Study on the Hydro-Mechanical Behavior of Fiber Reinforced Fine Grained Soils, with Application to the Preservation of Historical Monuments

Dissertation

as a requirement of the degree of
Doktor-Ingenieur (Dr.-Ing.)

at the Faculty of
Civil and Environmental Engineering
Ruhr-Universität Bochum

submitted by
Houman Soleimani Fard
from Isfahan, Iran

Reviewers
Prof. Dr.-Ing. habil. Tom Schanz
Prof. Dr.-Ing. Norbert Vogt
Prof. Dr.-Ing. Markus König

Bochum, March 2014

This work is dedicated to my beloved parents

Ali and Iran

Vorwort des Herausgebers

Herr Dr. Fard beschäftigt sich in seiner vorliegenden Promotion im weitesten Sinne mit Fragen des Denkmalschutzes. Im Mittelpunkt stehen historische Gebäude, welche aus Lehmziegeln mit einer Zumischung von Stroh und anderen Fasern gebaut wurden. Bei diesen oftmals religiösen Gebäuden treten in Folge der Änderung der Umweltbedingungen bzw. des Klimas Änderungen in den verwendeten Materialien auf, die unmittelbare Konsequenzen für die Nutzung bzw. die Standsicherheit dieser Gebäude haben.

Insbesondere beschäftigt sich Herr Fard mit der Situation eines derartigen Gebäudes in einem ariden Klima, wobei sich aus den genannten Gründen oftmals eine Befeuchtung der Wandstrukturen "von unten" ergibt. Ursache kann zum einen eine Änderung des lokalen Grundwasserspiegels als auch geänderte Niederschlagsverhältnisse sein.

Die normalerweise trockenen Materialien dieser Lehmbauweise weisen im charakteristischen Zustand relativ hohe Werte der Kapillarspannung auf. Bei einer Bewässerung können sie sich deshalb relativ schnell aufsättigen. Dadurch ändern sich ihre bodenmechanischen Eigenschaften, wie etwa die Durchlässigkeit, die Steifigkeit und die Festigkeit. Bei gleichbleibenden oder durch eine geänderte Nutzung sogar gesteigerten Lasten führt diese Degradation in zunehmendem Maße zu einer geringeren Gebrauchstauglichkeit, zum Teil auch einer geringeren Standsicherheit. Die genannten hydraulischen Belastungen sind ihrer Natur nach von zyklischer Art.

Ziel der Arbeit von Herrn Fard war es, unter Verwendung der Grundlagen der Bodenmechanik teilgesättigter Materialien eine Prognose zum Zeitverhalten derartiger Bauwerke zu ermöglichen. Ausgehend von einer Analyse an historischen Baumaterialien werden deren gekoppelte hydraulische und mechanische Eigenschaften in Laborversuchen quantifiziert.

Besonders die Laborversuche an Lehmmaterial, welches mit Stroh bewehrt ist, sind von internationaler Bedeutung. Die Ergebnisse in der Biaxialzelle unter Kontrolle der Teilsättigung stellen einen entscheidenden Fortschritt bei der Charakterisierung dieser Materialien dar.

Mit einem Technikumsversuch einer Ziegelwand im Maßstab 1 : 1 wird anschliessend die Aufsättigung der Lehmziegeln detailliert untersucht und mit vielfältigen Sensoren und Messkonzepten dokumentiert. Mittels der Laborversuche und des Technikumsversuchs wird ein numerisches Simulationsmodell kalibriert und validiert. Mit dem Modell ist es

anschließend möglich, größere Tragwerke bzw. unterschiedliche hydraulische Randbedingungen im Sinne von numerischen Experimenten zu studieren.

Die Ergebnisse der Arbeit von Herrn Fard ermöglichen es in Zukunft, geplante Sanierungsmaßnahmen in ihrer Wirksamkeit zu bewerten bzw. Ursachen für auftretende Schäden besser eingrenzen zu können.

Herr Dr. Fard leistet mit seiner Arbeit einen international sehr bedeutenden quantitativen Beitrag zur Sanierung historischer Kulturgebäude in Lehmbauweise. Mittels eines an Laborversuchen und Technikumsversuchen kalibrierten, THM-gekoppelten numerischen

Simulationsmodells, ist er in Lage den Wassertransport in derartigen Lehmgebäuden phy-sikalisch, realistisch zu simulieren. Dabei berücksichtigt er die komplex gekoppelten Temperatur-, Hydraulik- und Mechanikeffekte.

Die Ergebnisse der Promotion sind von einem internationalen Standpunkt aus als sehr wertvoll zu beurteilen. Verließ man sich bisher bei der Sanierung dieser Gebäude eher auf die langjährige Erfahrung, so ist es mit den Ergebnissen von Herrn Fards Promotion nun möglich, Ursachenforschung zu betreiben und die Wirksamkeit von Sanierungsmaßnahmen quantitativ realistisch zu bewerten.

Bochum, September 2014

Univ. Prof. Dr.-Ing. habil. Tom Schanz

Acknowledgements

All praises and thanks be to God for giving me strength and courage to achieve one of the challenging tasks of my life. This PhD thesis is a result of five years of research work carried out at Chair of Foundation Engineering, Soil and Rock Mechanics, Ruhr-Universität Bochum. I would like to thank first and foremost my supervisor, Prof. Tom Schanz, who gave me the opportunity to start my PhD and provided his continues support over all these years. My sincere gratitude goes to Dr. Diethard König, who helped me during my research and for his comments and suggestions throughout these years. Many thanks go to Prof. Norbert Vogt from Technische Universität München and Prof. Markus König from Ruhr-Universität Bochum for their agreement to be reviewers of this dissertation.

This work has been done with the financial support provided by Friedrich-Naumann-Stiftung. I would like to acknowledge the well organized scholarship as well as the whole supports offered by them.

I want to express my sincere thanks to "Cultural Heritage Organization of Iran" and Dr. Saberi, the Deputy Director of Research Institute of Culture and Art, University of Tehran, for many interesting and helpful discussions about historical buildings. I hereby express my special thanks to the Central Scanning Electron Microscope and the Chair of Building Materials of Ruhr-Universität Bochum for their kind cooperation and technical supports.

My gratitude should also be extended to all my current and former colleagues, laboratory staffs, and to all parties who indirectly assisted me during my period of stay in Bochum. Last but not least, I wish to gratitude my family for the whole support they have always given to me. Without their helps I would not be able to accomplish this work.

Bochum, Germany

September 2014

Houman Soleimani Fard

Abstract

Since several millenniums ago and still today adobes are being used in construction of buildings. The adobes are made from dried clayey soils. If water is in contact to the foundation of such buildings, it rises in the walls up. Building measures for example sealing the surrounding surfaces particularly for historical and culturally significant civil works gained recently more attentions. For non-burned adobes this uprising moisture is followed by reduction in strength of the material.

The aim of this research is to explain the uprising moisture in a masonry work made from adobes as a function of time and boundary conditions and to realize the effect of this raised water content on the shear strength of adobes unreinforced and reinforced with natural fibers. According to this basis the effectiveness of the selected countermeasure method is investigated.

Initially the materials used and the preparation of adobes are described. From this preparation method it is clear that in order to solve the problem the mechanics and hydraulics of unsaturated soils should be taken into account. In order to analyze the moisture transport in the fine grained soils of adobes, the water content-suction relationship and effect of reinforcement with natural fibers on that must be experimentally determined and discussed. The shear strength of this material is derived using a Biaxial device as a function of water content or its corresponding suction and also fiber content. In perception experiments the capillary uprising of moisture in a model wall which is in contact with water at the bottom are investigated and the volume changes related to this uprising are also monitored.

With a numerical simulation in which the input parameters are derived from basic investigations, the perception experiments are recalculated. The comparison of the results shows that the numerical modeling is able to represent the observed phenomenon. The model is then used to calculate the uprising of water with realistic dimension, to observe the efficacy of the countermeasure methods, and to evaluate the wall with the knowledge of changes in shear strength due to changes in water content and suction.

The investigations show that the uprising moisture over periods of several years can reach up to several meters height. The performance of the top surface of the wall is an essential boundary condition. The opening in the impermeable facades is an effective method

to reduce the height of wetted zone. An unobtrusive but effective method is to drill ventilation holes with regular intervals through the masonry work.

Zusammenfassung

Seit der Frühzeit bis heute bauen Menschen Gebäude aus Lehmziegeln. Die Lehmziegel werden aus tonhaltigen Böden geformt und getrocknet. Kommt die Gründung solcher Gebäude mit Wasser in Kontakt, steigt dieses in den Wänden auf. Durch Baumaßnahmen und z.B. Flächenversiegelung im Umfeld vor allem historischer und kulturell bedeutsamer Bauwerke wird dieses heute verstärkt beobachtet. Bei den nicht gebrannten Lehmziegeln führt die aufsteigende Feuchtigkeit neben anderen Einflüssen zu einer Reduktion der Festigkeit des Mauerwerks.

Ziel dieser Arbeit ist es, die Grundlagen zu legen, den Aufstieg der Feuchtigkeit in einem Mauerwerk aus Lehmziegeln in Abhängigkeit der Zeit und der Umgebungsrandbedingungen zu beschreiben und den Einfluss des erhöhten Wassergehaltes auf die Scherfestigkeit von Lehmziegeln mit und ohne Bewehrung aus natürlichen Fasern zu erfassen. Aufbauend auf diesen Grundlagen wird die Wirksamkeit ausgewählter Gegenmaßnahmen untersucht.

Zunächst werden die Ausgangsmaterialien und die Herstellung von Lehmziegeln beschrieben. Daraus wird deutlich, dass bei der Lösung der Fragestellung auf die Grundsätze der Mechanik und Hydraulik teilgesättigter Böden zurückzugreifen ist. Um den Feuchtetransport in dem feinkörnigen Bodenmaterial der Lehmziegel beschreiben zu können wird die Wassergehalts-Sättigungsbeziehung experimentell bestimmt und der Einfluss von Bewehrung aus Naturfasern auf diese ermittelt und diskutiert. Die Scherfestigkeit repräsentativer Materialien wird aus Biaxialversuchen in Abhängigkeit des Wassergehaltes und der damit verbundenen Saugspannungen sowie des Bewehrungsgehaltes abgeleitet. In Anschauungsversuchen wird der kapillare Aufstieg einer in der Sohle mit Wasser benetzten Modellwand beobachtet und dass damit verbundene Verformungsverhalten messtechnisch erfasst.

Mit einem numerischen Modell, in welches die Eingangsparameter abgeleitet aus den Grundlegenden Untersuchungen einfließen, werden die Anschauungsversuche nachgerechnet. Der Vergleich der Ergebnisse zeigt, dass das numerische Modell in der Lage ist, die beobachteten Phänomene abzubilden. Das Modell wird dann genutzt, um den Wasseraufstieg in Wänden mit realistischen Dimensionen zu berechnen und die Wirksamkeit von Gegenmaßnahmen zu beobachten und unter Einbeziehung der Kenntnisse zur Veränderung der Scherfestigkeit unter mit dem erhöhten Wassergehalt und Saugspannungen zu bewerten.

Die Untersuchungen zeigen, dass der Wasseraufstieg über Zeiträume von mehreren Jahren Höhen von mehreren Metern erreichen kann. Dabei ist die Ausführung der Oberfläche des Mauerwerks eine wesentliche Randbedingung. Die Öffnung von verfliesten Fassaden ist eine wirksame Methode die Höhe der durchfeuchteten Zone massiv zu reduzieren. Unauffälliger aber ebenfalls wirksam ist das Schaffen von Ventilationsbohrungen in regelmäßigen Abständen durch das Mauerwerk.

Contents

List of Figures

List of Tables

Nomenclature

Θ	Effective volumetric water content
χ	Bishop's effective stress parameter
ϵ_1	Maximum principal strain
ϵ_2	Intermediate principal strain
ϵ_3	Minimum principal strain
ϵ_p	Axial strain at peak stress
ϵ_v	Volumetric strain
$\epsilon_{50\%}$	Axial strain at 50% of maximum peak stress
κ	Fitting parameter of equations predicting χ
ϕ	Friction angle
ϕ'	Effective friction angle
ϕ^b	Angle of shearing resistance
ϕ_f	Post peak friction angle
ψ	Matric suction
ψ_d	Angle of dilation
ψ_d^f	Angle of dilation at failure
ψ_v^{max}	Maximum dilatancy angle
ψ_{AEV}	Suction corresponding to air entry value

ψ_{WEV} Suction corresponding to water entry value

ψ_r Residual suction

ρ_w Unit weight of water

σ Total stress

σ' Effective stress

σ_1 Maximum principal stress

σ_2 Intermediate principal stress

σ_3 Minimum principal stress

σ_d Deviator stress

σ_d^{max} Maximum deviator stress

τ Shear strength

τ_{oct} Octahedral shear stress

θ Volumetric water content

θ_m Angle of shear band inclination

θ_m Shear band inclination

θ_{res} Residual volumetric water content

θ_{sat} Saturated volumetric water content

a Fitting parameter of SWCC models

a, b, c Dimension of countermeasures' configurations

B Skemptons factor

b True triaxial stress condition factor

c Cohesion

c' Effective cohesion

e Void ratio

e_0 Initial void ratio

e_1 After-swelling void ratio

e_f Interfine void ratio

e_s Intergranular void ratio

E_{100} Moduli of elasticity at peak stress

E_{50} Moduli of elasticity at 50% of peak stress

f_c Fine content

G_s Specific gravity

h Water head

h_0 Initial height of the specimen

h_e Washburn's fitting parameter

$k(\psi)$ Unsaturated coeficient of permeability

$k_r(\psi)$ Relative coeficient of permeability

K_s Saturated hydraulic conductivity

k_s Saturated coeficient of permeability

LL Liquid limit

m Fitting parameter of SWCC models

M_w Molecular weight of water

n Fitting parameter of SWCC models

p Mean normal effective stress

PI Plastic index

PL Plastic limit

q Shear stress

q_ψ Steady state volumetric water flux

r Fitting parameter of equations predicting χ

R_g The universal gas constant

RH Relative humidity

S_e Effective degree of saturation

S_r Degree of saturation

$S_{r\,AEV}$ Degree of saturation corresponding to AEV

$S^w_{r\,max}$ Degree of saturation corresponding to minimum suction in the wetting path

$S_{r\,res}$ Residual degree of saturation

$S_{r\,sat}$ Saturated degree of saturation

$S_{r\,WEV}$ Degree of saturation corresponding to WEV

s_t Total suction

T Absolute temperature

u_a Pore air pressure

u_w Pore water pressure

v_x Velocity of water flow in direction of x

1 Introduction

1.1 Background and motivation

Hydro-mechanical properties of soils depends strongly on their moisture content. What differentiates unsaturated from saturated soils and unlocks a new field in soil mechanics is the presence of negative pressure in pore water, also called "Suction". Suction affects the effective stress and consequently all mechanical properties of soil (i.e. strength, volumetric behavior, hydraulic properties, etc.). Correspondingly, the most important property of an unsaturated soil can be defined as the relation between water content and suction, called the Soil-Water Characteristic Curve (SWCC).

Capillary uprising moisture occurs in dry and unsaturated soils under which a low suction or saturated zone is located. This phenomenon changes the suctions of the soil non-uniformly, and as stated in the present study as well as in previous works, all hydro-mechanical properties will be impressed. Uprising rate, as presented in the literature, besides material properties and geometrical configuration, is a function of saturated hydraulic conductivity and SWCC. Hydraulic conductivity of a soil is one of the most sensitive geotechnical parameters of variation of humidity. In unsaturated conditions, even for a single soil it is possible to have a coefficient of permeability that ranges by 10 orders of magnitude by a change in water content. Since many constructional materials are porous, uprising water from subsoil is a common problem in masonry materials and can cause serious problems in terms of their stability. In this case we encounter a fundamental process which is the movement of water through a permeable material and its subsequent influences.

Negative effects of uprising moisture on buildings can be considered from several points of view (e.g. weathering and erosion, salt crystallization, biological molds, facade deterioration, etc.), but this research concentrates on changes in hydro-mechanical properties. Masonry buildings generally have huge gravimetric loads transported to subsoil through wide walls. A reduction in the shear strength of masonries makes the walls more vulner-

able to unexpected loads such as an earthquake or they may even fail under their own constant gravity loads. Regarding to the fact that in clayey materials change in water content is followed by volumetric change, if the uprising moisture occurs disparately in the walls, differential settlement or heave in the building is unavoidable which endangers its overall structural behavior.

Sun-baked clay brick is maybe the earliest basic building materials produced by man and in spite of some weaknesses (i.e. poor response to earthquake, low compressive and shear strength, short service life, etc.) for various socio-economic reasons and the unavailability of suitable alternatives they are indeed still used today. Raw masonry materials behave in a similar way to consolidated soil, therefore they can be analyzed and investigated under the principles of soil mechanics.

Soil reinforcement is an old stabilizing method that even nowadays not only attracts the attention of researchers, but has also been widely used in several practical projects. Due to some shortcomings in the mechanical properties of soil and in order to improve them, some reinforcing elements are added to it, either as geotextiles with predefined locations or as randomly oriented discrete fibers. For this purpose, for a long time natural fibers such as straw have been implemented for bettering the properties of clay bricks (e.g. strength characteristics, crack control, and moisture resistance).

Since brick-working walls mainly have plane-strain behavior, to have more reliable physical simulation instead of conventional triaxial experiments, tests with plane strain condition should be carried out. Biaxial devices are not as common as triaxial or direct shear devices for geotechnical investigations and have more complexities to overcome in comparison to them. The difficulties are mainly related to the need for special mold, membrane, accessories, and the preparation of a prismatic soil specimen.

However, although masonry materials have been used for over five millenniums, there are only a few analytical studies on shear strength and volumetric behavior of reinforced soils used as masonries, and among the published data in this field, hydro-mechanical behavior of hard clayey materials under unsaturated conditions is very limited. It is evident that there is lack of knowledge of masonry materials, especially unsaturated soil. This lack of knowledge will be more obvious when the properties of reinforced soil under plane strain conditions is considered.

1.2 Scope and objectives

The main objective of the study is to investigate the hydro-mechanical properties and behaviors of unsaturated reinforced clay bricks (i.e. SWCC, uprising moisture, and shear strength). In this order three main series of experiments were performed:

(i) SWCC tests: The objective of this study was to investigate the influence of the fiber reinforcement on the SWCC by several experiments on soil reinforced with different fiber inclusions of 0, 0.5, 1, 2, and 3 gravimetric percent.

(ii) Biaxial tests: To determine the effects of suction and fiber inclusion on shear strength under plane strain conditions, a series of biaxial shear strength tests was performed on materials with 0, 0.5 and 1 percent fiber content with suctions varying from 0 (saturated conditions) to 55 MPa.

(iii) Large scale wall tests: In this research, based on the above discussion, uprising moisture in clay masonry materials with non-uniform degrees of saturation was investigated by large scale tests and numerical simulations. Effect of fiber reinforcement on the rate of uprising moisture was also studied. Proposed countermeasure methods against this problem were discussed above and one of the frequently used methods was analyzed more deeply by numerical and experimental modelings, and a new method is introduced.

The objectives of this research can be summarized as:

- Determine the basic properties of reinforced and unreinforced clayey soil typically used in the preparation of clay bricks.
- Determine the SWCC of a fine-grained soil, unreinforced and reinforced with 0.5, 1, 2, and 3% straw content.
- Investigate the effects of suction on shear strength, dilatancy, and shear band inclination of a clayey soil with 0, 0.5. and 1% straw content under a plane strain condition.
- Observe uprising moisture through large scale masonry walls with 0 and 1% straw content, and compare them with numerical results.
- Evaluate a countermeasure method used against uprising moisture by experimental and numerical modelings.
- Suggest a new method to prevent uprising moisture in thick walls.

1.3 Organization of the dissertation

This dissertation includes eight chapters. The first chapter presents the background, objectives, and scope of this research, as well as the organization of the thesis. The second chapter includes the motivation and outline of the main research problem in this thesis. The third chapter presents a literature review on the basics of unsaturated soil mechanics, a plane strain condition, fiber-reinforced soils, uprising moisture from underground water, and countermeasure methods commonly used against this problem. In the fourth chapter the materials used are introduced, which are clay-silt-sand mixture reinforced with different percentages of straw. In this chapter the experimental program is also presented. The fifth chapter describes the testing devices, experimental procedures, and implemented methods as well as calibrations and validations. The sixth chapter presents the results of tests and required corrections. In the seventh chapter analyses and discussions of experimental results and numerical simulations are given. Eighth chapter summarizes the research, provides conclusions and recommendations, and propounds further studies in this field.

2 Problems of uprising moisture and possible treatments

2.1 Introduction

Largely due to capillary action, water rises upward through all porous materials, which is located over saturated or low suction zones. The height and rate of uprising depend on the properties of a liquid (e.g. surface tension, viscosity, and density) as well as the transporting medium (e.g. pore size distribution, permeability, and SWCC). Therefore masonry materials like stones, rammed walls, fired and sun-dried bricks can simply absorb water from an underground water table which rises in some seasons up to the foundation of buildings. This humidity is in the main does not lead to serious problems for the stability and functionality of buildings made of materials like concrete, fired brick, stone, and modern materials; however, sun-dried brick (also called raw bricks or adobes), on which this research focuses, due to its micro-structure is very sensitive to the presence of humidity. Since the uprising humidity in the subsoil is a periodic phenomenon (over the seasons) the consequent problems also occur or increase each year, and can cause severe problems and even failure for such buildings.

In this chapter the preparation of adobes is explained from the geotechnical point of view. Most important aftermaths of uprising moisture on adobes and proposed countermeasure methods for various applications are presented. The so far unanswered questions which will be answered in this research together with the steps and methods of this approach are also explained in this chapter.

2.2 Brick preparation method and micro-structure of adobes

Adobe bricks have been used for over five millenniums and even today they are widely used in rural regions all around the world. Interestingly, during this long and extensive usage of adobes, their preparation method has not changed much. Generally (in the past) adobes were made from the soils available near the construction site, intact or with small modifications to the mixture. A wide range of soils employed for the preparation of adobes are cited in the literature (see Section 4.2); however, in general terms the percentage of fine and coarse contents should not exceed or fall below certain values. If the mixture contains too much clays, desiccations cracks occur during drying, and if it contains too much sand, the durability and strength of adobes reduce. The soil must be mixed with enough water to prepare soft and flowing slurry. The mixture should be stirred completely to get a uniform and homogeneous material, and left for a while to be sure that water is uniformly distributed and has reached all particles, and that all clay clusters are opened. Then, as shown in Figure 2.1, special molds are filled with the slurry thoroughly. Now molds can be removed slowly and gently so as not to disturb straight edges. For the drying process, they should be placed in an open atmosphere for several days. Unlike fired bricks, in sun-dried bricks the mineralogy of particles does not change. Process of drying is explained in more detail in Section 7.2.

Figure 2.1: Adobe preparation.

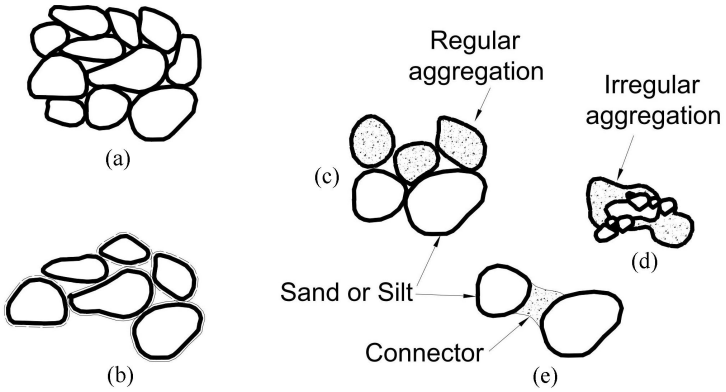

Figure 2.2: (a) Individual coarse grains interaction; (b) coarse grains covered with clay platelets; (c) regular clay aggregates formed beside coarse grains; (d) irregular clay aggregates; and (e) clay aggregates act as a connector between coarse grains (Koliji 2008).

2.2.1 Clay-sand mixtures

Depending on the conditions and formation path of a soil mass consisting of clay and sand particles, the interaction of clay and sand (or silt) may occur in different types of assemblages. As shown in Figure 2.2, clay platelets forming clay aggregates can have several assemblages. According to Collins & McGown (1974), aggregation might be regular or irregular. In regular aggregation, unlike irregular aggregation, aggregates have a definite physical boundary and therefore particular hydro-mechanical properties can be attributed to aggregates themselves.

Due to sample preparation of masonry materials, in which samples start from soft slurry of clay-silt-sand mixtures, the formation of clay aggregates separated from sand or silt grains is not expected, and it is plausible that coarse grains are clothed and covered with clay platelets and connected to each other via clayey connectors, as shown in Figures 2.2b and 2.2e. This will be explained in Chapter 4.

For sand-bentonite mixtures, Agus (2005) reported that sand content influences on the mechanical behavior of a mixture only with low clay content, i.e. when the intergranular contact between sand grains appears. There is a certain clay content beyond which the contact between sand disappears and clay fraction dominates the mixture properties. But it should be taken into consideration that compared to sand grains clay particles have a large specific surface area and -depending on the clay type- a very low percentage of clay

may cover all sand grains. The state of sand grains in the compacted mixture can be seen in Figure 2.3.

2.2.2 Bonding, fabric and structure

"Bonding" is defined as the combination of all the interparticle forces, which are not of a purely frictional nature. In general interparticle forces are the factors acting to keep the soil particles together. They are explained in this section.

The soil "fabric" is defined as the arrangement of soil particles, groups of particle, and pores in the soil. Two type of categorization for soil fabrics are introduced: (i) based on association of clay particles which can be "dispersed" (when no face-to-face contact exists) or "aggregated" (where several clay particles are grouped with face-to-face association to form an aggregate), and (ii) based on flocculation which can be "deflocculated" (when no aggregations of clay particles exist) or "flocculated" (where edge-to-edge and edge-to-face association of aggregates or particles exist) (van Olphen 1977 and Mitchell 1993).

The term "structure" will be used here to define the combination of fabric, arrangement of the component particles, and bonding (Gasparre 2005). A soil with a given mineralogy might be found with different internal structures arising from different physico-chemical causes. These differences are usually addressed by the concept of soil structure.

Elementary particles tend to group together rather than exist as individual particles. These groups of elementary particles may regroup in larger order and form what is termed here as particle assemblages. Depending on the type, environmental conditions and origin of the structuring process (formation of structures), different types of assemblages may exist. Connectors, for example, are bridge-like assemblages that connect two (or more) other assemblages which are usually of a larger size (Koliji 2008).

In general, interparticle forces are the factors acting to keep the soil particles together. Some of the interparticle forces are listed below:

Van der Waals forces:

The elementary layers stacked together to form a particle (platelet or crystal). In dry conditions, bonding between the elementary layers is provided by van der Waals and by exchangeable cations. These types of bonding are weak and broken when water inserts between them (Mitchell 1993).

Capillary forces:

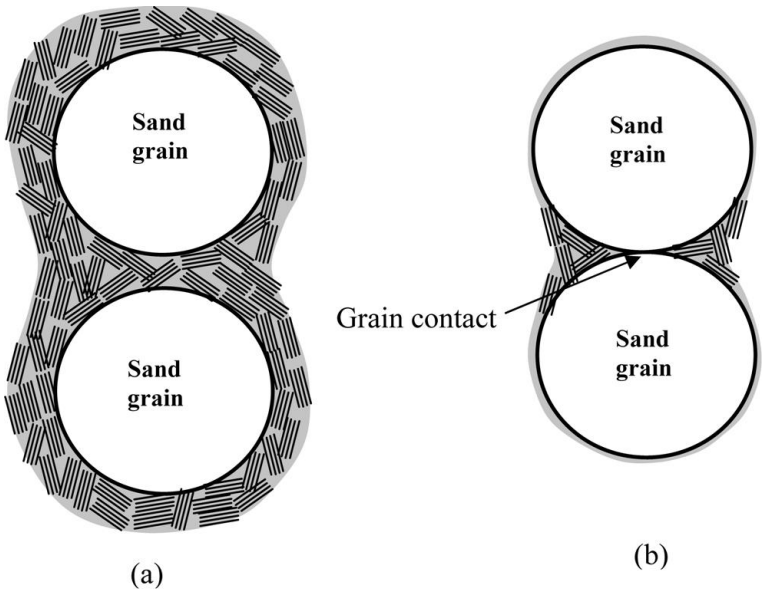

Figure 2.3: Two possible states of sand grains in a deflocculated clay system: (a) clay particles coating sand grains and (b) clay particles welding sand grains (Agus 2005).

By presence of an air bubble inside the soil body, water rings form around particle contact areas and the negative pore water pressure in menisci at particle contacts increases the interparticle forces.

Electrostatic attractions:

When particle edges and surfaces are oppositely charged, there is attraction due to interactions between double layers of opposite sign. Fine soil particles are often observed to adhere when dry. Electrostatic attraction between surfaces at different potentials has been suggested as a cause. In the gap between parallel particles separated by distance at different potentials, an attractive force exists per unit area (Ingles 1962). For coarse-grained soils such as sand, double-layer forces are essentially nonexistent.

Chemical force:

These forces arise from chemical cementation at the grain contacts.

2.2.3 Application of soil mechanics

Studies on masonries and brick-workings are generally categorized under branches of structural engineering. However, with a deeper view on the hydro-mechanical properties of sun-dried bricks and mortars it can be clearly understood that in fact principles of soil

mechanics govern the behavior of such material, at least as long as raw adobes are being considered.

Regarding the preparation method of raw adobes (Section 2.2), they can be counted as consolidated fine-grained soils. Dried bricks normally have a very low as-prepared water content in the range of 0.5 to 1.5 percent depending on the used materials and weather conditions at the building site. If this masonry material is subjected to uprising moisture, the consequences cannot be interpreted without implementation of principles of unsaturated soil mechanics. For example, with an increase in water content, as with any other consolidated clayey soil, adobes may swell or shrink (regarding the loading conditions). Unsaturated hydraulic conductivity of adobes is an essential parameter to investigate the capillary uprising moisture. Moreover, shear strength of a consolidated soil decreases with an increase in water content, therefore safety factors and other stability analyses must be carried out based on strength parameters of soil with varying degrees of saturation, which are presented and calculated in unsaturated soil mechanics.

2.3 Problems arising from uprising moisture

The risen water typically does not make an uprising front in the wall below which the masonry is saturated, but the water content (due to uprising moisture) has a gradient from saturated or nearly saturated in the bottom to dry or as-prepared water content in the top of the wall. Of course, the higher the water content in the adobes we have, the more significant and hazardous are the expected problems from uprising moisture. These problems can be studied from different points of view; for example, regarding stability, functionality and serviceability, facade and appearance, health of residents, or preservation of historical monuments. For buildings in which load is carrying through masonry walls the above mentioned problems are even more dangerous. Some of the common problems are as follows (the emphasis of this research is on the 3^{rd} and 4^{th} items):

1. Growth of molds or other biological species
2. Salt crystallization
3. Lowering in shear strength (Figure 2.4)
4. Volumetric changes (swelling or shrinkage) and their subsequences (Figure 2.6)
5. Facade deterioration (Figure 2.6d)

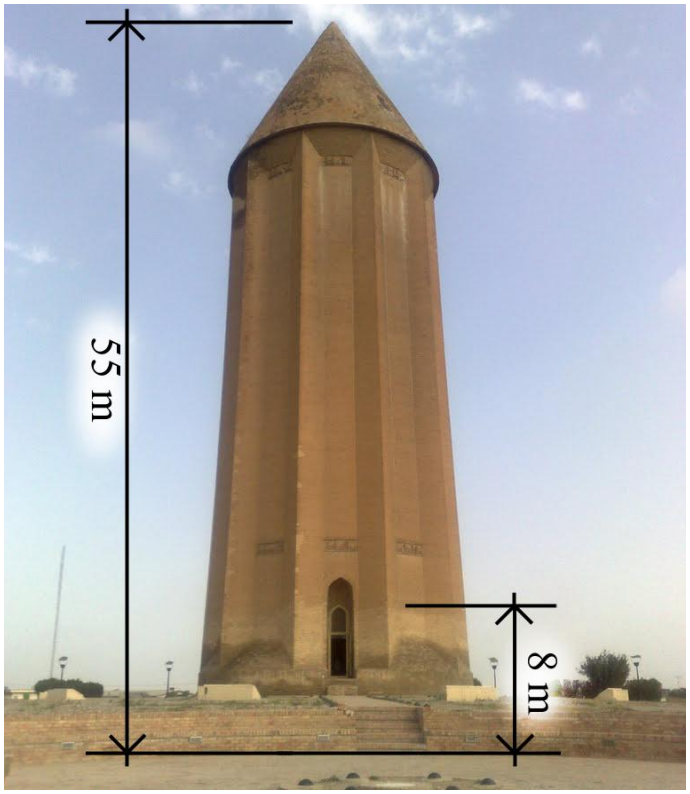

Figure 2.4: Tower of Gonbad-e Qabus, northeast of Iran.

In wet seasons amount of vapor in soil's air phase increases. This vapor can be released into the open atmosphere via the ground's surface. But in recent years due to impermeable pavements this moisture condensates in foundations and lower parts of masonry buildings. In Figure 2.5 the middle platform is made of old bricks which are permeable but the pavement of surrounding areas is built from cemented mosaics which prevent the moisture from passing through. Therefore, reaching open atmosphere, beneath-surface vapors from the entire yard come to this platform. Remaining salts on the brick platform -especially at the sides and corners- clearly confirm this phenomenon.

Figure 2.5: Impermeable pavement and condensation of water in the foundations.

Figure 2.6: Consequences of uprising moisture in historical masonry buildings; (a) horizontal crack due to differential settlement; (b) deformation on the dome due to differential settlement; (c) swelling in the wall; and (d) facade deterioration.

2.4 Proposed countermeasure methods against uprising moisture

Countermeasures will help prevent further damp problems and may reduce the severity of an existing problem so that major works are not necessary. Young (1997) and Torres & Freitas (2007) have reviewed the countermeasure methods commonly used against uprising moisture. Some of these methods are described below.

2.4.1 Creating a physical or chemical barrier

The main objective of this technique is to create a physical or chemical barrier at the base of the affected walls to prevent rising damp. It is possible to reduce the absorbent area, place watertight barriers, or apply hydrofuge products.

Reducing the absorbent section:

This technique basically consists of diminishing the absorbent area by replacing part of the porous material (wall) with air pockets. This is followed not only by a reduction in the amount of water absorbed, but by an increment in evaporation.

Placing watertight barriers:

A watertight material (bitumen, polymer-based mortar, corrugated sheets of stainless steel or lead sheets) is inserted into the wall's buried section to prevent water from migrating to upper levels. Creating watertight barriers might cause vibration and can threaten stability, especially in old masonry buildings.

Chemical barriers:

Chemical treatments have become popular in recent years. They aim to create an impermeable barrier in the wall by injecting water-repellent compounds into masonry pores via a series of pre-drilled holes along the base of the wall. Critical to the success of any chemical treatment is the formation of a continuous water-repellent zone through the entire wall thickness. In practice this may be difficult to ensure, and must be judged by the operator, whose experience and skill are essential. There are two methods of impregnating walls with chemicals: injection under pressure, and gravity feeding. Both require a series of closely spaced holes; two holes per brick are common.

Pressure injection is quicker, but has a number of disadvantages. It is generally not possible to inject into soft lime mortars as the pressure of injection may lead to blow out of the mortar. Consequently the chemical is injected into the bricks or stones.

Gravity feeding is slower and allows the chemical to penetrate fully into the pore structure of mortar, stone, and brick and is a more appropriate treatment for walls of hard dense stones (e.g. bluestones) set in soft lime mortars. The chemical is fed into holes in the mortar, and the higher suction of the adjacent dense stones draws it into them too (see Figure 2.7).

2.4.2 Creating a potential against the capillary potential

This is an old technique that delays rising of the water by creating an electrical potential against the capillary potential. This technique is no longer popular because it is not considered to be effective.

2.4.3 Changing the facades and pavements

Another efficient method is changing outer coatings of buildings that let uprising moisture evaporate easier and faster from inside the walls, which also impedes salt from crystallizing on the facades.

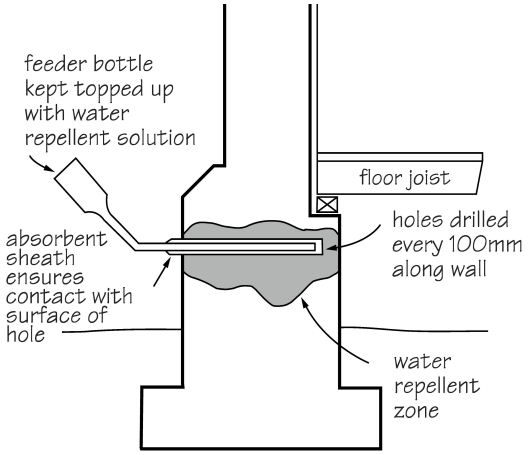

Figure 2.7: Chemical barrier injected inside the wall to limit uprising moisture phenomenon (Young 1997).

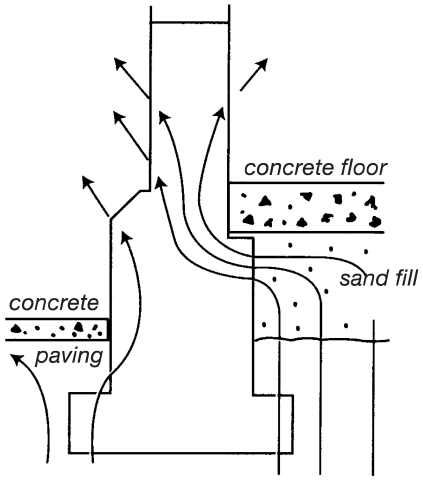

Figure 2.8: Impermeable pavements increase the uprising moisture inside the walls (Young 1997).

One of the worst mistakes made by renovators is to remove a ventilated timber or brick floors and replace it with a concrete slab or stones installed with cemented mortars which are impermeable compared to previous ones. As shown in Figure 2.8, these materials prevent evaporation and all the soil's moisture rising beneath the building is now focused on the walls. Rising damp problems are almost guaranteed, whereas before there may have been no significant damp. Depending on the variation of underground water table, this method can be suitable for raw masonries.

2.4.4 Concealing anomalies

When the causes of rising damp cannot be eliminated, we can decide to put up a new wall separated from the original wall with a ventilation space, which is a type of damp-proof course system concealing the anomalies. Concealing anomalies behind a wall built with a ventilation space separating it from the original wall would undoubtedly be effective if done correctly. Nevertheless, in addition to reducing space, concealing original walls may not be viable for historical buildings.

2.4.5 Base ventilation

It is important that water does not lie against the base of walls; surrounding paths and ground levels should be sloped so as to drain water away from walls. This practice is

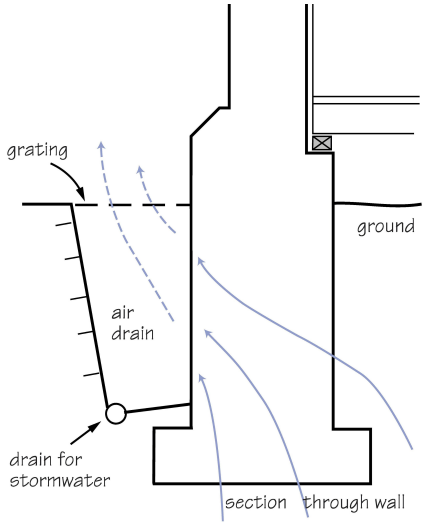

Figure 2.9: Ventilating the wall base (Young 1997).

extended in the technique known as air drains, a method for controlling damp by encouraging evaporation to occur at the lowest possible level.

Creating ventilated peripheral channels, in addition to diminishing water contact with porous walls, increases the evaporation of absorbed water. This evaporation takes place below ground level. Installing a hygro-regulated mechanical ventilation device can increase this system's effectiveness (see Figure 2.9). Depending on the thickness of the wall, this method may reduce the uprising height considerably. In Sections 6.4 and 7.4 this method has been evaluated.

2.5 Approaches of this research

This research investigates the effect of uprising moisture on hydro-mechanical behavior of fiber-reinforced masonry material, evaluates a commonly used countermeasure method, and proposes a new method to reduce uprising rate and height. Regarding the feature of capillary moisture in a masonry wall in which the degree of saturation has a gradient between minimum and maximum values, in order to cover all suctions, analyses and studies of the present work should be done in unsaturated conditions with suction ranging from saturated to as-prepared values.

As mentioned in Section 2.3, change in water content can significantly affect the shear strength of materials. Most elements, which are under treat of uprising, are foundations

and walls that have plane strain behavior (see Section 3.6). Therefore, in order to determine their behavior more realistically the effect of moisture on shear strength was investigated using a series of biaxial shear strength experiments.

Uprising rate in a wall made of adobes over a period of two months was experimentally observed and numerically simulated. Similar test but on a wall protected by a countermeasure method named "base ventilation" (explained in Section 2.4.5) illustrated the efficiency of this method on uprising circumstances.

Before performing the above tests the required information and data had to be gathered. SWCC of the used materials is perhaps the most important requirement in calculating and analyzing unsaturated shear strength parameters. Also, numerical results of uprising moisture is very sensitive to SWCC. This parameter together with other basic data (e.g. saturated permeability of reinforced and unreinforced soils, specific gravity, void ratio, atterberg limits, etc.) had been determined in advance.

Finally, according to this study for walls with any other configuration (i.e. geometry, countermeasure method, periods of presence of water, etc.) and regarding SWCC and other basic parameters, suction (or degree of saturation) can be obtained through numerical simulations for given heights and times. For each range of suction the shear strength is known, which makes the stability analyses of a wall with a gradient of humidity possible.

Some of the investigations and studies accomplished in this research were done (to the best of the author's knowledge) for the first time. For example, as mentioned before and explained later, this work has combined capillary rise and shear strength in the field of unsaturated soil mechanics. Furthermore, unsaturated shear strength characteristics of fiber-reinforced soil was studied in this work. Plane strain behavior of fiber-reinforced soils has not been studied before (neither saturated nor unsaturated). Moreover, investigation of SWCC of reinforced soil has not been reported in the literature so far.

2.6 Summary

In this chapter the uprising phenomenon in porous materials (e.g. masonries) was described. Preparation method of raw masonry brick was explained and discussed from geotechnical points of view. Possible formations of particles in sans-clay mixtures (e.g. masonry materials) and existing attraction between them were explained, and the necessity and performance of soil mechanics in interpretation of hydro-mechanical behavior of

such material were described. Problems that may be caused by uprising water and suggested methods to reduce them (none here as countermeasure methods) were mentioned and discussed. Finally, the aims and approaches, together with points which make this research new and (up to now) unique were presented and explained.

3 Literature review

3.1 Introduction

This chapter summarizes a review of the relevant literature to provide a background to the basics of unsaturated soil mechanics, effective stress and shear strength of unsaturated soil, plane strain conditions, fiber reinforced soil, hydraulic conductivity of saturated and unsaturated soil (theoretical and experimental approaches), and structure of fine-coarse grain mixture. At the end of this chapter proposed countermeasures against uprising moisture will be explained.

3.2 Basics of unsaturated soils

From the beginning of the twentieth century, geotechnical science has been based on the characterization of soil as a two-phase material (solid+water or solid+air). However, a considerable proportion of geotechnical engineering problems are involved with partially saturated (or unsaturated) soils, which have three phases (solid, water, and air), with significant behavioral differences from a two-phase system. Due to the existence of air and water together in the pore space, phenomena that are impossible to observe in two-phase media, such as capillary due to the surface tension of water at a water-air interface, affect both soil parameters and behavior. As a result, unsaturated soils present a variety of engineering challenges that require tools that are beyond those available for saturated soil mechanics. Examples of challenges include problems associated with failure due to rainfall (especially in slopes), expansive soils, and trafficability in semi-arid regions. Interest in such unsaturated problems started in the late 1950's, and has increased in the last decades.

In the early part of the 19^{th} century, geotechnical scientists separated the existing water in the body of soils into three groups which are presented in saturated porous media (Briggs 1897):

Gravimetric or bulk water: This water fills the pore volume. When the suction reaches to air entry value, the bulk water starts to reduce.

Capillary or pendular water: This moisture is liquid bridges around particle-to-particle contact. When all of the bulk water is drained due to the increase in suction, the pendular water can also be drained in the presence of enough suction.

Hygroscopic or adsorbed: Absorbed water is a few-molecule thick cover on all solid particles. Atmospheric condition of a normal and temperate climate cannot separate this water from soil particles.

3.2.1 Total potential of soil water

Aitchison (1965) defined the total potential of soil water as the amount of required work that must be done per unit quantity of pure water to transfer reversibly and isothermally an infinitesimal quantity of water from a basin of pure water at the reference elevation and external gas pressure to the soil water at the elevation of the soil under consideration. Soil water potential can be separated into different components: elevation (gravitational potential), pressure, matric, and osmotic.

First discovery of water tension strength was by the Bernoulli brothers in 1730. Euler, in 1754, found that if the velocity of water significantly increases its pressure it could become negative, and this was the first mathematical description of water's ability to withstand tension. Berthelot did the first test in which water sustained an amount of tension equal to 5 MPa greater than vapor pressure of water which is 99 kPa.

3.2.2 Concept of suction

Since in the soil science, soil pore water does not change its elevation at a certain point under consideration, and the external gas pressure (i.e. barometric pressure) varies negligibly, among the potential components described above, the first two (gravitational and pressure) cease to exist, and the last two potential components, which are matric and osmotic suctions, remain. In this research, the term "soil suction" refers to sum of these two components. It is also called total suction, negative pore water pressure, or moisture tension.

According to Aitchison (1965) the complete and exact definition of soil suction, which is similar to the definition above, is: Soil suction (matric + osmotic potential) is the

amount of useful work that must be done per unit quantity of pure water to transfer reversibly and isothermally an infinitesimal quantity of water from the soil water to a pool of pure water at the same elevation and atmospheric pressure. Although thermodynamical aspects of soil suction (capillarity, water tension, and water potential) have been addressed in theoretical ways by several researchers in the past (van der Waals 1983, Fisher 1923, Aitchison 1965, and Coussy & Fleureau 2002), the mechanical considerations were largely studied from a practical point of view.

3.2.2.1 Matric suction

Based on Toker (2002)'s definition, matric suction is a component of suction due to physics of the water-air interfaces, and is equal to positive of the matric potential value. Any soil may have pores small enough where the surface forces are large enough to prevent the body forces from draining the pores, i.e. the soil has a capacity to store water. Some energy (in the form of negative pressure) has to be applied to withdraw the water, which is held in place by the potential energy of the tensile forces created due to curved air-water interfaces. These forces in the pore water are termed matric suction or capillary potential.

In other words, the matric suction is related to the air-water interface, which provides surface tension and causes the capillary uprising phenomenon. Matric suction is calculated as the difference between pressures of pore air (u_a) and pore water (u_w) in the soil.

3.2.2.2 Osmotic suction

Osmotic suction is present in both saturated and unsaturated soils. This component is the suction due to salts and other solute concentration differences, which is equal to the absolute value of the osmotic potential. In the field of soil mechanics this suction can be provided with soluble materials. In most of the practical problems in geotechnical engineering, significant changes in osmotic suction is not a common phenomenon (Nelson & Miller 1992).

3.2.3 Suction measurement

Suction measurement is one of the fundamental experimental affairs in the field of unsaturated soil mechanics. Since suction value plays a central role in unsaturated soil aspects, an inaccurate measurement affects laboratorial results. Many methods for measuring the

Table 3.1: Some of the techniques introduced for measuring soil suction

Technique (ASTM Code)	Suction Type	Parameter Measured	Range (kPa)
Axis Translation Technique	Matric	u_a and u_w are controlled	0 - 1500
Suction probe	Matric	u_a and u_w are controlled	0 - 1500
Filter Paper (D5298-94)	Matric	contacting paper water content	0.3 - 1500
Filter Paper (D5298-94)	Total	nearby paper water content	2000 - 100000
TDR	Matric	dielectric constant of device	almost entire range
Tensiometer	Matric	water tension	0 - 100
Squeezing (D4542-95)	Osmotic	ion concentration	0 - 35000
Psychrometers	Total	temperature at evaporation	100 - 8000

suction are presented in the literature (Fredlund & Rahardjo 1993, Lee & Wray 1995, Ridley & Wray 1995, Toker 2002) which measure suction by two main methods: direct and indirect measurements. Indirect methods measure parameters of soil which correspond to osmotic, matric, or total suction via predetermined calibrations.

Although various methods have been suggested, so far no unique method is proposed to cover the entire range of total suction. Table 3.1, summarized by Toker (2002), presents the known methods of obtaining soil suction.

3.2.3.1 Direct measurements

Matric suction can be determined through direct measurement of the negative pore water pressure. The pore air pressure usually is equal to in situ atmospheric pressure and matric suction is the difference between air pressure and pore water pressure. The direct measurement of matric suction requires a separation between water and air phase by

means of a ceramic disk or a ceramic cup. Among these techniques are “tensiometer sensor”, “axis translation technique”, and “suction probe”.

3.2.3.2 Indirect measurements

As mentioned before, indirect methods measure the negative pore pressure, but by another parameter of soil which can be converted to soil suction through mathematical equations or experimental calibrations. Three of the indirect methods are described here:

Time domain reflectometry (TDR):

Time domain reflectometry is a method basically to analyze the reflected pulses which are emitted into a media. These reflections can reveal some of the properties of materials in which the wave travels. Application of TDR in soil mechanics is derived from the measurement of volumetric water content of the soil by Hoekstra & Delaney (1974) and Topp et al. (1980). Since then the method has been significantly developed and used for measuring.

In the TDR technique, apparent dielectric constant of the soil (i.e. the mass of soil and water) is measured, which is related to volumetric water content of the soil by means of a precise calibration (Topp et al. 1980). A fundamental assumption used in the application of TDR technology is that the dielectric properties of the soil water are similar to those of bulk water (White et al. 1994). As can be seen schematically in Figure 3.1, TDR sensors have a pulse generator unit which provide and send a pulse to the coaxial cable and finally wire transmission lines. The frequency of the pulse must be high enough (30 MHz - 1 GHz) to travel not inside the wire but through a body of soil. The time during which the pulse is emitted and reflected is based on the dielectric of surrounding soil (which depends on its water content). The reflected pulse is analyzed by an oscilloscope.

To relate the volumetric water content obtained from TDR to the matric suction, the soil-water characteristics curve of tested soil is required. Yu & Drnevich (2004) improved this technique by adding the ability to measure gravimetric water content without separately testing the soil to determine its specific gravity. This method is accepted and standardized by ASTM 2003 under ASTM D-6780.

Relative humidity sensor:

The amount of water vapor in the air at any given time is usually less than that required to saturate the air. The relative humidity is the percent of saturation humidity, generally calculated in relation to saturated vapor density as stated in Equation 3.1.

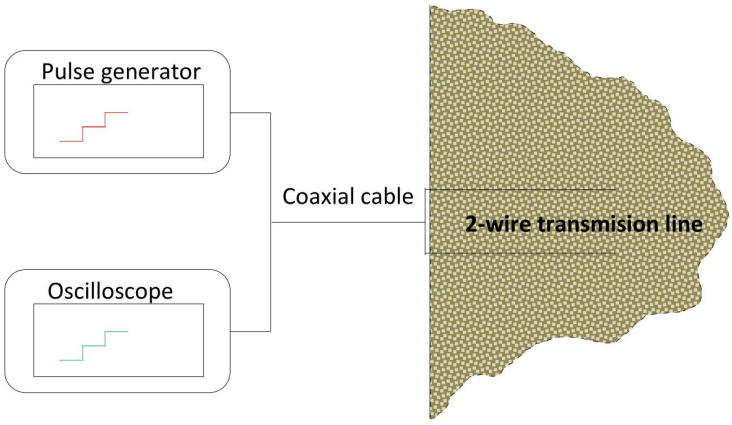

Figure 3.1: Schematic setup of TDR.

$$RH = \frac{Actual\ \ vapor\ \ density}{Saturated\ \ vapor\ \ density} \times 100 \tag{3.1}$$

The relative humidity (RH) and temperature of vapor space of the soil are measured and total suction (s_t) can be computed using Kelvin's law (Fredlund & Rahardjo 1993).

$$s_t = \frac{-R_g T}{M_w\,(1/\rho_w)} \times \ln\left(\frac{RH}{100}\right) \tag{3.2}$$

where s_t is total suction in kPa, R_g the universal gas constant (i.e. 8.31432 $J/molK$), T the absolute measured temperature in degrees K, M_w the molecular weight of water (i.e. 18.016 $kg/k.mol$), ρ_w the unit weight of water in kg/m^3 as a function of temperature and RH is the measured relative humidity in percent. This type of sensor is a polymer capacitance sensor consisting of two electrodes that are separated by a thermoset polymer film. Depending on the RH value being measured, the film absorbs or releases water. The RH is determined by measuring changing capacitance of the polymer film. With this technology, a rapid response of the sensor in measuring relative humidity is obtained. Albrecht et al. (2003) used a polymer capacitance sensor for measuring the relative humidity of a number of soils ranging from sand to clay. They used chilled mirror hygrometry to calibrate and assess the performance of a polymer capacitance sensor (as follows).

Chilled mirror hygrometry:

Chilled mirror hygrometer technique was developed for measuring the humidity of food products and pharmaceuticals. Later, it was used in soil science and geotechnical engi-

neering applications to measure the water potential or total suction of soils (Gee et al. 1992, Brye 2003, Leong et al. 2003, Albrecht et al. 2003, and Agus 2005).

The chilled mirror hygrometry technique measures the dew point and temperature of the sealed chamber in which the soil sample is placed. The relative humidity or water activity of the specimen is calculated from the measured due point and temperature. The temperature of the space is precisely controlled by a thermoelectric cooling system. A mirror and photo detector detects the appearance of first condensing water. Circulating of the air over the sample can fasten the process. In this order a fan is installed inside the chamber. The measured relative humidity can be converted to suction using Kelvin's law (Equation 3.2).

In this research, chilled mirror hygrometry is also used to measure the suction produced by various salt solutions in the vapor equilibrium technique (see Section 5.2.3).

3.3 Soil-water characteristics curve (SWCC)

The relation between amount of water in the soil and the associated suction in pore water is described by the Soil-Water Characteristic Curve (SWCC). This curve represents the ability of soil to retain water at different suctions. The amount of water can be expressed by any of the parameters showing the wetness of soil (i.e. degree of saturation, volumetric water content, or gravimetric water content). SWCC is one of the most useful characteristics in unsaturated soil mechanics and related to many geotechnical and hydro-mechanical properties of a soil such as hydraulic conductivity, effective stress, and volume change (Fredlund & Rahardjo 1993).

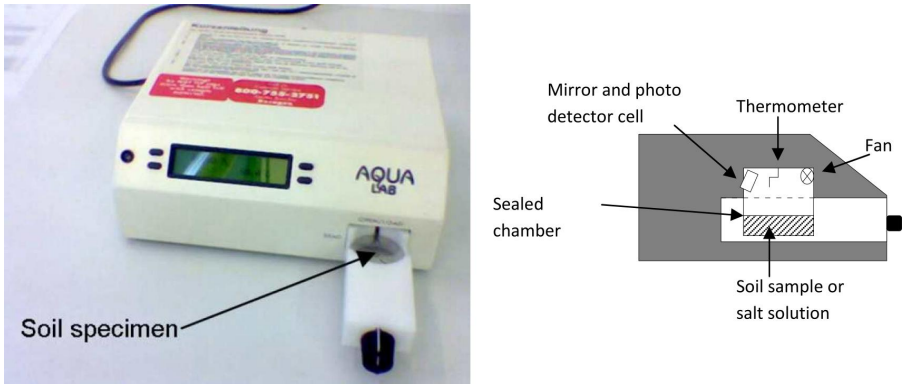

Figure 3.2: Chilled mirror hygrometer.

A typical SWCC of a non-expansive soil is drawn in Figure 3.3 which is presented as a relationship between degree of saturation and suction (Leong & Rahardjo 1997). SWCC shows different paths for imbibition and drainage conditions. If a sample of saturated soil undergoes suctions, increasing a little at a time, starting from a very low suction, it loses its water content and follows the drainage path which is also called desorption or the drying path. The increase in suction starting from the saturated condition can be performed under zero net applied stress (unconfined) or under any specific net stress (isotropic or one-dimensional compression). The reverse (i.e. wetting path) is the process where the water content of soil increases with a decrease in suction. If an oven-dried sample experiences suctions decreasing stepwise starting from very high suction, the soil starts absorbing water.

Usually the drying path ends in the oven-dried condition (105 $°C$). The suction corresponding to the oven-dried condition is about 1000 MPa as found by Croney & Coleman (1961). Fredlund & Rahardjo (1993) also found from the gravimetric water content versus suction relationship for various sand and clay soils that at zero water content the suction approaches a value of approximately 980 MPa. This value is also supported by thermodynamic considerations (Richards 1966).

The SWCC is influenced by type, texture, and mineralogy of soil. The soil behavior can be indicated by the consistency or Atterberg limits (Sridharan & Nagaraj 1999). Atterberg limits indicate variation of the soil properties with water content.

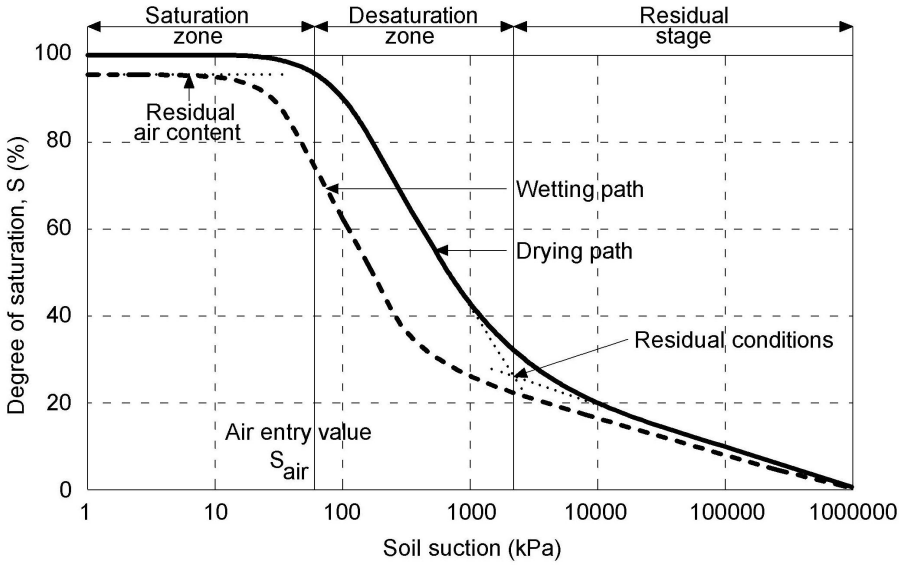

Figure 3.3: A typical SWCC (Leong & Rahardjo 1997).

Specimens compacted at different water contents result in different fabric of the soil (Lambe & Whitman 1979, Gens et al. 1995, and Delage & Graham 1996). Vanapalli et al. (1999) stated that there is a significant difference in the SWCC of clay untill compacted at different water content (i.e. at wet of optimum, optimum, and dry of optimum) using the same compaction energy. They stated that the SWCC appears to be approximately the same over suction ranging from 20000-1000000 kPa for specimens tested with different initial water content. Fleureau et al. (2002) found that the drying path of specimen from slurry represent the highest capability to retain water or can be used as the main drying curve of a soil. They also reported that the wetting path of specimen compacted at optimum water content was almost the same as the wetting path of specimen from slurry.

Al-Mukhtar et al. (1999) investigated the effect of axial compaction stress on the drying curve of compacted smectite. It was found that the drying curve, in terms of water content for relative humidity (RH) in the range of 100% to 98%, for a specimen with a lower axial stress, was placed over that of specimen with a higher axial stress. For RH less than 98% (or total suction higher than 2700 kPa), the drying curves of specimens were similar. They stated that for RH from 0 to 98%, suction is controlled by micro-pores; their size and distribution are not influenced by the compaction process, while suction is controlled by macro-pores at RH 98% or greater.

The SWCC normally has a sigmoidal shape if drawn in a semi logarithmic coordinate. In a logarithmic scale at or around a certain point the inclination of drying curve increases. The suction corresponding to this point is called the air entry value (ψ_{AEV}). By increasing the suction this slope remains almost constant until another point at which reduces again. This position is called the residual condition. The zone before AEV is called the saturation zone, although the soil is perhaps not fully saturated. The zone between AEV and the residual condition, and after the residual condition are called the desaturation zone and residual stage respectively (see Figure 3.3).

3.3.1 Hysteretic behavior

In general, soil can retain more water in drying conditions than in wetting conditions (see Figure 3.3). This means that under a given suction, the sample started from a fully saturated condition contains more water compared to the sample started from an oven-dried condition. There are an infinite number of scanning curves inside the hysteresis loop. The hysteresis of SWCC can occur for several reasons (Klausner 1991). The fundamental

reasons for this phenomenon are not clearly understood. The hysteretic behavior of SWCC could be attributed to these mechanisms:

1. The ink bottle effect, or the effect of non-homogeneous pore size distribution.

2. In a pore channel of any given size, the larger radius of an advancing interface implies a smaller value of suction than would occur at the same spot if the interface was retreating (which would involve the interface being correspondingly more tightly curved). This phenomenon is described by the difference in contact angle of water drop in advancing and receding interfaces (Childs 1969 and Lu & Likos 2004).

3. Entrapped airs might remain within the soil particles in the wetting path.

4. Condensation or absorption of a water film on the surface of fine-grained particles.

5. Swelling or shrinkage during wetting and drying can alter the soil structure differently.

All the above mentioned mechanisms do not contribute in all conditions. In coarse grained materials, surface adsorption is probably negligible, and hysteresis is mostly due to the ink bottle and contact angle effects. The ink bottle effect is a relatively macroscopic effect acting among the interparticle arrangements and particle groups, and applies for higher degrees of saturation. But the contact angle effect is to some extent a microscopic effect acting in the interparticle scale of the individual particles and particle contacts. Therefore, it applies to lower degrees of saturation when the water is in the form of separate menisci between the particles. On the other hand, due to surface attraction of particles and volume change during drainage and wetting phases, “absorption” and “swelling or shrinkage” mechanisms applies mostly to clayey soils.

Slope ratio is defined as the ratio of the slope of drying curve to the slope of wetting curve, both at boundary states. According to Pham et al. (2005) there are particular ranges of values for the slope ratio and the distance between the two boundary curves for the collected soil datasets. Values for the slope ratio between the two boundary curves on the semi logarithmic soil suction scale vary from 2.5 for sandy soils to 1 - 1.5 for fine-grained soils. The distance between the two boundary curves (wetting and drying) on the logarithmic scaled suction for sand and clay can be from 0.2 to 0.5 (log-cycles).

3.4 Effective stress in unsaturated soils

According to the principles of soil mechanics by Terzaghi (1943), in order to analyze behavior a two-phase soil mass (either water- or gas-saturated) and one stress state variable is enough. The stress state variable σ' (effective stress) is defined as $\sigma' = \sigma - u_w$, where σ is the total stress and u_w is the pore-water pressure. Effective stress is the portion carried by soil particles' skeletons and pore water pressure is the stress carried by trapped water between the solid particles. Currently, there are two approaches to describe the unsaturated soil behavior; namely the effective stress approach (Bishop 1959), and the two independent state variables approach (Fredlund & Morgenstern 1977).

3.4.1 Effective stress approach

Bishop (1959) modified Terzaghi's theory to extend the effective stress idea for unsaturated soils by taking into account the two-phase nature of the pore fluid in the unsaturated soil. Bishop proposed Equation 3.3:

$$\sigma' = (\sigma - u_a) - \chi.\,(u_w - u_a) \tag{3.3}$$

where σ' is effective stress, σ is total stress, u_a is pore air pressure, u_w is pore water pressure, and χ is Bishop's effective stress parameter, which is 1 for saturated soils and 0 for dry soils. Therefore, effective stress is always larger in an unsaturated soil compared to the same soil at a fully saturated condition.

3.4.2 Two independent stress variables approach

Fredlund & Morgenstern (1977) explained and described the stress state variables governing the behavior of unsaturated soil. They reported that the stress state variables have to be created from the individual force components acting on the solid, water, and air phases, as well as the air-water contractile skin. They proposed that the variables are: the net stress $(\sigma - u_a)$ and the matric suction $(u_a - u_w)$. In the same study they validated the concept of stress state variables by carrying out a series of null tests. In these experiments it was found that as long as the state variables remain constant, changing the air, water, or the total pressure, causes no changes in the state of the soil. Using a new laboratory apparatus, Tarantino et al. (2000) investigated these variables. Their outcomes confirmed the usage of matric suction and the net stress as stress state variables.

3.5 Shear strength of unsaturated soil

There are two fundamental approaches dominating the determination of shear strength of unsaturated soils; namely the effective stress approach and the independent state variables approach. Both originated from the Coulomb strength equation:

$$\tau = c' + \sigma' \cdot \tan(\phi') \tag{3.4}$$

where τ is the shear strength of unsaturated soil, c' is the effective cohesion, and ϕ' is effective friction angle.

3.5.1 Effective stress approach

Following Bishop's effective stress equation, the shear strength of unsaturated soils can be calculated via a failure envelope (such as Coulomb strength equation) by substituting Equation 3.3 into the strength equation of the envelope Equation 3.4:

$$\tau = c' + (\sigma_n - u_a)\tan(\phi') + (u_a - u_w)\chi \tan(\phi') \tag{3.5}$$

where $(\sigma_n - u_a)$ is net normal stress.

3.5.2 Independent state variables approach

The inability to use the conventional effective stress principle for accurate representation of unsaturated soil behavior led Fredlund & Morgenstern (1977) to describe the stresses in a new framework with two independent stress state variables: the net normal stress, $(\sigma_n - u_a)$, and matric suction, $(u_a - u_w)$. They expressed the shear strength in a modified form of the Coulomb strength equation as:

$$\tau = c' + (\sigma_n - u_a)\tan(\phi') + (u_a - u_w)\tan\left(\phi^b\right) \tag{3.6}$$

ϕ^b is angle of shearing resistance with respect to matric suction and can be measured for a specific soil through a series of shear strength tests with suction measurements. It is

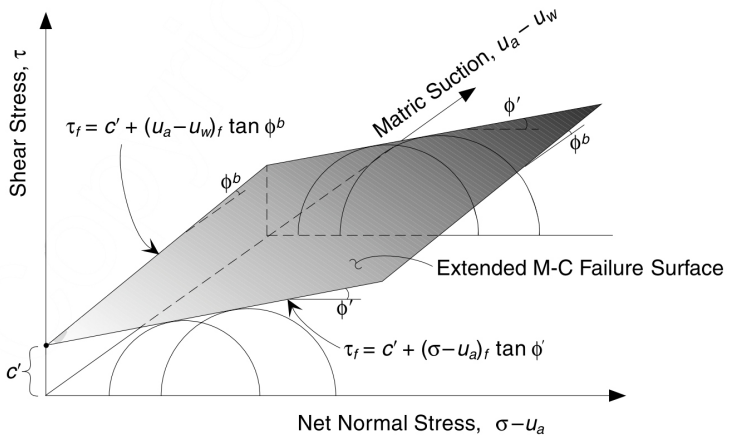

Figure 3.4: Extended Mohr-Coulomb failure surface for unsaturated soil (Lu & Likos 2004).

usually defined not as a constant strength parameter, but as a function of the matric suction. In Figure 3.4, Lu & Likos (2004) schematically drew the extended Mohr-Coulomb failure envelope as a 3D surface.

Figure 3.5 shows a conceptualized soil-water characteristic curve along a drainage path and the corresponding shear strength envelope with respect to increasing matric suction for a typical soil. As we can see in this figure in relatively low matric suctions (before the air entry value), where the pores are more or less saturated, the shear strength envelope is linear and ϕ^b is almost equal to ϕ'. Beyond the air entry value suction, where desaturation starts, a nonlinear behavior for ϕ^b is observed.

3.5.3 Laboratory measurement of shear parameter for unsaturated soil

The most important factor in testing shear strength of unsaturated soil is to reach pre-designed suction before the test and keep it constant during the shearing. The method of applying suction can vary regarding the range of suction. For lower suctions (< 10 kPa) hanging column is enough, while for higher suction the Axis Translation Technique (ATT), proposed by Hilf (1965), must be implemented. The sample can reach this suction using the Axis Translation Technique (ATT), in which especial ceramic discs are used. When this disc is fully saturated it enables water to pass through but prevents air. This air pressure at which the air can pass through the ceramic disc is called the air entry value (AEV) of the ceramic disc. Ceramic discs are commercially available with different

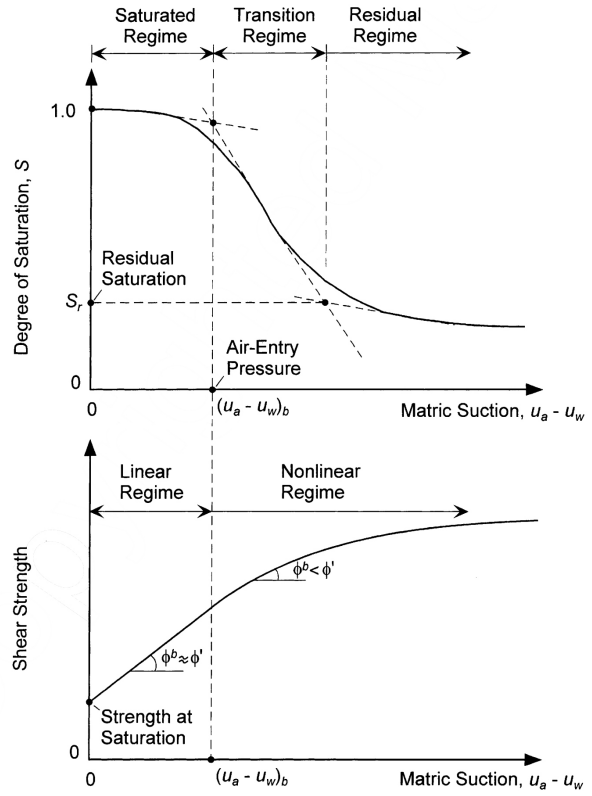

Figure 3.5: Conceptual relationship between soil-water characteristic curve and unsaturated shear strength envelope (Vanapalli et al. 1996).

diameters, thicknesses, and AEVs for various purposes. The AEV of ceramic limits the maximum suction that can be applied via this method. For higher suction other methods such as the Vapor Equilibrium Technique (VET) can be used, in a way that a vapor circulates over a salt solution with a given concentration and gets a specific relative humidity. This vapor is pumped over the specimen and when the moisture of the sample and humidity of the vapor reach to an equilibrium condition, the sample's suction is constant and, using Kelvin's law (Equation 3.2), can be calculated from the relative humidity of the vapor.

The most widely used method for measuring shear strength is the triaxial test, and compressibility characteristics have usually been studied using oedometers and similar one-dimensional testing devices. Anderson et al. (1997) performed one-dimensional compression and triaxial tests on granular soils with suction control and measurement by ATT. Fleureau et al. (1998) did a similar study on a low-plasticity material. Wong et al. (2001) managed to incorporate three miniature tensiometers into an ATT-equipped triaxial setup.

Summary:

As explained in this section, hydro-mechanical behavior of a saturated soil differs considerably from that in an unsaturated condition. The influencing parameter on behavior of unsaturated soils is the suction which can be measured or applied in a soil. Changes in effective stress and consequently shear strength parameters are one of the critical effects of the suction on soil properties. The methods - introduced in the literature to calculate the effective stress and shear strength of unsaturated soils - have been summarized here.

3.6 Plane strain state

The strength and volume change behavior of material from the geotechnical point of view are often evaluated by conventional axisymmetric triaxial compression or extension tests, where a cylindrical soil specimen under different loading conditions is tested to simulate field conditions. However, most of the field problems, such as strip footings, embankments and slopes, are three-dimensional or close to a plane strain condition. In the plane strain state the deformation of the soil is considered to be, approximately, zero in one direction ($\epsilon_2 = 0$) and the soil is free to deform in the two other directions ($\epsilon_1 \neq 0$ and $\epsilon_3 \neq 0$) (see Figure 3.6). In general it is assumed that: $\sigma_1 \geq \sigma_2 \geq \sigma_3$.

The stress, strain, and strength behavior under a plane strain condition may differ from those measured under a rotational symmetric condition. Vaid & Campanella (1974) stated that use of triaxial results in a field situation where plane strain conditions prevail would lead to a conservative design. However, same researchers in another study (Campanella & Vaid 1974) showed that in clayey soils for the same creep rate the conventional isotropic triaxial test would result in an unconservative estimate by a large factor of about 4 if the real situation corresponds to plane strain. Cornforth (1961) stated that the conventional triaxial test may still be the most widely used test in the commercial laboratories of soil mechanics to determine the soil strength parameters, but in some fields or projects of soil mechanics a good knowledge of the plane strain state is essential and has its especial applications.

As can be seen in Figure 3.7, plane strain state predicts the behavior of historical ramparts and castles better than axisymmetric triaxial condition. With regard to the objective of this research, which is the evaluation and analyses of historical masonry buildings, shear strength of material under plane strain condition has been experimentally determined. To evaluate the soil behavior in plane strain condition, a variety of biaxial or true triax-

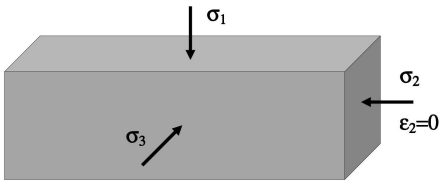

Figure 3.6: Plane strain condition.

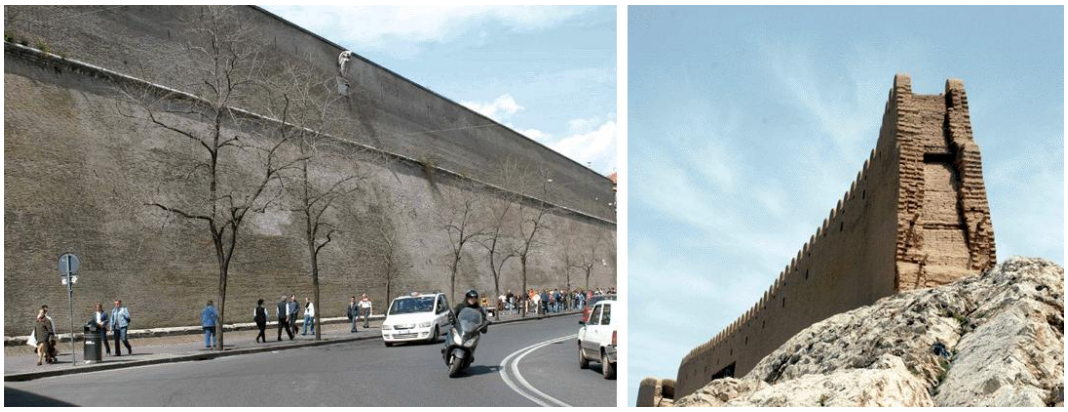

Figure 3.7: Examples of plane strain state.

ial devices were developed. In Section 3.6.2 some of the developed apparatuses will be described.

3.6.1 Plane strain concept in geotechnical engineering

The plane strain condition, as shown in Figure 3.8, is accompanied with the $\epsilon_2 = 0$ and occurs at "Lade angle" of θ=15-30°. As Nakai (2007) mentioned, for triaxial compression test and triaxial extension test, this angle is 0° and 30°, respectively. Figures 3.8 and 3.9 show the failure criteria in deviator plane and the stress path for plan-strain and triaxial tests, respectively.

Hambly (1972) stated that under the conditions of plane strain there is not a unique relationship between the three principal stresses, and it is necessary to consider them as three independent variables. Shibata & Krube (1965) and Shibata & Krube (1967) used a modified true triaxial apparatus to study the undrained plane stress (σ_3 is constant) behavior of Osaka alluvial clay with $\sigma_1 \geq \sigma_2 \geq \sigma_3$ and found that the magnitude of the intermediate stress slightly influenced the undrained stress strain curves, and ϕ' is greater in plane strain than under axially symmetric conditions.

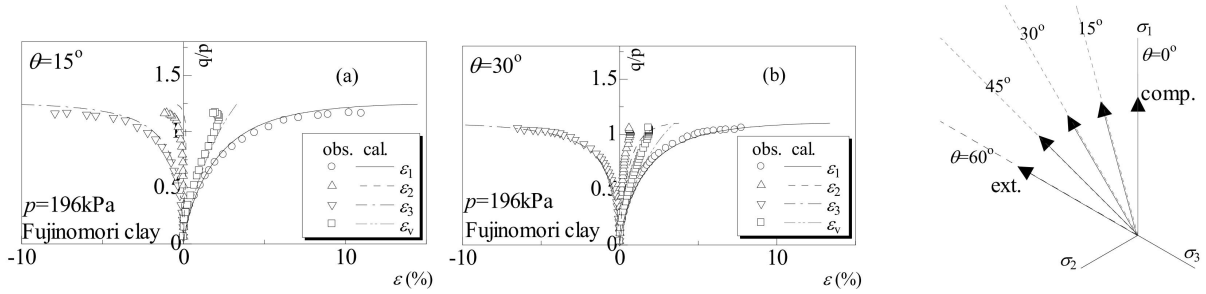

Figure 3.8: Stress path for different values of Lade angle in true triaxial tests (Nakai 2007).

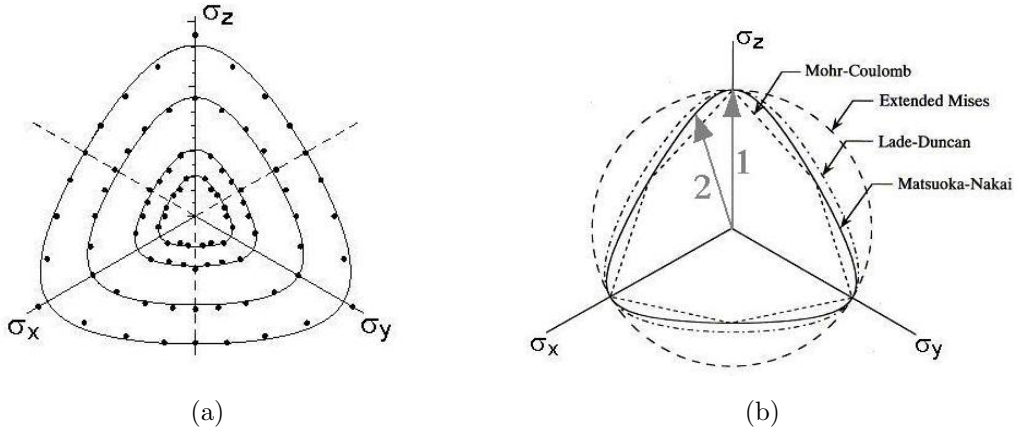

(a) (b)

Figure 3.9: (a) Experimental results of true triaxial on deviatoric plane, and (b) developed models to predict the true triaxial behavior and triaxial and biaxial test (arrows 1 and 2 in the figure).

Wu et al. (1963) stated that intermediate principal stress exercises no influence over the value of friction angle of clayey samples from glacial lake deposit under undrained conditions. Broms & Casbarian (1965) found from some tests on kaolin that, when the intermediate principal stress lay between the major and minor principal stresses, the value of ϕ' varied from 25° (extension) to 21° (compression). They also found that rotation of the principal axes of stress produced the same variation in the magnitude of 4°.

Hambly & Roscoe (1969) and later Hambly (1972) reported the ratio $\sigma'_2/(\sigma'_1 + \sigma'_3)$ can be considered constant during consolidation and shear of samples prior to failure (see Figure 3.10).

Also, Campanella & Vaid (1973), as seen in Figure 3.11, found that in a clayey soil the ratio $\sigma'_2/(\sigma'_1 + \sigma'_3)$ stayed remarkably constant during the shearing process and corresponded

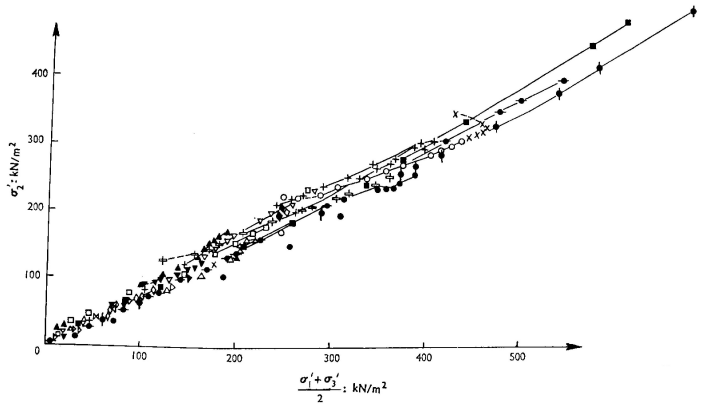

Figure 3.10: Relationship between σ_2' and $(\sigma_1' + \sigma_3')/2$ for all plane strain tests (Hambly 1972).

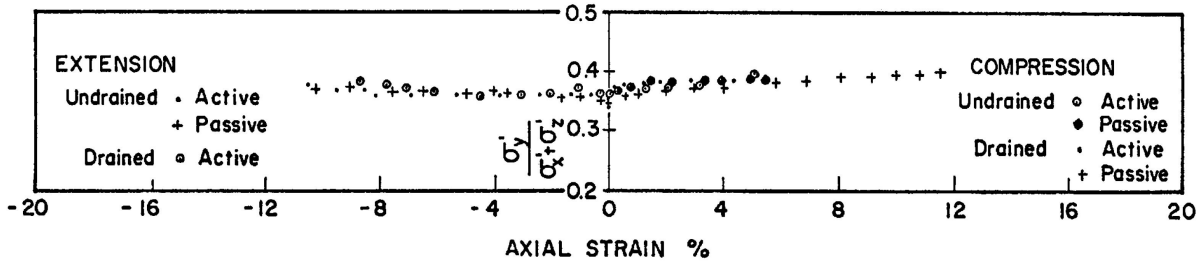

Figure 3.11: Variation of stress ratio $\sigma_2'/(\sigma_1' + \sigma_3')$ with axial strain in plane strain shear (Campanella & Vaid 1973).

to a value of between 0.36 to 0.39. Thus, a good approximation σ_2' might be considered to be a constant fraction of $(\sigma_1' + \sigma_3')$ during plane strain shear.

Green (1971) developed a true triaxial apparatus and performed compression and extension tests on sandy soils. The sample dimension was: $81 \times 53 \times 76mm$. He defined b factor as:

$$b = \frac{\sigma_2' - \sigma_3'}{\sigma_1' - \sigma_3'} \tag{3.7}$$

b is 0 for triaxial compression, 1 for triaxial extension conditions, and for all other values of σ_2', $0 < b < 1$. Starting from triaxial compression ($b = 0$) the maximum value of σ_1' as well as friction angle (ϕ') increases up to plane strain condition (in this case $b = 0.28$) and thereafter both remain relatively constant at $b = 1$. By increasing the void ratio of

the same material, the parameter b, at which the plane strain condition happens, also increases. Green (1971)'s outcomes showed identical results for triaxial tests ($\sigma'_2 = \sigma'_3$) in conventional cylindrical and in cuboidal specimens.

3.6.2 Developed laboratory devices used for plane strain state

In order to improve the testing conditions and increase the accuracy of the measured shear strength parameters, several plane strain or biaxial devices have been developed in the past (e.g., Cornforth 1964, Green 1971, Tatsuoka et al. 1986, Drescher et al. 1990, Alshibli et al. 2003, Wanatowski & Chu 2007). However, many of the biaxial apparatuses used in the previous studies had shortcomings. For examples, the biaxial apparatuses used by Lee (1970), Drescher et al. (1990), Desrues & Viggiani (2004), and Alshibli et al. (2004) could not measure σ_2, whereas the apparatus used by Topolnicki et al. (1990) was completely sealed so the development of shear bands could not be observed. These devices were used mainly in the investigation of the shear strength, deformation characteristics, and shear banding of saturated or dry soils under plane strain conditions.

The biaxial shearing tests required more sophisticated equipment than triaxial tests (Wanatowski & Chu 2006 and Alabdullah 2010). These difficulties are mainly due to the need for special mold, membrane, accessories, and the preparation of a prismatic soil specimen. Moreover, performing plane strain "extension" shear tests changes the boundary conditions and it is very difficult to keep all the boundaries in the situation necessary for extension shear tests in plane strain conditions.

3.6.2.1 Devices for saturated and dry conditions

An early plane strain device was designed and developed at the Imperial College, London. Wood (1958) has presented the details of this apparatus. Figure 3.12 shows a photograph of the device and the specimen after failure. Using the null technique in this plane strain apparatus, the intermediate stress (σ_2) was measured, similar to that used in measuring the pore water pressure of soil specimen. Silicon grease was used in between the membrane and the metal side walls. This lubrication reduced the coefficient of friction to the value of 0.02.

Hambly (1972) performed plain strain tests on saturated, remolded, and normally consolidated kaolin. The biaxial apparatus they used had been introduced earlier by Hambly & Roscoe (1969) and Hambly (1969). This apparatus could accommodate samples in the

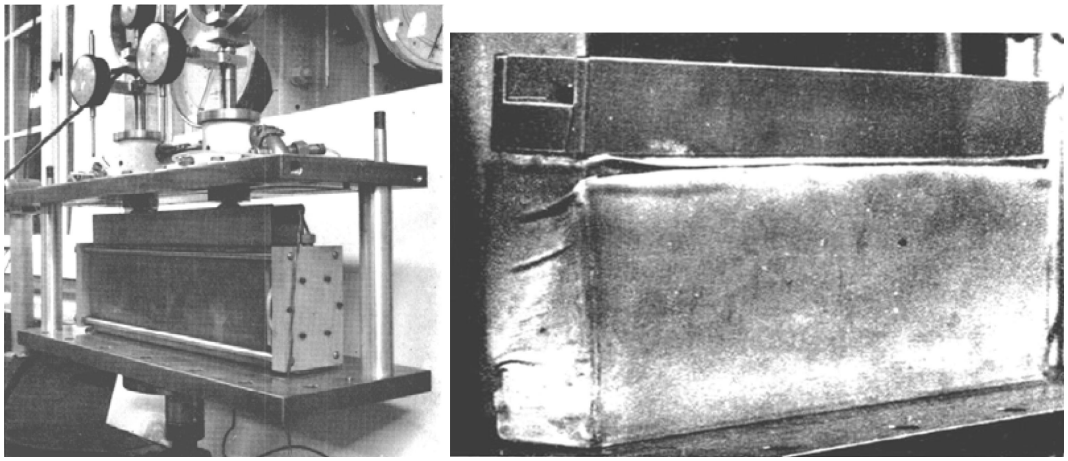

Figure 3.12: Imperial college plane strain device, loading system and specimen after failure (Wood 1958).

form of rectangular prisms of up to $135 \times 135 \times 50\,mm$ between four movable rigid platens and two fixed rigid glass plates held above and below.

Another biaxial apparatus was developed by Campanella & Vaid (1973) for saturated drained and undrained samples with dimensions $100 \times 25 \times 57.5\,mm$ which was fixed in the direction of its length between two rigid end plates which provided the plane strain condition. This apparatus was equipped to measure intermediate principal stress (σ_2) as well. Vertical load was transmitted to the sample by means of a rigid loading cap (for σ_1), whereas a pair of flexible and water filled rubber diaphragms which were sealed to stiffened support plates were employed to furnish the lateral principal stress (σ_3). This apparatus was also designed to measure all boundary stresses, even side friction.

Anisotropic shear strength in a plane strain device was investigated by Oda et al. (1978). The anisotropic parallel alignment of particles effects the shear strength of sand and the changes in the shear strength is more clearly observed in the plane strain test ($\epsilon_2 = 0$) than in axisymmetric triaxial stress conditions. In this plane strain device the four rigid platens were polished and lubricated using two greased rubber membranes to ensure frictionless sliding surfaces. The specimen had dimensions of 60 mm high, 80 mm long, and 44 mm wide. The intermediate principle stress was controlled by null techniques similar to those used in measuring pore water pressure.

Vardoulakis & Goldscheider (1981) outlined a theoretical and experimental analysis of the spontaneous shear band formation in the biaxial tests. The design of the biaxial apparatus was based on some experiences with a similar apparatus in the University of

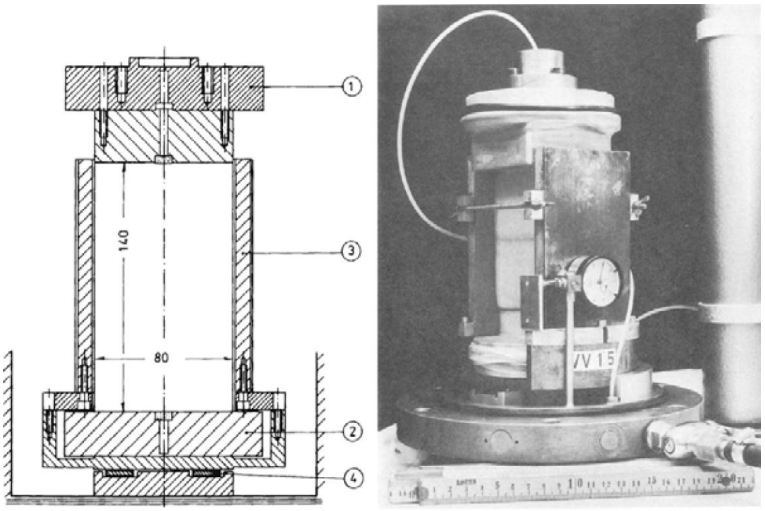

Figure 3.13: Schematic setup and specimen conditions of the biaxial apparatus (Vardoulakis & Goldscheider 1981 and Vardoulakis 1978).

Karlsruhe, Germany. Figure 3.13 shows the first biaxial apparatus used by Vardoulakis & Goldscheider (1981). The deformation was restricted along the long direction of the cross section of the specimen. Vardoulakis & Goldscheider (1981) and Vardoulakis & Graf (1985) modified the original biaxial apparatus by using a submersible load cell. In addition, lateral displacements were measured in two opposite points of the specimen's faces.

Drescher et al. (1990) improved the biaxial apparatus developed by Vardoulakis & Goldscheider (1981) by equipping it with a linear bearing platform which allowed the free lateral displacement of the lower part of the specimen, for investigation of shear band formation and growth for dry and saturated clay and sand specimens. The sample is a prismatic specimen with dimensions of $140 \times 40 \times 80\,mm$. The 80 mm dimension is corresponds to the intermediate stress (σ_2).

Alshibli & Sture (2000) developed a new biaxial apparatus. The tests were carried out to observe the effects of confining pressure, density, and grain size on the constitutive and instability behavior of coarse grained materials. The deformation of the sample was recorded using a camera. In this biaxial apparatus the end platen was fixed against rotation and lateral deformations.

Later, Alshibli et al. (2004) modified and improved the plane strain device developed earlier. The design of this apparatus took into consideration the geometry configuration for optical measurements and instrumentation, tracking of the development of shear band,

and the flexibility in altering boundary conditions. This device was provided with a lateral displacement track assembly to enable free development and propagation of the shear band.

Alshibli & Akbas (2007) worked on the apparatus of Alshibli et al. (2004). An instrumented control panel was used to apply the desired cell/pore water pressures and vacuum using the principle of pressurized air-water interface. Cell pressure and pore pressure were also monitored and recorded using very sensitive pressure transducers having an accuracy of about 0.08 *psi*. Three submergible Linear Variation Displacement Transducers (LDVT) were used to record specimen's lateral displacement at the bottom end platen. These three LDVTs passed through the wall of the water jacket where grommets were used to seal around the LVDTs' body (see Figure 3.14).

In Wanatowski & Chu (2007)'s study two rigid vertical platens were fixed in position by two pairs of horizontal tie rods to impose a plane strain condition. The lateral stress in this direction (σ_2) was measured by four submersible total pressure transducers. As shown in Figure 3.15, two transducers were used for each platen, so that the lateral pressures at the top and the bottom of the specimen could be measured and any non-uniform stress distribution could be detected. The total lateral pressure was evaluated as the average of the values obtained from the four individual transducers.

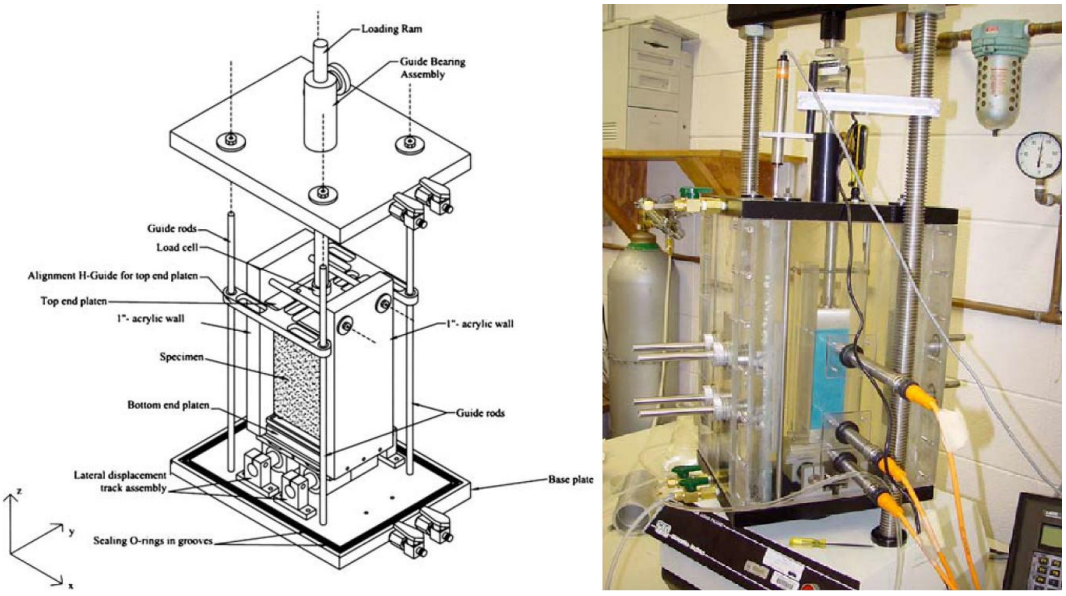

Figure 3.14: Schematic setup and photograph of apparatus used by Alshibli & Akbas (2007).

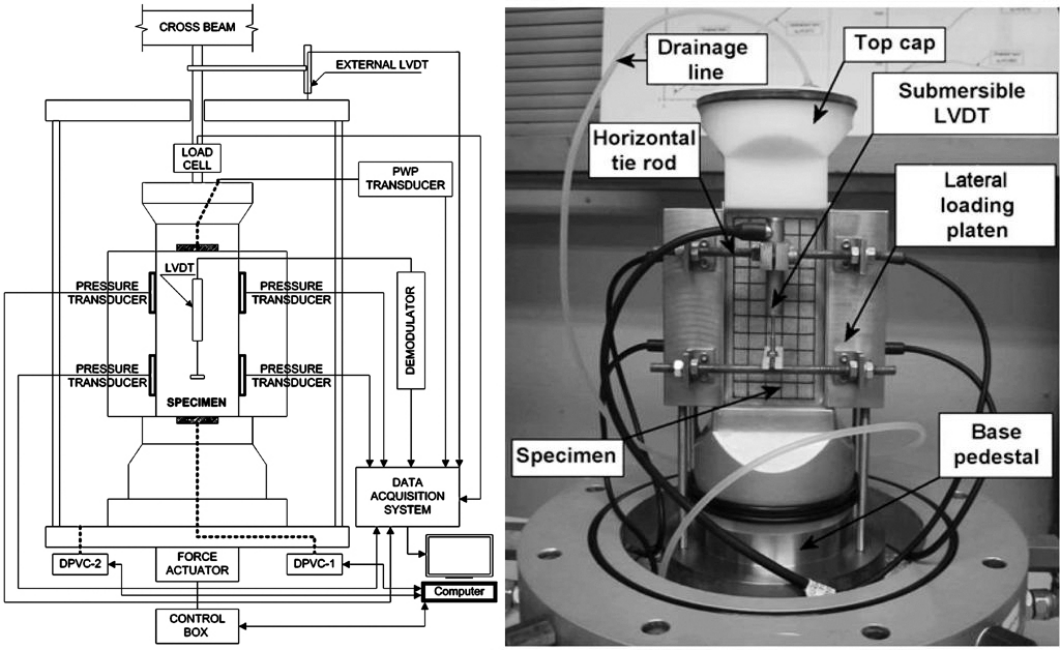

Figure 3.15: Setup of device developed by Wanatowski & Chu (2007).

Röchter et al. (2010) and Röchter (2011) developed a biaxial device (Figure 3.16) which consisted of an opposing pair of rigid walls to ensure plane strain conditions and an opposing pair of flexible walls to permit free shear band formation in simple shear mode. The flexible walls were constructed as water cushions, in which the water pressure was controlled via software and a pressure control valve up to 300 kPa. The horizontal stress was measured by pressure transducers in two positions in one rigid wall. The horizontal deformation was measured locally by six contact free displacement sensors, which ware integrated into the water cushions. The vertical pressure was determined redundantly by a load cell measuring the vertical force outside the biaxial cell and by pressure transducers in the top and bottom end plates.

Kumruzzaman & Yin (2012) made plane strain tests in a true triaxial testing system with four rigid loading plates used for plane strain testing. This device had been presented earlier by Yin et al. (2007). The sample dimension was $7 \times 7 \times 14\,cm$. It should be pointed out that the original loading plates could not slide and a small gap between two plates should be left before testing. This original design had problems of non-uniform stress/strain in the specimen and interferences of the plates at large strains. The device included four hydraulic load rams equipped with LVDT, which were placed outside the chamber along each piston for measuring displacement of the piston (see Figure 3.17).

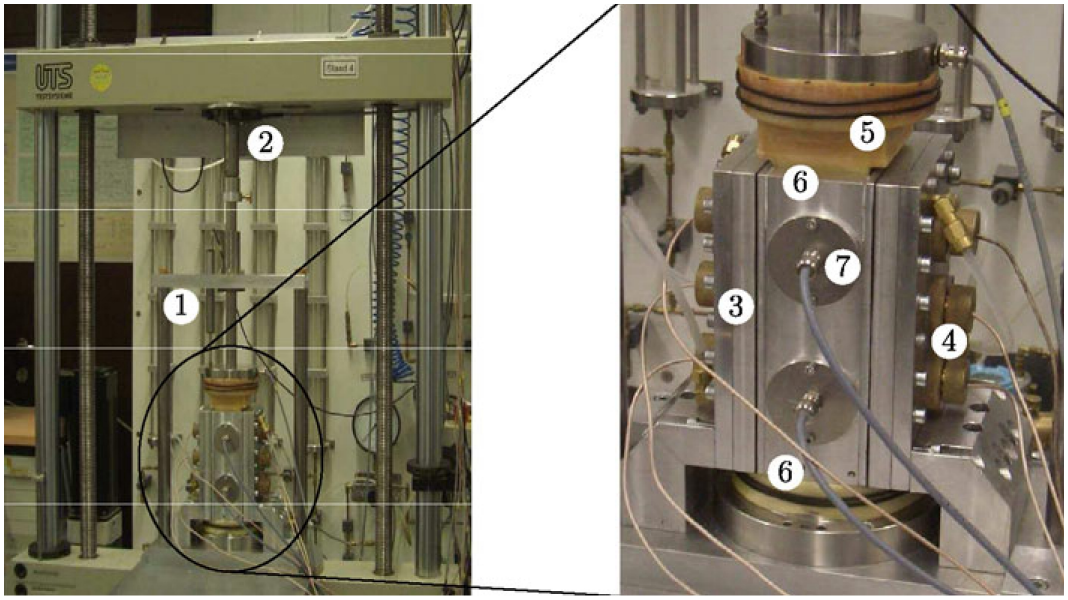

Figure 3.16: Setup of device developed by Röchter (2011).

3.6.2.2 Devices for unsaturated conditions

Fauziah & Nikraz (2007*a*) and Fauziah & Nikraz (2007*b*) studied the behavior of unsaturated overconsolidated clay under plane strain conditions. They worked with a newly developed biaxial device. Same researchers, Fauziah & Nikraz (2008), reported tests under plane strain conditions of unsaturated compacted clay. This biaxial apparatus was instrumented with high air-entry value discs at the interface between the unsaturated clayey specimen and the pore-water pressure measuring system. The height of the specimen was 72 mm and the cross section was 72×36 mm. The specimen was confined laterally by two rigid perspex walls with a 36.7 mm distance. In this apparatus the axial load was measured by a submersible load cell. The axial displacements of the specimen were measured by an external LVDT. Laser sensors were used to monitor the volume change of the specimen. In Figure 3.18 a photograph of the specimen and its schematic setup of the biaxial apparatus are shown. This device was not able to measure intermediate principal stress.

Cruz et al. (2011) designed a plane strain apparatus based on the biaxial device of Vardoulakis & Goldscheider (1981) (geotechnical laboratories of the University of the Andes, Bogota, Colombia). They modified the device for suction-controlled tests at the University of Texas at Arlington. Plane strain condition was imposed on the soil sample by means of two 8-mm thick rigid walls, each 106 × 55 mm. Intermediate principal stress σ_2

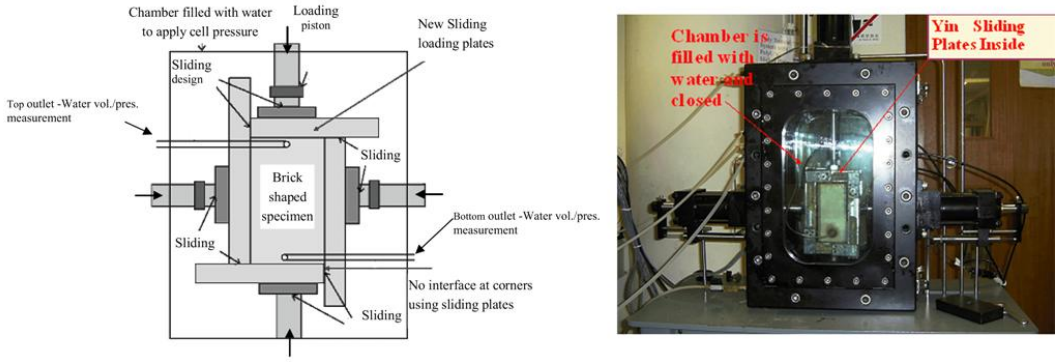

Figure 3.17: Schematic setup and photograph of apparatus used by Kumruzzaman & Yin (2012).

was measured using Sensotec model pressure cells, with one installed at each of the rigid lateral walls.

The suction was applied via the axis-translation technique. Pore-air pressure u_a was controlled and supplied to the soil pores through the loading platen via a coarse porous stone. The bottom pedestal supports the specimen and also had a high-air-entry ceramic for control and measurement of pore-water pressure (u_w).

Samples were made from uniaxially consolidated slurries, which were later trimmed to the required size of the biaxial device ($90 \times 60 \times 30\,mm$). A sliding bottom with very low friction provided an additional degree of freedom to facilitate the non-forced formation of the failure surface during shearing. The formation of a failure surface or shear band could be readily detected by sensing the start of the motion of the sliding table (bottom cap) with the LDVT.

Another biaxial device for determining shear strength parameters of soils in unsaturated conditions was developed by Alabdullah (2010) for suctions up to 100 kPa. Shear strength tests performed in the present research have been done using Alabdullah (2010)'s device which is explained in detail in Chapter 5.

3.6.3 Results of plane strain conditions

Several studies have been performed using tests under plane strain conditions. Some of the results stated in the literature are presented here. In this sections the results are categorized concerning (1) shear strength parameters, (2) failure type and shear band inclination, and (3) volumetric strain (dilation) in plane strain conditions.

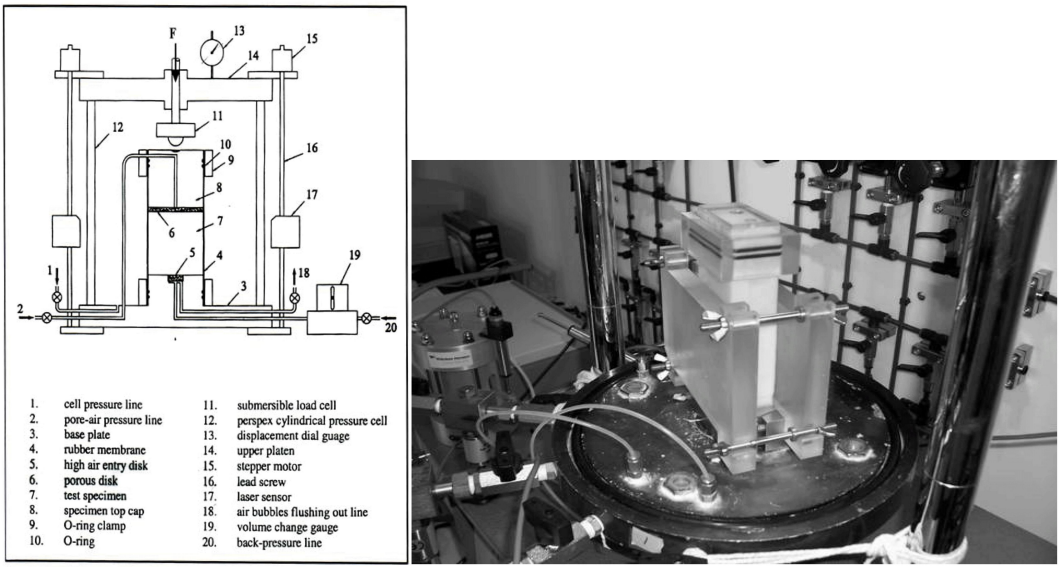

Figure 3.18: Biaxial device developed by Fauziah & Nikraz (2007*a*) and Fauziah & Nikraz (2007*b*) for unsaturated soils.

3.6.3.1 Shear strength

Comparative studies between plane strain and triaxial test results have been performed by many researchers. The studies generally revealed that the plane strain specimens pose higher strengths than triaxial specimens. Increase in soil density and confining pressure has a significant effect on the difference between strength parameters measured in triaxial and plane strain conditions. Failure strains of triaxial specimens are always larger than those of plane strain specimens, if other conditions remain constant. In drained conditions they performed only active extension and not passive extension.

Campanella & Vaid (1973) performed drained and undrained shear strength tests on normally consolidated undisturbed clay in plane strain conditions with four different stress paths; namely passive compression ($b = 0$), active compression ($b = 0$), passive extension ($b = 1$), and active extension ($b = 1$). In compression tests for both active and passive conditions the same peak effective stress was developed, but the strains required to mobilize the maximum strength and reach to failure were considerably different: 12% in passive compared to only 4% in active compression conditions.

Rectangular prismatic samples of normally consolidated remolded clayey soil were sheared under undrained plane strain conditions by Wade (1963). By comparing his results with those from the axially symmetric tests on the same batch of clay, Wade concluded that the friction angle of this clay in plane strain conditions was about 1.2° greater than that in

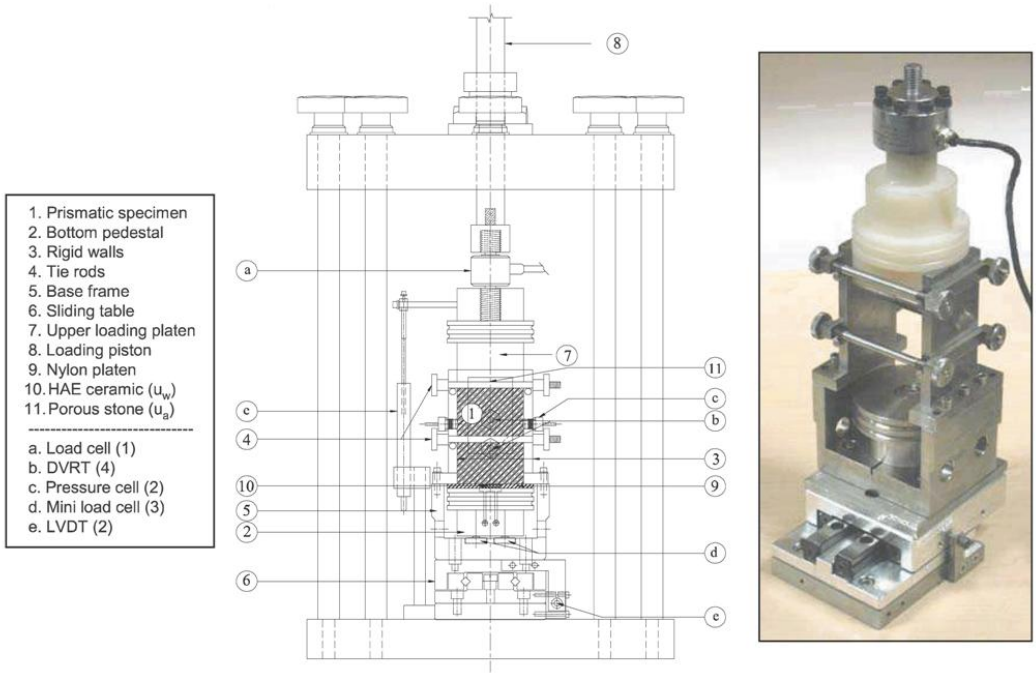

Figure 3.19: Photograph and main components of suction-controlled biaxial apparatus of Cruz et al. (2011).

axially symmetric conditions. Similarly Mochizuki et al. (1993) reported that when soil is tested under plane strain conditions, it exhibited a higher compressive strength and lower axial strain. Cornforth (1964), Lee & Shubeck (1971), Marachi et al. (1981), Alshibli et al. (2003), and Wanatowski & Chu (2007) also proved that the friction angle was higher in plane strain conditions than triaxial axisymmetric conditions, and by increasing void ratio the above-mentioned difference reduced. Figure 3.20 shows the comparison done by Marachi et al. (1981). As seen here, for loose material the results of both conditions resembled each other in large strains.

Vaid & Campanella (1974) studied the behavior of undisturbed clayey soil under triaxial and plane strain loading conditions and reported that friction angle of undisturbed clay in plane strain conditions is some 10% higher than that in triaxial. And in undrained conditions at very large strains (more than 16% axial strain) the strength was the same for both plane strain and triaxial tests. Their results showed that for undisturbed clayey samples the strain corresponding to peak deviator stress was essentially the same in plane strain as in the corresponding triaxial tests. But the results of Henkel & Wade (1960) on a remolded clay showed that failure strain in triaxial compression was several times larger than that under plain strain. The similarity of the strains corresponding to failure in

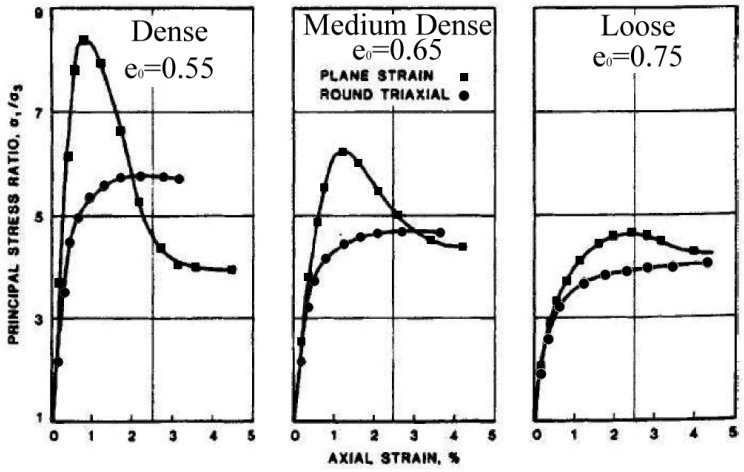

Figure 3.20: Stress-strain curves for plane strain and triaxial conditions (Marachi et al. 1981).

unsaturated conditions was probably due to the brittleness of samples in this condition. Samples fail with first cracks. However, in saturated conditions failures are ductile and have enough time to follow the boundary conditions (rotational symetric or plane strain).

However, Hambly & Roscoe (1969) found the friction angle was identical in plane strain and in axially symmetric tests. Green (1971) showed that for loose samples (compared to dense samples) the results in plane strain conditions were closer to that of triaxial compression, and the higher the density, the more obvious the difference observed. Schanz & Vermeer (1996) have also demonstrated this fact. Rowe (1971) expressed a similar tendency for ϕ_f, which is a constant volume friction angle in the post peak zone.

Higher peak stress values followed by severe softening have been reported in the literature for sand specimens tested under plane strain compared to cylindrical triaxial conditions, and by an increase in specimen's density and confining pressure, the difference between peak stresses of two loading conditions increased (Lee 1970, Marachi et al. 1981, and Peters et al. 1988). For clay also Vaid & Campanella (1974) found in plane strain condition, shearing was associated with loss in post peak shear resistance which was not observed in the corresponding triaxial condition.

Lee (1970) performed plane strain and triaxial compression shear experiments on fully saturated sands with different densities and showed that plane strain specimens reached higher values of maximum principal stress ratio than triaxial specimens, and the difference decreased as void ratio increased. Moreover, plane strain specimens failed at smaller axial strain with a severe softening compared to triaxial specimens. He concluded that

the difference between plane strain and triaxial results was greatest for dense specimens tested under low confining pressure and that the difference decreased as confining pressure increased. Later, Alshibli et al. (2003) proved that the failure of specimens subjected to plane strain loading conditions was characterized by distinct shear bands accompanied by softening in the stress response depending on the specimen density and confining pressure.

Alshibli & Akbas (2007) also compared the behavior of K_0 consolidated kaolin specimens under those two conditions and the experimental results led to the same conclusion reached by Vaid & Campanella (1974).

Kumruzzaman & Yin (2012) found that the peak friction angle for plane strain tests was higher than that from axisymmetric loading conditions. In both drained and undrained tests the deviatoric stress in plane strain conditions was always higher than that in triaxial condition, and by increasing void ratio this difference increased. However, Wanatowski & Chu (2006) showed that the stress ratio (q/p') for axisymmetric conditions was higher than that in plane strain conditions for same void ratio, even though the friction angle was greater in plane strain conditions.

Cruz et al. (2012) performed some biaxial shear tests on an unsaturated soil compromised 25% Kaolin and 75% silty sand. Peak stress values of 724.8 kPa and 309 kPa, corresponding to axial strain values of 6.16% and 6.42%, were attained under matric suctions of 100 kPa and 50 kPa, respectively. Peak strength was followed by a sharp drop in stress until an apparent residual state was achieved at maximum axial strain values of 8.32% and 8.83%, respectively. The results reflected the important role played by matric suction in the stress-strain-strength response of unsaturated soils under plane strain conditions.

Fauziah & Nikraz (2010) reported that in unsaturated clayey soils under the same matric suction and net normal stress the specimen tested under plane strain conditions exhibited a higher compressive strength compared to the specimen tested under triaxial test setup.

3.6.3.2 Failure type and shear band inclination

The failure patterns of materials under a plane strain state are different from the failure patterns that can be observed in triaxial tests. Under plane strain conditions the specimens fail along a well defined shear plane (compared to rotational symmetric conditions). But in the conventional axisymmetric triaxial compression test, either localized shear plane or bulging diffuse failure modes occur, depending on the confining pressure and the density of the soil specimen.

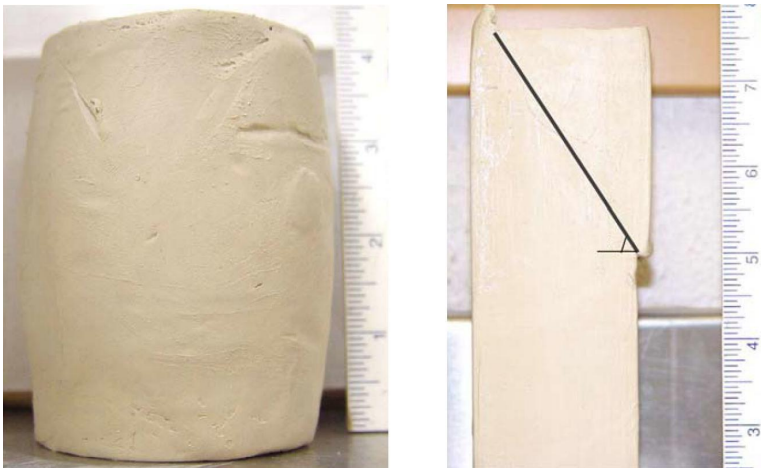

Figure 3.21: Differences in failure mode in triaxial and biaxial tests (Alshibli & Akbas 2007).

The stress conditions of a triaxial test do not allow free development of failure planes; that is why there is a fundamental difference between the failure modes of specimens tested under plane strain compared to axisymmetric triaxial loading. Lee (1970), Marachi et al. (1981), Peric & Hwang (2002), and Alshibli et al. (2003) concluded that failure of the plane strain specimens always occurred along a single well-defined shear plane, whereas in the axisymmetric triaxial tests, either localized shear plane or bulging diffuse failure modes occured depending on the density of the specimen and the confining pressure. Peters et al. (1988) performed a theoretical and experimental study on the formation of shear bands in plane strain, triaxial compression, and triaxial extension. They also found that shear bands were more readily initiated under plane strain than under triaxial conditions. Alshibli et al. (2003), Desrues & Viggiani (2004) concluded that the stress conditions for plane strain and triaxial specimens had a large effect on the strength of soil as well as the shear band formation.

As Alshibli & Akbas (2007) showed (see Figure 3.21) that the plane strain specimens failed via a well-defined shear band that began to develop during the hardening stress regime whereas triaxial specimens failed through a diffuse bulging mode.

Peric & Hwang (2002) performed undrained plane strain tests on Georgia kaolin and pointed out that the failure of the specimens happened with distinct shear bands as the specimens approach the critical state regardless of stress histories and strain rates.

Desrues et al. (1985) experimentally showed that the initiation of localizations in plane strain experiments was observed in a very early stage of the deformation process before

the peak stress value, which implies that localization initiated in the hardening part of the test. However, Vardoulakis (1978) found that localized deformations develop at the peak. Similarly, Alshibli et al. (2003) showed that the first shear band was developed at the peak stress and there was no evidence that it was developed in the hardening regime before the peak.

Shear bands are defined as the localization of deformations into thin layers of intensively shearing material. Classical solutions for shear band inclination in frictional materials subjected to plane strain are referred to as the Mohr-Coulomb (static) and Roscoe (1970) (kinematic) solutions. According to the Mohr-Coulomb criterion, the inclination angle of the shear band is given by:

$$\theta_m = \left(45^\circ + \frac{\phi'_f}{2}\right) \tag{3.8}$$

where θ_m is the angle between the shear band and the direction of the minor principal strain, and ϕ'_f is the effective angle of internal friction at failure. Equation 3.8 is a purely static statement along a plane defined by the inclination angle θ_m under the stress obliquity, (i.e. the ratio of shear stress to normal stress reaches its maximum value). Only one static constitutive parameter (ϕ'_f) is contained in Equation 3.8, and no deformation variables or parameters appear.

Roscoe (1970) observed that the inclination angle of the shear band corresponds more closely to the plane of maximum strain obliquity in terms of strain rates, as presented by:

$$\theta_m = \left(45^\circ + \frac{\psi_d^f}{2}\right) \tag{3.9}$$

where ψ_d^f is the angle of dilation at failure.

Based on experimental observations, Arthur et al. (1977) obtained the following equation:

$$\theta_A = 45^\circ + \frac{1}{4}\left(\phi'_f + \psi_d^f\right) \tag{3.10}$$

Alshibli & Akbas (2007) found that the measured shear band inclination values were slightly smaller than the Coulomb solution. The Roscoe's and Arthur's solutions underestimate the inclination angle of the shear band for specimens tested under undrained conditions.

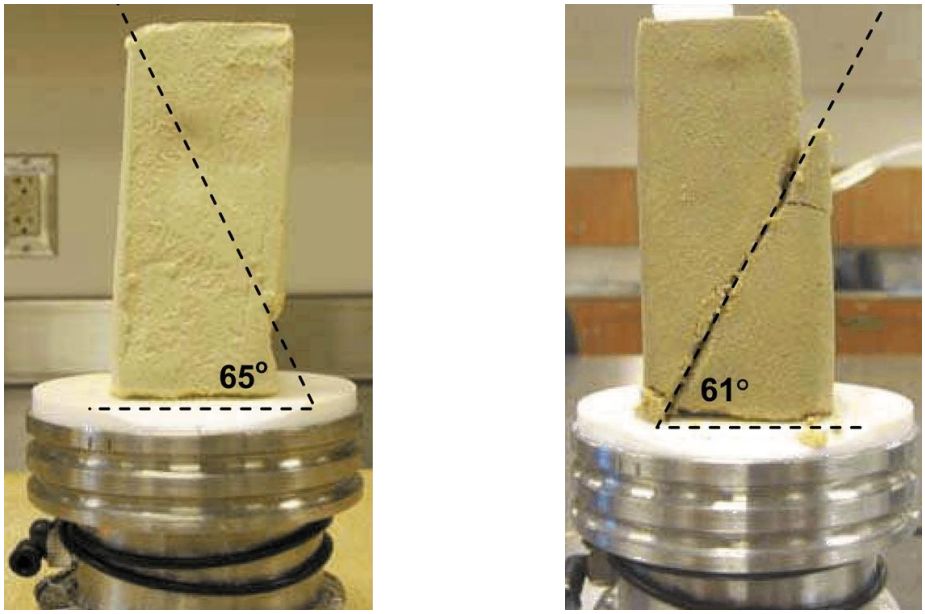

(a) (b)

Figure 3.22: Samples failed under biaxial shearing at suctions (a) 100 kPa, and (b) 50 kPa (Cruz et al. 2012).

Cruz et al. (2012) in plain strain conditions observed a fully developed failure surface for unsaturated silty sand, with failure angles of 61° and 65° for suctions of 50 and 100 kPa respectively (Figures 3.22a and 3.22b).

3.6.3.3 Volumetric strain

The hypothesis that a unique relationship exists between void ratio and effective stress during shearing of clays was first advanced by Rendulic (1937) and Henkel (1960). Roscoe et al. (1958)'s concept of a unique state boundary surface was an alternate statement of Redulic's concept of uniqueness of void ratio and effective stresses. A unique surface in $s - t - e$ space implies that in triaxial conditions void ratio is a function of mean normal effective stress (s) and shear stress (t). But in plane strain conditions octahedral shear stress is a more appropriate measure of shear stress, which means a surface in the $s - \tau_{oct} - e$ space (Campanella & Vaid 1973).

$$\tau_{oct} = \frac{1}{3}\sqrt{(\sigma_1 - \sigma_2)^2 + (\sigma_2 - \sigma_3)^2 + (\sigma_3 - \sigma_1)^2} \tag{3.11}$$

Alshibli et al. (2003) and Kumruzzaman & Yin (2012) mentioned that volumetric strain of drained triaxial experiments was much higher than that of plane strain experiments.

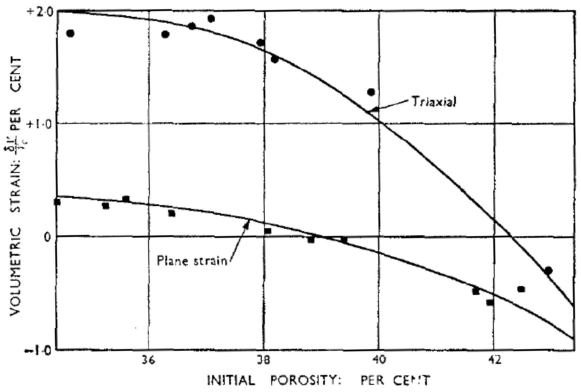

Figure 3.23: Volumetric strain for plane strain and triaxial conditions (Cornforth 1961).

It was also observed that specimens in plane strain tests are stiffer and experience smaller volume changes than those in triaxial tests (Cornforth 1961, Bishop 1966, Lee 1970, and Marachi et al. 1981). Cornforth (1961) presented a comparison of the failure characteristics of the plane strain and triaxial compression tests in which the cell pressure was kept constant. He concluded that the triaxial specimens showed a greater positive volume change (dilation) at failure. The volume change curves in the triaxial and plane strain tests tend to converge at looser densities (see Figure 3.23). In addition, the axial strain at failure in the triaxial test was found to be almost three times higher than that in plane strain tests for the same densities.

Volumetric strains (ϵ_v) at failure reported by Green (1971) are shown in Figure 3.24 versus b factor defined in Equation 3.7. In these tests the b value corresponding to plane strain conditions was 0.28. As can be seen here the volume change reaches its minimum very close to plane strain conditions.

Summary:

As discussed in this section, the shear strength of soil cannot be interpreted in all loading conditions, only with axisymmetric triaxial experiments. In some cases plane strain conditions dominate the behavior of a sample, and, as illustrated in the literature, there are clear differences between the results of plane strain and triaxial tests. So far several biaxial shear devices have been developed in order to determine the shear strength of saturated and unsaturated soils.

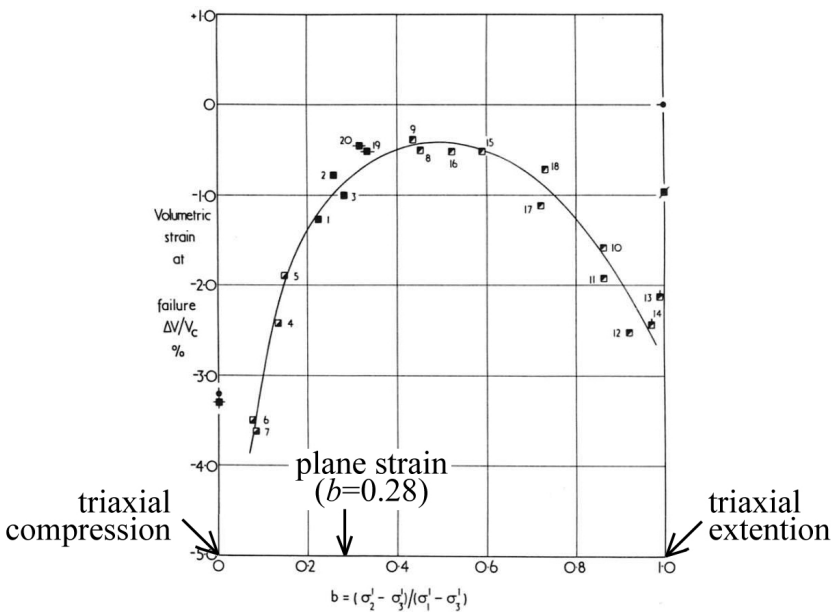

Figure 3.24: Volumetric strain vs. b factor in true triaxial tests (Green 1971).

3.7 Fiber-reinforced soil

3.7.1 General

Soil generally has low tensile and shear strength and its characteristics may depend strongly on the surrounding conditions (water content, void ratio, etc.). On the other hand, some stabilizing methods have been introduced to overcome the shortcomings of soil. Of theses, soil reinforcement has recently received the attention of researchers. Reinforcement consists of incorporating certain materials with some desired properties within other material which lack those properties. Soil reinforcement is defined as a technique to improve the engineering characteristics of soil in order to develop the parameters such as shear strength, compressibility, density, and hydraulic conductivity. Soil reinforcement can consist of stone columns, root piles or micro-piles, soil nailings, geo-textiles, and randomly distributed fibers. Fiber-reinforcement of soil is a procedure where natural or synthesized additives are used to improve the properties of soil. The standard fiber-reinforced soil is defined by Li (2005) as a soil mass that contains randomly distributed discrete elements (i.e. fibers), which provide an improvement in the mechanical behavior of the soil composite. Hejazi et al. (2012) has reviewed and summerized the recent studies on soil reinforcement using discrete natural and synthetic fibers. Most of

the published research in this field has generally shown that strength and stiffness of the soil was improved by fiber-reinforcement.

One of the advantages of randomly distributed fiber-reinforcement compared to systematically oriented geosynthetics (strips, geotextile, geogrid, etc.) is the maintenance of strength isotropy and the absence of potential failure planes, which can develop in parallel to the oriented reinforcement (Maher & Gray 1990 and Chakraborty & Dasgupta 1996).

The effectiveness of the reinforcement is influenced by fiber properties, sample preparation, volume fraction, length, aspect ratio, modulus of elasticity, orientation, and also soil characteristics including particle size, shape, and gradation, as well as stress levels and density.

3.7.1.1 History

The stabilization of soils has been employed over millennia. The concept of fiber-reinforcement was recognized more than 5000 years ago. For example, ancient civilizations used straw and hay to reinforce mud blocks in order to create reinforced building blocks (Hejazi et al. 2012). There are several examples of reinforcing soil like the Great Wall of China (earliest example of reinforced earth using branches of trees as tensile elements), the Ziggurats of the Elam civilization in western Iran and eastern Iraq (woven mats of read were used), etc. In the modern history of soil stabilization, the concept and principle of soil reinforcement was first developed by Vidal (1969). He demonstrated that the inclusion of reinforcing elements in a soil mass increases the shear resistance of the medium. At present, the soil reinforcement technique is well established and is used in various applications such as improving bearing capacity, filters, and drainage control.

3.7.2 Types of fibers

3.7.2.1 Natural fibers

Natural fibers are mostly prepared from plants. Since natural fibers consumes no fossil energy to be produced and leaves no pollution, from an environmental perspective they fits the green planet, and recently usage of such material in the industrialized world is essential and is worthy of attracting significant attention worldwide in all branches of engineering sciences.

Figure 3.25: Straw inclusion in preparation of adobes.

Natural fibers can include several materials, e.g. straw, coconut coir, sisal, palm, jute, flax, bamboo, and cane.

Straw fibers:

Barley or wheat straws are widely cultivated and harvested once or twice annually in rural areas all over the world and could be used in the production of composite soil blocks with better characteristics, but relatively few published data are available on its performance as reinforcement to soil or earth blocks. It is interesting to know that in ancient Egypt, straws or horsehairs were added to mud bricks, while straw mats were used as reinforcements in early housing construction (Mansour et al. 2007, Li 2009, and Salehan & Yaacob 2011). Barley straw is claimed to be the most cost-effective mulch practice to retain soil in artificial rainfall tests. Abtahi et al. (2010) showed that barley straw fibers are more effective on the shear strength of the soil than Kenaf fibers. The optimized fiber content was 1%. In addition to these benefits, the straw could act as a thermal insulating material for the unpleasant weather conditions to create a pleasant indoor temperature. Other studies on straw as a reinforcing element have been published by Key (1988), Bouhicha et al. (2005), Kazragis (2005), Ashour et al. (2010), Qu et al. (2013), and Estabragh et al. (2013).

Coconut coir fiber:

Due to its high lignin content, degradation of coconut coir fiber takes place much more slowly than in other natural fibers (Rowell et al. 2000). Other studies on coconut coir fiber

are Ayyar et al. (1989), Viswanadham (1989), Ravishankar & Raghavan (2004), Khedari et al. (2005), Sivakumar-Babu & Vasudevan (2008*b*), and Ramesh et al. (2010).

Sisal fibers:

This fiber is extracted from the leaves of the plants, which vary in size, between 6-10 *cm* in width and 50-250 *cm* in length. In general, Brazil, Indonesia, and east African countries are the world's main producers of sisal fibers. Ghavami et al. (1999) found that inclusion of 4% sisal imparted considerable ductility and slightly increased the compressive strength. Prabakara & Sridhar (2002) and Mattone (2005) are other research studies on fiber-reinforcement using sisal fibers.

Palm fibers:

Palm fibers in date agriculture have filament textures with special properties such as low costs, plenitude in the region, durability, being lightweight, tension capacity, and relative strength against deterioration. Swamy (1984), Marandi et al. (2008), Yusoff et al. (2010), Jamellodin et al. (2010), Ahmad et al. (2010), and Salehan & Yaacob (2011) also have worked on reinforcement with palm fibers.

Jute fibers:

Jute is grown abundantly in Bangladesh, China, India and Thailand. Jute fibers are extracted from the fibrous bark of jute plants which grow as tall as 2.5 *m* with the base stem diameter of around 25 *mm*. Swamy (1984), Aggarwal & Sharma (2010), and Islam & Iwashita (2010) have studied the properties of reinforced soils with jute.

Flax fibers:

Flax is probably the oldest textile fiber known to mankind. It has been used for the production of linen cloth since ancient times. Flax is a slender, blue flowered plant grown for its fibers and seeds in many parts of the world. Swamy (1984), Harriette (2004), Segetin et al. (2007) and Cheah & Morgan (2009) have worked on this material as a reinforcing fiber.

Bamboo fibers:

Bamboo is a regenerated cellulose fiber. It is a common fact that bamboo can thrive naturally without using any pesticide. Kozlowski (2011) reported that bamboo fibers are remarkably strong in tension but have low modulus of elasticity. Ramaswamy et al. (1983) and Coutts (1995) are some of the other studies on implementation of this fiber in reinforcement.

Cane fibers:

Cane or sugarcane belongs to the grass family and grows up to 6 m high and has a diameter up to 6 cm and bagasse is the fibrous residue which is obtained in sugarcane production after extraction of the juice from the cane stalk. Cement boards produced from sugar cane waste have been recently introduced to the market.

3.7.2.2 Synthetic fibers

Synthetic fibers are the most widely used materials in the laboratory testing of soil reinforcement. Their durability is much more than natural fibers and most of them are not decomposable and pollute the environment. But due to mass production of such fibers in industry and their high strength and predesigned behavior they are broadly used in soil reinforcement projects worldwide. Research and studies on soil reinforcement using randomly distributed fibers are mostly concentrated on synthetic rather than natural fibers.

Since synthetic fibers are beyond the scope of this research they are mentioned briefly here. Most important synthetic fibers are: Polypropylene fibers (Setty & Rao 1987, Setty & Murthy 1987, Puppala & Musenda 2000, Santoni & Webster 2001, Consoli et al. 2003, Punthutaecha et al. 2006, and Freilich et al. 2010), Polyester fibers (Consoli et al. 2002, Kumar et al. 2006, Kumar et al. 2007, Furumoto et al. 2002, Maheshwari 2011, Kaniraj & Havanagi 2001, and Jadhao & Nagarnaik 2008), Polyethylene fibers (Orman 1994, Bueno 1997, Dutta & Sarda 2007, and Sobhan & Mashnad 2002), Glass fibers (Consoli et al. 2004, Maher & Ho 1993, Maher & Ho 1994, and Al-Refeai 1991), Nylon fibers (Gosavi et al. 2004, Murray et al. 2000, Boyd 1997, and Wang 2006), Steel fibers (Boominathan et al. 1991, Murray & Farrar 1988, and Gray & Al-Refeai 1986), and Polyvinyl alcohol fibers (Park et al. 2008 and Park 2009).

3.7.3 Effects of reinforcement

3.7.3.1 Mechanism of behavior in fiber-reinforced soils

Tang et al. (2010) investigated the micromechanical interaction behavior between soil particles and reinforcing polypropylene fibers. They concluded that the interfacial shear resistance of fiber-reinforced soil depends primarily on the rearrangement resistance of soil particles, effective interface contact area (the area through which soil in connected

to the fiber, and normally is less than the surface area of fiber), fiber surface roughness, and soil composition. Jamellodin et al. (2010) observed that the fibers act to interlock particles and groups of particles in a unitary coherent matrix, thus the strength properties of the soil can be increased. The Scanned Electron Microscopy (SEM) photos of Tang et al. (2007) also indicated that the bond strength and friction at the interface seem to be the dominant mechanisms controlling the reinforcement benefit. It can also be seen that the fiber surface is attached by many clay minerals which make the contribution to bond strength and friction between the fiber and soil matrix. Jacob et al. (2005) also stated that the adhesion between fiber and composite matrix was a major factor in determining the response of the interface and its integrity under stress. The interfacial shear strength was a critical factor that controls the toughness and mechanical properties of composite materials. Similarly, Tang et al. (2007) indicated the distributed discrete fibers act as a spatial three dimensional network to interlock soil grains and help grains to restrict the displacement. As expected this bonding network will reduce the liquid limit of soil as Ikizler et al. (2009) reported for bentonite.

Effect of fiber-reinforcement is more pronounced when the strain in any strength test is increasing. It means the fibers play a role or contribute to the transporting load, only if they are mobilized. Chen & Loehr (2008) found that volumetric strain plays an important role in the mobilization of fiber resistance. Heineck et al. (2005) and Diambra et al. (2010) stated that the contribution of fiber-reinforcement is more effective after a certain level of shear strain, and at very small strains, the inclusion of fiber-reinforcement did not influence the initial stiffness and the elastic shear modulus.

Behavior of fiber-reinforced soil is not only influenced by strain range but also by stress level. Consoli et al. (2007) stated that the failure envelope of reinforced sand was distinctly nonlinear, with a well defined kink point, so that it could be approximated to a bilinear envelope (see Figure 3.26). It could be suggested that for failure occurring at mean stresses below the kink point separating the bilinear failure envelope, there is a composite of slippage and yielding of fibers, with some fibers showing limited stretching and others possibly slipping due to the low confining stress. For specimens failing on the higher pressure part of the bilinear failure envelope, there is more pronounced fiber stretching but no breakage because the fibers are highly extensible and the fiber strains necessary to cause breakage were not reached under triaxial conditions at these strain levels in the sample.

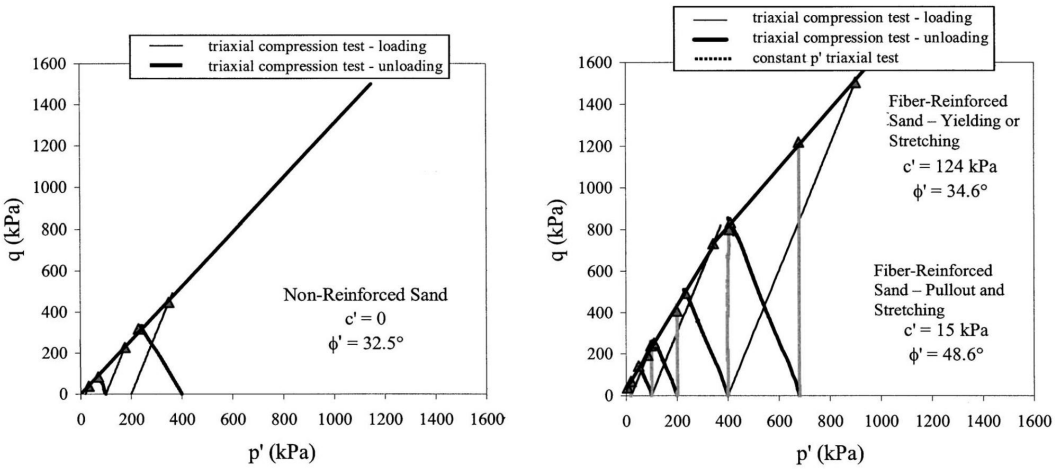

Figure 3.26: Failure envelope for unreinforced and fiber-reinforced sand (Consoli et al. 2007).

3.7.3.2 Compaction

Ravishankar & Raghavan (2004), Esna-ashari & Asadi (2008), Marandi et al. (2008), and Chegenizadeh & Nikraz (2011*a*) experimentally confirmed that in proctor compaction by increasing fiber content the maximum dry density (MDD) of a silty soil decreases but the optimum moisture content (OMC) of the soil increases. These results were also proved by Neeraja (2010) and Aggarwal & Sharma (2010). Amir-Faryar & Aggour (2012) also reported that by increasing the fiber content in kaolin optimum moisture content increased and maximum dry density decreased. Ikizler et al. (2009) found the same behavior for bentonites. The decrease in density is probably a result of the fiber filaments having less specific weight in comparison with the soil grains, and the fibers prevent the soil particles from approaching one another. The increase in moisture content is most likely the result of the fibers having a greater water absorption capacity than the surrounding soil.

Naeini & Sadjadi (2009) and Malekzadeh & Bilsel (2012*a*) reported that an increase in fiber content causes a reduction in maximum dry density, but has almost no influence on optimum moisture content. The results from the standard proctor compaction tests of Maher & Ho (1994) showed that increasing fiber length (from 64 to 254 *mm*), and fiber content (from 0.5 to 4% weight) did not produce significant effects on the magnitude of the dry density or the optimum moisture content of the mixture. Malekzadeh & Bilsel (2012*a*) and Illuri & Nataatmadja (2007) stated that by adding fibers maximum dry density decreases but there is no significant variation in optimum moisture content.

3.7.3.3 Strength characteristics

Bouhicha et al. (2005) and Ravishankar & Raghavan (2004) found that the compressive and tensile strength of soil increase by increases with the fiber content, if an optimized reinforcement ratio is used. Salehan & Yaacob (2011) reported that the addition of 3% palm fibers improves the compressive strength of composite bricks. Malekzadeh & Bilsel (2012*a*) showed that the split tensile strength of highly plastic clay increases by 270% only with the inclusion of 1% polypropylene fiber. Maher & Ho (1994) and Islam & Iwashita (2010) also confirmed the increase in tensile strength after fiber inclusion. Mesbah et al. (2004) proposed the development of a direct tensile test for compacted earth blocks reinforced with sisal fibers. Benefits of the inclusion of this natural fiber-reinforcement include both improved ductility in tension in comparison with plain earth blocks and the inhibition of tensile crack propagation after initial formation. Prior to cracking, the fibers appeared to have no noticeable effect on the material behavior.

Puppala & Musenda (2000), Cai et al. (2006), Kumar et al. (2006), Tang et al. (2006), Tang et al. (2007) and Consoli et al. (2007) indicated that reinforcement with polypropylene fibers enhanced the unconfined compressive strength of the soil which increases with the increase in fiber content and length. Santhi & Sayida (2009) and Malekzadeh & Bilsel (2012*a*) also have confirmed this outcome. Marandi et al. (2008) reported that longer fibers resulted in higher unconfined compressive strength but this effect is more pronounced in lower fiber contents than higher fiber contents.

Some previous studies have shown that the inclusion of fibers increases both the cohesion and friction angle compared to values for unreinforced soil. Pradhan et al. (2012) and Prabakara & Sridhar (2002) found that the shear strength is increased non-linearly with the increase in length of fiber and beyond, where an increase in length reduces the shear strength. Maher & Ho (1994) and Nataraj & McManis (1997) found that a significant improvement in the strength and shear strength parameters (c and ϕ) of the soil reinforced with various fibers, which is also supported by Tang et al. (2007), Jamellodin et al. (2010), Ahmad et al. (2010), and Diambra et al. (2010). However, Gray & Ohashi (1983), Gray & Al-Refeai (1986), Ranjan et al. (1996), and Chen & Loehr (2008) found that the inclusion of fibers did not significantly affect the friction angle. Esna-ashari & Asadi (2008) reported that fiber content increases the friction angle but has insignificant effects on cohesion.

Setty & Rao (1987) and Setty & Murthy (1987) carried out triaxial and tensile strength tests on silty sand and black cotton soil reinforced with polypropylene fibers. The test results illustrated that both of the soils showed a significant increase in the cohesion

intercept and a slight decrease in friction angle with an increase in fiber content up to 3% in weight. Naeini & Sadjadi (2009) and Al-Adili et al. (2012) also reported an increase in shear strength with an increase in fiber content but after a certain amount of fiber the strength reduced. Similarly, Cai et al. (2006) stated that too much fiber added could reduce the effectiveness of the improvement in the strength and toughness, inasmuch as the fibers adhere to each other to form lumps and cannot contact with soil particles fully.

Gray & Ohashi (1983) conducted a series of direct shear tests on dry sand reinforced with different synthetic, natural, and metallic fibers to evaluate the effect of different aspects such as fiber orientation, fiber content, fiber aspect ratios (ratio of fiber's diameter to fiber's length), and fiber stiffness on the shear strength. Based on the test results, they concluded that an increase in shear strength is directly proportional to the fiber area ratio. Jiang et al. (2010) also performed a series of direct shear tests on clayey soil reinforced with polypropylene fibers and reported that the cohesion and internal friction angle of fiber-reinforced soil exhibited an initial increase followed by a rapid decrease with increasing fiber content and fiber length.

As Consoli et al. (2003) reported, the reinforced specimens showed a marked hardening behavior up to the end of the tests, at axial strains larger than 20%, whereas the unreinforced specimens demonstrated an almost perfectly plastic behavior at large strain.

Ghiassian et al. (2004) found that at any fiber length, the peak strength and total volume change increases with fiber content whereas the rate of increase reduces with increasing fiber content. Ola (1989) and Diambra et al. (2010) also proved that fiber-reinforcement increases the peak strength and modifies the stress deformation behavior in a significant manner. It increases the peak shear strength and limits the amount of post peak reduction in shear resistance. Similarly, Consoli et al. (2002) and Tang et al. (2007) indicated that the inclusion of fiber in fine sand improves both peak and post peak which is dependent on fiber content. Esna-ashari & Asadi (2008) observed that fiber-reinforcement increases the peak shear strength in direct shear tests. However, the peak shear strength of specimens is insignificantly affected by the fiber length. Casagrande et al. (2006) concluded in their study on the behavior of fiber-reinforced bentonite that the inclusion of randomly distributed fibers increased the peak shear strength, whereas the residual strengths of both unreinforced and reinforced bentonite were found to be the same.

Moreover, when local cracks appear in a specimen, some fibers crossing these cracks are responsible for the tension in the soil by fiber-soil connection, which effectively impedes the further development of cracks and accordingly changes the failure mode of the reinforced specimens to a more ductile one with less distinct failure plane (see Figures 3.27 and 3.28).

With an increase in fiber content there are a greater number of failure surfaces and the surfaces' orientations were regular with a higher angle in respect to the horizontal line. The reason for this behavior suggests that increasing the fiber inclusion (i.e. the number of filaments per unit volume) makes the soil more homogenous and isotropic (Marandi et al. 2008). Freilich et al. (2010) showed that axial deformation of the unreinforced specimen resulted in the development of a failure plane, while reinforced specimens tended to bulge, indicating an increase in the ductility of soil-fiber mixture.

Maher & Ho (1994) studied the mechanical properties of a kaolin-fiber composite. The study showed that fibers inclusion increased the ductility of kaolin. Islam & Iwashita (2010)'s study showed that fibers in the matrix provide a means to prevent the crack growth in the shear band when cracks propagate due to the imposed loads. Thus fibers can improve the ductility and flexural strength of the material. They also studied the effect of water content on the shearing behavior of reinforced and unreinforced adobes. Park (2001) reported that at a 1% polyvinyl alcohol fiber dosage the values of ductility of sandy soil are greater than four. Yetimoglu & Salbas (2003), Bouhicha et al. (2005), Cai et al. (2006), Tang et al. (2007), Marandi et al. (2008), and Esna-ashari & Asadi (2008) have also proved that reinforced specimens show more ductile failure. Cai et al. (2006) clearly showed that by increasing the fiber content big cracks gradually vanish and small ones appear in their place.

Bauer & Oancea (1996), based on their triaxial test results, indicated that the secant modulus as an indication of the stiffness within the initial vertical strain of 2% decreased

with increasing fiber contents. Consoli et al. (1998), by conducting triaxial compression tests, showed that fiber-reinforcement increased the peak and residual strengths, but decreased stiffness. However, Gray & Ohashi (1983) found no increase in stiffness of the fiber-sand composite. Freitag (1986) reported that randomly distributed fibers in a compacted fine-grained soil could result in greater strength and stiffness. Gray & Al-Refeai (1986) found that conducting triaxial compression tests on a sand reinforced with synthetic fibers resulted in a loss of compressive stiffness at low strains. They also showed that fiber-reinforcements increased the axial strain at failure, and in most cases reduced post-peak loss of strength. Michalowski & Zhao (1996), based on triaxial test results, indicated that the steel fibers led to an increase in the peak shear stress and in the stiffness prior to failure. They also reported that polyamide fibers produced an increase in the peak shear stress for large confining pressures, but the effect was associated with a considerable loss of stiffness prior to failure and a substantial increase of the strain to failure. In Esna-ashari & Asadi (2008)'s study, initial stiffness (initial tangent modulus)

Figure 3.27: Variation of the failure characteristics with fiber content, the fiber content from left to right respectively: 0, 0.05, 0.15, and 0.25 gravimetric percent (Cai et al. 2006).

decreased with an increase in the length and dosage of fibers. Yetimoglu & Salbas (2003) and Naeini & Sadjadi (2009) reported that fiber-reinforcements have no discernible effect on the initial stiffness of the sand.

One of rare studies showing reduction in shear strength with an increase in fiber content is the done by Islam & Iwashita (2010). As Figure 3.29 shows, compressive strength of adobes decreased but the ductility increased with the increase of straw content irrespective of the straw length. The mechanisms behind the above-mentioned observations can be explained as follows: the straw is not flexible enough to move in phases with soil particles during the drying shrinkage of adobe, either separation of straw from soil or lowering in shrinkage might occur, which both provide less dry density and less strength for material. Hoare (1979) also found a decrease in strength for a compacted reinforced compared to unreinforced soil.

3.7.3.4 Swelling and shrinkage

When swelling occurs in a soil-fiber mixture, the fibers in the soil are stretched and the tension in the fibers resists further swelling. Consequently, the swelling potential of the soil reduces while fiber content increases. Tang et al. (2007) observed the micro-structure of clay-silt-sand mixture reinforced with polypropylene fiber by using Scanning Electron Microscopy (SEM). As can be seen in Figure 3.30a, the fiber surface is attached by many clay minerals which contribute to bond strength and friction between the fiber and the

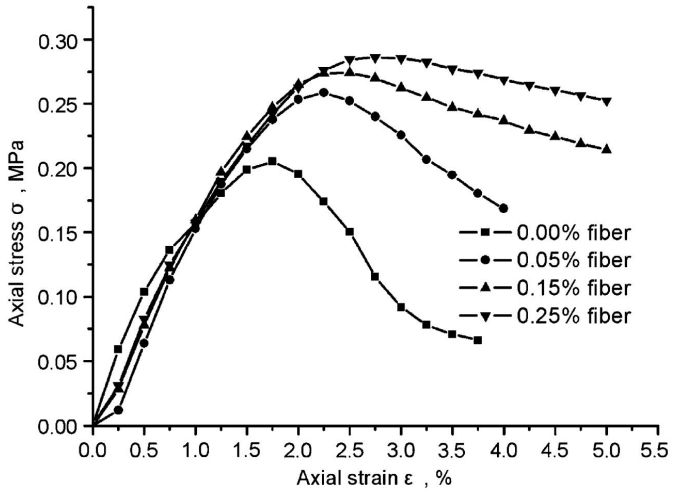

Figure 3.28: Change from brittle failure to ductile one by increase in fiber content (Tang et al. 2007).

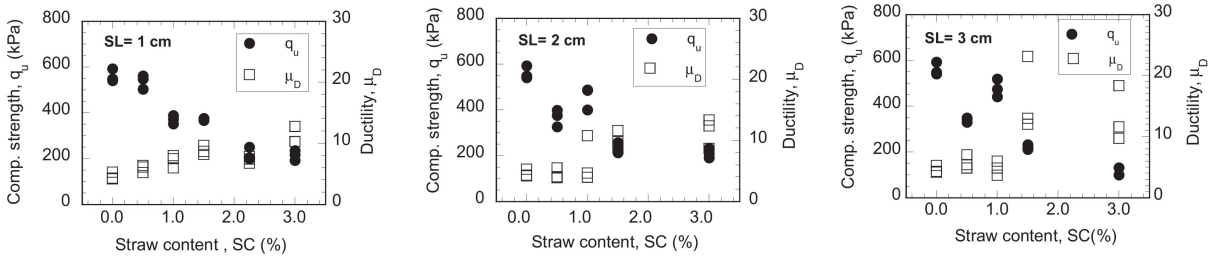

Figure 3.29: Reduction in compressive strength with increase in straw content for 3 different straw lengths (Islam & Iwashita 2010).

soil matrix. They concluded that the distributed discrete fibers act as a spatial three dimensional network (Figure 3.30b) to interlock soil grains, help grains to form a unitary coherent matrix and restrict the displacement. Consequently, the stretching resistance between clay particles and strength behavior was improved. Because of the interfacial force, the fibers in the matrix limit the shrinkage and swelling in soil structure.

Ayyar et al. (1989) have worked on the efficacy of randomly distributed coir fibers in reducing the swelling tendency of soil. Puppala & Musenda (2000) and Punthutaecha et al. (2006) showed that fiber-reinforcements reduced the swelling potential of expansive clays. Cai et al. (2005), Cai et al. (2006), and Viswanadham et al. (2009) also found the same trend for fiber-reinforced clayey soils. Al-Azzo et al. (2009) reported that increasing the weight of fibers by 10% to expansive clayey soil eliminates about 80% of the original swelling pressure. Ikizler et al. (2009) found the same behavior with bentonite soil.

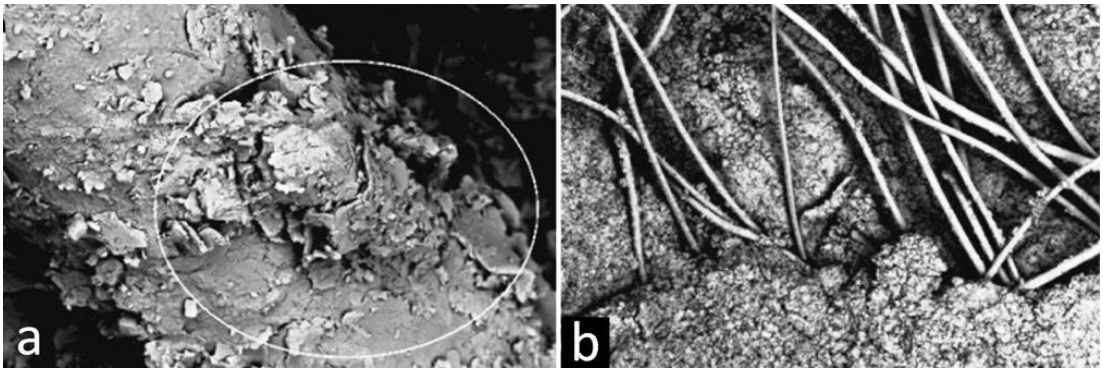

(a) (b)

Figure 3.30: (a) Bonding between fiber and soil, and (b) spatial three dimensional network observed in SEM photos of Tang et al. (2007).

Phanikumar & Kashliwal (2010) stated that the amount of heave over a foundation built on a reinforced low plastic clay decreased with an increase in fiber inclusion (sisal fibers) in the soil.

As shown in Figure 3.31, Bouhicha et al. (2005) stated that shrinkage decreased with the increase in fiber content and fiber length. Shrinkage was higher for soils with higher levels of clay. The addition of straw reduces the shrinkage as the fibers tend to oppose the deformation. In similar research studies Malekzadeh & Bilsel (2012*a*) and Kinjal et al. (2012) stated that fiber inclusion reduces shrinkage settlements during desiccation in a highly plastic clayey soil. Al-Wahab & M.A. (1995) found that reinforcement with polypropylene fibers reduces tension cracks as well as the amount of shrinkage and swelling in compacted clays.

3.7.3.5 Hydraulic properties

The studies of Maher & Ho (1994) and Chegenizadeh & Nikraz (2011*b*) showed that an increase in fiber content increases the saturated hydraulic conductivity of the soil, for the same fiber types and lengths tested. Similarly, Abdi et al. (2008) indicated that hydraulic conductivity of a clayey soil due to random inclusion of fibers was slightly increased as a function of both fiber content and length.

Furumoto et al. (2002) conducted a series of permeability tests and large-scale levee models to examine the piping resistance of polyester fiber-reinforced soil. From the permeability tests, they found that the piping resistance of soil becomes higher by mixing short fibers.

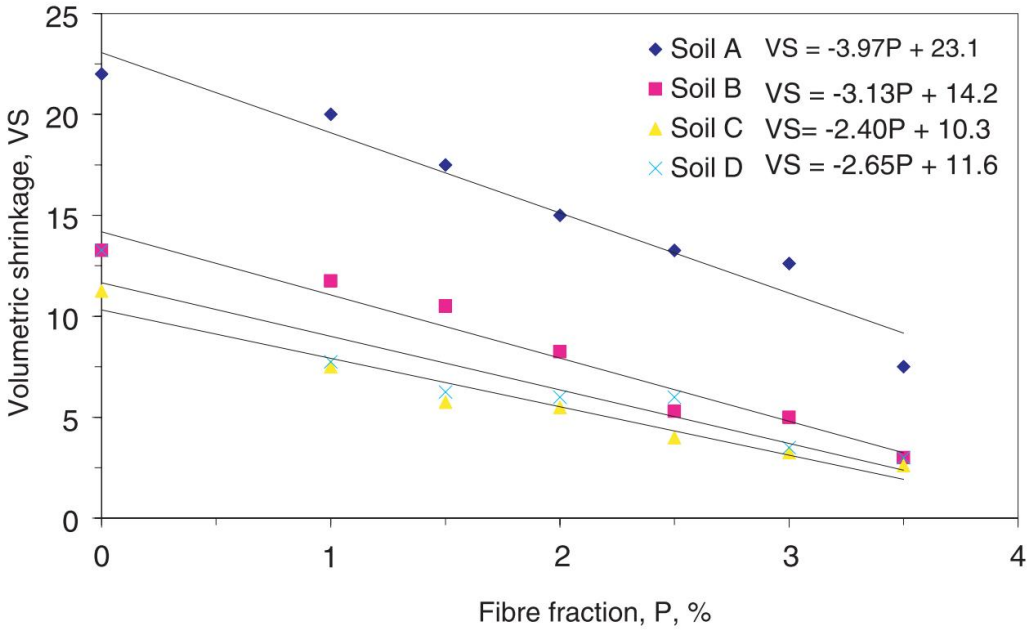

Figure 3.31: Effect of fiber content on shrinkage (Bouhicha et al. 2005).

Miller & Rifai (2004), based on their test results, indicated that fiber inclusion reduced the crack propagation which decreased the hydraulic conductivity of compacted clayey soil.

Efficacy of natural fiber-reinforcement in reducing the seepage velocity and improving the piping resistance of soils was investigated by Sivakumar-Babu & Vasudevan (2008*a*). They carried out a number of experiments to determine the seepage velocity and piping resistance of different types of soils mixed randomly with coconut coir fibers. Three types of sandy soils were used in their study. The experiments were carried out for various hydraulic heads, fiber contents, and fiber lengths. As Figure 3.32 shows, it was observed that fibers reduce the seepage velocity of plain soil considerably and thus increase the piping resistance of soil, while fiber length does not have considerable effect on seepage velocity.

Since fibers are distributed throughout a soil mass, they impart strength isotropy and reduce the possibility of formation of weak zones and contribute to improved piping resistance.

Das et al. (2009), using one-dimensional piping tests, have determined the effect of flexible polyester fiber inclusion on the seepage velocity and piping resistance of fly ash. Reinforcing fly ash specimens with polyester fibers reduced seepage velocity and improved

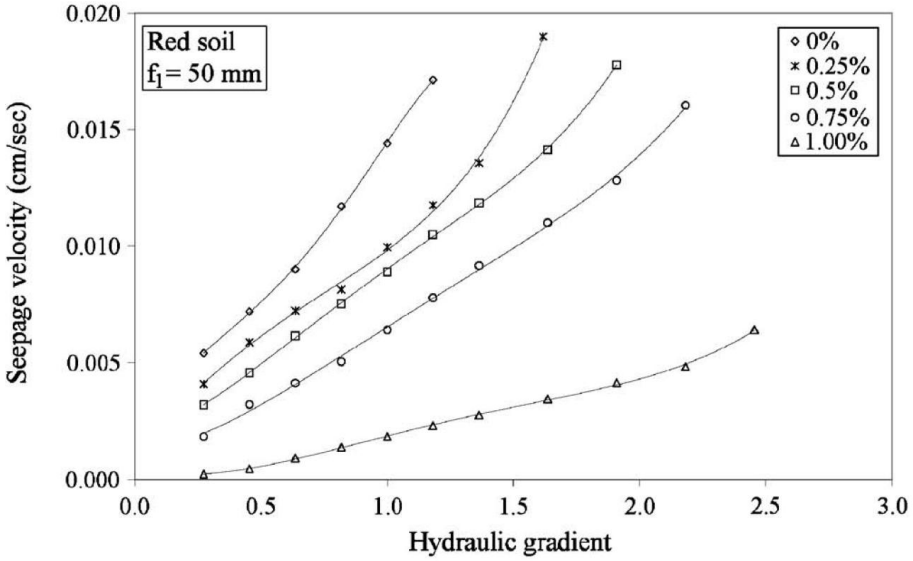

Figure 3.32: Seepage velocity versus hydraulic gradient for various fiber contents (Sivakumar-Babu & Vasudevan 2008*a*).

piping resistance. Reduction in seepage velocity and improved piping resistance can be attributed to the effective contact area of fly ash and fibers, which results in the blocking of pore spaces of fly ash by fibers replacing fly ash solids.

3.7.3.6 Desiccation cracks

Islam & Iwashita (2010) showed that straw fibers will help to prevent the desiccation cracks in adobe block and mortar during drying. Abdi et al. (2008) stated that polypropylene fiber-reinforcement significantly reduced the extent and distribution of desiccation cracks in a soil consisting of 75% kaolinite and 25% montmorillonite as observed by the reduced number, depth, and width of cracks (see Figure 3.33). Azadegan et al. (2012) reported that as the amount of fibers increases the type of cracks changed from wide and long to tiny and distributed ones.

Summary:

Fibers have been employed to stabilized soil for a long time. Recently, synthetic fibers have been used in addition to natural fibers. Fiber-reinforcement can affect some of the properties of soils, such as: proctor compaction, shear strength, swelling and shrinkage, hydraulic conductivity, and desiccation cracks. Studies on the micro-structure of fiber

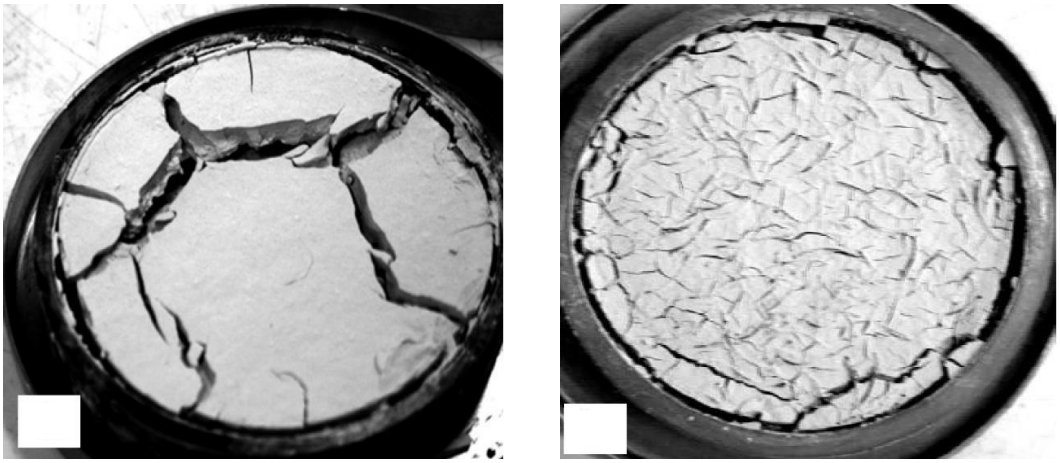

(a) (b)

Figure 3.33: Desiccation cracking for (a) unreinforced and (b) reinforced sample (Abdi et al. 2008).

reinforced soils, using ESEM photos, showed how the interaction between soil particles and fiber surface affects the mechanisms of behavior.

3.8 Hydraulic conductivity

3.8.1 General

In the past, geotechnical engineers have been primarily interested in the saturated hydraulic conductivity of soils. With the growth of geo-environmental practice many geotechnical engineers now need to quantify flow in the unsaturated zone. Applications where unsaturated flow must be characterized include the assessment of contaminant leaching in the unsaturated zone, designing earthen caps for waste containment, capillary uprising moisture in materials, etc. An essential element required for analyses and calculations in each of these applications is the relationship between hydraulic conductivity and water content or matric suction.

3.8.2 Saturated hydraulic conductivity

The flow of water within a fully saturated soil is normally taken to behave in accordance with Darcy's law, which for one-dimensional flow has the form:

$$v_x = -k_x \frac{\partial h}{\partial x} \tag{3.12}$$

where v_x, k_x, and $\partial h/\partial x$ are velocity of water flow in direction of x, coefficient of permeability (for water flow) in the direction x, and hydraulic gradient in the same direction.

3.8.3 Unsaturated hydraulic conductivity

Buckingham (1907) was the first to present experimental evidence for the validity of flux in unsaturated medium. As Childs (1969) reported, vapor phase flow is much slower compared to liquid phase and can be neglected when fluid flow occurs. Once the water phase within the soil has discontinued, water will no longer be able to flow in its liquid form, but will only be possible in its vapor phase. Therefore, for unsaturated soils with a very low degree of saturation, which have a non-continues water phase, the water flow rate is almost zero.

It is generally accepted (for example, Ng & Shi 1998 and Smith 2003) that Darcy's law, and its associated assumptions, remains applicable to flow through unsaturated soil, except that it now takes the following form:

$$v_x = -k_x(\psi) \frac{\partial h}{\partial x} \tag{3.13}$$

where $k_x(\psi)$ is the coefficient of permeability as a function of suction. Freeze & Cherry (1979) developed an equation for continuity of flow for transient flow through an unsaturated soil, incorporating Darcy's law in its unsaturated form, as shown in Equation 3.14.

$$\frac{\partial}{\partial x}\left[k(\psi)\frac{\partial h}{\partial x}\right] + \frac{\partial}{\partial y}\left[k(\psi)\frac{\partial h}{\partial y}\right] + \frac{\partial}{\partial z}\left[k(\psi)\frac{\partial h}{\partial z}\right] = \frac{\partial \theta}{\partial t} \tag{3.14}$$

Freeze & Cherry rewrote Equation 3.14 to give Equation 3.15. In this form it is known as the Richards equation.

$$\frac{\partial}{\partial x}\left[k(\psi)\frac{\partial \psi}{\partial x}\right] + \frac{\partial}{\partial y}\left[k(\psi)\frac{\partial \psi}{\partial y}\right] + \frac{\partial}{\partial z}\left[k(\psi)\left(\frac{\partial \psi}{\partial z} + 1\right)\right] = C\frac{\partial \psi}{\partial t} \tag{3.15}$$

where C is specific moisture capacity, so that:

$$C = \frac{\partial \theta}{\partial \psi} \tag{3.16}$$

The right hand side in Equation 3.15 or the Richards equation represents the change in water storage within soil, and this behavior is reflected by the slope of the SWCC. The slope of this curve indicates the quantity of water that flows in or out of a soil element in response to a given change in suction.

The equation contains two functional relationships characterizing the soil: (i) the soil-water characteristics curve (SWCC), $\psi(\theta)$, describing the relation between suction and water content, and (ii) the unsaturated hydraulic conductivity function, $k(\psi)$, describing the unsaturated hydraulic conductivity as a function of suction, or using $\psi(\theta)$ can be converted to function of water content. To solve the Richards equation, prior knowledge of these unsaturated hydraulic properties is required. Methods for determining the unsaturated hydraulic properties are described in the following section.

3.8.4 Determination of unsaturated hydraulic conductivity

Saturated coefficient of permeability can vary by several orders of magnitude for different soils. In the case of partial saturation, even for a single soil, it is possible to have a coefficient of permeability that ranges over 10 orders of magnitude.

When the coefficient of permeability at different suctions, $k(\psi)$, is referenced to the saturated coefficient of permeability ,k_s, the relative coefficient of permeability, $k_r(\psi)$, can be written as follows:

$$k_r(\psi) = \frac{k(\psi)}{k_s} \tag{3.17}$$

The relative coefficient of permeability as a function of volumetric water content, $k_r(\theta)$, can be defined similarly.

3.8.4.1 Theoretical methods

Fredlund et al. (1994) stated that for unsaturated soils there could be different permeability functions in desorption and sorption processes. However they believed that

both functions have a similar characteristic shape and can be fitted by a similar form of mathematical equation. There are two theoretical approaches to obtain the permeability function of an unsaturated soil:

Empirical equations:

Several empirical equations for the permeability function of unsaturated soils are listed in Table 3.2. These equations can be used in engineering practice when measured data are available for the relationship between the coefficient of permeability and suction, $k(\psi)$, or for the relationship between the coefficient of permeability and volumetric water content, $k(\theta)$. The smallest number of measured points required to use one of the permeability equations in Table 3.2 is equal to the number of fitting parameters in the adopted equation. When the number of measurements exceeds the number of the fitting parameters, a curve-fitting procedure can be applied to determine the fitting parameters. This approach allows a closed-form analytical solution for unsaturated flow problems.

Brooks & Corey (1966) reported that for a medium containing two immiscible fluids (for example, air and water), the permeability of the wetting phase is a function of the difference in pressure between the two phases, which means they found that permeability is actually a function of soil suction. Some of the empirical equations based on soil suction are listed in Table 3.3.

Statistical models:

Statistical models have also been used to determine the permeability function for an unsaturated soil using the parameters of the soil-water characteristic curve. This approach

Table 3.2: Empirical equations of k_r

Function	Reference
$k_r = \Theta^{0.35}$	Averjanov (1950)
$k_r = (S_e)^4$	Corey (1957)
$k_r = \exp\left[\alpha\left(\theta - \theta_{sat}\right)\right]$	Davidson et al. (1969)
$k_r = \left[\frac{\theta}{\theta_{sat}}\right]^n$	Campbell (1973)

Table 3.3: Empirical equations of k_r based on suction

Function		Reference
$k(\psi) = a\psi + b$		Richards (1931)
$k(\psi) = \alpha\psi^{-n}$		Wind (1955)
$k_r = \exp(-\alpha\psi)$		Gardner (1958)
$k_r = 1$	$\psi \leq \psi_{AEV}$	Brooks & Corey (1964)
$k_r = \left(\frac{\psi}{\psi_{AEV}}\right)^{-n}$	$\psi \geq \psi_{AEV}$	
$k(\psi) = k_s$	$\psi \leq \psi_{AEV}$	
$k(\psi) = \exp[-\alpha(\psi - \psi_{AEV})]$	$\psi_{AEV} \leq \psi \leq \psi_r$	Rijtema (1965)
$k(\psi) = k_r\left(\frac{\psi}{\psi_r}\right)$	$\psi_r < \psi$	
$k_r = S_e^{1/2}\left[1 - \left(1 - S_e^{1/m}\right)^m\right]^2$		van Genuchten (1980)

where ψ_r is the residual suction and k_r is its corresponding coefficient of permeability.

is based on the fact that both permeability function and the soil-water characteristic curve are primarily determined by the pore-size distribution of the soil under consideration and can be related to each other.

Burdine (1953) proposed the following equation for the relative coefficient of permeability:

$$k_r(\theta_w) = \Theta^2 \frac{\int_0^{\theta_w} \frac{d\theta_w}{\psi^2}}{\int_0^{\theta_s} \frac{d\theta_w}{\psi^2}} \tag{3.18}$$

Mualem (1976) derived an equation as follows:

$$k_r(\theta_w) = \Theta^{0.5} \left(\frac{\int_0^{\theta_w} \frac{d\theta_w}{\psi}}{\int_0^{\theta_s} \frac{d\theta_w}{\psi}} \right)^2 \tag{3.19}$$

Similarly, a more general form can be written as:

$$k_r(\theta_w) = \Theta^x \left(\frac{\int_0^{\theta_w} \frac{\theta_w - \xi}{\psi^y} d\xi}{\int_0^{\theta_s} \frac{\theta_w - \xi}{\psi^y} d\xi} \right)^z \tag{3.20}$$

where Θ is the effective volumetric water content and is calculated from Equation 3.21:

$$\Theta = \frac{\theta - \theta_{res}}{\theta_{sat} - \theta_{res}} \tag{3.21}$$

θ_{sat} and θ_{res} are saturated and residual volumetric water contents. Agus et al. (2003) compared some of the above-mentioned models for various soils.

3.8.4.2 Experimental methods

Several ways have been proposed to find the hydraulic conductivity of unsaturated soils in the laboratory as a function of suction or water content. These methods are divided into two main groups: namely, steady state and unsteady methods. Benson & Gribb (1997) and Masrouri et al. (2008) reviewed the proposed experimental steady and unsteady states techniques for measuring unsaturated hydraulic conductivity.

Steady state methods:

In the steady state methods, either a "constant flow rate" (e.g. Olsen 1966, Olsen et al. 1985, Aiban & Znidarcic 1989, Znidarcic et al. 1991, Bicalho et al. 2000, Likos et al. 2005, and Lu et al. 2006) or a "constant hydraulic gradient" (e.g. Corey 1957) is applied under a specific average matric suction. Measurements are then made of matric suction (constant flow rate test) or flow rate (applied gradient test). Hydraulic conductivity is computed using Darcy's law. Most steady state methods are similar to those used for saturated soils. Detailed descriptions of these methods are provided in Klute (1972), Klute & Dirksen (1986), and Dirksen (1991).

In the traditional steady method as shown in Figure 3.34 a sealed chamber is used to apply suction via the ATT method, and simultaneously a constant head is applied from one side of the soil sample.

When the constant head method is employed the unsaturated hydraulic conductivity is computed as:

$$K(\theta_w) = q_\psi \left[\frac{L}{\Delta H_s} \right] \tag{3.22}$$

where q_ψ is the steady state volumetric water flux at applied matric suction ψ, L is length of specimen, and ΔH_s is the drop in total head across the specimen.

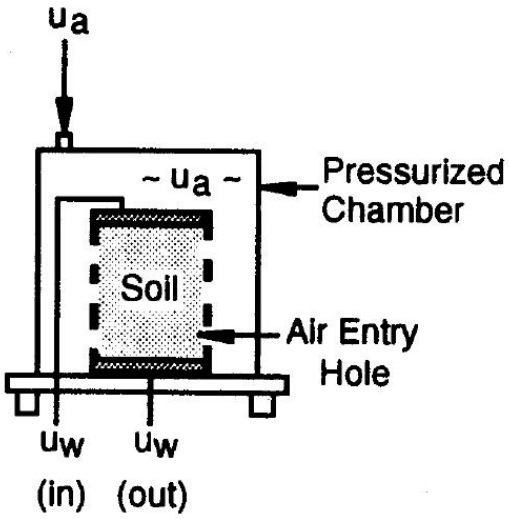

Figure 3.34: Measurement of unsaturated hydraulic conductivity of unsaturated soil under constant suction (Benson & Gribb 1997).

Unsteady methods:

The steady state method may be costly, tedious, and lengthy in low permeability materials. In contrast to steady methods, transient conditions (water content, matric suction, etc.) are imposed when using one of the unsteady methods. Hydraulic conductivity is computed from the transient data using analytical solutions describing transient flow or by applying Darcy's law over time, during which conditions are approximately steady.

There are two main categories of unsteady methods, namely the "outflow methods" (e.g. Miller & Elrick 1958, Rijtema 1959, and Kunze & Kirkham 1962), and the "instantaneous profile methods" (e.g. Richards & Weeks 1953, Bruce & Klute 1956, Daniel 1983, and Chiu & Shackelford 1998).

Outflow methods consist of subjecting a soil specimen to small incremental steps in matric suction and recording the rate of outflow and total outflow during each step. The method assumes that during the outflow process k_r is constant, and the relation between water content and matric suction is linear.

The instantaneous profile method consists of inducing transient flow in a long cylindrical sample of soil and then measuring the resulting water content and/or pore water pressure profiles at various time intervals. The method cannot be used for measuring k_r functions at high degrees of saturation.

3.8.5 Uprising moisture

Capillary rise in porous media has been studied for many years, since the pioneering work of Washburn (1921). The Washburn equation was derived originally for a liquid rising in a cylindrical capillary tube from the effects of capillary forces, but using a fitting parameter it can be developed for soil or other construction materials. Washburn assumed that water rises as a saturated front in a material. That means that up to a certain height of the wall the material is saturated and above that it is dry, which is not a correct assumption in fine-grained soils. Washburn's equation relates height and time of uprising together:

$$t = \frac{\theta_s(h_e + z_R)}{K_s} \ln\left(\frac{z_R + h_e}{z_R + h_e - z_f}\right) - \frac{\theta_s z_f}{K_s} \tag{3.23}$$

As shown also in Figure 3.35 z_f is the height of the wetting front, z_R is the positive pressure head imposed at z=0 (z_R can be zero), θ_s is the volumetric water content of the saturated sample (often taken as equivalent to the effective porosity), K_s is the saturated hydraulic conductivity, h_e is the equilibrium height for a capillary tube but is a fitted parameter for complex porous media typically corresponding to the equivalent saturated height of the cumulative mass absorbed, and t is time. Some limitations of the Washburn equation have been discussed in the literature and an excellent review can be found in Dullien (1992).

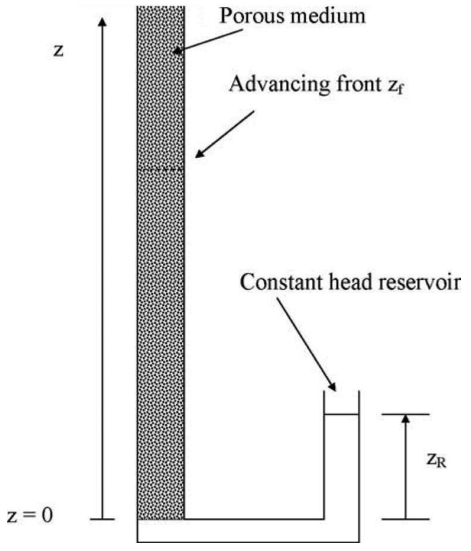

Figure 3.35: Capillary rise experiment (Lockington & Parlange 2004).

Hall (1977) proposed a method for steady state flow in construction materials between two parts of a building which are assumed to have constant water content (e.g. completely dry and saturated). This flow can be either horizontal or vertical. With some simplifications on separation of θ and t in equations he also introduced a method to solve the time dependency of the flow.

Yuan & Lu (2005) derived an analytical solutions for vertical flow in unsaturated soils using the Richards equation to describe the distribution of pressure head, water content, and fluid flow for rooted, homogeneous soils with varying surface fluxes. The solutions assume that (i) the constitutive relations for the hydraulic conductivity and water content as a function of the pressure head are exponential, (ii) the initial water content distribution is a steady-state distribution, and (iii) the root water uptake is a function of depth. Three simple forms of root water uptake were considered: uniform, stepwise, and exponential functional forms.

3.8.5.1 Uprising moisture in walls protected with countermeasure methods

Several countermeasure methods have been suggested in the literature to control uprising moisture and some are more common in practice. Main methods are presented in Section 2.4. In order to evaluate the efficiency of the base ventilation technique for treating rising damp in the walls of masonry buildings, Torres & Freitas (2007) performed several large scale experimental and numerical studies. Their techniques consisted of ventilating the base of walls through a natural ventilation process. To trace the distribution of moisture inside the walls, RH sensors were located at different heights and depths. The experimental tests consisted of prismatic walls with the dimensions $158\times200\times20$ cm, exposed or waterproofed on the facades to control the transport of moisture in these directions. The bricks were made of limestone slabs. To apply water to the lower parts of the wall a water reservoir was built in which the wall itself was constructed. The geometry and boundary conditions used are presented in Figure 3.36. Configuration 4 was comparable with what was accomplished in the present study. They concluded that this method can successfully limit uprising moisture. The comparison of configurations 3 and 4, with initial RH of 60%, showed that at a height of 60 cm relative humidity of a

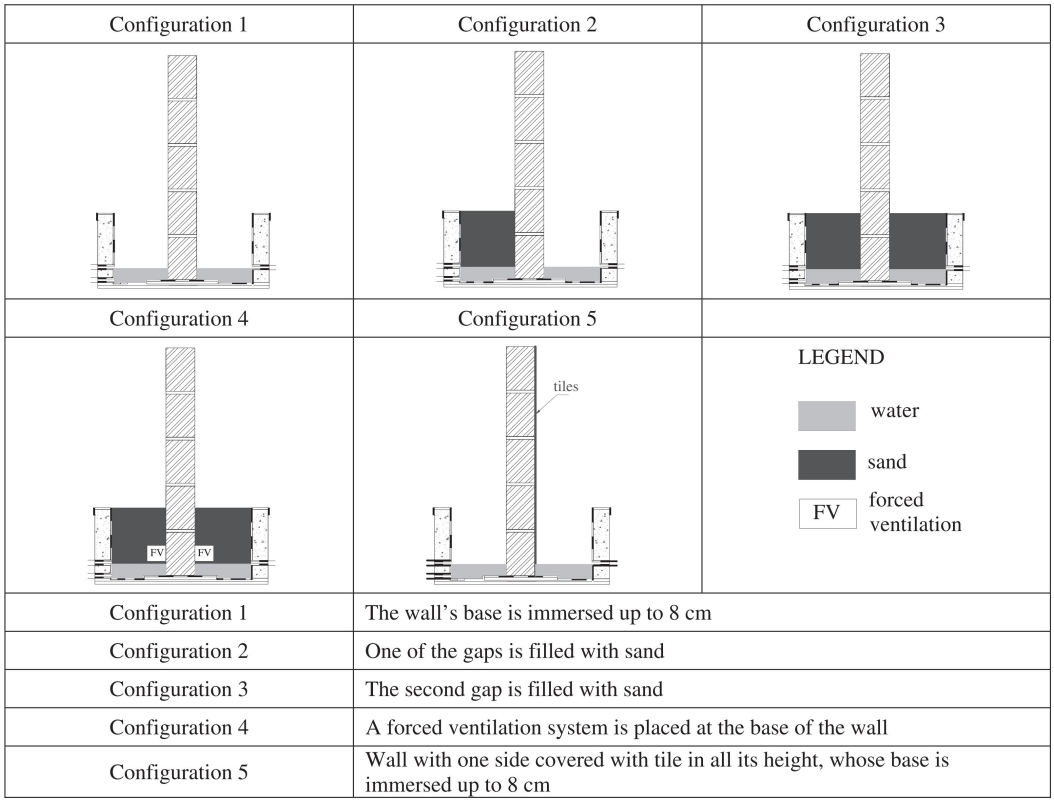

Configuration 1	The wall's base is immersed up to 8 cm
Configuration 2	One of the gaps is filled with sand
Configuration 3	The second gap is filled with sand
Configuration 4	A forced ventilation system is placed at the base of the wall
Configuration 5	Wall with one side covered with tile in all its height, whose base is immersed up to 8 cm

Figure 3.36: Different base ventilation methods implemented by Torres & Freitas (2007).

protected wall (configuration 4) increased from 60 to 65%, while this value at the same height of an unprotected wall (configuration 3) increased to 100% after 800 hours.

3.9 Summary

In this chapter the relevant literature for analyzing uprising moisture in masonry walls has been reviewed,

- General definitions and the basics of unsaturated soil (e.g. suction, SWCC, etc.);
- Concept of effective stress in unsaturated soil (two different approaches);
- Shear strength of unsaturated soil;
- Fiber-reinforcement of soil (as an efficient method to improve some hydro-mechanical properties); and
- Hydraulic conductivity of soil (for saturated and unsaturated conditions, with experimental and analytical methods to obtain its dependency on suction, which will be used

in calculations of uprising moisture).

With regard to the reviewed literature and to the best of the author's knowledge, there are still some gaps in terms of analyzing the consequences of uprising moisture in masonry materials. SWCC of fiber-reinforced soil has not yet been investigated. Shear strength of fiber-reinforced soils under unsaturated conditions has not been considered until this research. However, there are very few experimental or numerical studies on masonry walls subjected to uprising moisture with and without a protecting countermeasure method (as well as proposing of alternative methods) in the literature, and further research is needed in this field.

4 Material used and experimental program

4.1 Introduction

In this chapter the materials used in the present study are introduced and their basic properties are presented. Using Scan Electron Microscopy (SEM) photos the micro-structure of samples are observed in more detail. Pore-size distributions of samples are also observed using Mercury Intrusion Porosimetry (MIP).

In addition, the experimental programs adopted in this study are introduced. The need and motivation for performing these tests are explained in Sections 2.5 and 3.9. Methods and techniques to obtain SWCC, as well as the experimental programs for biaxial shear tests and large scale wall tests are presented.

4.2 Materials used

As mentioned in previews chapters, this study concentrates on typical masonry materials from which old buildings used to be constructed. The materials used in this study were soil-straw mixtures with different dosages. The soil itself was a composite of two types of clay, i.e. kaolin and a calcium-type bentonite (called also Calcigel), silt, and sand. The fiber used for reinforcing masonry materials was straw, a byproduct of harvesting wheat.

The material used for making adobe bricks is mostly prepared from local sources and can have different mixtures from area to area and climate to climate. The mixture should not contain too much clay, otherwise the soil tends to shrink and crack severely as it dries. If sand is in excess, the bricks will erode easily in wet weather. Desirable soils for brick making are those classified as loamy sands, sandy loams, or sandy clay loams. These textural names are given to soils that contain sand, clay, and silt (Hohn 1971).

4.2.1 Soil mixture

Bahar et al. (2004) defined a range of grain size distribution for soil that can be used as adobe bricks. Schicker & Gier (2009) worked on the optimization of mechanical strength of adobe bricks. They used a loam soil containing 26% clay size, 67% silt size, and 7% sand size particles. Kouakou & Morel (2009) studied the strength and elasto-plastic behavior of adobe bricks. The soil mixture they used was 25.5% clay (90% kaolin and 10% illite), 30% silt, and 44.5% sand. Bui et al. (2009) also worked with 3 types of materials (named a, b, and c in Figure 4.1), containing clay, silt, and sand. Molnár (2011) did an experimental study on adobe bricks to eliminate some of the disadvantages of this material (e.g. water sensitivity, tensile strength, and cracking). The grain sizes distribution curves of materials introduced by the above-mentioned studies together with the soil used in this research is presented in Figure 4.1. As can be seen in this Figure, a range of mixtures for masonry materials varies widely.

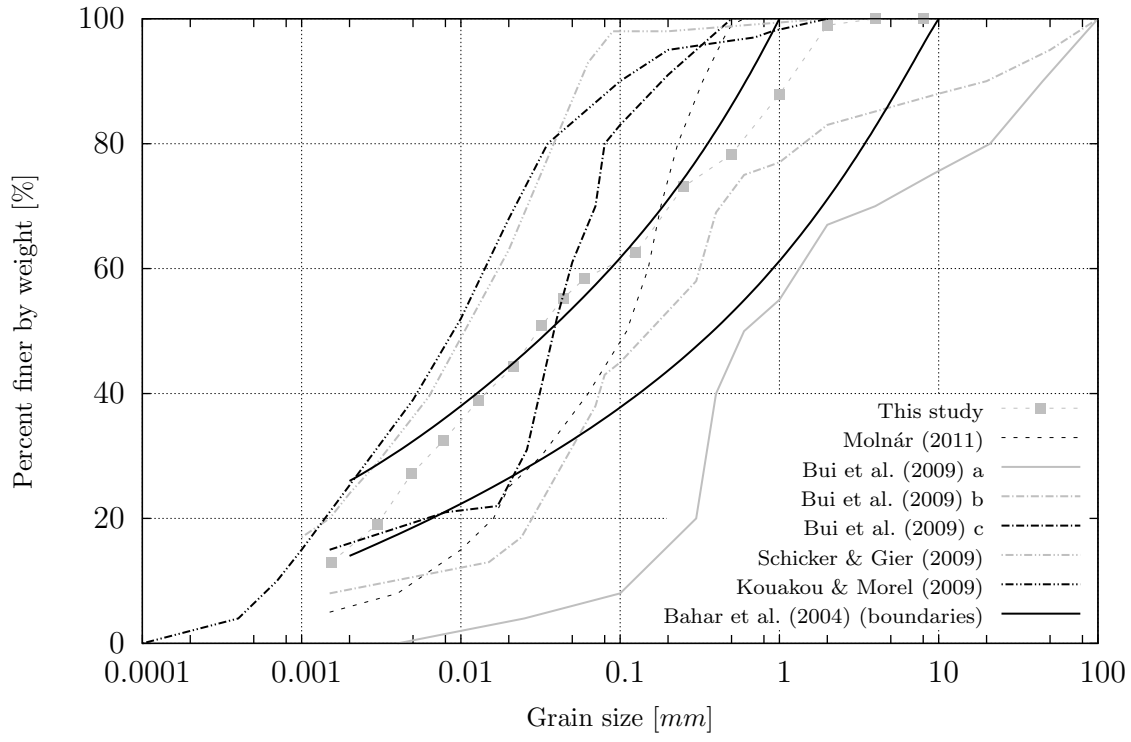

Figure 4.1: Grain size distribution curve of different soils used in preparation of masonries.

Figure 4.2: Wheat straw used in this study.

The grain size distribution curve for soil used in this research is shown in Figure 4.1 together with other studies soil mixtures. The selection of this material was based on the typical soils used for the preparation of clay bricks in central parts of Iran, presented in Khak-Paye Cons. Eng. Report (Amirshahkarami 2005). Grain size distribution curve of this soil is shown in Figure 4.1. As can be seen, the soil mixture in this study is almost in the range found by Bahar et al. (2004), and goes between others' curves. In the unified soil classification system this soil is classified as CL.

4.2.2 Straw

Unlike most of the research studies in the field of fiber reinforcement of soils, the selected fiber for reinforcement in this research was a natural fiber, typical wheat straw (Figure 4.2), available worldwide, which is a nonhazardous byproduct of agriculture. The amount of straw content in this study varied from 0 to 3 gravimetric percent of total weight. Unlike synthetic fibers, straw pieces consumes no fossil energy in its production, and also disintegrates and does not contaminate nature. The specific gravity of straw used in this study was 1.68 g/cm^3.

The moisture absorption characteristics of the straw fibers were examined by soaking the fiber samples and weighing them at various times. The results are shown in Figure 4.3. The results indicate that the maximum gravimetric water content of almost 900% was achieved after a period of 40-50 hours. There was an insignificant increase in water

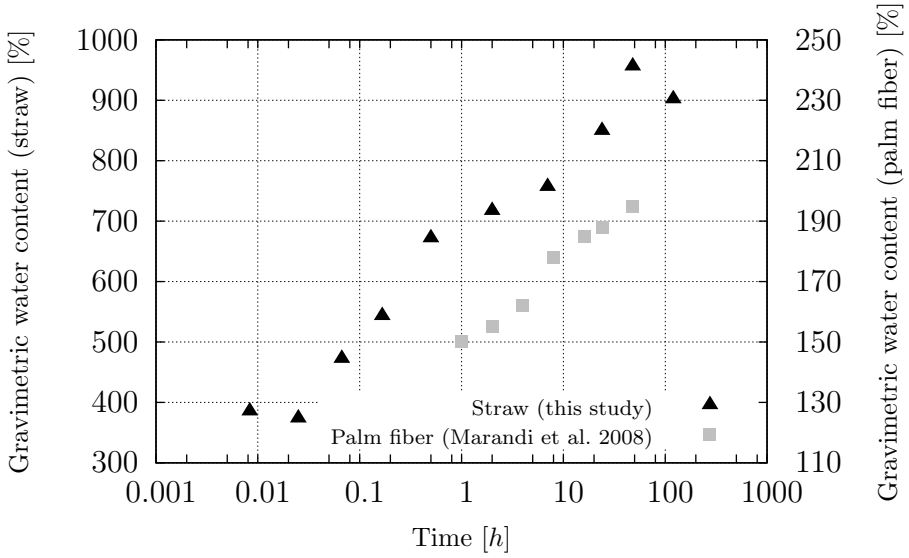

Figure 4.3: Fiber water absorption vs. time.

content above this value. High value of water content was probably due to the shape of straw pieces which are like hollow tubes and can retain water inside. The initial gravimetric water content was around 7%. Marandi et al. (2008) reported similar results on palm fibers which are presented in the same figure. The maximum water content of palm fibers, as found by Marandi et al. (2008), was 190%. The big difference between these two water adsorptions is rooted in the fiber shape. Marandi et al. (2008) used palm fibers which are not as porous as straw fibers and unlike straw do not have a hollow tube inside.

4.3 Properties of material

4.3.1 Basic properties

The soil had a liquid limit of 20.5%, plastic limit of 11.5%, and plasticity index of 9%. Liquid limits of soil-straw mixtures are presented in Table 4.1. Ikizler et al. (2009) also reported an increase in LL with an increase in fiber content. Due to instructions, it was not possible to perform a plastic limit test for samples containing straw. In this table e_0 is the void ratio of saturated slurry with 1.25×LL water content (see Section 5.2.1).

Table 4.1: Specific gravity and liquid limit of soil-straw mixtures.

Straw [%]	Soil [%]	G_s(average) [-]	LL [%]	e_0 [-]
0	100	2.67	20.5	0.7
0.5	99.5	2.67	21.5	0.705
1	99	2.66	25	0.72
2	98	2.65	28.5	0.74
3	97	2.64	37.8	0.77

The specific surface area (SSA) is the surface area of the soil particles measured in m^2/g. It is also a strong indicator of the retention and sorption capacity of clays. The SSA was determined using the Ethylene Glycol Monoethyl Ether (EGME) adsorption method (Eltantawy & Arnold 1973, Cerato & Lutenegger 2002, Yukselen & Kaya 2006, and Jotisankasa et al. 2009). The stepwise instruction is provided in the above-mentioned references. The SSA of the soil presented in this chapter is 25.9 m^2/g which is the average of the three measurements employed in this research.

4.3.2 Proctor compaction

Compaction only reduces the air fraction of voids. In theory, the most effective compaction process should completely remove air fraction. However, in practice, compaction cannot completely eradicate air fraction, only reduces it to a minimum.

The soil-fiber composite was compacted in three layers, each with 25 blows in the standard Proctor mold, following the ASTM D698 using the standard effort of 600 $kN.m/m^3$. The mixture for compaction was prepared by first mixing a measured amount of dry soil (about 2 kg for each test) with a predetermined amount of water. In case of fiber addition, the weight of specific fiber content was calculated based on the weight of the dried soil. The required amount of fiber was first mixed with the dry soil and then water was gradually added. Mixing continued until a uniform mixture was produced. The fiber inclusion was 0, 0.5, 1, 2, and 3% of total soil-fiber weight.

The compaction curve usually represents the relationship between the molding water content of the soil and its dry unit weight or dry density. As Figures 4.4 and 4.5 show, after the compaction of soils by an increase in fiber content maximum dry density decreased

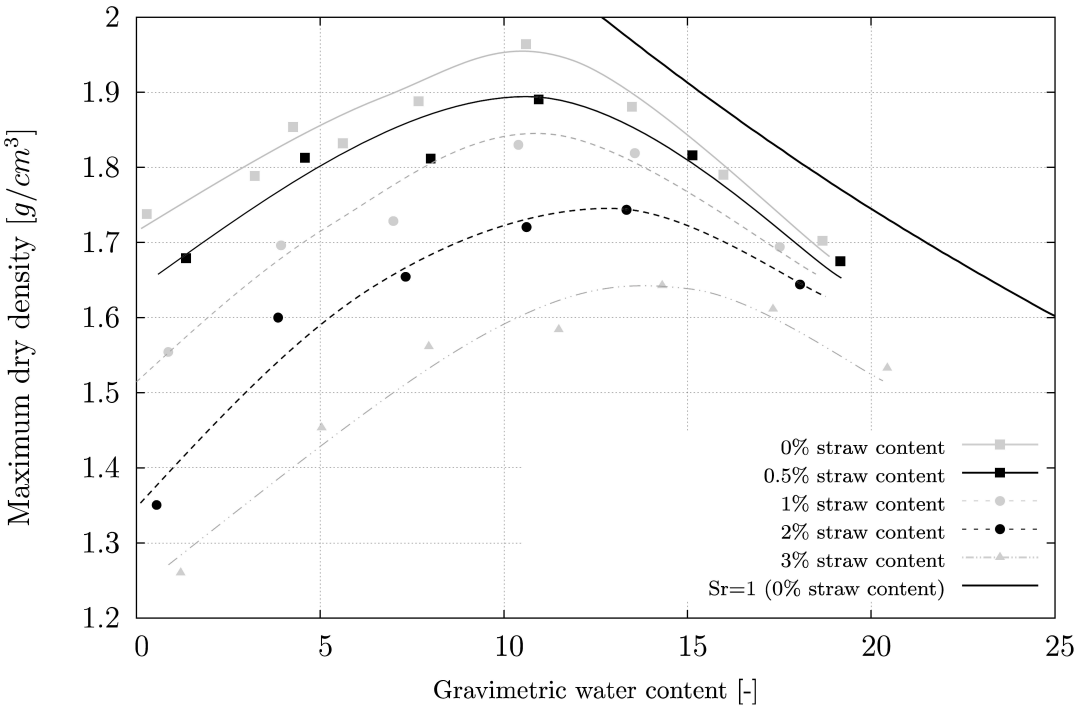

Figure 4.4: Compaction curves of unreinforced and reinforced soils with straw fibers.

and optimum water content increased. Both are almost linear functions of straw content in the range of 0 to 3% gravimetric inclusion. As explained in Section 3.7.3.2, most of the studies working on proctor compaction of fiber-reinforced soils declared that with an increase in fiber content the optimum moisture content increases but the maximum dry density decreases.

The decrease in density was most likely a result of the less specific weight of fiber filaments in comparison with the soil grains and the elasticity of fibers that prevent the soil particles approaching each other. And the increase in moisture content was most likely the result of the greater water absorption capacity of the fibers than that of the surrounding soil (see Figure 4.3).

4.3.3 Scanning electron microscopy (SEM)

SEM photos of the fiber-reinforced soil used in this study are shown in Figure 4.6, taken in the center of scanning electron microscopy of Ruhr-Universität Bochum. As explained in Section 2.2.1, after the compaction of a clay-sand mixture clay clusters do not change

their bonding and connection between sand grains and clay clusters are mostly frictional (see Figure 2.2c). Figure 4.7 shows a SEM photo of a compacted sand-clay mixture taken by Ghahremani et al. (2007). As we can see in this figure, clay clusters are formed independent of sand grains. But the samples used in this observation were first mixed with water content equal to 1.25 × LL to reach to a soft and uniform slurry and then dried in laboratory conditions. In slurry conditions clay clusters opened and had a possibility of changing their arrangement during drying. In this situation clay platelets covered the sand grains and also made connections between them which worked as solid bridges (see Figure 2.2e). They are the main reason for the high strength of masonry materials compared to compacted soils. As can be seen in Figures 4.6a and 4.6b, sand grains are covered with clay platelets and connected to each other via solid bridges, and no sand-sand connection is observed. Figures 4.6d and 4.6e show that the fibers' surfaces were covered by many clay minerals which made the contribution to bond strength and friction between the fiber and soil matrix. Also, as shown in Figure 4.6c, at some points clay platelets penetrated even into very thin vessels of straw, which was another reason for increasing the strength of the bondings between the soil matrix and straw filaments. Due to these connections straw pieces limited movement of soil particles during volume changes. This phenomenon considerably reduced swelling and shrinkage of the reinforced soil.

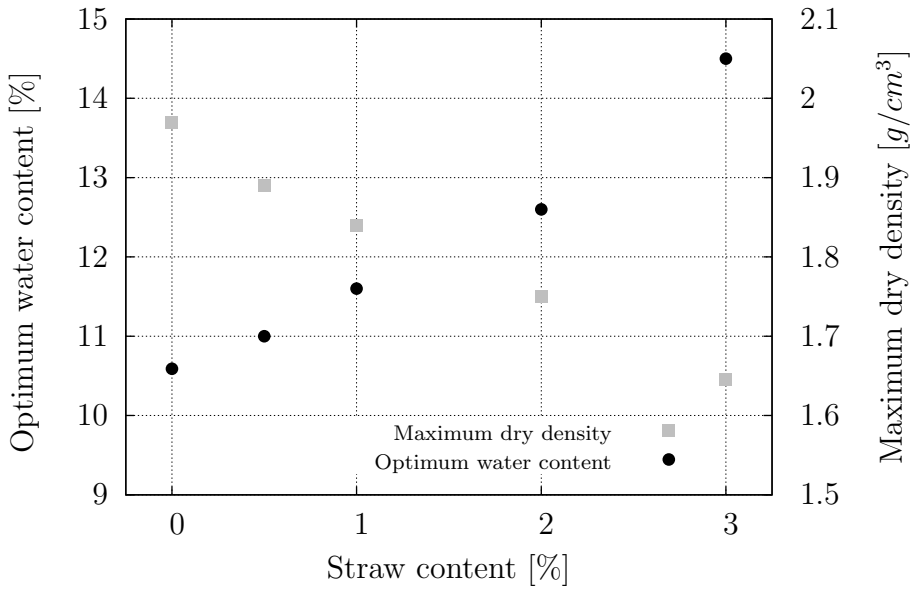

Figure 4.5: Optimum water content and maximum dry density vs. straw content.

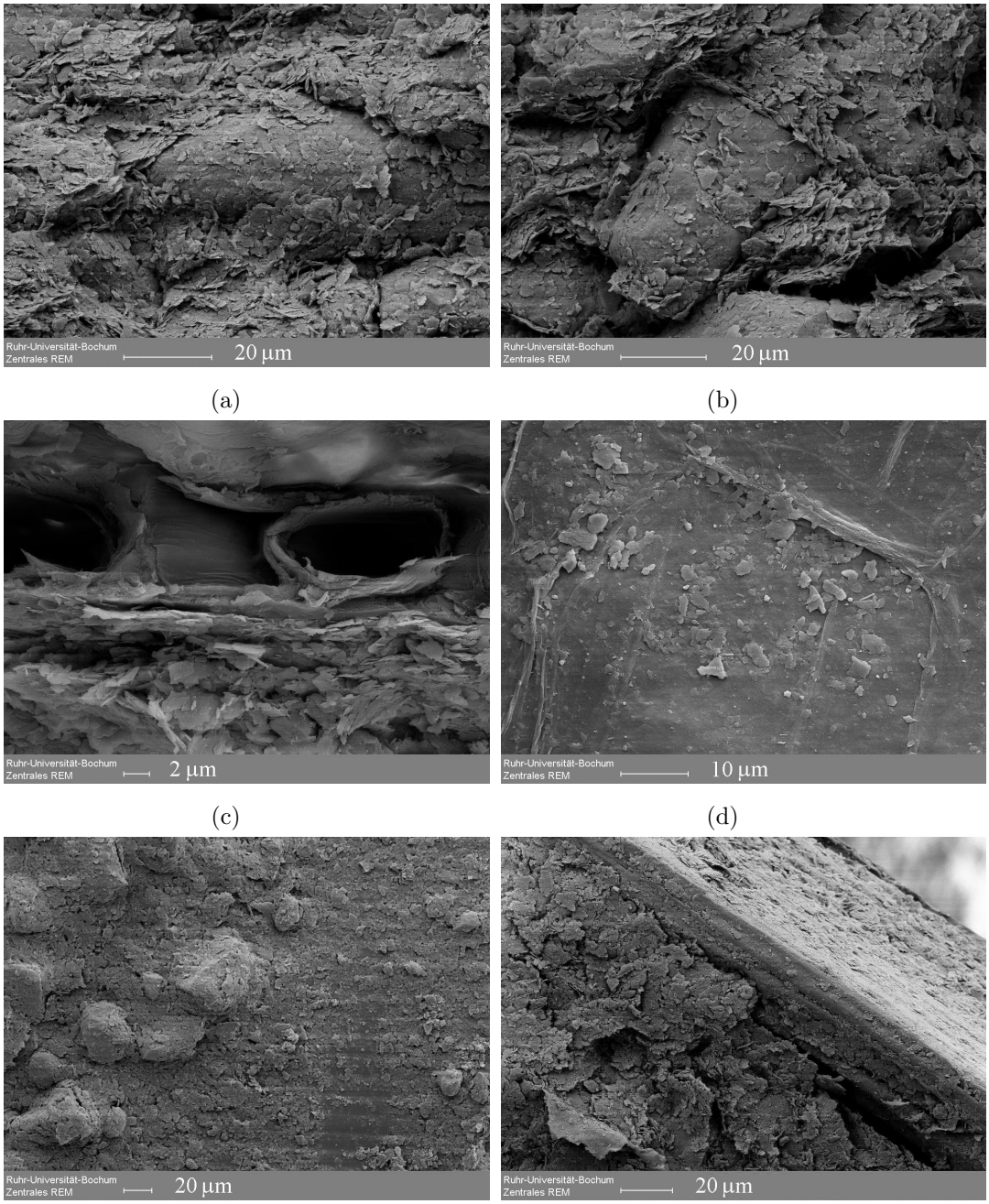

Figure 4.6: Scanning Electron Microscopy (SEM) photos taken from dried sample: (a) sand grains are covered with clay platelets; (b) connection between sands are through formed clay clusters; (c) penetration of clay platelets inside vessels of straw; (d) connection between clay and surface of straw; (e) connection between sand grains and surface of straw are through clay clusters; and (f) separation between soil and straw due to shrinkage.

Figure 4.7: Scanned electron microscopy photo of mixture of 60% sand and 40% clay (Ghahremani et al. 2007).

4.3.4 Porosimetry

In this research the pore size distribution obtained from the mercury intrusion porosimetry (MIP) method was used to study the micro-structure of straw-reinforced soils. In this technique a non-wetting liquid (here mercury) is intruded to a sample with various pressures in a porosimeter device. The pore size distribution can be determined from the external pressure required to push the liquid into a pore with a particular size against the opposing force of the liquid's surface tension. Details of this method have been presented in several papers (e.g. Delage et al. 1996, Agus & Schanz 2005, Thom et al. 2007, Arifin 2008, etc.).

Pore size distribution curve for three materials was analyzed and drawn; namely unreinforced and reinforced soils with 1% straw content, but with different lengths of 1 and 20 mm. The void ratios obtained by this observation were not the same as calculated from measuring the mass and volume of samples (the effect of straw length on void ratio will be explained in Section 7.2.2). In Table 4.2 void ratios are presented and compared. Void ratios derived from porosimetry were smaller to those of mass-volume measurements. The reason for this could be due to the size of the sample which was relatively small in MIP observation ($5\times5\times5$ mm). Such a small sample might not include as many large pores as exist in larger samples. As we see in this table, the largest difference was found in

the reinforced sample with 20 mm straw filaments. This matter was probably due to the absence of large straws thicker than 3-5 mm which could not exist in the small sample.

In spite of the differences in void ratios, the pore size distribution curves of the three materials mentioned above had a similar trend. Figure 4.8 shows the cumulative volume of voids in mm^3/g. This figure shows that for all the materials the majority of pores were in the range of 0.1 to 1 μm. Although the unreinforced material had a smaller void ratio, its distribution over pore radius was similar to those of reinforced materials.

Table 4.2: Void ratios obtained from MIP and from mass-volume calculations.

Material	Void ratio from porosimetry	Calculated void ratio
0% Straw	0.33	0.39
1% Straw content (1 mm)	0.39	0.42
1% Straw content (20 mm)	0.40	0.55

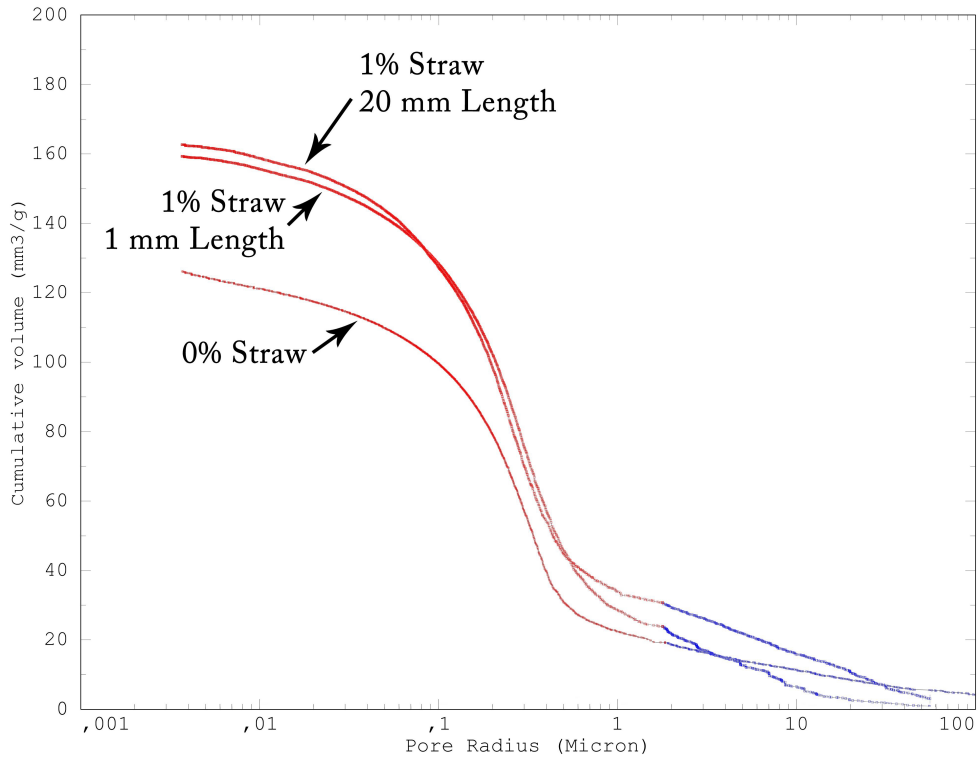

Figure 4.8: Pore size distribution curves for unreinforced and reinforced soil with 1% straw content, with 1 and 20 mm length.

4.4 Experimental program

Besides the primary and prerequisite tests and observations explained above, the laboratory program of this study consisted of experiments to obtain the effect of fiber-reinforcement on the soil-water characteristic curve of fine-grained soil, shear tests using a biaxial device to investigate the effect of reinforcement on the shear strength of saturated and unsaturated soils under various suctions, and large scale tests to analyze the rate of uprising moisture under unprotected unreinforced, unprotected reinforced, and protected unreinforced conditions which were also simulated numerically.

As mentioned before, SWCC is the most essential parameter in calculations of unsaturated soils. Series of tests was performed to draw SWCC for soil, presented in Section 4.2, together with its mixtures with different dosages of straw added as reinforcing elements. Whole range of suction required for this material was covered (i.e. from saturated conditions to more than 200 MPa). Methods of applying suction were chosen on the basis of the range of suction, and were the Axis Translation Technique (ATT) and the Vapor Equilibrium Technique (VET). Details are presented in Section 5.2.

In all biaxial tests the specimens, after being prepared, were sheared under drained conditions. Firstly, samples reached the pre-designed suction and then during the test the suction was applied while samples sheared. For all materials biaxial tests were carried out under suctions of 80, 400, 3000, 9500, and 55000 kPa and under saturated conditions too. Several researchers have worked on shear strength of unsaturated clayey soils, but rarely the applied suction exceeds the residual zone. The materials used in the biaxial tests were the soil introduced in Section 4.2, unreinforced and reinforced with 0.5 and 1 % straw content. The selected void ratios for each material and suction depended on the sample preparation method and shrinkage process which are presented in Sections 6.3 and 7.3. The void ratios are summerized in Table 4.3.

For realizing the uprising moisture phenomenon three large scale tests were performed on unreinforced and fiber-reinforced with 1% straw content, and protected unreinforced

Table 4.3: Void ratios of biaxial tests for different straw contents and suctions.

Suction $[kPa]$		Sat.	80	400	3000	9500	55000
Void ratios for:	0% straw	0.45	0.44	0.43	0.39	0.39	0.39
	0.5% straw	0.56	0.55	0.53	0.52	0.52	0.52
	1% straw	0.60	0.59	0.58	0.57	0.57	0.57

materials. The void ratios were similar to those mentioned in Table 4.3 for the highest suction.

Free water table with no back pressure or suction rose up from the bottom surface of the walls. Facades were covered with silicon glue and nylon foils in order to prevent the evaporation and simulate the boundary conditions of impermeable facades of the buildings. Details of these tests are presented in Section 5.4.

4.5 Summary

In this chapter characteristics of soils and fibers used in this study have been presented by determining their mixture and basic properties (i.e. liquid and plastic limits, specific gravity, specific surface area, and proctor compaction curves). For better understanding of sand-clay-straw mixture SEM photos were also taken and discussed in this chapter. In order to observe the effect of straw inclusion and straw length, MIP analyses were carried out and presented.

Moreover, the experimental program which this study followed has been explained for three main tests which were SWCC tests, biaxial tests, and large scale wall tests.

5 Experimental techniques and procedures

5.1 Introduction

This chapter presents the experimental techniques and procedures used in this study. The devices, techniques, and experiments carried out for determination of SWCC are described here. The double-wall biaxial device developed by Alabdullah (2010) for sandy soils is also introduced, as well as the calibrations and modifications done in this study. In addition, the large scale wall tests, including methods of calibration and test procedures, is presented in this chapter.

5.2 Techniques and procedures used for SWCC tests

As mentioned in Section 3.3, SWCC has 2 main paths, namely drying and wetting. In order to draw drying and wetting paths, saturated and dry samples (respectively) must be subjected to constant suctions to loose or receive water until they reach the equilibrium condition. In this study two methods were implemented for controlling the suction, the Axis Translation Technique (ATT) for suctions $< 1500\ kPa$ and the Vapor Equilibrium Technique (VET) for suctions $> 2000\ kPa$.

5.2.1 Sample preparation

Sample preparation in this study followed the traditional adobe preparation method (the brick preparation method is explained in Section 2.2). The mixtures introduced in Section 4.2 and with various straw contents described in Table 4.1 first were mixed with 1.25 $\times$ LL to produce a uniform slurry. These saturated slurries with void ratio of 0.7, 0.705,

0.72, 0.74, and 0.77 for unreinforced soil, and reinforced soils with 0.5, 1, 2, and 3% straw contents respectively, were the initial points of drying paths of SWCC.

Plexiglas rings with a diameter and height of 50 and 15 mm were filled with the slurries to be placed in the pressure plate or desiccators. To be sure that the samples were fully saturated they were placed over saturated porous stones and covered with nylon foil. After a few days in these conditions the samples reached constant weights. These weights were supposed to be equal to the pre-calculated weight of saturated samples, and as such they were assumed to be fully saturated. During this process, since the samples started from saturated uniform slurries, the increase in their weight was very low or even zero.

As will be presented in Sections 6.2 and 7.2, samples with various straw content shrank dissimilarly and reached different void ratios. Completely dry samples with different void ratios (as a function of straw inclusion) were initial points for wetting paths, because in reality dry adobes are used in the construction of masonry buildings which are already shrunk.

5.2.2 Pressure plate apparatus (for ATT)

The pressure plate extractor is a well-known testing device for determination of the relationship between the degree of saturation, volumetric water content, or gravimetric water content and suction in a soil (ASTM C1699-09). The axis translation technique, introduced by Hilf (1965), is used in this device for applying suction to the samples. In this study the pressure plate extractor was used to apply suction values between 10 to 800 kPa with three ceramic discs with different air-entry values used depending on the applied suction (100, 500, and 1500 kPa discs). High air-entry ceramics are not always desirable, as due to their very low coefficient of permeability sometimes an equilibrium takes several months. Figure 5.1 shows the schematic setup and a photograph of this device.

The tests started with the saturation of the ceramic disc by placing it under deaired water. Afterwards, in order to remove all the air bubbles from inside the ceramic disc, it was subjected to water pressure less than its air-entry value in the pressure plate apparatus. In this way the water followed through the ceramic disc and brought the air bubbles out. This water pressure lasted until no bubbles were seen in the out-flow pipe.

Diffused air bubbles in the water results in discontinuity between the specimen's pore water and the source of water. During the testing procedure, in order to be sure that the ceramic disc is saturated and to remove the diffused air bubbles collected underneath,

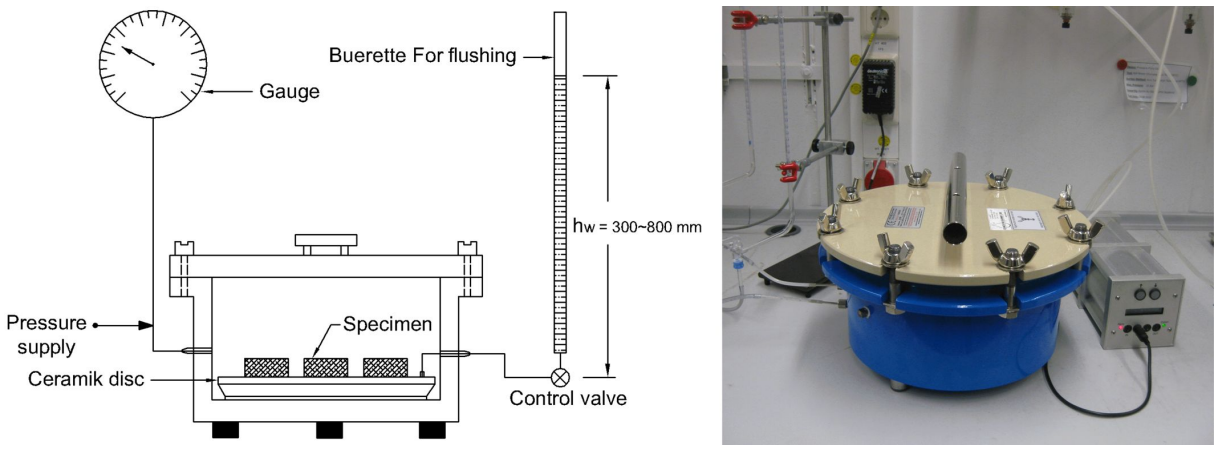

Figure 5.1: Schematic sketch and a photograph of the pressure plate device.

flushing of the water compartment was carried out periodically. Same procedure that was done at the beginning of the test was repeated for each period of flushing. Of course, during flushing samples were kept in a small closed chamber so as not to lose their water content by evaporation.

The specimens were weighed from time to time until equilibrium occured. A precision balance with an accuracy of 0.0001 g was used to weigh the specimens. In this situation the dimension of the specimens were monitored using a vernier caliper with an accuracy of 0.01 mm. When all specimens in the apparatus reached equilibrium, the next step of suction could be applied.

5.2.3 Desiccators (for VET)

The Vapor Equilibrium Technique (VET) has been used in several research studies for the determination of the soil-water characteristic curve of clayey soils (e.g. Croney & Coleman 1961, Agus et al. 2001, Blatz & Graham 2003, Schanz et al. 2004, and Al-Badran 2011).

Generally, the VET can be used to control almost the whole range of total suction. But the use of VET for applying total suction less than 2000 kPa suffers from inaccuracies since this technique is extremely sensitive to temperature gradient between the salt solution, the vapor space, and the soil specimen (Agus & Schanz 2003). If the temperature fluctuation can be maintained at as high as 0.5 $°C$, the VET can be used to apply and control the suction higher than 1000 kPa (Arifin 2008).

Several salt solutions were used to induce total suction to the specimen by changing the relative humidity of the vapor space in the desiccators. The relative humidity of the

vapor above the salt solution was verified using the chilled-mirror hygrometer technique. The chilled mirror hygrometer used in this study was a water activity meter type 3TE produced by Decagon Devices Inc. (Figure 3.2). Figure 5.2 shows the vapor equilibrium technique schematically and a photograph of the arrangement.

Procedures similar to those used in the pressure plate apparatus (ATT) to determine the changes in water content and void ratio were adopted here. At the end of the test, the relative humidity of the solution was measured using the chilled mirror technique to compute the actual total suction applied to the specimens.

5.3 Techniques and procedures used for plane strain tests

The so-called "Biaxial Apparatus" was used in this study to measure plane strain shear strength of unsaturated material. This device has been developed in Bauhaus-Universität Weimar, Germany, by Alabdullah (2010), also mentioned in Schanz & Alabdullah (2007). The device was designed to apply suction via ATT up to 100 kPa, but in this study with minor modifications the applied suction increased to the whole VET range.

The device consisted of two cells (i.e. the outer and inner cells), base platen and top cap equipped with porous and ceramic discs. The required connections and valves were provided to facilitate the application of the inner and outer cell pressures, pore-air pressure, and pore-water pressure. All data, such as volume changes, applied load, and vertical displacement were recorded by a data acquisition system connected to a computer. The device and its equipments are explained in the following sections.

5.3.1 Sample description

The rectangular (prismatic) soil specimen of this test had a 120 mm height, 100 mm width, and 40 mm thickness. The deformation was restricted ($\epsilon_2 = 0$) along the long dimension of the cross section by two immovable side steel platens (i.e. the specimen had a constant width of 100 mm). Figure 5.3 shows the geometry of the specimen and deformation conditions. The slenderness ratio is defined as the ratio of the height of the specimen to the dimensions within which the specimen is free to deform. In this study, the slenderness ratio was $120/40 = 3$. The high slenderness ratio was chosen to allow free formation of shear band without reflecting on the end platens. Desrues (1995) observed that for specimens with a slenderness ratio of 2 the shear band reflected to the end platen or deviated towards the corner.

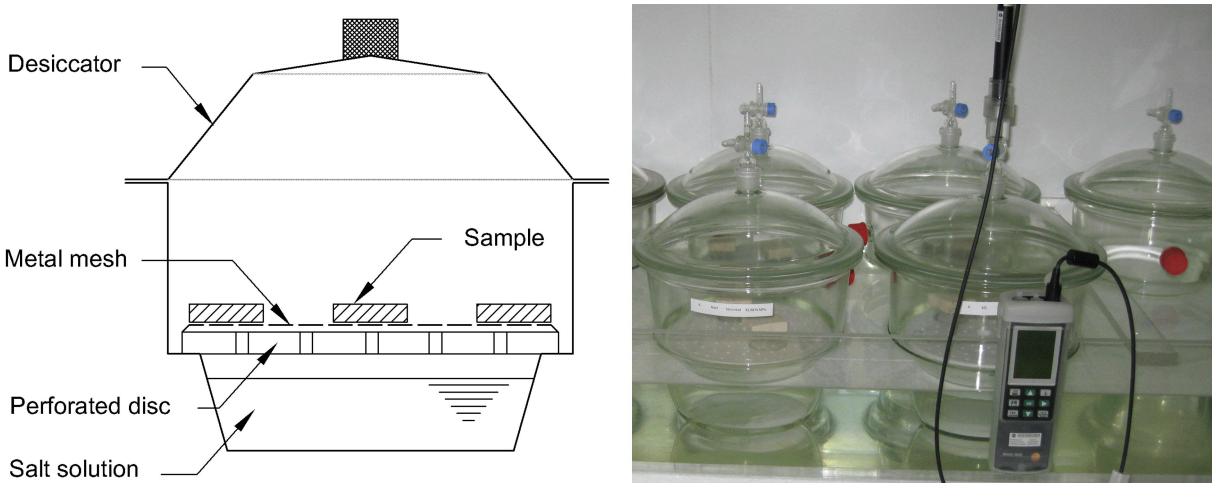

Figure 5.2: Schematic sketch of VET and photograph of the desiccators used.

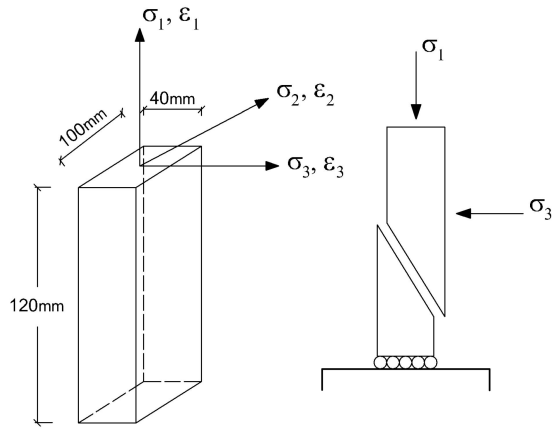

Figure 5.3: Geometry of the specimen, stress and strain conditions (Alabdullah 2010).

5.3.2 Biaxial device

Biaxial apparatus used was a double-wall device which consisted of several parts and pieces: loading frame and pistons, inner and outer cells, top cap, bottom platen, side platens, draining pipes and connections (for saturated samples), system of applying suction (for unsaturated conditions), volume change indicators, membrane and O-rings, air and water pressure suppliers and controllers, load cell, pressure transducers, linear variable differential transformer (LVDT), and data loggers. Listed parts are shown in Figures 5.4, 5.5 and 5.6. All data produced during the test (from load cell, pressure transducers, LVDT, and volume change indicators) were logged automatically onto a computer using a software called HP-Vee version 5.01 produced by Hewlett-Packard Co.

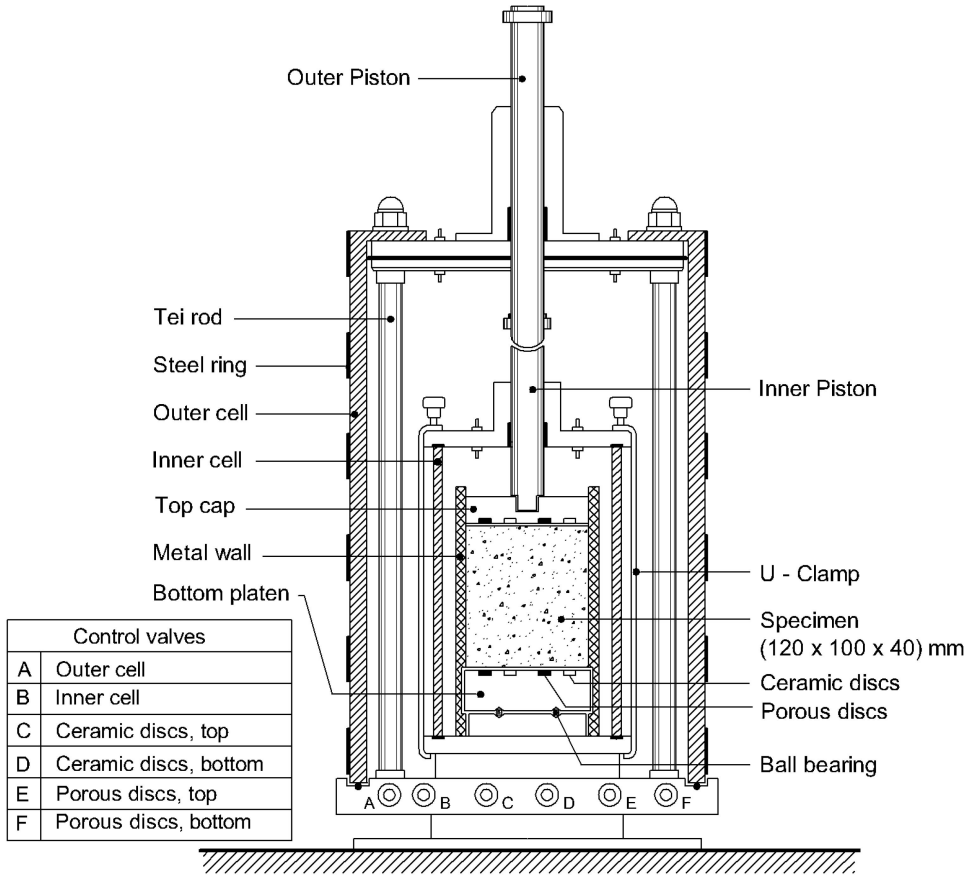

Figure 5.4: Schematic diagram of biaxial apparatus (Alabdullah 2010).

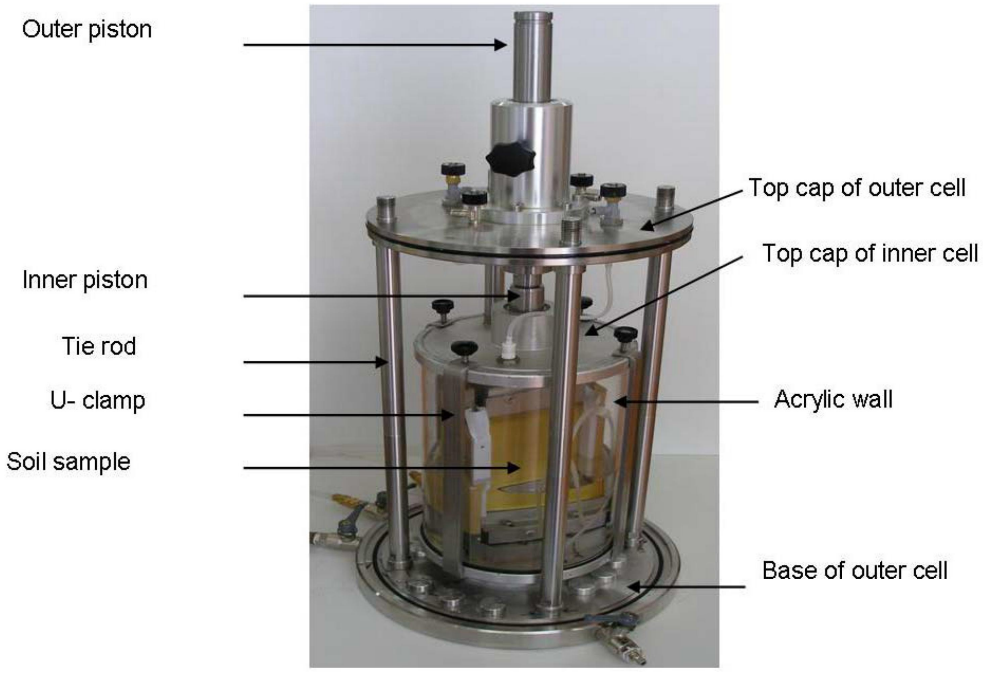

Figure 5.5: Photograph of biaxial apparatus without outer cell (Alabdullah 2010).

5.3.2.1 Loading system

Loading system consisted of a loading frame, outer and inner pistons, and a load cell. The frame can be seen in Figure 5.6. This frame was capable of applying static forces to the specimen with minimum deformation rate of 0.0001 mm/min. Two load cells with maximum capacities of 10 and 50 kN were used in this study, depending on the range of applied axial loads. As shown in Figure 5.6, the load cell was installed above the outer piston and below the horizontal beam of the frame.

The outer and inner pistons with diameters of 30 mm carried the axial load from frame to the sample. The outer piston penetrated the top cap of the outer cell, and the inner piston penetrated the top cap of the inner cell. Due to the fact that the cell pressure was the same inside and outside the inner cell, there was no hydraulic gradient between point 1 and point 2 in Figure 5.7, and no leakage was expected between the shaft and the inner loading piston. This will avoid errors in volume change measurements caused by water leakage.

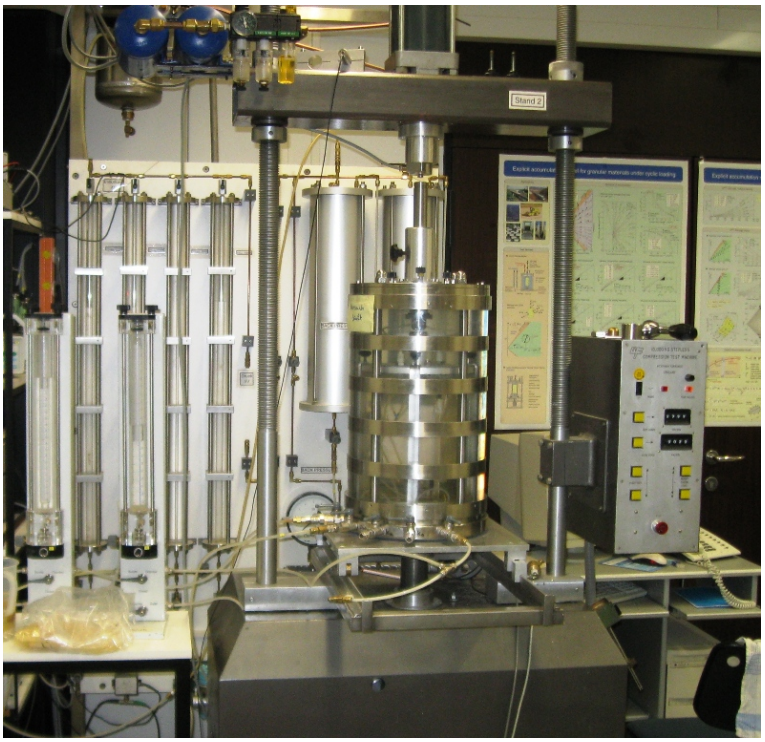

Figure 5.6: The biaxial cell installed and placed in the loading frame.

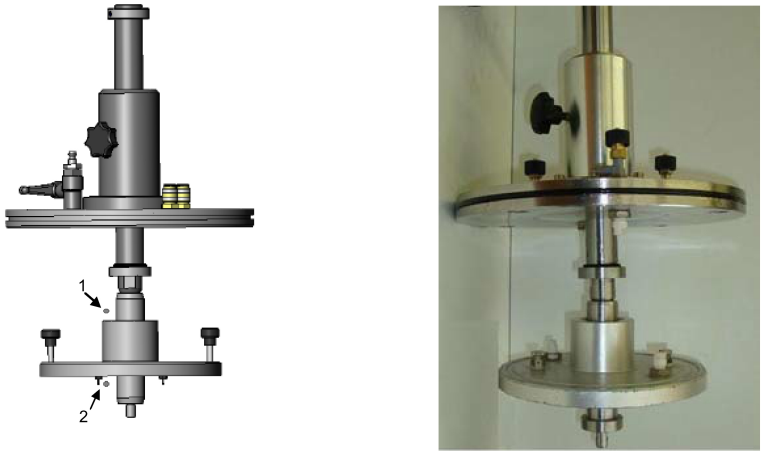

Figure 5.7: Outer and inner pistons (Alabdullah 2010).

5.3.2.2 Double wall technique, inner and outer cells

In order to measure volumetric changes for unsaturated samples a so-called "double-wall technique" was implemented, in which the sample was mounted inside two concentric cylindrical cells. Figure 5.8 shows the principle of the double-wall technique. As shown in this figure, in this system both inner and outer cells are pressurized by the same value of pressure during the test. Theoretically no volume change (expansion or contraction) is expected from the inner cell and the transport of water inside the inner cell observed during the test will be assumed to be the volumetric change of the soil specimen tested, after required corrections and calibrations.

Bishop & Donald (1961) introduced the double cell technique with an open inner cell device. The liquid of the inner cell was mercury whereas the outer one was filled with water. The changes in the level of the mercury surface were observed by the movement of a stainless steel ball floating in the mercury. Cui & Delage (1996) implemented same technique, but both inner and outer cells were filled with water, while a thin layer of silicon oil separated the cell liquids. Yin (1998) proposed almost the same system of Bishop & Donald (1961), but with water (instead of mercury) to fill the open-top cylindrical container, whereas the outer cell was filled with air. Later, Ng et al. (2002) developed a double-wall triaxial cell using deaired water to fill the inner and outer cells. Ng et al. (2002) proposed a double-wall cell but with an open-top bottle-shaped inner cylindrical container achieving a more accurate reading in the changes of the water surface in the container. Mendes et al. (2012) introduced a new double cell triaxial device. They used a glass inner cell to avoid any water absorption.

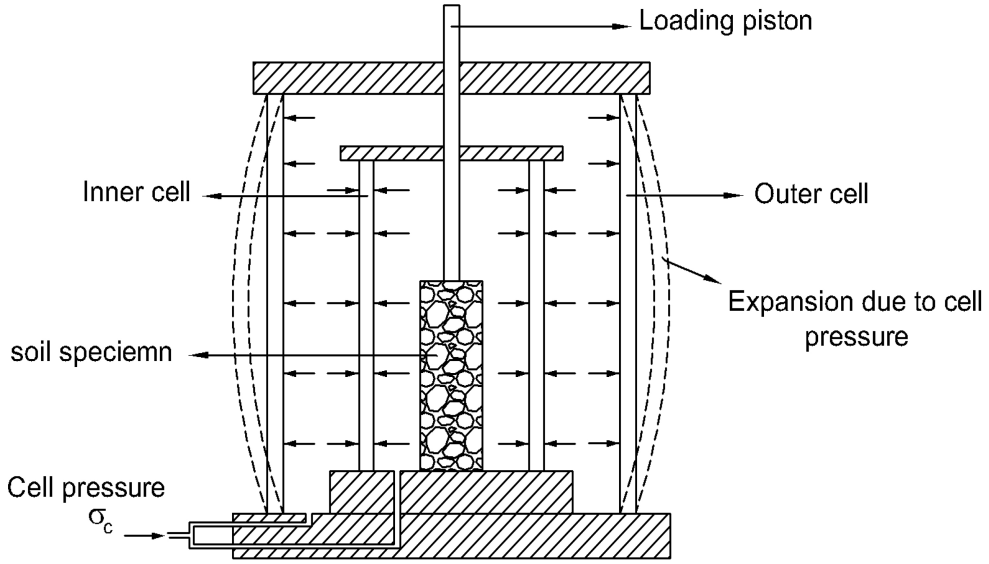

Figure 5.8: The concept of double-wall cell.

In this study two cylindrical cells were used as inner and outer cells, both made from high quality acrylic and filled with deaired water. Their dimensions are presented in Table 5.1. The outer cell was reinforced with steel bands (rings) to sustain confining pressures up to 1000 kPa, whereas no metal or fiberglass reinforcing ring was needed for the inner cell. In Figure 5.4 the inner and outer cells are shown schematically. In Figures 5.5 and 5.6 photographs of inner and outer cells can be seen respectively.

The top cap of the outer cell is equipped with four plugs for air bleeding. Two of these plugs are connected to the top cap of the inner cell. These connections facilitate filling and emptying the inner and outer cells. Figure 5.7 shows the top caps of inner and outer cells. The top cap of the inner cell was placed over it and fixed with four U-shape clamps to the pedestal (see Figure 5.4) in order to avoid any volume change due to vertical movement of the cap.

Table 5.1: The dimensions of the inner and outer cells.

	Inner cell $[mm]$	Outer cell $[mm]$
Diameter	175	270
Height	270	470
Thickness of the acrylic wall	5	8

5.3.2.3 Side platens, top cap, and bottom platen

Figures 5.9a and 5.9b show top cap, bottom platen, O-rings, and two stainless still plates (which were in contact with the sample through filter papers). Three pairs of such plates were used in this study: (1) with two 100 kPa air-entry ceramics and two porous discs; (2) with two 500 kPa air-entry ceramics and two porous discs; and (3) with four porous discs. Plates (1) and (2) were used for unsaturated conditions with the ATT method and plate (3) for saturated as well as unsaturated conditions with the VET method. In the following section the systems of applying suction will be explained.

The porous and ceramic discs were glued to the metal plates using an epoxy resin on its periphery. A tight seal between the disc and metal plate ensured that air would not leak into the water compartment under the ceramic disc. To isolate the pore-water phase from the pore-air phase, four O-rings were used between the metal plate and the top cap or the bottom platen. Figures 5.9c and 5.9d show schematic cross sections of these systems.

The plane-strain condition was imposed using two immovable stainless steel walls with 15 mm thickness and 101 mm width. Two 0.25 mm teflon sheets lubricated with silicon grease were used to reduce friction between the membrane and the metal side wall. Teflon sheets and silicon grease were used also by Wanatowski (2005) to reduce the side friction. Silicon grease was used in biaxial devices by Tatsuoka et al. (1986) as well.

To reduce the friction between the bottom end platen and the cell base, ball bearings with a slide were provided at the base of the sample. This anti-friction system allowed the translation of the lower portion (block) of the specimen relative to the top portion after the onset of the shear band. In Figure 5.10 immovable side walls and bottom end platen equipped with ball bearings are shown. Other techniques have also been cited in the literature to reduce the end restrain effect such as a greased membrane (Oda & Kazama 1998 and Wanatowski 2005) and pillow block bearings (Alshibli et al. 2004).

In the present study a rectangular latex membrane was used. The membrane had a 0.4 mm thickness and 200 mm height. Figure 5.11 shows the prismatic-shape membrane before it is cut to the desired height of the specimen. Due to the special shape of the specimen and membrane, the O-rings with their circular shape could not fit the membrane to the top cap and bottom platen. Therefore, four metal plates were predicted to tighten the membrane at the periphery of the top cap and base platen. In Figure 5.11 the tightening metal plates can be seen.

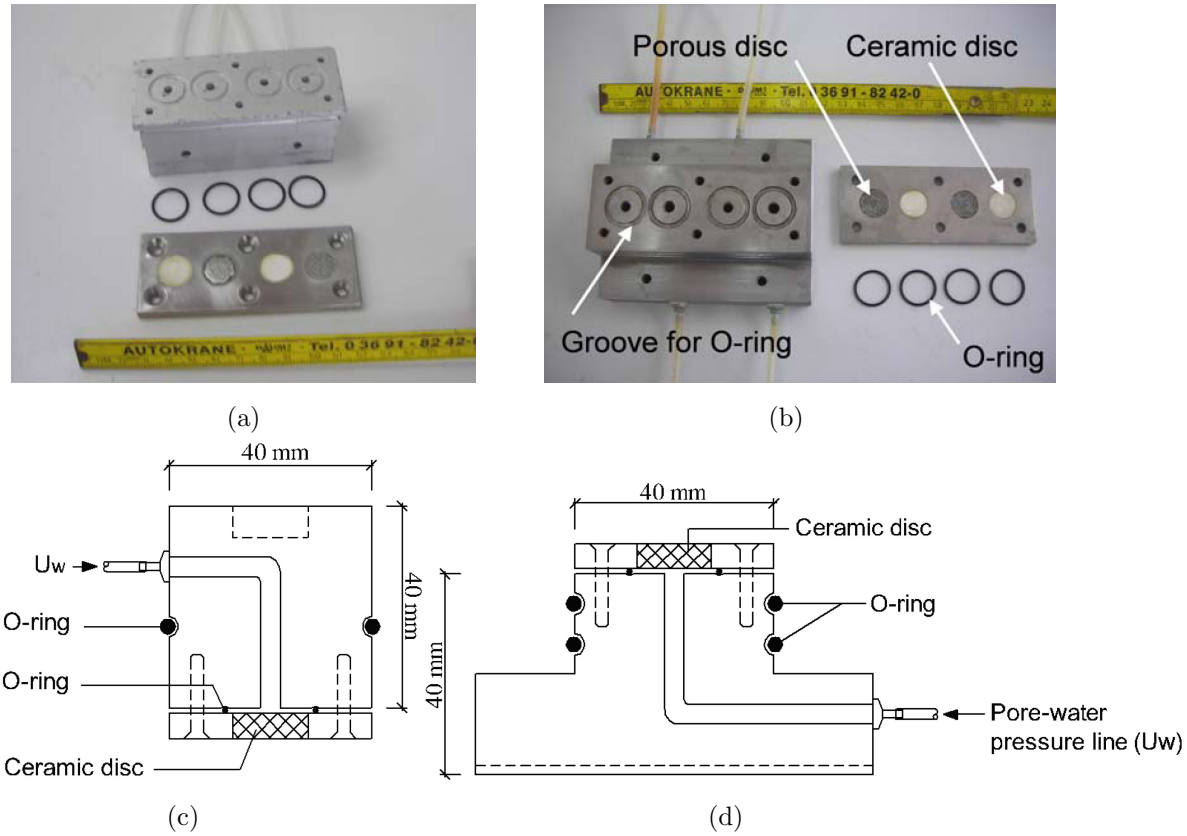

Figure 5.9: Photographs of (a) top cap and (b) bottom platen, schematic cross section of (c) top cap and (d) bottom platen (Alabdullah 2010).

Figure 5.10: Ball bearings and immovable side walls covered with teflon sheets.

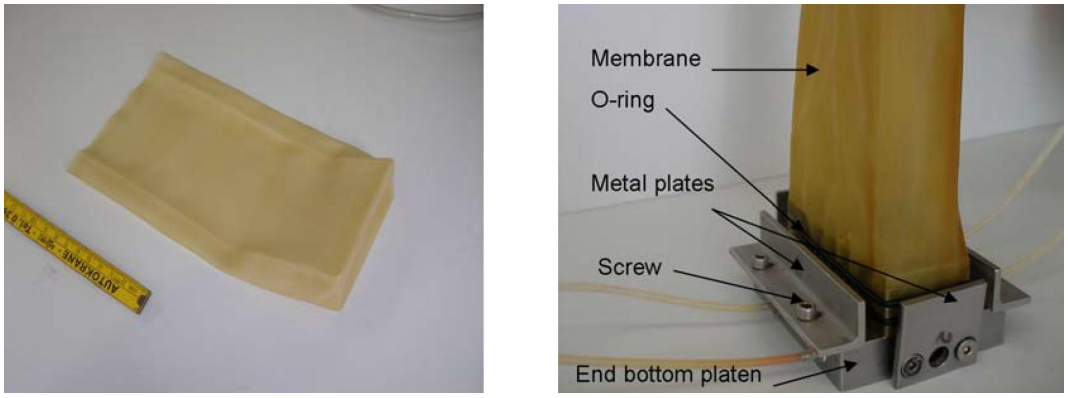

Figure 5.11: The membrane and its installation to the platen (Alabdullah 2010).

5.3.2.4 Systems to apply suction

As mentioned in Section 4.4, biaxial tests were performed under saturated and unsaturated conditions. Applied suctions had a wide range from 80 to 55000 kPa. For 80 and 400 kPa the ATT method and for 3000, 9500, and 55000 kPa VET method were used.

The porous and ceramic discs were used to apply pore-air and pore-water pressures (u_a and u_w) to the soil specimen. The ceramic discs and the porous discs were fixed to the metal plate as shown in Figure 5.9. The metal plates can be simply replaced with other plates equipped with ceramic discs with higher air-entry value, enabling the application of higher values of matric suction and thus testing unsaturated soil in a wide range of matric suctions. In this research 100 and 500 kPa ceramic discs were used. Figure 5.12 shows the schematic setup of applying suction via ATT in this study.

This device was able to apply gradient of suction, so that both the pore-water pressure (u_w) and pore-air pressure (u_a) could be independently controlled at the top and bottom of the specimen. In this way, a suction gradient could be applied enabling investigation of soil characteristics such as permeability and compressibility under suction gradient. Gradient of suction was not within the scope of this research.

The vapor equilibrium technique (VET) has also been used in several studies for controlling total suction in unsaturated oedometer and triaxial tests (e.g., Cuisinier & Masrouri 2002, Lloret et al. 2003, Blatz & Graham 2003, and Al-Badran 2011). The concept of this method is explained in Section 5.2.3. For controlling higher suctions in the biaxial device, vapor produced from salt solutions with given molalities of various salts was circulated

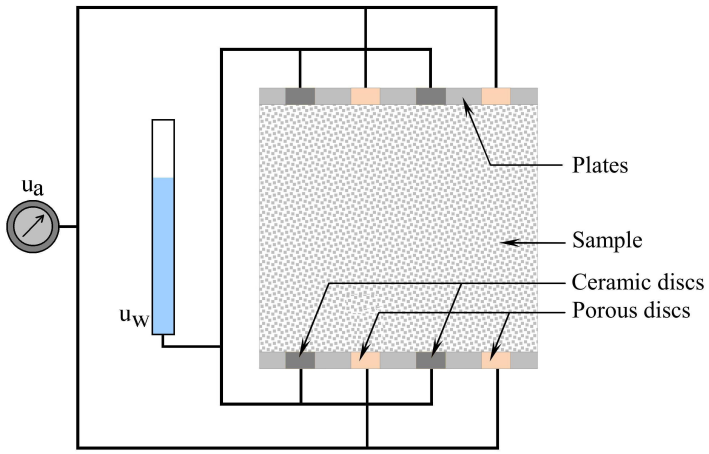

Figure 5.12: Schematic setup of applying suction via ATT (this figure is not scaled).

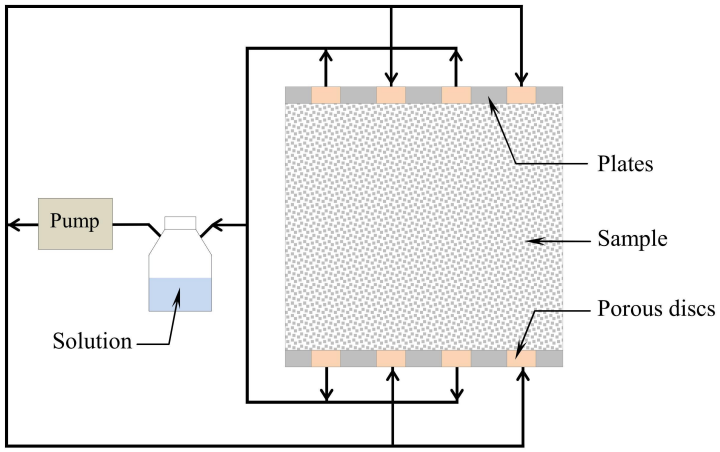

Figure 5.13: Schematic setup of applying suction via VET (this figure is not scaled).

over the sample. This circulation was carried out using a pump as schematically shown in Figure 5.13. The top and bottom metal plates with four porous discs were used here. Saturated tests had also been performed by the same metal plates. The salt solutions used for controlling suction in the biaxial device were the same as the solutions in the desiccators of the SWCC tests. But to be sure that the produced suctions were still the same as they were during SWCC tests, before starting each biaxial test the suction was measured by the chilled mirror. For more details see Section 5.3.4.

5.3.3 Calibrations

To enable the biaxial device to be used accurately in unsaturated soil testing, it was essential to calibrate it for the following items: apparent volume change measured by

volume change indicators, load cells, pressure transducers, ram displacement measured by LVDT during the shearing, and pressure suppliers used for controlling water pressures.

5.3.3.1 Calibration of volume change indicators

Two volume change indicators were used to measure the volume change of the pore water phase and the overall volume change of the specimen, which corresponds to the volume changes of inner cell. One of the volume change indicators which measured the inner cell volume changes was installed on the board behind the biaxial device (as seen in Figure 5.6), and the other one from which changes in the sample's pore water phase were measured was a mobile buret. Both volume change indicators were calibrated by a thin buret with an accuracy of 0.1 ml. Deaired water was filled and - in a separate path - drained stepwise from the indicators into the thin buret. At each step one reading was taken and recorded onto the computer. The relation between readings and the applied values of volume change (read from the thin buret) was almost linear oscillating around 1-1 line as shown in Figure 5.14.

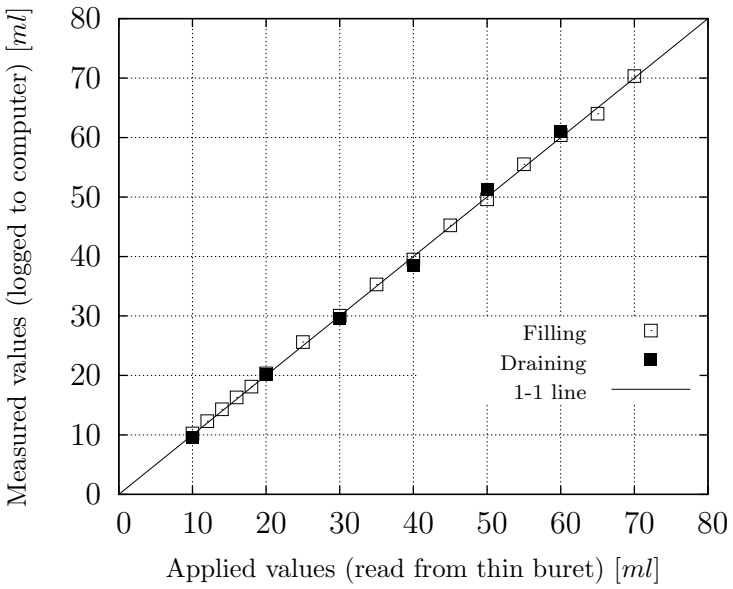

Figure 5.14: Calibration of the volume change indicator installed on the board.

5.3.3.2 Calibration of inner cell volume change

Theoretically no volume change is expected to occur in a double-wall cell system, but volume changes may occur in the inner cell for several reasons. The most important factors affecting on inner cell volume changes are:

- Time delay in pressurizing inner and outer cells (Sivakumar 1993)
- The absorption of water by the acrylic inner cell: Wheeler (1986) coated the inner cell's surface with waterproofing material to limit absorption. Mendes et al. (2012) replaced the acrylic inner cell with a glass cell in order to avoid any absorption. All these trails and measures failed to prevent the absorption by the wall of the inner cell.
- The compression of water within the inner cell: Wheeler (1986) stated that the compressibility of water accounts for about one third of the total volume changes of the inner cell.

In this study the inner cell was made of acrylic materials and was kept always in water even when the test was not running and the device was open. In this way, the acrylic cell took its maximum capacity of water in, and no more water could be absorbed during the test by the cell.

Compressibility of water caused no error in data in this research. Because the shearing did not start before or immediately after increasing the cell pressure, but as will be explained in experimental procedures (Section 5.3.4) the shearing started a minimum of three days after the beginning of the constant situation (i.e. suction and cell pressure).

However, the inner cell was pressurized equally from both sides; it showed a small amount of creep over time. This creep was calibrated using a metal dummy. The overall slow volume change that accrued after the immediate change was assumed to be creep, while the acrylic cell had absorbed as much water as it could before the test. The cell pressures for this observation were 50, 100, and 150 kPa. Figure 5.15 shows the inner cell's creep for various pressures versus time. In these curves creep is normalized by dividing it by dummy's volume ($40\times100\times120$ mm). As we can see in this figure, after around three days volume change reached its stabilized value. The creep depends not only on the cell's material and pressure, but also on the setup of the device (for example how tight the screws and clamps are, which could vary from test to test). Therefore, before performing a test the cell pressure had been applied and kept constant for three days.

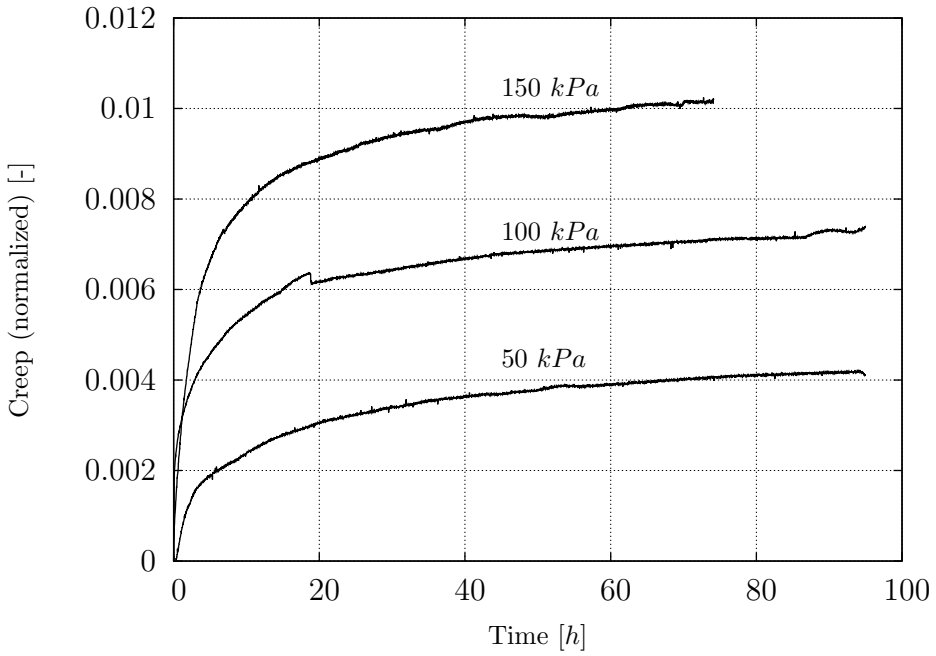

Figure 5.15: Inner cell's normalized creep for various pressures; cell pressures are written on the curves.

Finally, the reliability of measured volume change was checked by testing a saturated sample in isotropic compression conditions. For a saturated sample, the volume change of the specimen during the test (water exchange of the inner cell) must be equal to the volume of water drained from the specimen.

A saturated Silver sand specimen was prepared with an initial void ratio of 0.6. The cell pressure was applied simultaneously to the outer and inner cells. The volume change of the saturated specimen was measured using two methods: with double wall technique (i.e. by measuring the volume changes of the fluid in the inner cell), and the volume of water expelled out from the specimen.

In this experiment, as mentioned before (in order to eliminate the effects of creep and cell's water absorption on results), the draining valve of the sample was left open for three days from the start of pressurizing the cells. Three separate tests with cell pressures equal to 50, 100, and 150 kPa were carried out. Figure 5.16 shows the volume changes measured by the two methods versus the applied confining pressures. The measurements showed good agreement between the volume changes measured by both methods.

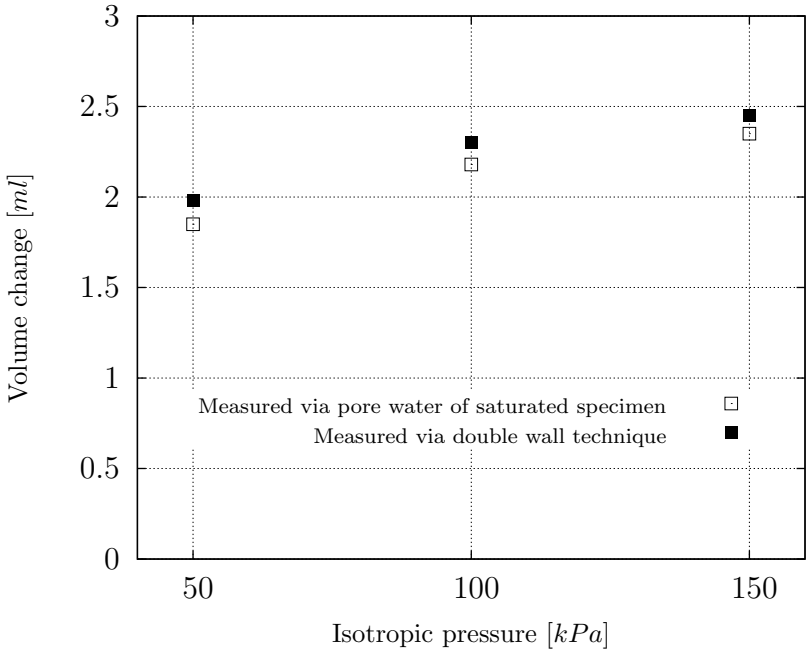

Figure 5.16: Volume changes of saturated sample measured by two methods.

5.3.3.3 Calibration of other parts

The load cells installed above the device were calibrated using a simple lever. By adding counterweights certain amounts of load were applied to the load cells, and simultaneously data of load cells were logged by the software HP-Vee. Load cells were calibrated by comparison of measured and applied loads.

Water pressure at different points of the experiment (i.e. inside saturated samples, in inner and outer cells) were checked by pressure transducers during the test (Figure 5.17a). The data were recorded using the software mentioned above. These sensors were calibrated using a precise differential pressure meter (Figure 5.17b).

Using an LVDT the axial deformation of the sample during shearing was measured. This device was calibrated with a micrometer screw gauge with an accuracy of 0.01 mm installed on a stand (Figure 5.17c).

Air pressure controllers (Figure 5.17d) were used to apply and control the confining pressure in the inner and outer cells, as well as pore-air and pore-water pressures. The accuracy of the applied pressure was of great importance, specially in testing the soil under low

confining pressures or low matric suctions. Since the minimum and maximum applied pressures were 50 and 550 kPa, a range of 50 to 600 kPa was selected for pressures in the calibration. The same precise differential pressure meter implemented for calibration of pressure transducers was also used in this calibration.

5.3.4 Test procedure

5.3.4.1 Sample preparation and setup

The biaxial device, developed by Alabdullah (2010), was equipped to mount the sample inside the membrane during the setup, either by pluviation or water sedimentation methods for samples with dry and saturated initial conditions respectively. But if the sample is stable enough (for example, consolidated clayey soils) it is possible to prepare the sample out of the biaxial device and place it inside the membrane and continue the setup.

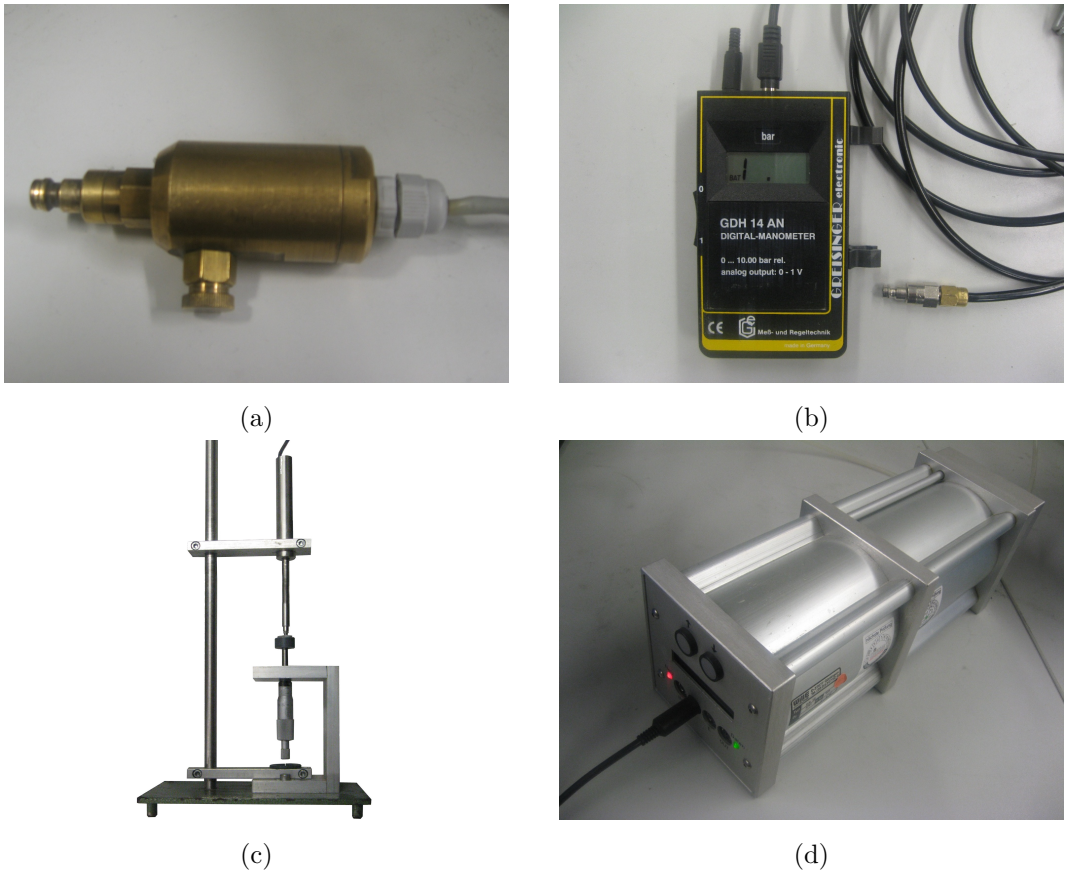

(a) (b)

(c) (d)

Figure 5.17: Photographs of (a) pressure transducer; (b) precise differential pressure meter; (c) LVDT and micrometer screw gauge; and (d) air pressure controller.

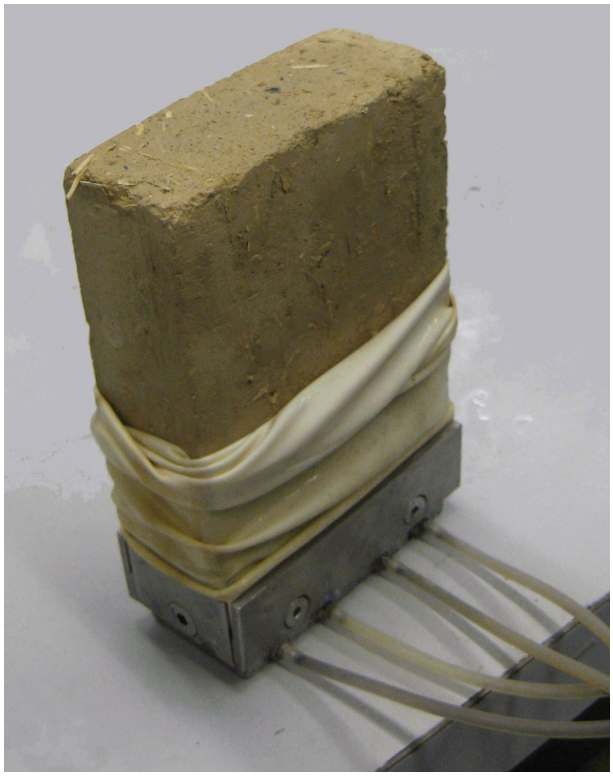

Figure 5.18: Placing a prepared sample inside the membrane.

In this study the samples were made from clayey slurry (with 1.25 × LL water content) which was poured into especial molds. After drying and shrinkage, the samples were still bigger than the required dimensions of the biaxial device. In this condition the samples were stable enough to be cut exactly to the required dimensions of the device (i.e. $40 \times 100 \times 120$ mm). With these dimensions the sample was placed inside the membrane after sealing the membrane to the bottom platen. Regarding the hardness of the sample, the top cap was installed easily over the sample and tightened to the membrane. Two filter papers were placed at the bottom and at the top of the specimen. In Figure 5.18 a sample is shown, which is placed inside the membrane.

After the whole block (i.e. specimen, platen, cap, pedestal, and side walls) was mounted and placed over the base of the inner cell, as shown in Figure 5.19a, the tubes had to be connected as required (explained in following 2 sections). Then the inner cell and its cap were placed over the base. The inner cell chamber was isolated by four clamps fixing the cell over two rubber rings, one attached to the base and one to the cap of the inner cell. Cap of the outer cell had to be placed and connected to the pipes through which the inner cell chamber could be vented (Figure 5.19b). The inner piston was pushed into the top cap.

(a) (b) (c)

Figure 5.19: Installation of the inner and outer cells.

The outer piston was pushed down until it came into contact with the inner piston. The outer cell was placed and supported by four screws from the top as shown in Figure 5.19c. Finally, both cells were filled with fresh deaired water. The inner and outer cells were connected to the same pressures via the volume change indicator and a water reservoir respectively, because the volume change of the outer cell was not of interest.

5.3.4.2 Test procedure for saturated samples

For saturated samples, metal plates screwed to the bottom platen and the top cap (shown in Figure 5.9) contained only porous discs, allowing the sample to saturate with deaired water and allowing drainage of the water during shearing. In saturated conditions porous discs at the top and bottom of the sample had to be connected to the same water pressure via a volume change indicator (see Figure 5.20).

Since hydrogen dissolves in water faster than normal air, to have better saturation, hydrogen was inserted from the bottom and let out from the top to replace the air in the soil voids with this gas. For saturation a constant back pressure was applied equally to the top and bottom of the sample. The applied cell pressure increased to the summation of the predetermined surrounding pressure (σ_3) and saturation back pressure. Pressure of 200 kPa was used in this study as back pressure for saturation. Le Bihan & Leroueil (2002) reported that as the water pressure increases, the entrapped air in soil dissolves better in the water. The cell and back pressures were kept constant until the sample was

completely saturated. If Skempton's factor B exceeded 0.92 the sample was assumed to be saturated. To control the cell and back pressure two pressure transducers were employed (Figuer 5.17a).

When the saturated condition was reached, the shearing phase started. By keeping the cell and back pressure constant and applying a constant strain rate, the maximum principal stress increased until the sample failed. The strain rate for all tests was 0.002 mm/min according to Fredlund & Rahardjo (1993) for clayey soft soils with pore pressure measurement.

5.3.4.3 Test procedure for unsaturated samples

In the unsaturated tests, samples had to reach constant suction before they were sheared. Regarding the material used (Section 4.2), which was a fine grained soil, equilibrium took a long time to establish. In order to accelerate the process, first the sample was subjected to the required suction outside of the biaxial device and when the equilibrium condition was detected the setup procedure explained above was carried out. For this purpose for suctions in the VET suction range the dry samples were directly placed in desiccators with certain salt solutions (see Figure 5.21). The equilibrium was achieved when the samples' weight reached constant values. To be sure about the suction values, after equilibrium the applied suction by the solution was checked again with the chilled mirror. For suctions in the ATT range, with regard to the wetting path of SWCC, the dry samples received water to reach the required water content and its corresponding suction. Volume changes of samples during the wetting process were also recorded.

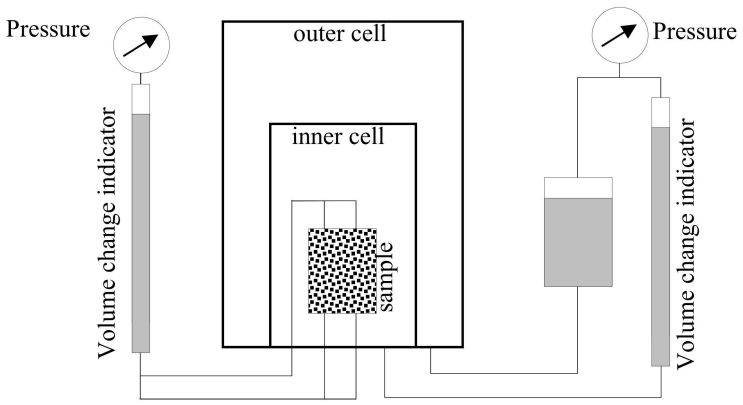

Figure 5.20: Setup for saturated conditions.

Figure 5.21: Applying suction to the samples with VET method.

As mentioned earlier, the sample remained three days under a constant condition in the biaxial device (suction and cell pressure) before shearing. During this period and also during shearing the same suction was applied.

For controlling suction with the ATT method, unlike the setup of saturated conditions, the metal plates contained both ceramic and porous discs (Figure 5.9). Based on the applied suction, ceramics with air-entry values of 100 and 500 kPa could be selected. Suction in the ATT range was applied as explained in Section 5.3.2.4. Cell pressure (σ_3) and pore water pressure (u_w) were controlled by two pressure transducers (Figuer 5.17a). Pore air pressure (u_a) was applied and controlled by the air pressure controller device (Figure 5.17d). The effective applied cell pressure was equal to $\sigma_3 - u_a$. The setup of the bixial device in unsaturated conditions with the ATT method is shown in Figure 5.22.

For the VET method, similar to the setup of saturated conditions the metal plates contained only porous discs through which vapor could be easily circulated at both the top and bottom of the sample. System of applying suction using the VET method is explained in Section 5.3.2.4. Cell pressure was controlled by a pressure transducer. The setup of the bixial device in unsaturated conditions with the VET method is shown in Figure 5.23.

In the shearing stage, the specimens were axially compressed by 0.002 mm/min (i.e. strain rate of $1.6{\times}10^{-5}$ $\%/min$); the low strain rate is vital to ensure the dissipation of induced pore pressures during the compression stage (Fredlund & Rahardjo 1993).

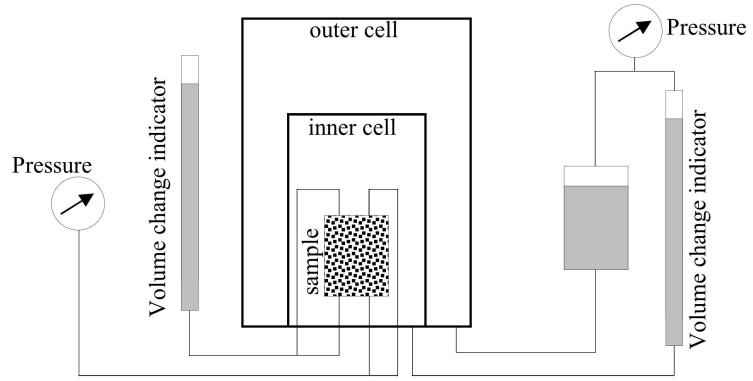

Figure 5.22: Setup for unsaturated condition with the ATT method.

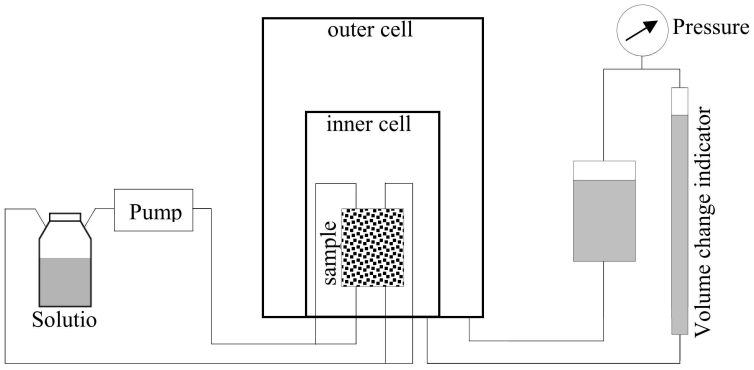

Figure 5.23: Setup for unsaturated condition with the VET method.

5.3.5 Repeatability and verification of the results

Repeatability of the test results is an important factor in experimental investigations. The repeatability of the test results in the biaxial device was examined by testing two series (A and B) of two identical samples (1 and 2), under saturated and unsaturated conditions. Void ratio, degree of saturation, and preparation procedure were the same for each test set. Initial conditions and a summary of results are given in Table 5.2, where θ_m, ψ_v^{max}, and σ_d^{max} are shear band inclination, maximum dilatancy angle, and maximum deviator stress.

Figures 5.24a and 5.24b show the deviator stress vs. axial strain, and Figures 5.24c and 5.24d the volumetric strain vs. axial strain of test series A and B. The curves and values in Table 5.2 imply a good agreement in the identical tests.

In order to check the accuracy of the results, a biaxial test performed by Röchter (2011) on pure sand was repeated using the biaxial device of this study. The sample was made of

Table 5.2: Identical tests.

Tests		Initial condition				Results		
		e [-]	Straw content [%]	Suction $[kPa]$	σ_3 $[kPa]$	θ_m [°]	ψ_v^{max} [°]	σ_d^{max} $[kPa]$
A	1	0.4	0	0	50	55	5	117.83
	2	0.4	0	0	50	57	5	124.18
B	1	0.52	0.5	9500	50	70	18	1022.28
	2	0.52	0.5	9500	50	68	23	1099.65

saturated Silver sand with an initial void ratio of 0.6. The dimension of Röchter (2011)'s specimen were 60×80×130 mm, whereas, as mentioned before, the dimensions of the sample in this study were 40×100×120 mm. σ_3 in the biaxial device of Röchter (2011) was applied by flexible walls, while in this study the cell pressure was supplied by water pressure in the inner cell. The biaxial device developed by Röchter (2011) is explained in Section 3.6.2.1.

As shown in Figure 5.25a, the manner of the stress ratio (σ_1'/σ_3') of both experiments are comparable. Figure 5.25b also shows the volumetric strain in those tests. There are some differences in peak values, however their trends are to some extent similar. The diversities in these results might be due to the differences and dissimilarities in the biaxial devices mentioned above (dimension of samples and methods of applying σ_3).

5.4 Techniques and procedures used for wall tests

Rising damp in masonry walls occurs as a result of the capillary action of moisture from the ground into porous building materials. All masonry materials (including stone, earth as adobe or rammed earth, clay brick, concrete block, and mortar) are to some extent porous and contain voids or pores. Capillary suction becomes stronger as the pore size gets smaller. It can be greater than the force of gravity, thus leading to water rising many meters if the pore size is small enough.

In order to realize the uprising moisture phenomenon and its effects, a series of large scale tests was performed (Figure 5.26a). In these experiments masonry walls with different conditions (which are explained in Section 5.4.3) were subjected to uprising moisture from the bottom and loaded from the top which represents the building's weight. Figure 5.32 schematically shows the test setup.

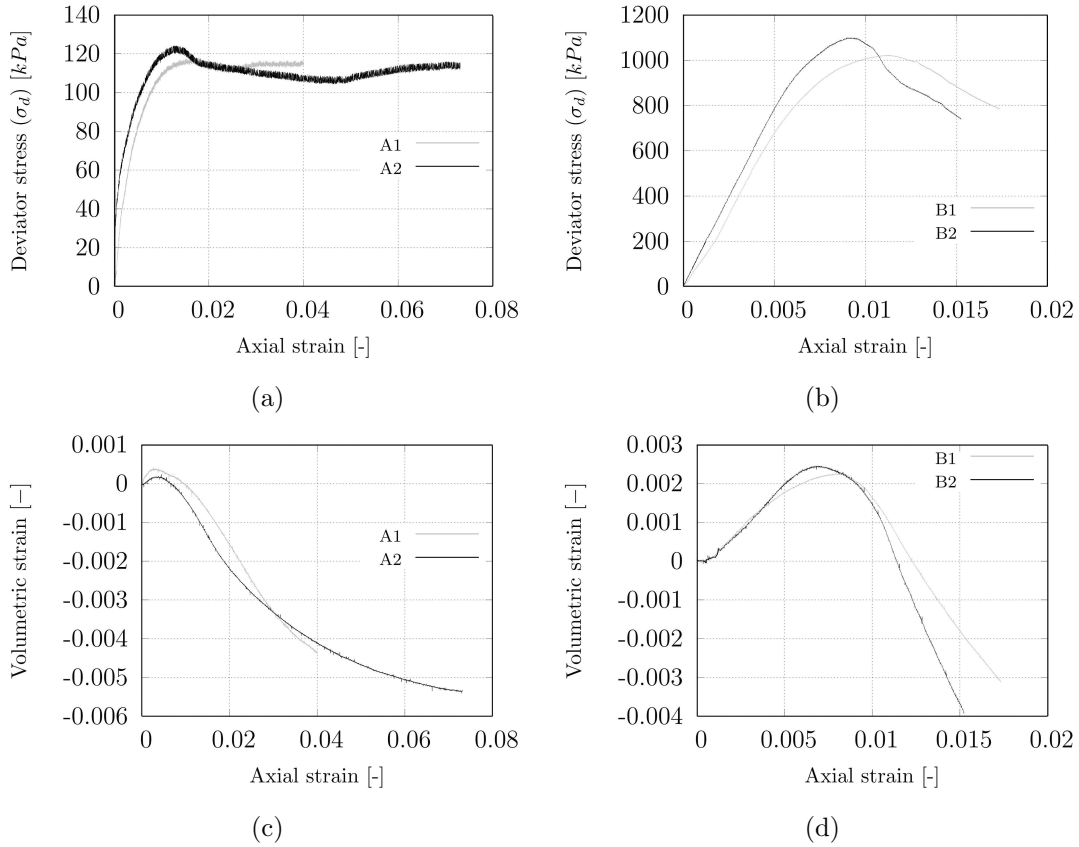

Figure 5.24: Identical tests to check the repeatability of results: (a) and (b) deviator stress-axial strain curves; (c) and (d) volumetric strain-axial strain curves, for materials listed in Table 5.2.

As can be seen in Figure 5.26b the wall was built over a geotextile and filter paper. This geotextile worked as a draining surface in order to transport water to the bottom surface of the wall. With continues drops from a water bucket which was located in a higher elevation, the geotextile was always kept saturated.

5.4.1 Measurements

5.4.1.1 Volumetric water content

In this experiment volumetric water content and temperature were measured by four TDR probes, as shown in Figure 5.26b. The TDR sensor consist of 2 parallel rods, a probe's body, and cables. The physical performance of this sensor was explained in Section 3.2.3.2. The TDRs were produced by the company Imko in Germany under the commercial name of Trim-Pico 32 (Figure 5.27). Unlike conventional TDRs which have separate units of

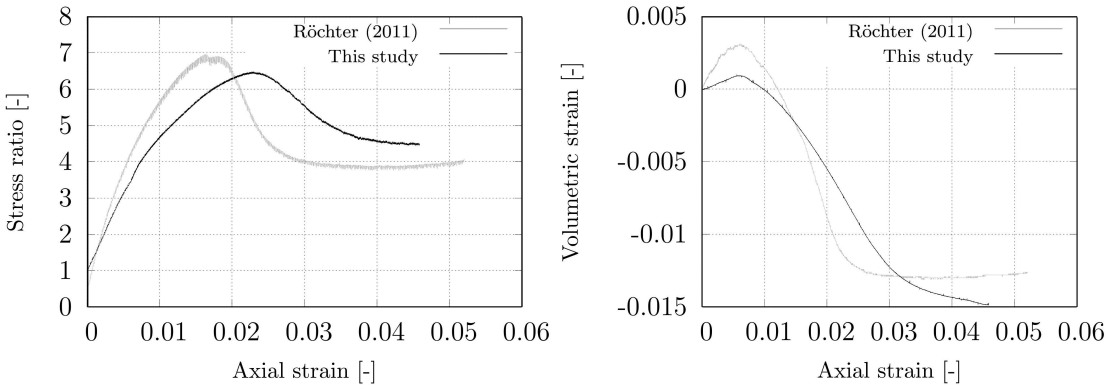

(a) (b)

Figure 5.25: Comparison of the biaxial results on saturated pure sand using the biaxial device of this study and Röchter (2011).

pulse generator and oscilloscope, this generation of TDRs emits and receives pulses from the probe's body (the blue cylinder in Figure 5.27). The data read by the probes was logged on a computer through a switch and a data converter, both shown in Figure 5.28. Special software, developed by the producer, allows the measurement of the pulse's speed and analysis of the dielectric constant of soil which is related to the volumetric water content. The accuracy of measurements in the ranges of 0 to 40% and 40% to 70% volumetric water content were ±1% and ±2% respectively. Measurement of temperature in the range of -15°C to 50°C had an accuracy of ±0.2°C.

5.4.1.2 Deformation

The settlement of the wall was measures by the Particle Image Velocimetry method (VIP). PIV is a technique that was originally developed in the field of fluid mechanics by Adrian (1991). This technique was implemented using double-flash photography of a seeded flow. The photographs contain image pairs of each seed particle. For PIV analysis, the photograph is divided into a grid of test patches. The displacement vector of each patch during the interval between the flashes is found by locating the peak of the autocorrelation function of each patch. The peak in the autocorrelation function indicates that the two images of each seeding particle captured during the flashes are overlying each other. The correlation offset is equal to the displacement vector (White et al. 2003).

A modified approach has been used to implement PIV for geotechnical applications. Unlike fluids, soils have their own texture in the form of different-colored grains and the light and shadow formed between adjacent grains when illuminated. This technique has

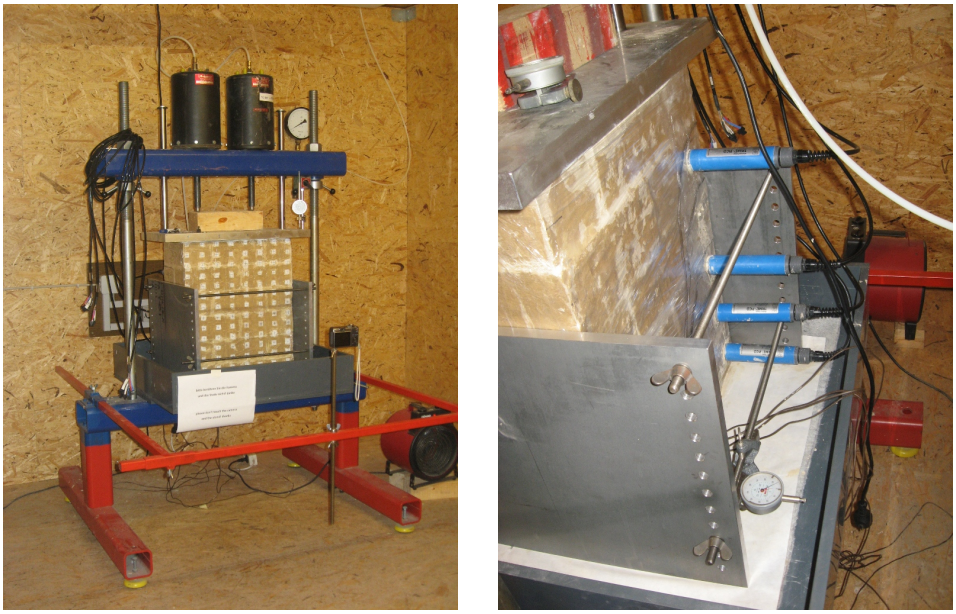

(a) (b)

Figure 5.26: (a) Test setup, wall, gauge, and installed camera; and (b) TDRs at different levels.

been used by several authors for geotechnical purposes (e.g. Paikowsky & Xi 2000, Nübel & Weitbrecht 2002, White et al. 2003, Rechenmacher & Finno 2004, Adam et al. 2005, Watanabe et al. 2005, Wolf et al. 2005, and Röchter 2011).

In this study the settlement was measured by detecting the position of indicators fixed on the wall's front surface using photos taken at given intervals by a fixed camera (as shown in Figure 5.26a) and a code written in Matlab. The software could distinguish the crosses attached to the wall and compare their position with a reference position which was the wall before the uprise of moisture. Horizontal deformation of the wall was measured using a vernier caliper at various points. Moreover, to double check the results one dial-gauge displacement transducers was installed on the top of the wall and two on the sides down.

5.4.2 Calibrations

5.4.2.1 Calibration of TDRs

Basic calibration serves to compensate the cable length and tolerances of the probe mechanics (thickness of the rod coating, rod length, etc.). After two measurements, one in dry, and one in water saturated glass beads, the calibration data were calculated and

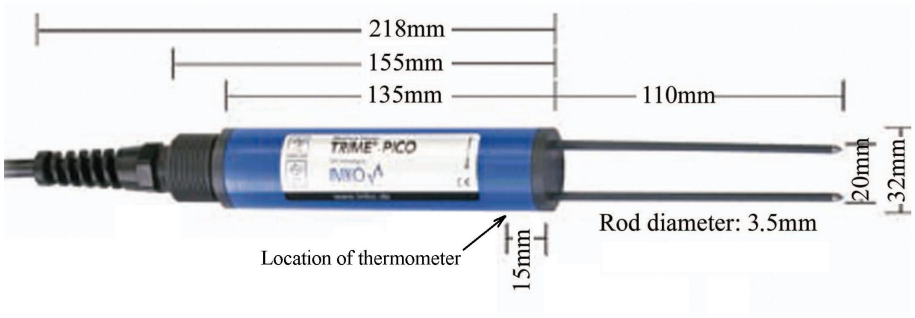

Figure 5.27: Dimension of the TDR probes.

Figure 5.28: (Left) The data converter, and (Right) the switch to accumulate data from all TDRs.

stored in the TDR sensor. Each Trime-Pico 32 sensor (used in this study) must be calibrated before it can supply proper measurement results. Basic calibration was carried out by the producer company in the factory prior to shipment. The sensors' measuring system operates with a universal calibration for mineral soils as a standard.

Although the TDR sensors had already been calibrated and did not need to be calibrated before installation, in order to observe the accuracy of calibration and results they were calibrated again on similar bricks and the same conditions. For this purpose 4 bricks similar to those being used in the wall were prepared, in which the sensors had been placed. Their water content was increased step by step. When the read data from sensors reached to an equilibrium it was assumed that the water was fully distributed through the brick's body, and we could go to the next step of water content. Figures 5.29a and 5.29b show a photograph of the calibration procedure and a curve showing a reasonable

(a)

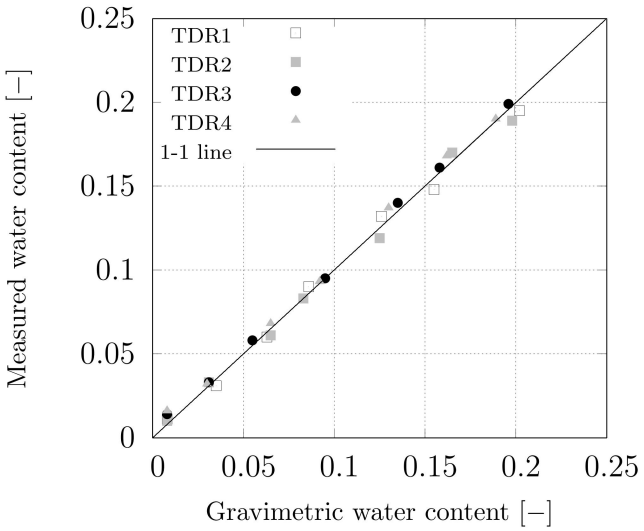

(b)

Figure 5.29: (a) A photograph of calibration of TDRs, and (b) comparison of applied and measured data.

agreement between the given and measured water contents. In this curve volumetric water content read by sensors has been converted to gravimetric water content.

5.4.2.2 Calibration of PIV

The Particle Image Velocimetry method (PIV) explained in Section 5.4.1.2 was calibrated before performing the tests. A code with the ability of finding the x and y coordinates of a given template in a bigger picture was written in Matlab. The templates used here were crosses of two 10 mm bars. For calibrating this code a paper with crosses arrayed at 20 mm horizontal and vertical distances placed on the wall (Figures 5.30a and 5.30b). By analyzing this photo in the software, position of each cross was obtained, however these positions were not in mm but in pixels of the original photo. Since the position of crosses were predetermined and known, another code in Matlab can simply transfer the values from pixel to mm. As can be inferred from Figure 5.30 a straight line on the wall will be curved in a 2D photo, and a known length looks smaller near to the edges of a photo than in the center. These errors were also corrected in the calibration.

After the above-mentioned calibrations and transformations, all crosses attached to the wall could be found numerically among the 550 crosses of the calibration paper. This means that from the calibration data, the position of crosses on the photos taken during the test can be interpolated from pixel to mm using the software Matlab, with a theoretical

accuracy of $\pm 0.2\ mm$. For example, a photo was taken with only four crosses on the wall and calibrated via the procedure explained above. Figures 5.30c and 5.30d are positions of calibration crosses and four - green - controlling points among them in pixel and mm respectively. During the test, the calibration paper was removed and 13 rows of 8 crosses were attached to the wall instead.

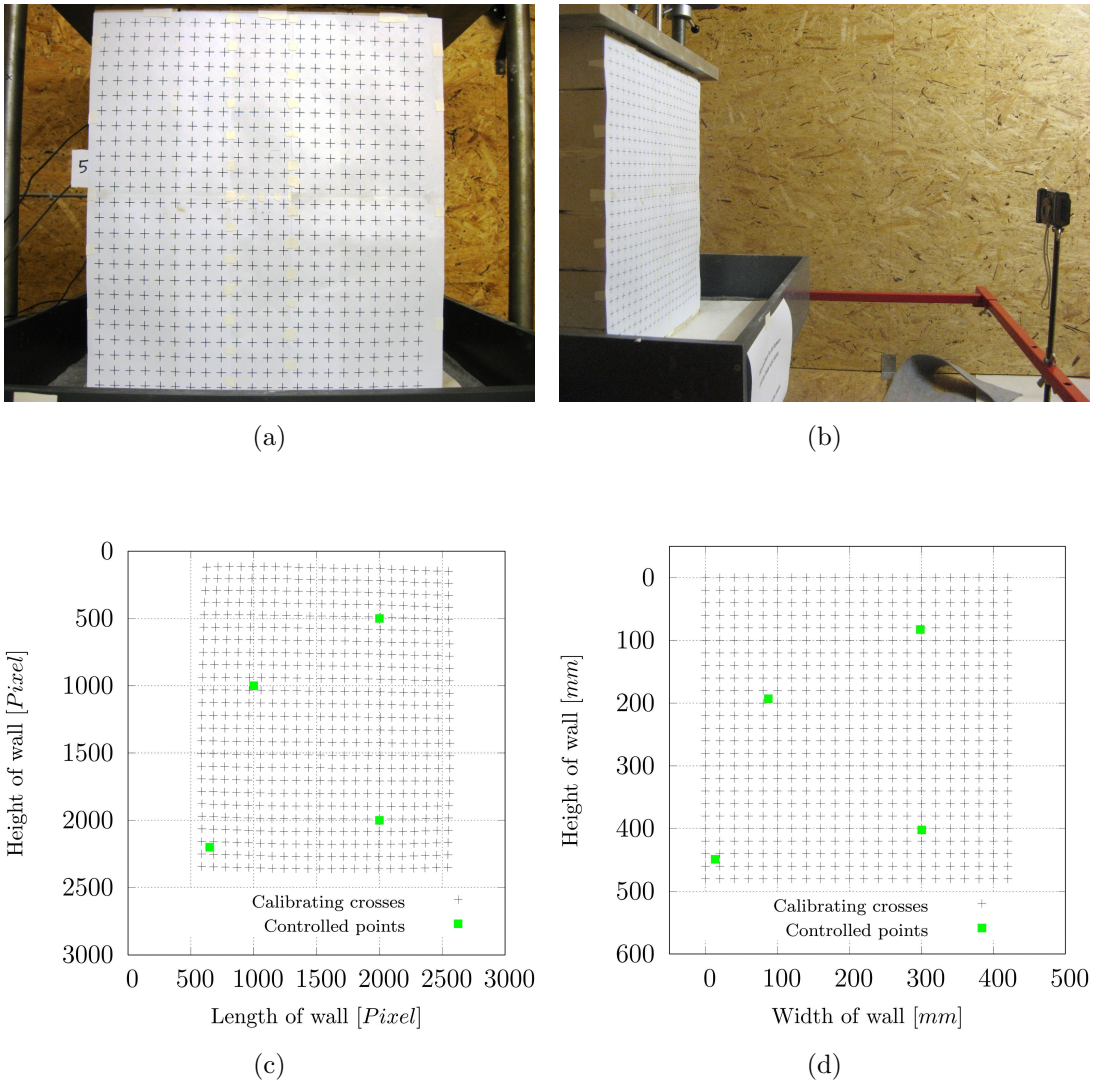

Figure 5.30: (a) Calibration of the PIV method using crosses with known positions; (b) location of camera in front of the wall; (c) positions of calibrating crosses and controlled points analyzed by software form taken photos; and (d) corrected position of the same crosses and points using calibration transfer.

5.4.3 Test procedure

5.4.3.1 Sample preparation

In this study the sample preparation method was similar to that of the traditional method of making adobe bricks used in the past. The soil mixture described in Section 4.2 was mixed and blended entirely with 1.25×LL water content to reach a soft and uniform slurry mud. To have a good distribution of water in all parts of the sample, the mud was left for 2 days in a closed container. Afterwards it was poured into molds to get the required form during drying process. The mold had dimensions of 100×120×240 mm, however, due to shrinkage the dried bricks were fairly smaller than the mold, namely ∼95×113×230 mm. Figure 5.31 shows the molds after being filled with the slurry mud. After 5 to 7 days and when the slurry had to some extent dried and shrunk, they were removed from the molds and stored in a place for completion of the drying process in a laboratory atmosphere. From time to time they were weighed to check if the equilibrium (i.e. constant water content) was achieved. In these conditions the wall was built with 6 rows of 4 bricks. As it can be inferred from Figure 5.32, the arrangement of bricks in 2 tandem rows was not similar. In odd rows all 4 bricks were parallel to the width of the wall, whereas in even rows 2 were parallel and 2 were perpendicular. The mortar used between the layers was the same material used in the preparation of adobe bricks but without very course sands larger than 2 mm. With regard to the roughness of the bricks, the thickness of mortar varied between 1 to 4 mm.

Figure 5.31: Preparation of bricks for wall tests.

5.4.3.2 Description of experiments

As mentioned in Section 3.6, in most historical masonry buildings plane strain conditions dominate the behavior of load-bearing walls. Provide the plane strain conditions in this test, 2 aluminum side-walls were employed, which were fixed to each other by 4 steel bars (see Figures 5.26). The first row of bricks was placed over a drainage geotextile through which water could be conveyed and reachs all of the bottom surface of the wall. Using two buckets of water, as shown in Figure 5.32, the water level was kept constant over the geotextile during the test.

In this study three different wall tests were carried out. The wall dimension, sample preparation method, loading conditions, equipment used, and instrumentations were the same in all three experiments. In order to simulate typical historical masonry monuments which are covered with impermeable facades in the experimental models, the evaporation of moisture from the surfaces of the walls had to be prevented. Therefore, all four vertical sides of the walls were covered with silicon glue and nylon foil, but the top and bottom surfaces were not covered. The experiments are explained below.

Test 1: Unprotected unreinforced wall

In the first test no straw fibers were included to the soil in the preparation of the bricks. The setup and position of TDRs are shown in Figure 5.32, which were located at heights of 50, 150, 250, and 450 mm.

Test 2: Unprotected reinforced wall

The second test followed the same procedure explained for test 1, except for the material used in the bricks which was reinforced with 1% straw fibers. This straw was added to the dry soil in the sample preparation procedure. From a comparison of the results from tests 1 and 2 the differences in uprising moisture in reinforced and unreinforced materials can be investigated.

Test 3: Protected unreinforced wall

In the third test one of the widely used countermeasure methods against uprising moisture, which is called “Base Ventilation”, was analyzed and evaluated. This method was explained in Section 2.4.5, and can be either from one side or both sides of the wall. In this experiment, as with tests 1 and 2, the wall was covered by silicon glue and nylon foil. But in the front and back facades 100 mm from the bottom was left open without covering from which moisture was allowed to evaporate. In this situation a slower rate and lower height for uprising was expected. Therefore, TDRs were located in lower positions

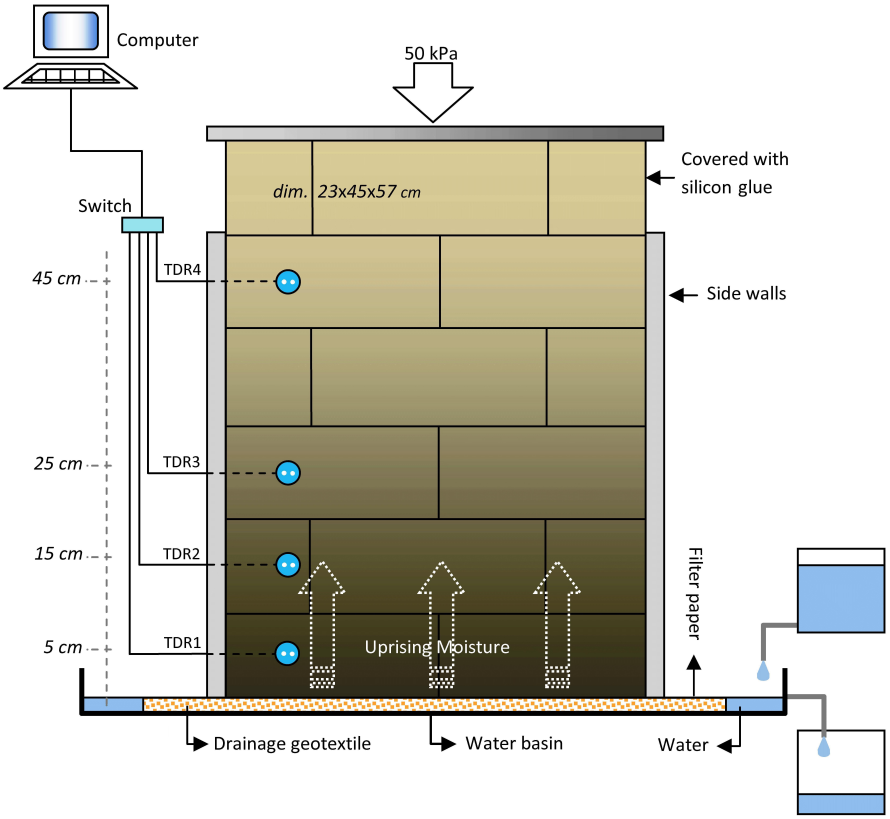

Figure 5.32: Schematic setup of test.

of 50, 100, 200, and 300 *mm* from the bottom. Unlike tests 1 and 2 in which impermeable covering resulted in unique water content in any horizontal plane, in test 3 water content did not have the same value at all points of a horizontal section, but its maximum value was expected to be located in the center-line of the horizontal plane and near the front and back facades lower values were expected. Thus, TDRs were placed on the side of the center-line. Figure 5.33 shows two photographs of this test.

5.5 Summary

In this chapter experimental procedures and utilized methods have been presented. Tests performed in this study were categorized into three main groups: SWCC tests, biaxial shear strength tests, and wall tests. For SWCC tests, which consisted ATT and VET methods, sample preparation and details of controlling suction have been explained. The biaxial shear device used in this study and calibration of different parts have been described. Procedures of saturated and unsaturated biaxial tests and repeatability of the

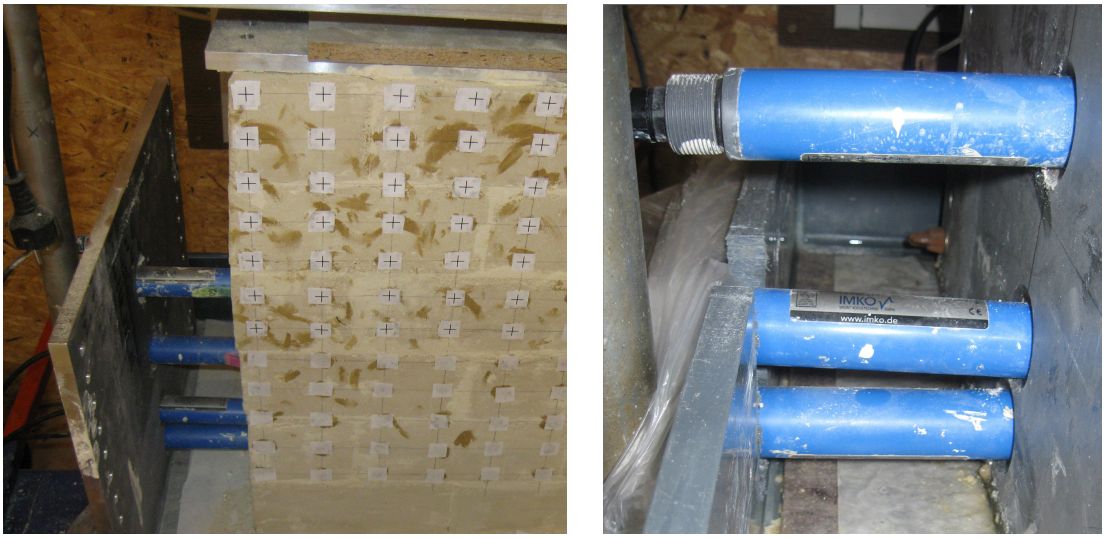

(a) (b)

Figure 5.33: (a) TDRs under installation on the center-line of the left surface; and (b) TDRs passed through aluminum side wall.

results have also been presented. Finally, the wall tests and the required measurements together with their calibrations and procedures have been explained.

6 Experimental results

6.1 Introduction

This chapter presents the experimental results of the laboratory test program described in Chapters 4 and 5. The aim of these tests was to determine and investigate the dependency of material properties on suction and fiber-reinforcement, and to experimentally simulate the uprising moisture and observe its consequences. The qualitative analysis to calculate the hydro-mechanical properties of unsaturated reinforced fine-grained soils will be undertaken in Chapter 7.

Results of SWCC tests, which were function of volumetric changes during drying and wetting, are presented in this chapter. Influences of reinforcement and suction on shear strength and volumetric strain of soil introduced in Section 4.2 over a wide range of suction and under plane strain conditions are presented here using the biaxial apparatus. Progress of uprising water table in the wall tests is also drawn over time and height of the wall.

6.2 Results of SWCC tests

Sample preparation and implemented methods for determining SWCC have been described in Section 5.2.1. The materials used for this experiment were reinforced soils with different dosages of straw content. Initial void ratios for the drying path of 0, 0.5, 1, 2, and 3 % straw content were 0.7, 0.705, 0.72, 0.74 and 0.77 respectively. The variation in void ratio at the beginning of the drying path (in the slurry condition) was due to a lower density of straw pieces compared to soil particles and voids inside the straw's body which could not be filled with grains. However, the differences in void ratios for the beginning of the wetting path were even more obvious; namely, 0.39, 0.52, 0.56, 0.63 and 0.72 for materials with 0, 0.5, 1, 2 and 3% straw content respectively. This higher veriation was not only because of the density of components, but was also due to differential shrinkage

which occured as a function of straw content, as also demonstrated in the literature (e.g. Ayyar et al. 1989, Puppala & Musenda 2000, Cai et al. 2005, Cai et al. 2006, Punthutaecha et al. 2006, and Viswanadham et al. 2009). This matter will be explained in Chapter 7.

Three samples from each material were prepared for suctions in the ATT range. When equilibrium was reached for a step of suction the same samples were subjected to the next step. But for suctions in the VET range several identical samples were prepared for each applied value of suction. The changes of mass in the specimens were recorded for each specimen over time. As examples, Figure 6.1a and Figure 6.1b show the mass of specimens versus time for four samples: two reinforced and unreinforced samples in the drying path under suction of 200 kPa (ATT range), and two reinforced and unreinforced samples in the wetting path under suction of 3000 kPa (VET range).

SWCC of all the materials mentioned above (in the form of volumetric water content versus suction) are shown in Figures 6.2 and 6.3 in drying and wetting paths respectively. In Figure 6.2 the saturated condition is represented by suction = 1 kPa. More detailed information and interpretations are given in Section 7.2.

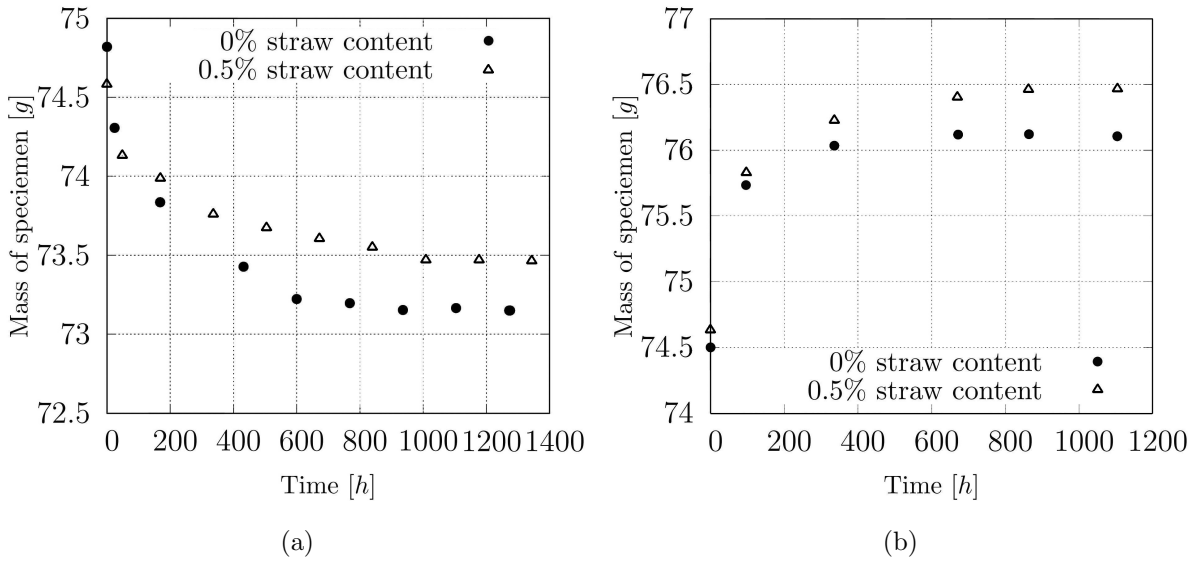

Figure 6.1: Measured mass of samples, (a) in drying path at 200 kPa suction (suction at starting point: 80 kPa) and (b) in wetting path at 3000 kPa suction (fully dry at starting point).

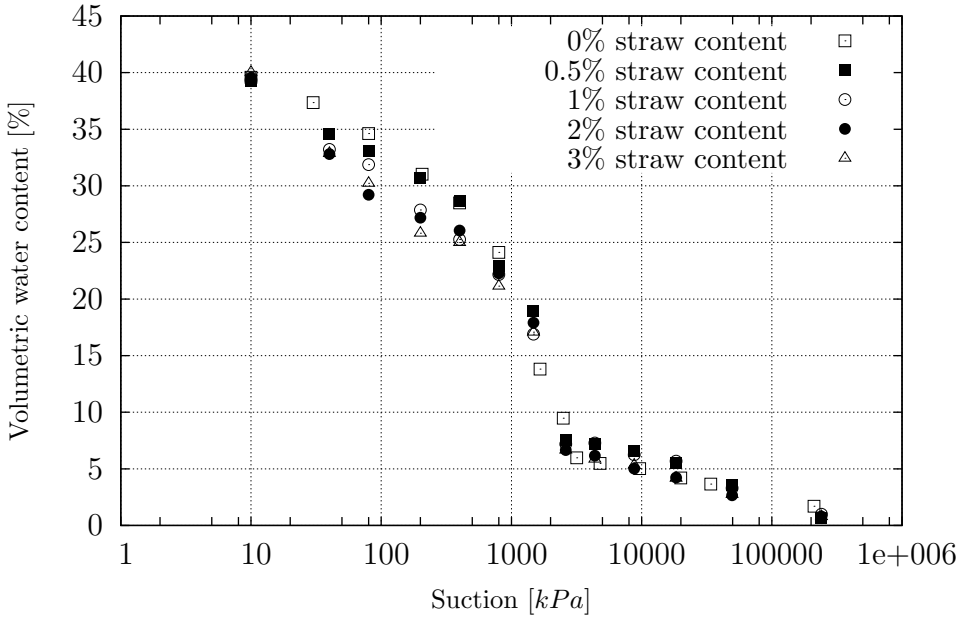

Figure 6.2: Volumetric water content vs. suction in drying path for the materials used.

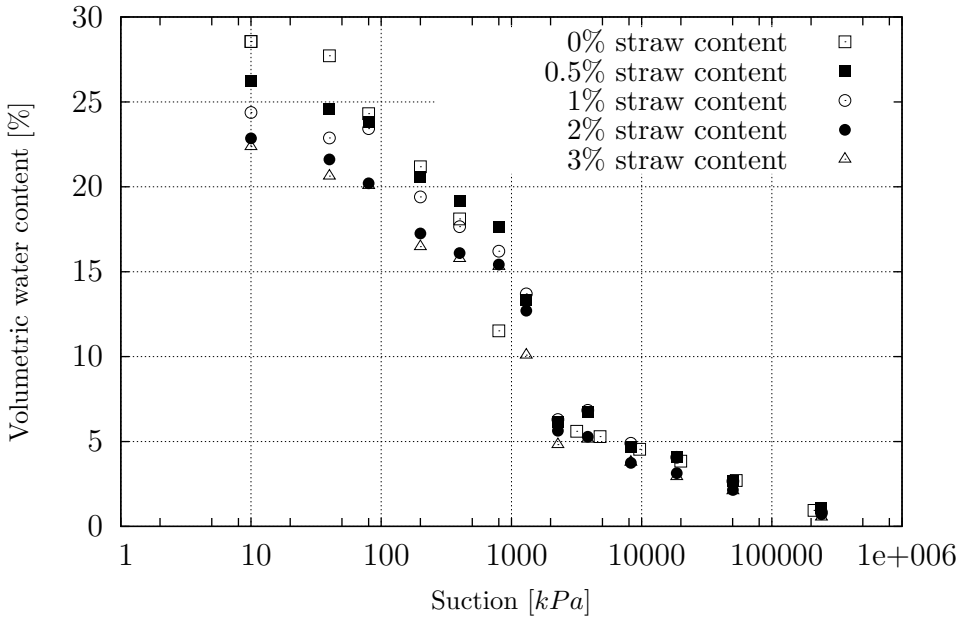

Figure 6.3: Volumetric water content vs. suction in wetting path for the materials used.

6.3 Results of biaxial tests

In this section the results of biaxial shear tests on unreinforced and reinforced soil in saturated and unsaturated conditions will be presented. In the calculation of the results axial strain (ϵ_1) and volumetric strain (ϵ_v) are defined using the following equations:

$$\epsilon_1 = \frac{\Delta h}{h_0} \tag{6.1}$$

$$\epsilon_v = \frac{\Delta v}{v_0} \tag{6.2}$$

where h_0 is initial height of the specimen, Δh change in height of the specimen, v_0 initial volume of the specimen, and Δv change in volume of the specimen. Strains ϵ_1 and ϵ_3 are the major and minor principal strains, respectively. In the plane strain condition $\epsilon_2 = 0$ and σ_2 could not be measured in the used device. The deviator stress (σ_d) is the difference between major and minor principal stresses (σ_1 and σ_3).

$$\sigma_d = \sigma_1 - \sigma_3 \tag{6.3}$$

For calculations instead of net stresses effective stresses must be used which are calculated depending on the suction and selected approach (see Section 3.4). Calculation of effective stress is presented in detail in Section 7.3.

As explained in Section 5.3.2.2, Δv was measured by in- or outflow of water of the inner cell. The acquired data later needed to be corrected in terms of factors affecting volume change in addition to the actual sample's volume change (as mentioned in Section 5.3.3.2), as well as entrance of the piston in the inner cell which had a constant rate during shearing.

The axial load was applied using a load frame and two pistons following each other. Weight of the upper piston did not insert any error in calculating deviator stress (σ_d). Because the reference point for calculations of σ_d were the force recorded at the beginning of shearing moment, in which only the inner piston applied its weight on the sample (regarding cell pressure which pushes the outer piston upward to the load cell). In order to correct the data, the weight of the inner piston must be added to the force detected by the load cell (see Figure 5.4).

Figures 6.4 to 6.12 show the deviator stress (σ_d) and volumetric strain (ϵ_v) versus axial strain (ϵ_1) for materials with three different straw contents and three steps of cell pressure

(σ_3). In each figure the left and right curves present stress-strain and volumetric strain changed during shearing for five different unsaturated conditions with 80, 400, 3000, 9500, and 55000 kPa suctions, as well as for the saturated condition. Initial void ratio for each sample is given in Table 4.3. Suctions of samples were applied using methods explained in Section 5.3.2.4.

As we can see in Figures 6.4 to 6.12 with an increase in suction stiffness, peak deviator stress, and consequently the shear strength, increased. The lower the suction is, the softer the material behaves. But the strain at failure points decreased with an increase in suction, and post peak drop had a direct relation with value of suction. All samples showed contraction in the first phase of shearing, and then slightly before failure the volumetric behavior changed its trend and dilation started. Maximum contraction increased with an increase in suction, but after a certain suction (mostly around 400 kPa) decreased by with further increase in suction. More description and analyses of the results are presented in Section 7.3.

Angles of shear band inclination were measured at the end of the test (residual state) in respect to the direction of the minor principle stress. In this biaxial device, the shear bands cannot be observed in the plane of the intermediate stress (σ_2) because the platens used to impose the plane-strain conditions were made of stainless steel. But with regard to the materials used and the sample preparation method explained in Section 5.3.4.1, it was possible to remove the failed sample from the membrane after the test finished and measure the failure plane inclination. Samples after failure with 0.5% straw content, under 50 kPa cell pressure, and suctions from 0 to 55000 kPa are shown in Figures 6.13a to 6.13f. Figure 6.14 shows the shear band inclination versus suction for three materials and three confining pressures. As can be seen here, shear band inclination increased with an increase in suction, but decreased with an increase in straw content and confining pressure. It should be noted that in all biaxial tests in the current study, the bottom platen was free to move laterally from the beginning until the end of the test.

In most of the tests, the shear bands were symmetric and both faces of the specimen show the same angle of inclination. If any difference was observed, the angles of shear band inclination were measured at both faces of the specimen and the average was considered. The same phenomenon (i.e. different angles of shear band in each side face) was observed by Vardoulakis (1978) and Alabdullah (2010). In some tests the shear plane was not completely straight but rather curved or zigzag. In such cases a fitting line was drawn and an average inclination was determined (Oda & Kazama 1998 and Alabdullah 2010).

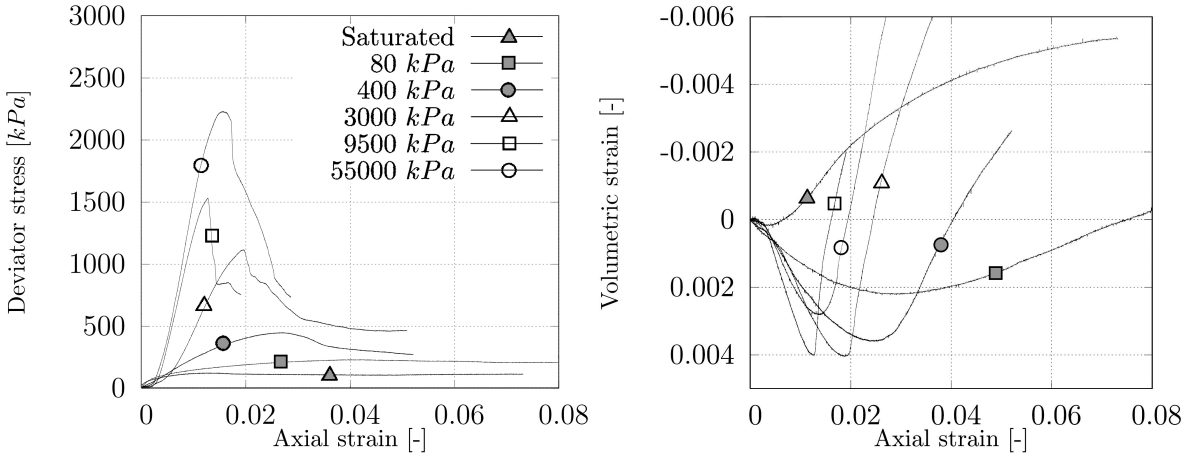

Figure 6.4: σ_d and ϵ_v vs. ϵ_1, straw content: 0%, σ_3 : 50 kPa.

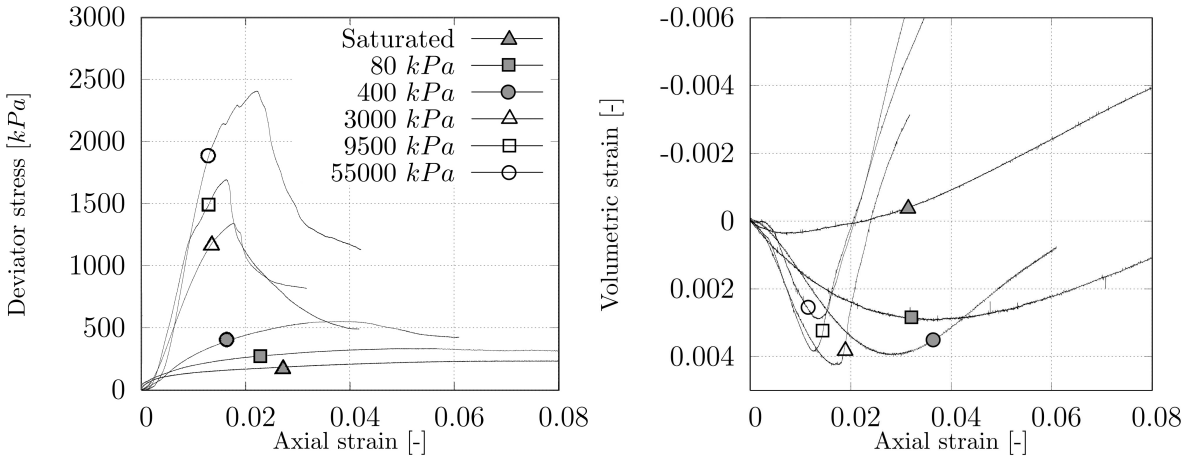

Figure 6.5: σ_d and ϵ_v vs. ϵ_1, straw content: 0%, σ_3 : 100 kPa.

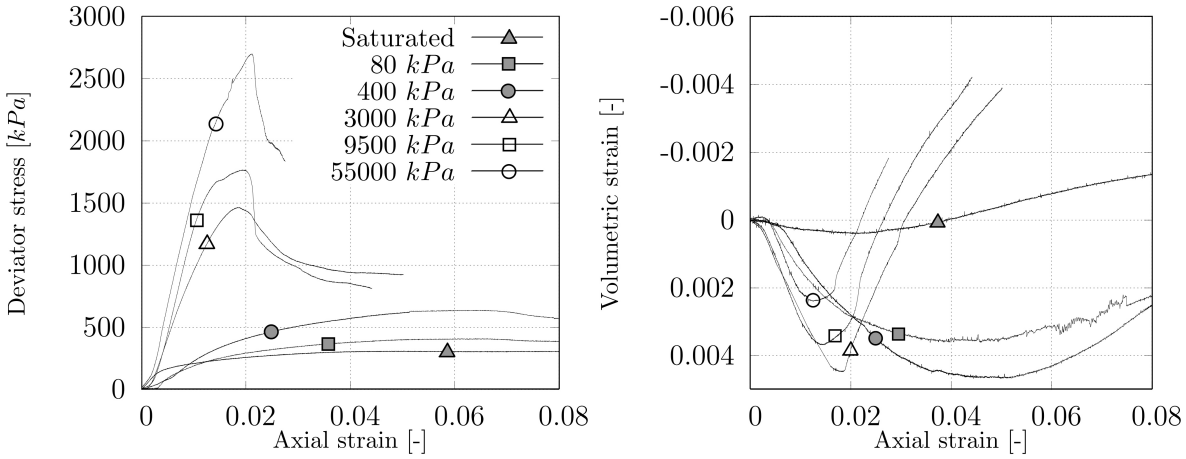

Figure 6.6: σ_d and ϵ_v vs. ϵ_1, straw content: 0%, σ_3 : 150 kPa.

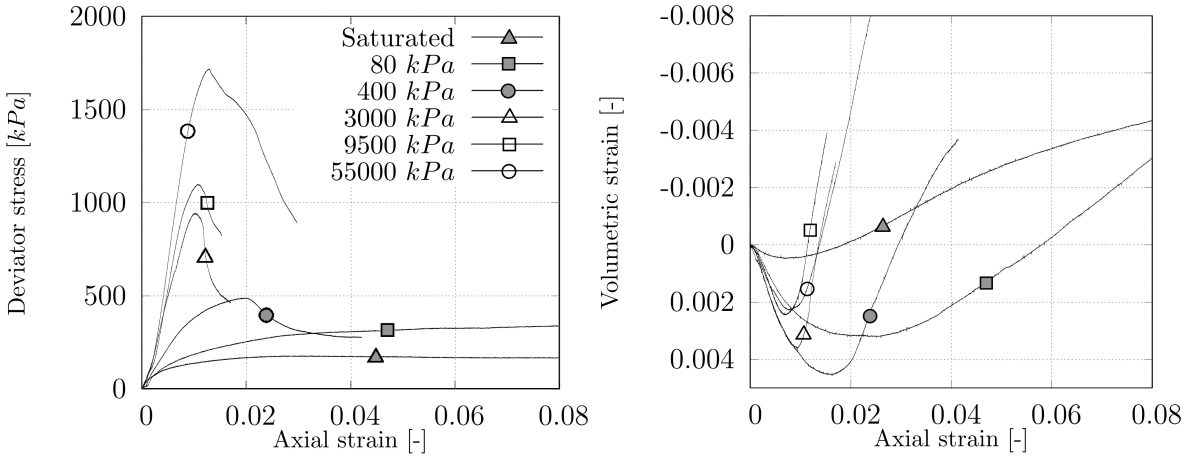

Figure 6.7: σ_d and ϵ_v vs. ϵ_1, straw content: 0.5%, σ_3 : 50 kPa.

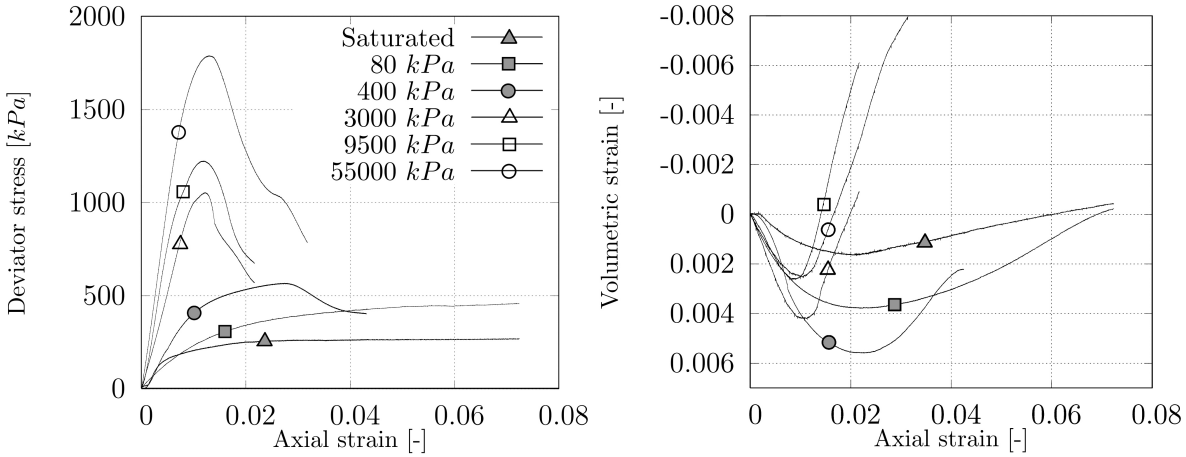

Figure 6.8: σ_d and ϵ_v vs. ϵ_1, straw content: 0.5%, σ_3 : 100 kPa.

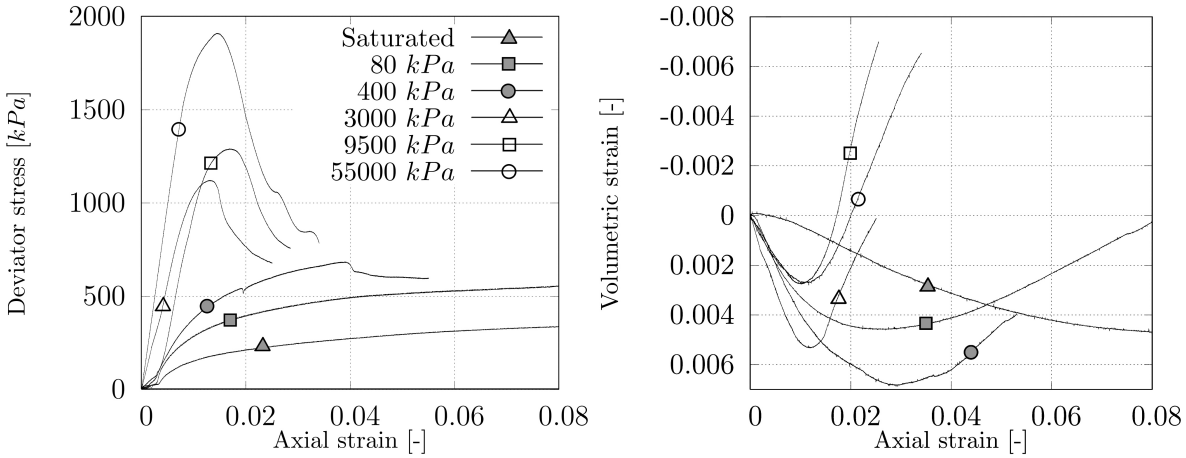

Figure 6.9: σ_d and ϵ_v vs. ϵ_1, straw content: 0.5%, σ_3 : 150 kPa.

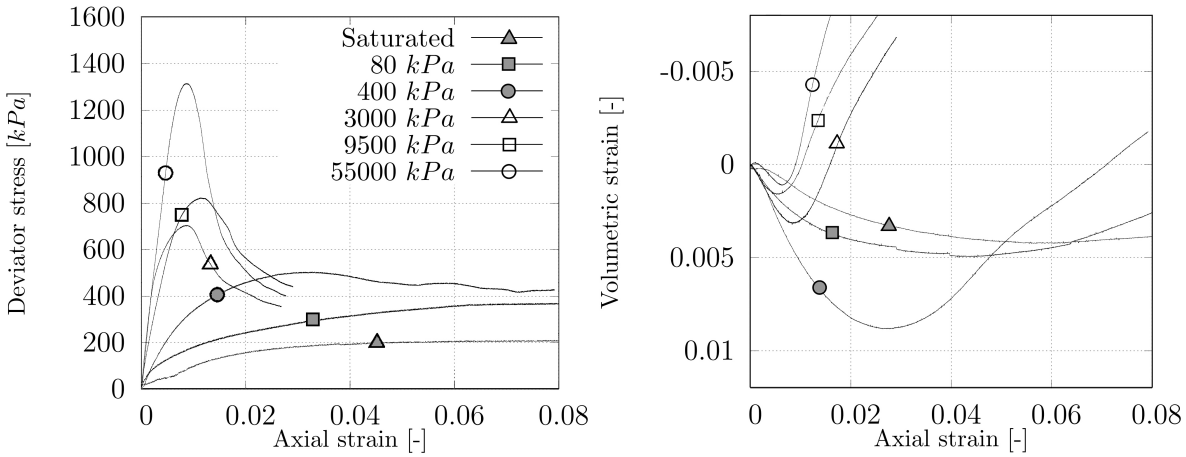

Figure 6.10: σ_d and ϵ_v vs. ϵ_1, straw content: 1%, σ_3 : 50 kPa.

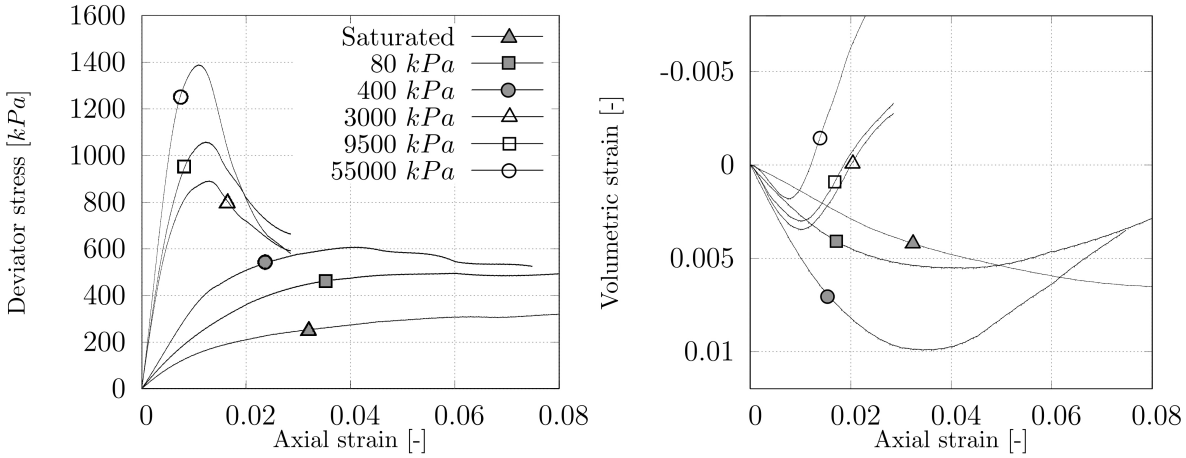

Figure 6.11: σ_d and ϵ_v vs. ϵ_1, straw content: 1%, σ_3 : 100 kPa.

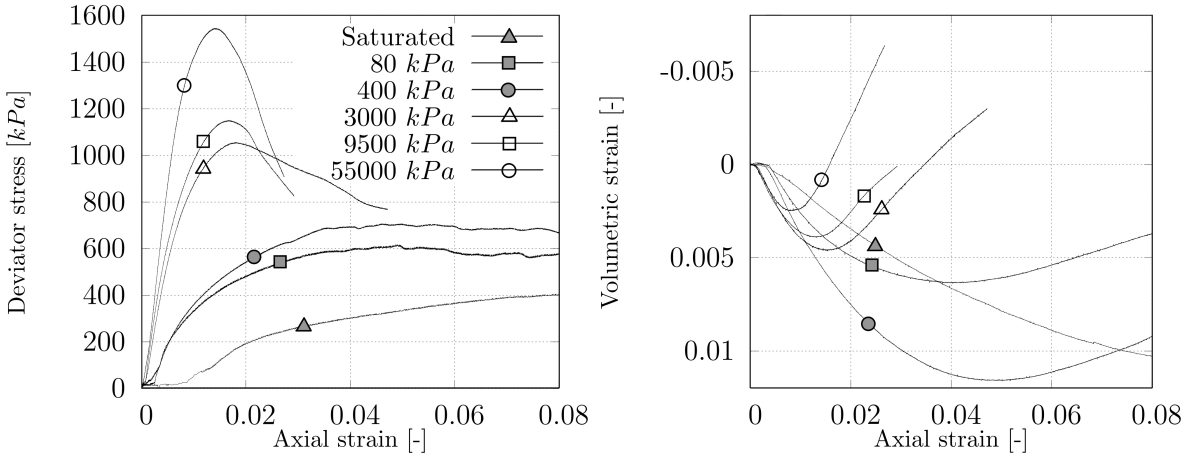

Figure 6.12: σ_d and ϵ_v vs. ϵ_1, straw content: 1%, σ_3 : 150 kPa.

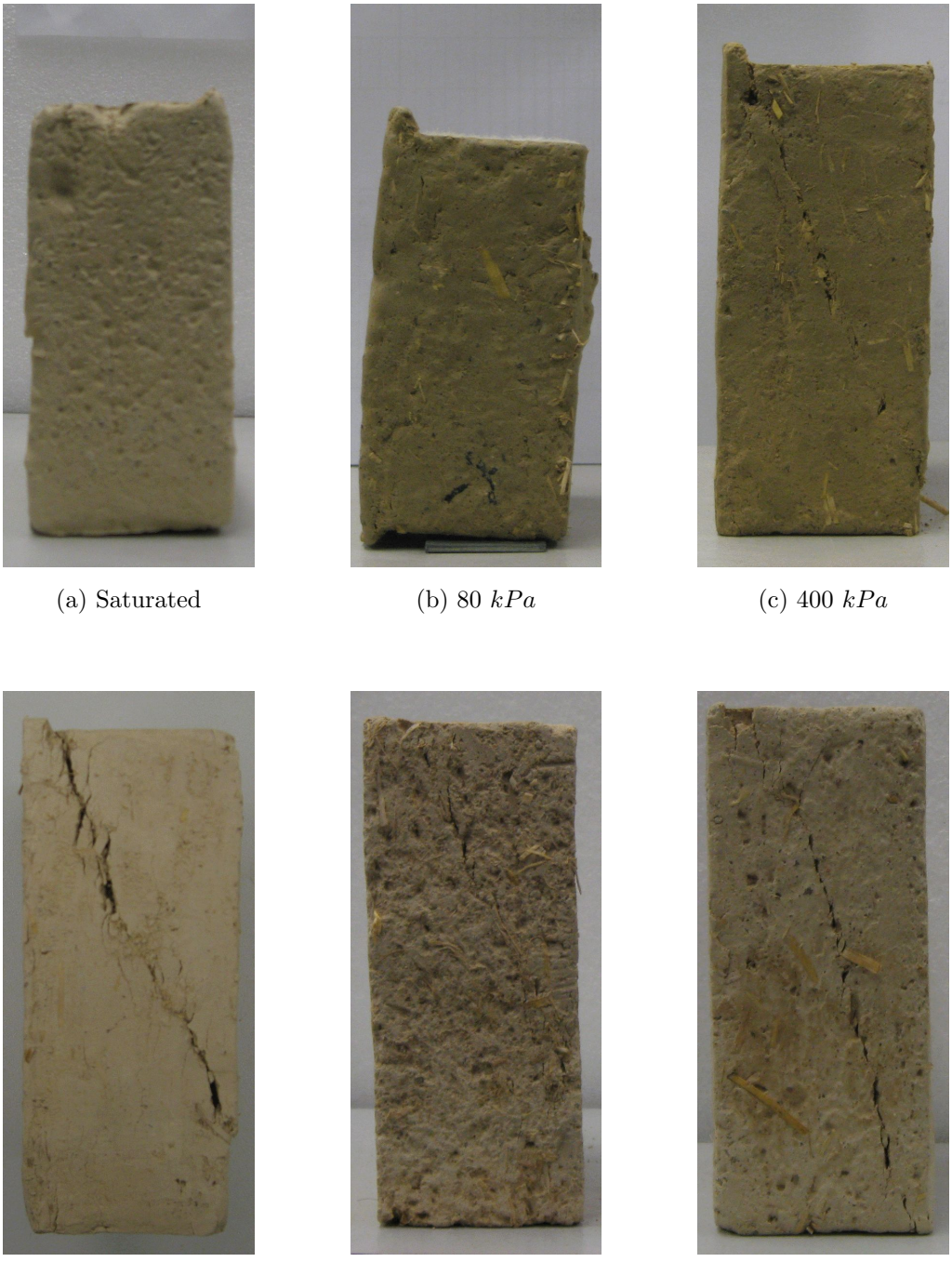

(a) Saturated (b) 80 kPa (c) 400 kPa

(d) 3000 kPa (e) 9500 kPa (f) 55000 kPa

Figure 6.13: Failed samples, 0.5% straw content, $\sigma_3 = 50\,kPa$, suctions are writen under the photos.

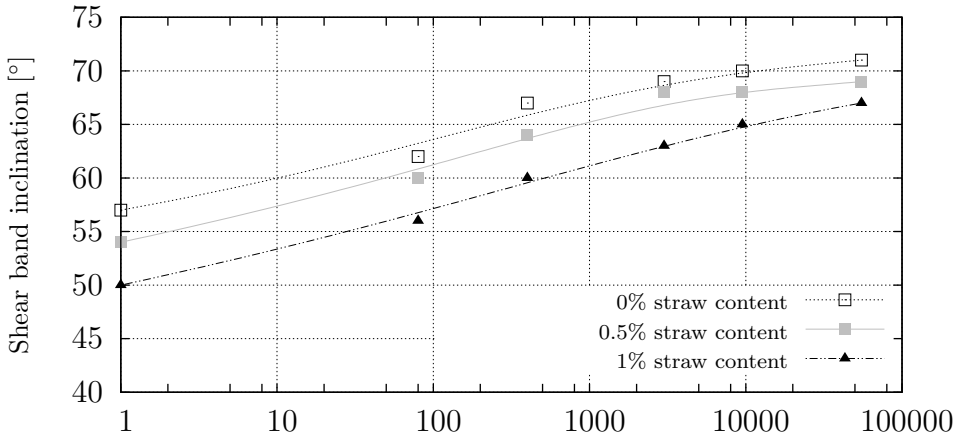

(a) σ_3=50 kPa

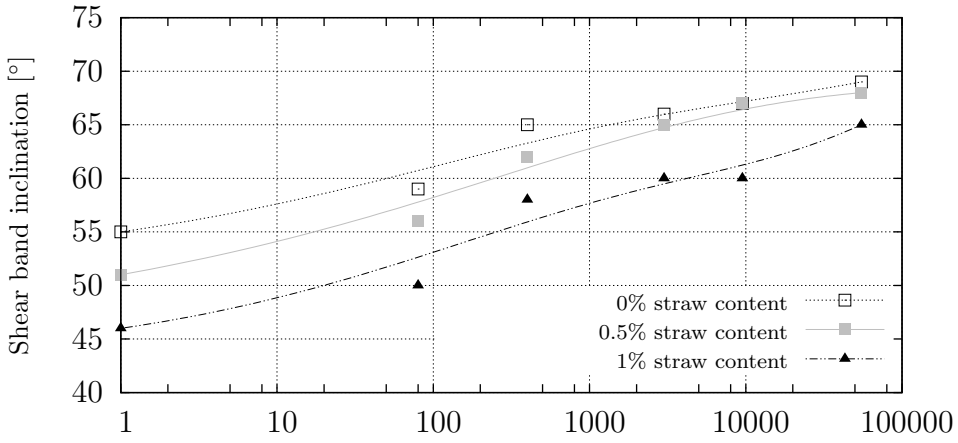

(b) σ_3=100 kPa

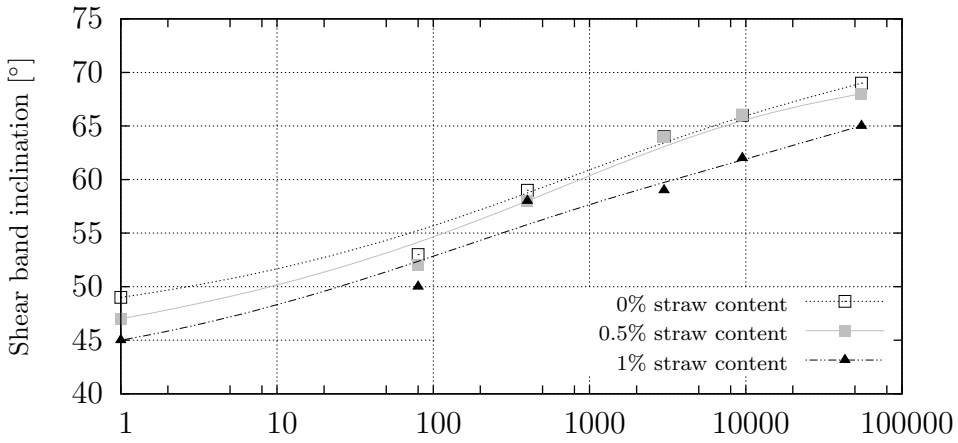

(c) σ_3=150 kPa

Figure 6.14: Angles of shear band inclination vs. suction for different cell pressures (saturated condition is represented by suction = 1 kPa).

6.4 Results of wall tests

Four TDR sensors were installed in different positions of the walls. For unprotected walls (with reinforced and unreinforced materials but without countermeasure) the TDRs were at heights of 5, 15, 25, and 45 *cm* from the bottom (see Figure 5.32). But for the protected wall, since the maximum rise of water was expected to be less than that of the unprotected wall, the sensors were at heights of 5, 10, 20, and 30 *cm*. In terms of the geometry of unprotected walls, uprising happened uniformly and in any horizontal section of the wall the water content was the same. Therefore, the position of TDRs in any elevation was not important. But the openings of the protected wall made uprising nonuniform and the position of sensors was very important. In this wall sensors were installed on the center-line which had the most distance from the openings. The conditions of these three walls are presented in Section 5.4.3.2.

TDRs measured the volumetric water content of samples. Using mass-volume relationships and in relation to the volume changes that happened during uprising of moisture (results of volume change are given in this section), gravimetric water content and the degree of saturation were calculated. Figures 6.15, 6.16, and 6.17 present gravimetric water content over time for walls without countermeasure protection and with 0% and 1% straw content, as well as the protected unreinforced wall. In these figures the positions in which TDRs were installed are written on the curves.

In Figure 6.18 the gravimetric water content of three walls at the end of the tests are presented. As can be seen here, the implemented method against uprising moisture could prevent this problem. It should be noted that in this figure the two unprotected walls cannot be compared with each other, because the duration of their tests was different. However, comparing the results of unprotected walls (with and without straw inclusion) in Figures 6.15 and 6.16 concludes that reinforcement also could reduce the uprising rate, but its efficiency was not considerable.

Figure 6.19 also shows gravimetric water content measured experimentally in the test from different positions of protected wall. For this measurement each row of bricks was divided into three vertical layers and six samples were taken from each layer. The distribution of samples could cover the thickness of the wall from one side to the other one. The bricks located in elevations higher than 40 *cm* were divided into two layers from which only four samples were taken.

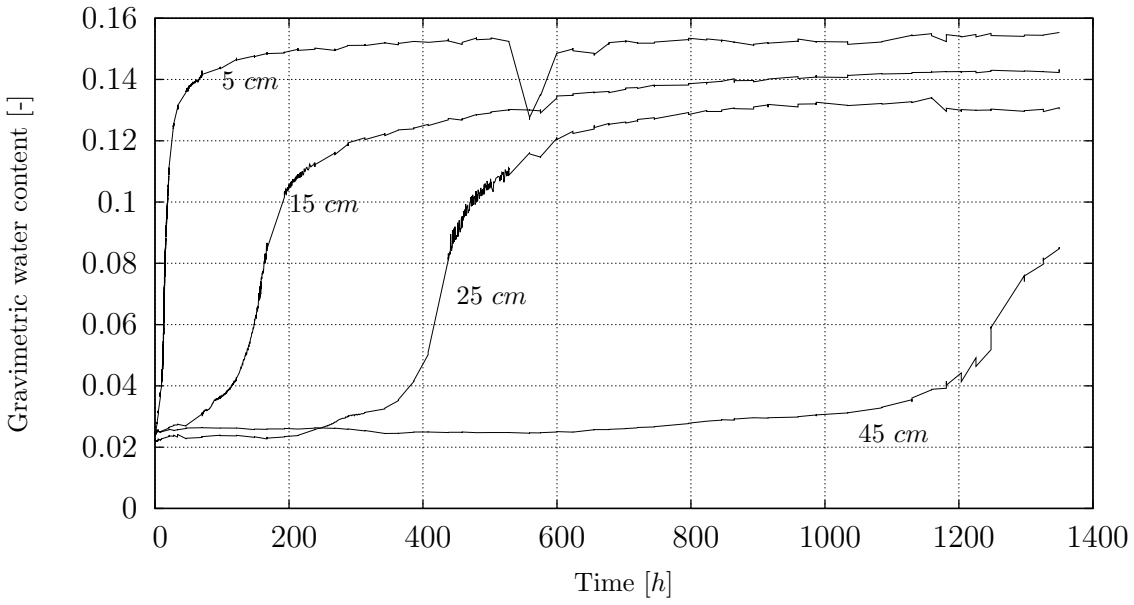

Figure 6.15: Experimental results for four TDRs at different elevations for unprotected wall with 0% straw contrent (see Figure 5.32).

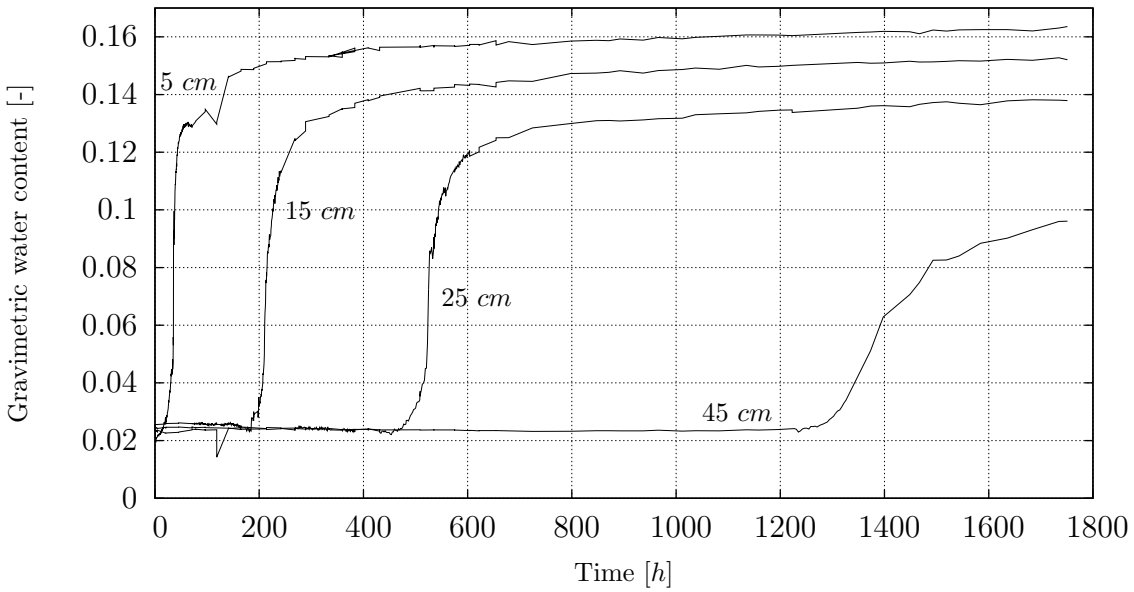

Figure 6.16: Experimental results for four TDRs at different elevations for unprotected wall with 1% straw contrent (see Figure 5.32).

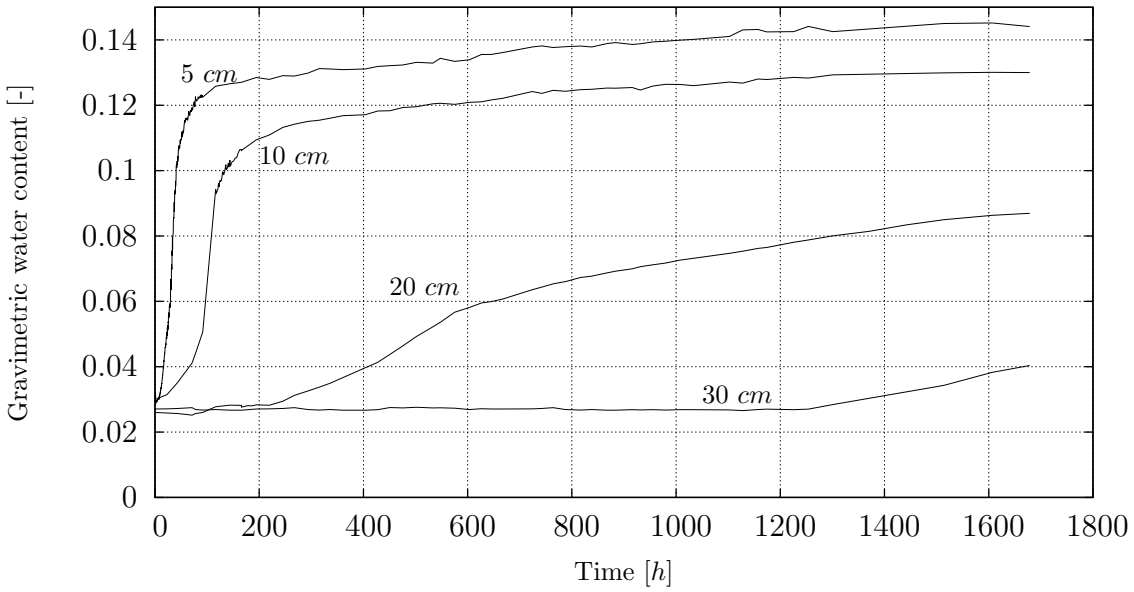

Figure 6.17: Experimental results for four TDRs at different elevations for protected wall with 0% straw contrent (see Figure 5.33).

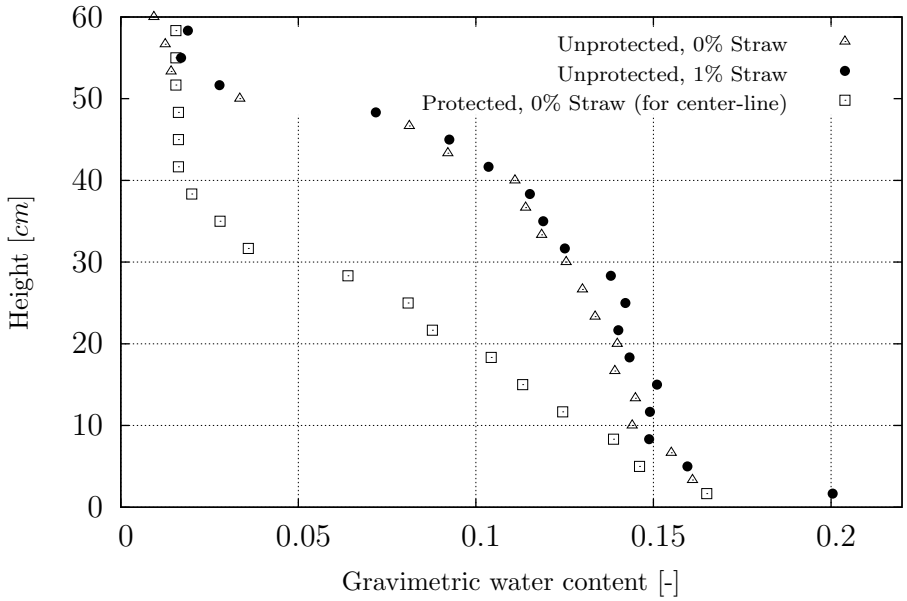

Figure 6.18: Gravimetric water content at the end of tests, for unprotected walls with 1% and 0% straw contrent, and for protected unreinforced wall (see Figures 5.32 and 5.33).

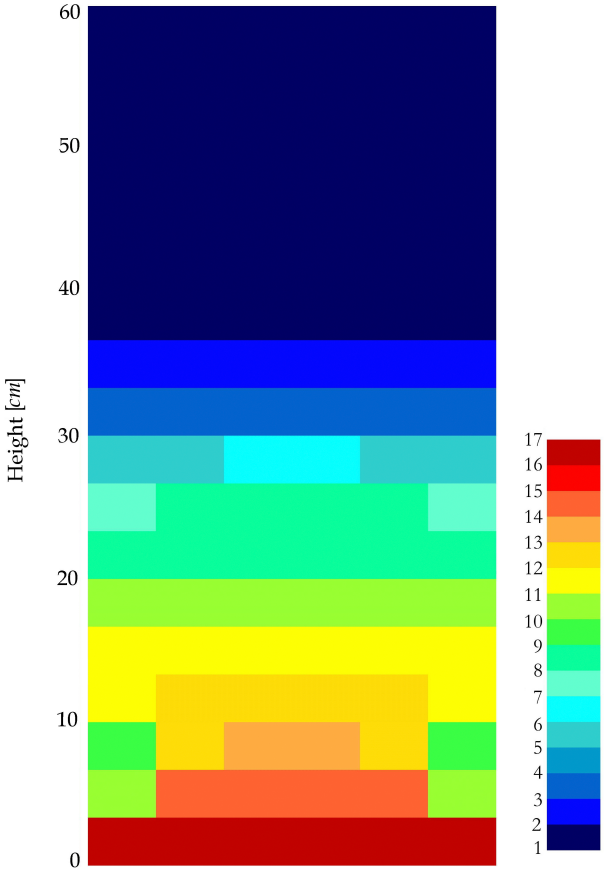

Figure 6.19: Gravimetric water content [%] at end of the test, for the protected wall with 0% straw content.

Vertical deformation of the wall was measured using the PIV method and horizontal deformation by a vernier caliper (see Section 5.4.1.2). Figures 6.20, 6.21, and 6.22 present vertical displacement of given points on the front surface of the walls over time. Elevation of the points are written in the curves' legends. Positive values of the curves show heave and swelling in the bricks. Although the wall was loaded and softening in material could cause settlement, in relation to swelling pressure and loading condition the overall deformation was swelling in all three walls.

As it can be seen here, straw inclusion could considerably reduce the volume change. The heave on top of the wall was reduced more than three times by adding 1% straw fibers to the bricks. This reduction in swelling was compatible with the outcomes of SWCC tests on similar materials (see Section 7.2 and Figure 7.2). The employed protection method also could limit the swelling to the two lowest rows of bricks. Discussion of the results is provided in the next chapter.

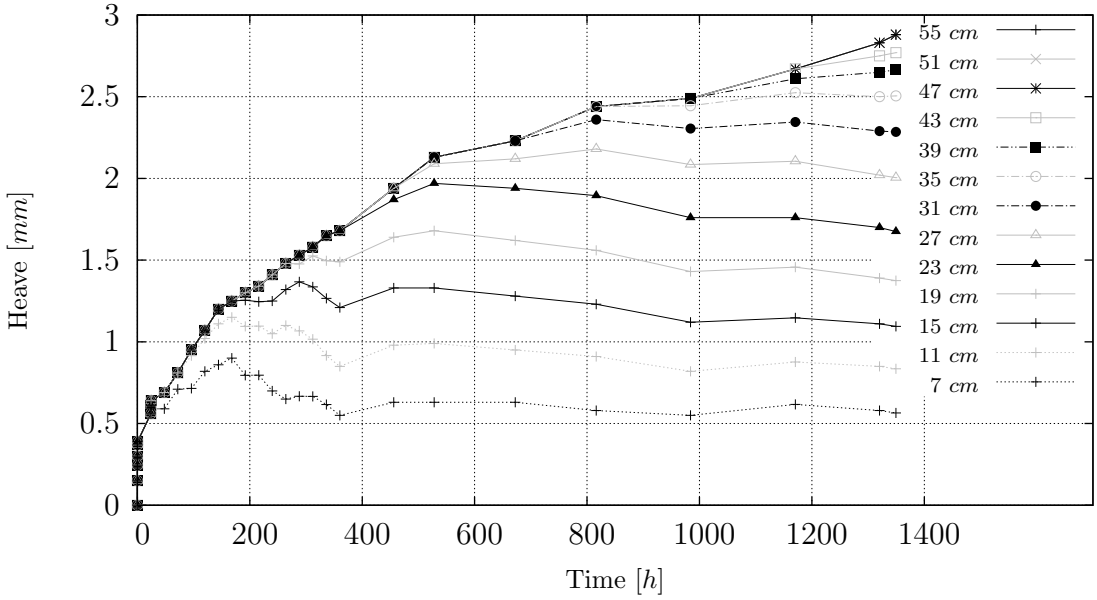

Figure 6.20: Vertical displacement of different points on the unprotected unreinforced wall

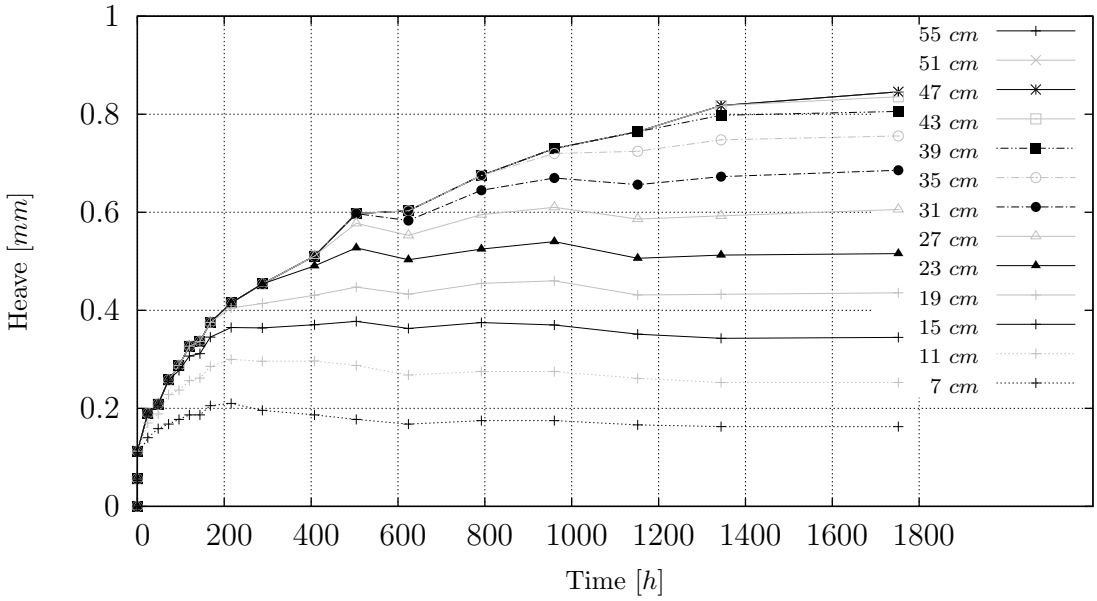

Figure 6.21: Vertical displacement of different points on the unprotected reinforced wall.

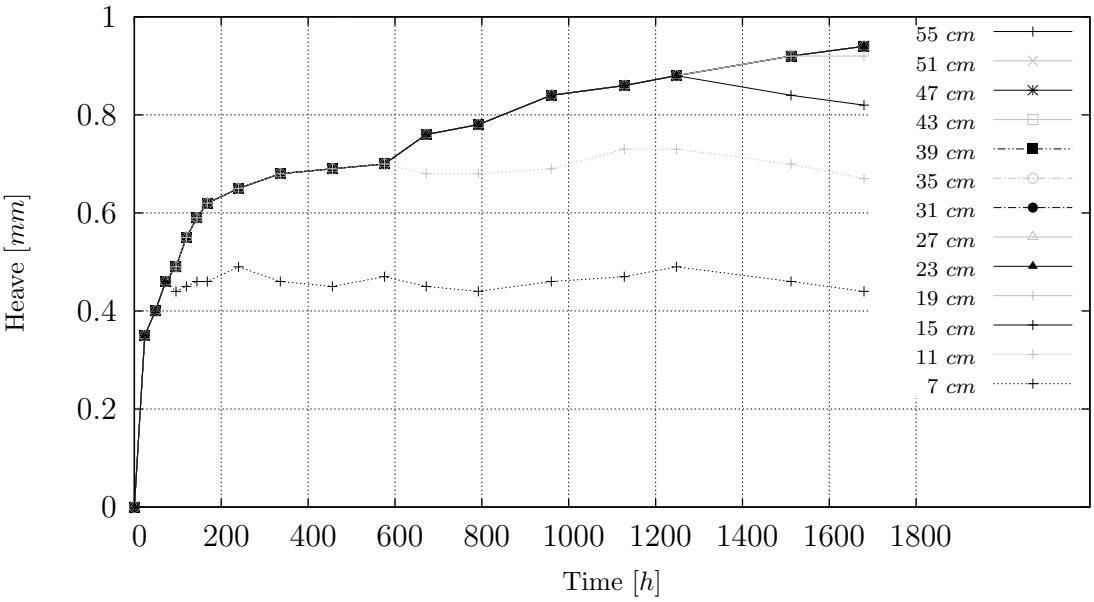

Figure 6.22: Vertical displacement of different points on the protected unreinforced wall.

6.5 Saturated hydraulic conductivity

In this study, in order to measure hydraulic conductivity of unreinforced and reinforced soils, the constant head permeability test was carried out. The samples were compacted in a cylindrical mold with 120 mm height and 100 mm diameter. For this purpose first soil was mixed with the predetermined dosage of straw. Afterwards water was added to the mixture gradually to reach a 5% gravimetric water content. In order to have same compaction at different levels, water must be distributed evenly through the mixture. In the compaction process the void ratio of soils with various straw dosages must reach to the void ratio of the bricks made from same materials after drying and when shrinkage finished. As previously mentioned, the void ratio of dried samples depended on straw inclusion. In this study the desired void ratios for measuring hydraulic conductivity were 0.39, 0.52, and 0.57 for samples with 0, 0.5 and 1% straw content respectively. After samples were made and saturated under isotropic water pressure, a back pressure of 350 kPa was kept constant during the test.

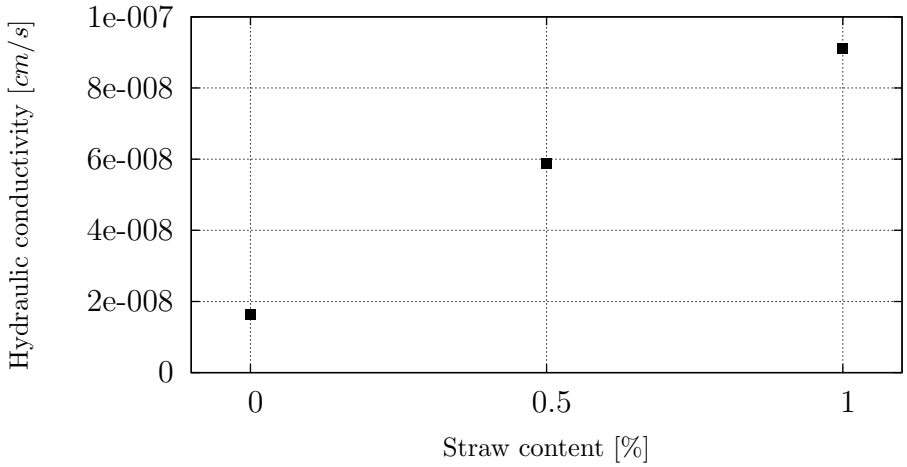

Figure 6.23: Hydraulic conductivity.

Effect of fiber inclusion on the hydraulic conductivity of samples tested is shown in Figure 6.23. Hydraulic conductivity increased with an increase in fiber content. This rapid increase might be due to two factors: (i) porosity of fibers which can function as long pipes and transport water through the sample, and (ii) void ratio of samples which increased with increase in straw content (see Section 7.2 and Figure 7.2).

Abdi et al. (2008) reported that hydraulic conductivity of a clayey soil was increased as a function of both fiber content and length. Chegenizadeh & Nikraz (2011*b*) and Maher & Ho (1994) have also demonstrated the increase in hydraulic conductivity with an increase in fiber content. More literatures review on effect of reinforcement on hydraulic conductivity are presented in Section 3.7.3.5.

6.6 Summary

In this chapter the experimental results of SWCC tests, biaxial tests, and large scale experiments (wall tests) have been presented. Effects of straw content on the shape of SWCC in drying and wetting paths have been shown. Deviator stress and volumetric strain have been drawn versus axial strain for saturated conditions and five applied suctions (80, 400, 3000, 9500 and 55000 kPa), and with three steps of confining pressure (50, 100 and 150 kPa) for materials with 0, 0.5 and 1% straw content. Angles of shear band inclination

observed in the biaxial tests have also been presented for different materials, suctions, and confining pressures. Progress of uprising moisture and the consequent deformation in the wall tests have been shown by separate curves for unprotected unreinforced, unprotected reinforced, and protected unreinforced walls. Finally, the effect of fiber-reinforcement on the hydraulic conductivity of materials used has been presented.

7 Analyses and discussions

7.1 Introduction

In this chapter the discussion of the experimental results of the tests performed is presented. Soil-water characteristic curve of soil without and with four different dosages of fiber content are given and explained in detail. Plane strain shear strength of unsaturated fine-grained soil reinforced with straw fibers is calculated using the effective stress concept for unsaturated soils and the outcomes are discussed and compared with the literature. The experimental results of the wall tests are presented and compared with the results obtained from numerical simulations. A commonly implemented countermeasure method against uprising moisture is controlled experimentally and numerically. Finally, the efficiency of this method together with another alternative method for various dimensions are evaluated using numerical simulations.

7.2 Discussion of SWCC results

It can be implied from Figures 6.2 and 6.3 that the SWCCs cover a wide range of suctions. Figure 7.1 shows the gravimetric water content versus suction (in all curves the saturated condition is represented by suction = 1 kPa). Due to the hysteretic behavior of SWCC, explained in Section 3.3.1, as we can see for all samples, the amount of water that samples could retain was different in wetting and drying paths. But the water content at certain suctions was almost independent from straw inclusion. This matter could be due to the similarity of the material in the five mixtures which contained 97 to 100% of the same soil and the difference was only within the remaining 0 to 3%. The main factors influencing the relationship between the degree of saturation and suction of the fine-grained soils are the surface area and the cation exchange capacity. The soil pore water is retained by molecular bonding, electrical field polarization caused by the negative charge on the

surface of the minerals, and Van der Waals attraction within the soil pore water interface between the molecules as well as the exchangeable cation hydration.

However, samples with different materials could contain relatively the same water content; at certain values of suction they had different shrinkage (in the drying path) and swelling (in the wetting path). As Figure 7.2 shows, although all samples had more or less the same void ratio in their saturated slurry (initial condition), in the drying procedure as the straw content increased the amount of shrinkage under the same suction decreased (or the void ratios increased). The presented results on shrinkage in this study are proven in the literature. Malekzadeh & Bilsel (2012*a*) and Kinjal et al. (2012) stated that fiber reinforcing with polypropylene and polyester reduces the shrinkage tendency in expansive clay specimens. A similar phenomenon also occurred in the wetting path (see wetting paths in Figure 7.2). Samples with higher dosages of straw content showed less swelling. For swelling also, the trend found in this study has been reported in the literature. Loehr et al. (2000), Viswanadham et al. (2009), and Malekzadeh & Bilsel (2012*b*) reported a reduction in swelling with increase in fiber content.

As mentioned before (Section 3.7.3.4), Tang et al. (2007), using SEM photos, found that the surface of fiber filaments was attached by many clay minerals which increases the bonding strength and leads to smaller volumetric deformation during shrinkage or swelling. In the captured SEM photos of the present study this phenomenon was observed (see Figures 4.6a to 4.6f). Besides, due to interfacial forces, the fibers in the matrix limit the shrinkage and swelling of the mixture.

Degree of saturation is the ratio of volume of voids filled with water over total volume of voids, or the water content divided by saturated water content (if void ratio remains constant). As explained above, in the drying path with an increase in straw content shrinkage reduced and the void ratio showed less tendency to decrease. This means that at a given suction the degree of saturation was greater for an unreinforced sample compared to those with straw inclusion, and decreased with an increase in straw content. Or, in other words, reinforcement caused a faster desaturation of material. This phenomenon steeped the SWCC in the drying path. Degree of saturation for drying and wetting paths are shown in Figures 7.3 and 7.4.

In wetting paths, since the void ratio of samples was a function of straw content (as shown in Figure 7.2), the degree of saturation decreased with an increase in straw content (at any given suction); however, they contained relatively the same amount of water. The final degree of saturation at the lowest suction of the wetting paths was higher for samples with less fiber dosage.

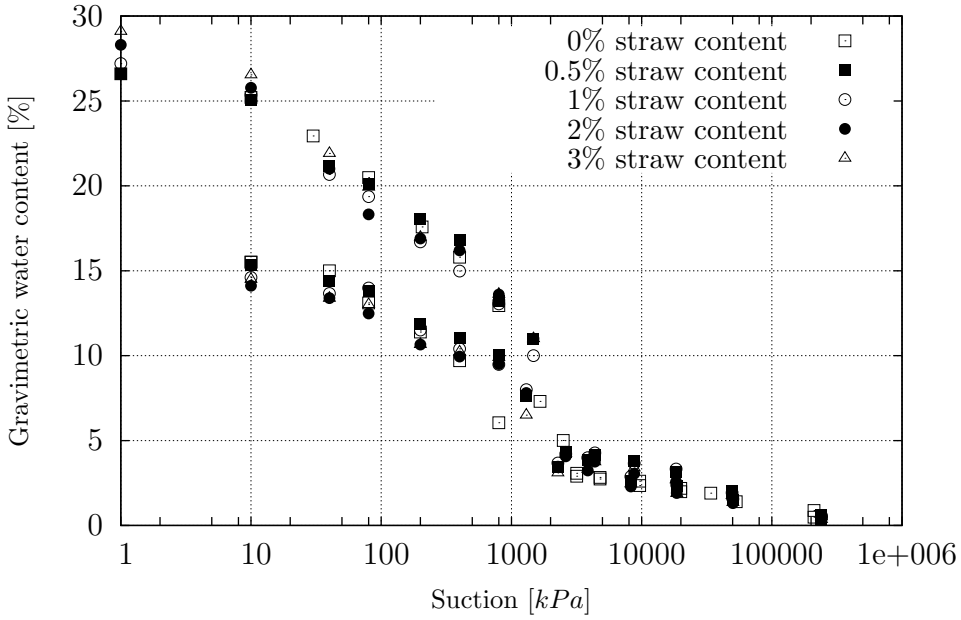

Figure 7.1: Grawimetric water content vs. suction in drying and wetting paths.

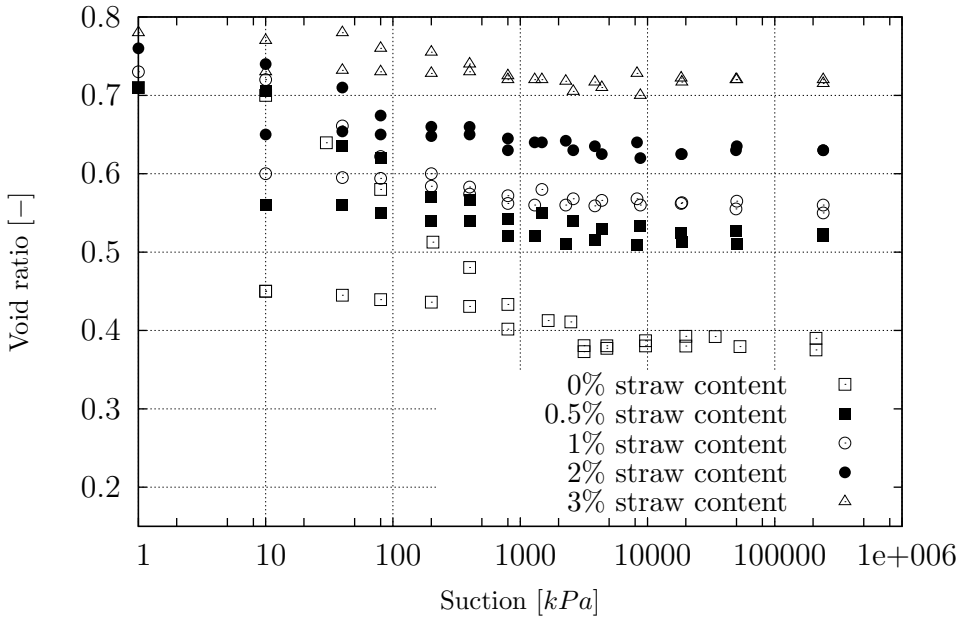

Figure 7.2: Void ratio vs. suction in drying and wetting paths.

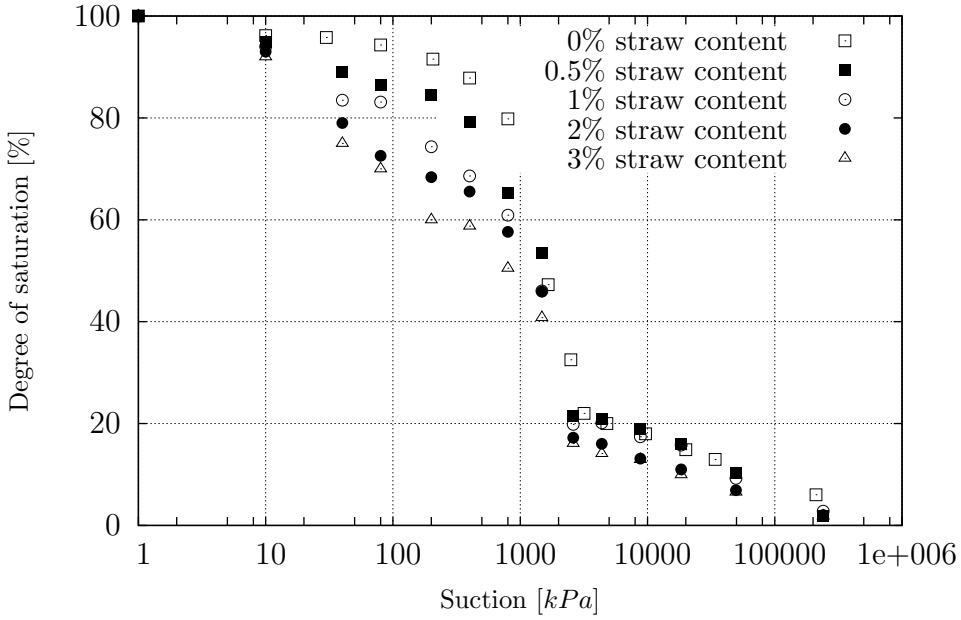

Figure 7.3: Degree of saturation vs. suction in drying paths.

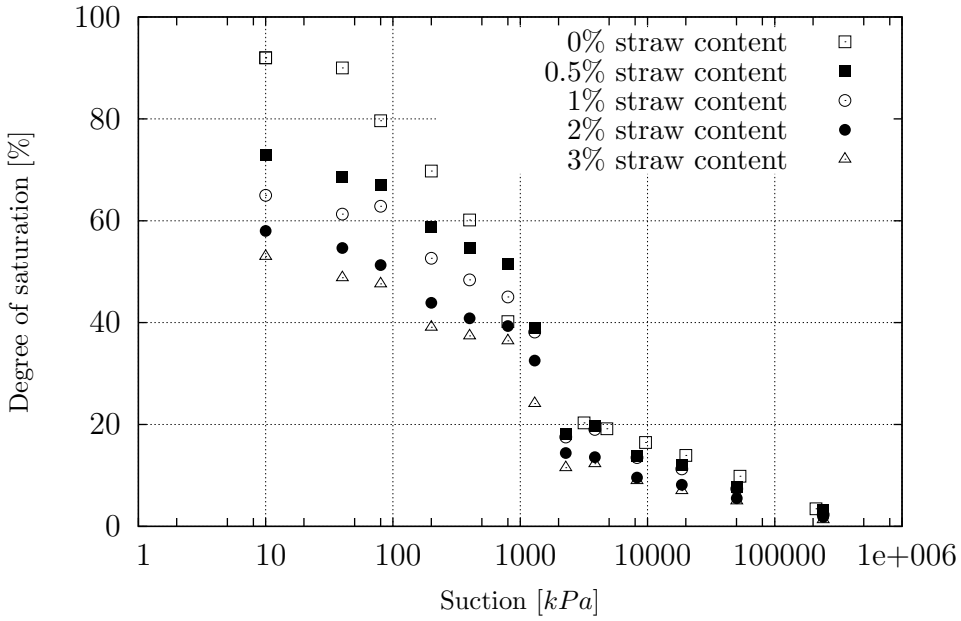

Figure 7.4: Degree of saturation vs. suction in wetting paths.

7.2.1 SWCC parameters

The SWCC parameters were determined by adopting methods suggested by Fredlund & Xing (1994), as below (see Figure 7.5):

(i) Air-entry value(ψ_{AEV}): The air-entry value is the value of suction at which air starts to enter the largest pores of the soil during the drainage process. In some studies in the literature, before AEV the soil is assumed to be saturated (e.g. Vanapalli et al. 1996 and Khalili & Khabbaz 1998). This assumption is not compatible with the reinforced soil used in this study.

(ii) Residual suction (ψ_r): The residual suction is the suction at which the water starts to be held in the soil by adsorption forces (Sillers 1997).

(iii) Water-entry value (ψ_{WEV}): The water-entry value is the suction at which water starts to enter the smallest pores during the wetting process. The water-entry value corresponds to the matric suction at which the water content of the soil starts to increase significantly during the wetting process (Yang et al. 2004).

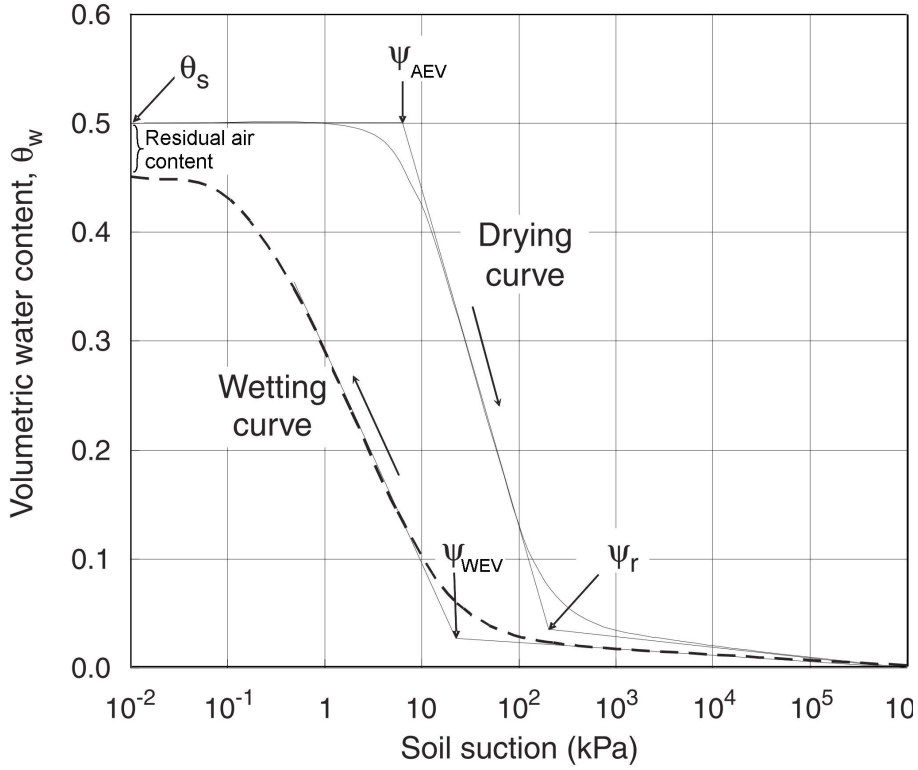

Figure 7.5: Idealized soil-water characteristic curves modified after Fredlund & Xing (1994) (Yang et al. 2004).

Table 7.1: SWCC parameters.

Straw content in the mixture	ψ_{AEV} $[kPa]$	S_{rAEV} [%]	ψ_r $[kPa]$	S_{rres} [%]	ψ_{WEV} $[kPa]$	S_{rWEV} [%]	$S_{r_{max}}^{w}$ [%]
0 %	750	82	3170	22	3000	20	92
0.5 %	600	74	2600	21.5	2300	18	73
1 %	650	64	2600	19.8	2300	17.5	65
2 %	700	60	2600	17.2	2300	14.4	58
3 %	670	52	2600	16.1	2300	11.5	53

The SWCC parameters of mixtures in this research can be determined from Figures 7.3 and 7.4 and were more or less independent from straw content, however, the residual air content (and consequently the degree of saturation at the lowest suction of wetting path ($S_{r_{max}}^{w}$)) were different as a function of straw content. Table 7.1 presents the SWCC parameters defined above for the materials used in this research. The hysteresis between drying and wetting paths increases with the increase in the straw content in the specimens.

In this table S_{rAEV}, S_{rres}, S_{rWEV}, and $S_{r_{max}}^{w}$ represent degrees of saturation corresponding to AEV, residual suction, water entry value, and minimum suction in the wetting path.

The pore size distribution mainly influences the shape and the slope of the SWCC. Poorly graded soils have steep soil-water characteristic curves, because the majority of pores are drained at a narrow range of soil suction. Well graded soils have flatter soil-water characteristic curves, because of their pore size distribution they are drained over wider range of suction.

7.2.2 Effect of sample and straw size on shrinkage and swelling

As explained before, the degree of saturation is strongly dependent on shrinkage of the sample which can be identified by comparison between initial and final void ratios (or void ratios at slurry and dry conditions). Dosage and size of straw (if size of sample remain constant) affects the shrinkage. This research was interested in variation in straw content, but to clarify the effect of length of straw filaments on shrinkage, one unreinforced and four reinforced samples with the same dimensions (cylinder shape with diameter: 50 mm and height: 15 mm) and same straw content (1%) but different lengths (1, 5, 10, and 20 mm) were made with 1.25×LL water content and with the same method of sample preparation for SWCC tests (see Section 5.2.1). As Figure 7.6a shows, the void ratio in the

slurry condition was almost independent of the length of straw, but in the dry condition as length of straw increased as much as the drop in void ratio decreased, which means longer fibers limit the shrinkage more than smaller ones. This phenomenon occurred due to the bondings between soil particles and straw surfaces which were more efficient for longer fibers. As shrinkage of the soil started, the fibers in the soil were compressed and the pressure in fibers resisted any further deformation. Bouhicha et al. (2005) has also reported the same trend. To observe the effect of sample dimensions on shrinkage (if the size of straw remains constant), four cylindrical samples were made with these dimensions: d=148, h=49; d=99.15, h=43.8; d=83.9, h=38; and d=49, h=20.1 mm, with 1% straw content (∼20 mm each piece). However, as can be seen in Figure 7.6b, the size of the sample did not have an important influence on void ratio. From these two curves one can conclude that if the length of straw exceeds a certain value, regardless of size of sample, shrinkage remains constant.

Viswanadham et al. (2009) examined the swelling behavior of fiber-reinforced soils, using fibers of different lengths and observed a reduction in heave. The swelling pressure was the maximum at low length at both fiber contents of 0.25% and 0.50%. Finally, the mechanism by which discrete and randomly distributed fibers restrain deformation of soil was explained with the help of soil fiber interaction. However, Abdi et al. (2008) stated that at constant fiber content the amount of swelling was not significantly affected by increasing fiber length. Maybe was due to the limited range of length they worked with

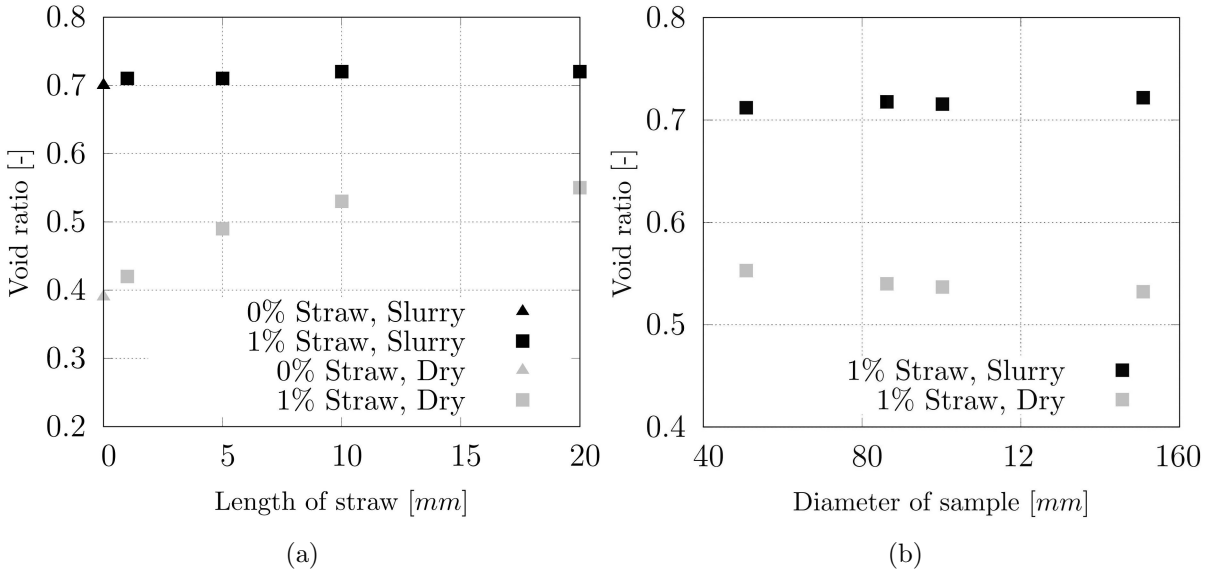

Figure 7.6: Influence of (a) length of straw on shrinkage (Diameter of sample: 50 mm), and (b) diameter of sample on shrinkage (Length of straw: ∼20 mm).

(5, 10, and 15 mm), which supported the idea that after a certain length, fibers do not have significant influence on volume change. Their soil mixture consisted of 75% kaolinite and 25% montmorillonite and the fiber used was polypropylene fibers having 5, 10 and 15mm lengths and contents of 1, 2, 4 and 8%. Unlike synthetic fibers, straw fibers can carry compressive loads if they are confined. Therefore, synthetic fibers have less effect on shrinkage compared to straw fibers. Bouhicha et al. (2005) observed a slight decrease in shrinkage with the increase in straw length at all dosages of reinforcement. This could be attributed to the sufficient length of the straws for the bond stresses at the straw-soil interface to develop and hence to oppose to the deformation and to soil contraction. They performed shrinkage tests on four soils. Two of them had high clay content, but the other two had Atterberg's limits and grain size distribution close to the soil of this study. Size of straw had a considerable effect on soils with high clay content, whereas this effect was much lower for soils with lower clay content (25% and 14% average reduction in shrinkage for soils with high and low clay content due to increase in straw length from 0.5 to 5 cm).

7.2.3 SWCC models

Several parametric models or equations have been suggested and developed to simulate the soil-water characteristics curve. Most of the models are based on a best fit to the experimental data. The "best fitting" curve minimizes the sum of squares of the deviations of the observed values for degree of saturation from those predicted by the regression equation and the method to obtain such a "best fitting" curve is called least sums of squares method. Some of the more frequently used models for representing the SWCC are presented in Table 7.2.

Table 7.2: Conventional equations of SWCC.

Equation	Reference
$S_e = \frac{1}{1+a\psi^m}$	Gardner (1958)
$S_e = \left(\frac{1}{1+a\psi^{1/(1-m)}}\right)^{-m}$	van Genuchten (1980)
$S_e = C(S)\frac{1}{\left\{\ln\left[e+\left(\frac{\psi}{a}\right)^m\right]\right\}^n}$ $C(S) = 1 - \frac{\ln\left(1+\frac{\psi}{\psi_r}\right)}{\ln\left(1+\frac{1000000}{\psi_r}\right)}$	Fredlund & Xing (1994)

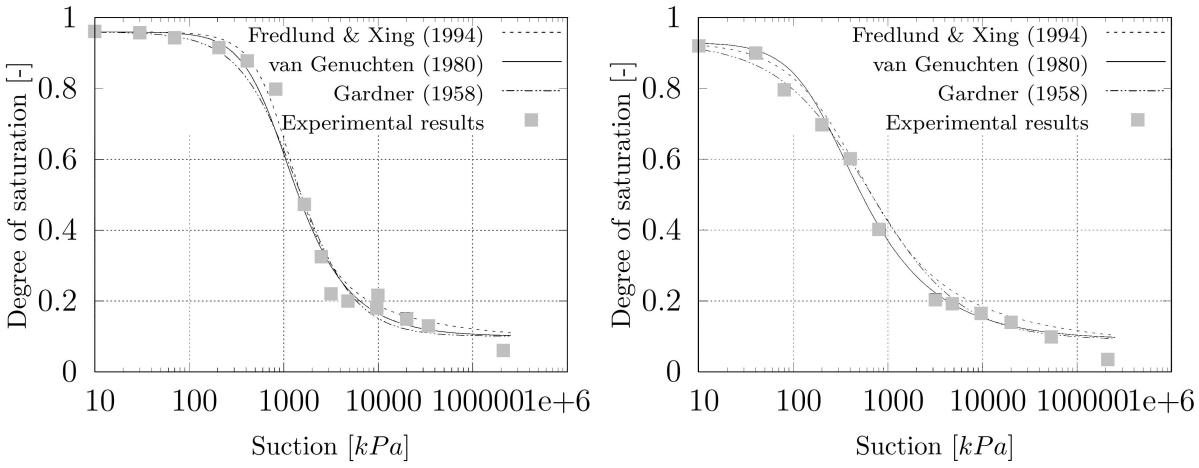

Figure 7.7: SWCC modeling for (a) drying, and (b) wetting paths.

where $C(S)$, S_e and ψ_r (in kPa) are correction factor, effective degree of saturation, and residual suction respectively. m, n, and a are fitting parameters. The parameter a is called the reference suction and is related to the AEV.

S_e in all above equations is:

$$S_e = \frac{S_r - S_{rres}}{S_{rsat} - S_{rres}} \tag{7.1}$$

where S_{rres} and S_{rsat} are residual and saturated degrees of saturation.

Fredlund & Xing (1994)'s model was developed by taking into consideration the pore-size distribution of the soil. The coefficient C is used in the equation to give a zero volumetric water content at a suction of 1000 MPa which approximately corresponds to the oven-dried condition of the soil.

Figures 7.7a and 7.7b show experimental results together with predictions of SWCC suggested by models given in Table 7.2 for unreinforced soil. Fitting parameter of equations are presented in Table 7.3.

Stoimenova et al. (2005) proposed a new simulation method of the SWCC using linearization on parameters. These types of modeling describes the relationship between suction and volumetric water content for suctions more than air entry value by means of two parameters (β_0 and β_1) which linearly relate $\ln\psi$ or $\ln\ln\psi$ to $\ln\theta$ or $\ln\ln 1/\theta$ as below:

Table 7.3: Fitting parameters of SWCC models for unreinforced soil.

Model	Drying			Wetting		
	a	m	n	a	m	n
Gardner (1958)	0.0004	1.4		0.003	0.9	
van Genuchten (1980)	750	0.5		350	0.5	
Fredlund & Xing (1994)	0.0011	2.2	1.3	0.003	1.15	1.5

$$\begin{cases} i) & \ln\theta = \beta_0 + \beta_1 \ln\Psi \\ ii) & \ln\theta = \beta_0 + \beta_1 \ln\ln\Psi \\ iii) & \ln\ln 1/\theta = \beta_0 + \beta_1 \ln\Psi \\ iv) & \ln\ln 1/\theta = \beta_0 + \beta_1 \ln\ln\Psi \end{cases} \tag{7.2}$$

where:

$$\Psi = \frac{\psi}{\psi_u} \tag{7.3}$$

Here, ψ_u is properly chosen regarding the units of suction measurements and is used to define the dimensionless suction measure Ψ which is bigger than 1. By changing the parameter vector (β_0, β_1) and correlating the experimental data on the predicting model, the best fit is obtained. Lins (2009) has also adopted this method for modeling the SWCCs of her experimental results on sand. In this study, Figure 7.8 shows the predictions using Equations 7.2 and compares them with experimental data. In the calculations ψ_u is assumed 1 kPa. The parameters β_0 and β_1 are determined by best fit of lines to the experimental results and are given in Table 7.4.

Table 7.4: Fitting parameters of statistical SWCC models for unreinforced soil.

Parameters	Equations 7.2			
	(i)	(ii)	(iii)	(iv)
β_0	1.183	6.234	-0.48	-2.41
β_1	-0.447	-4.158	0.165	1.566

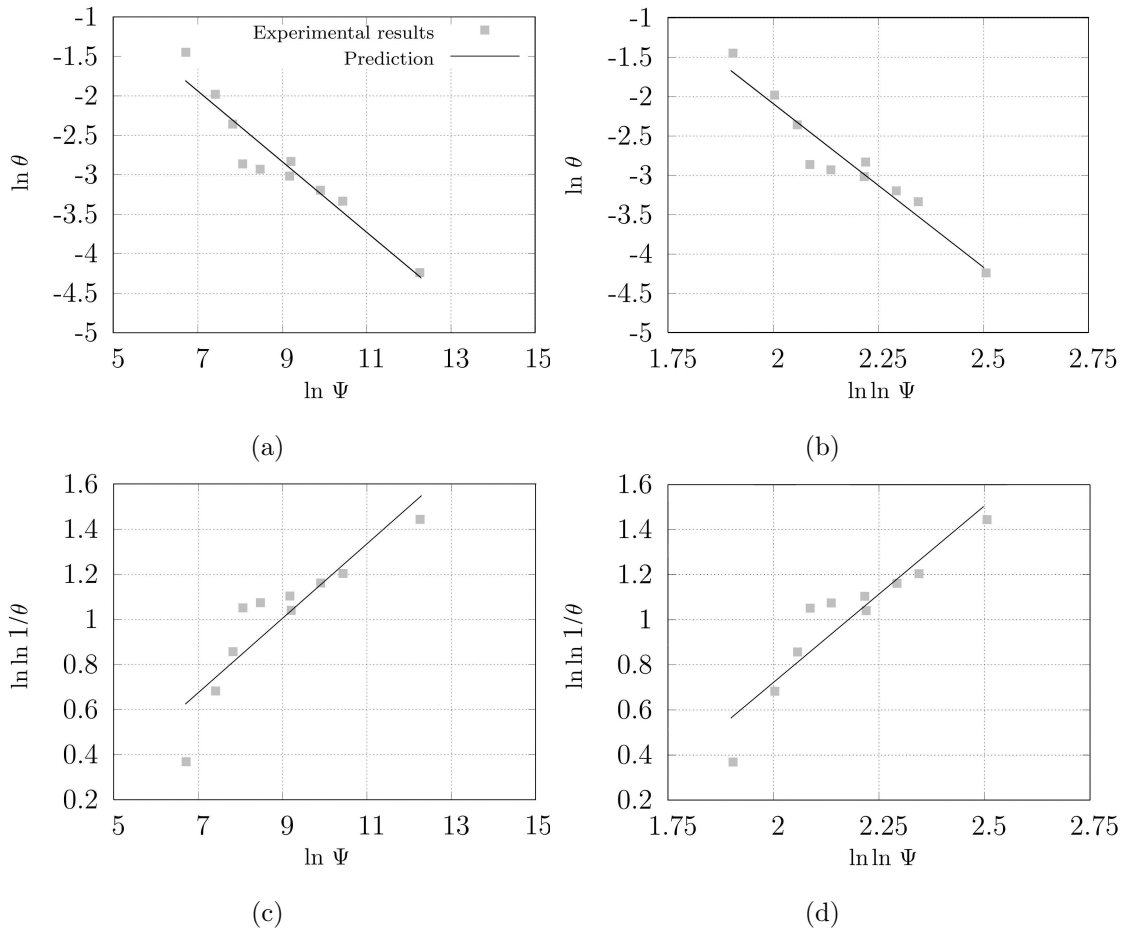

Figure 7.8: Comparison between experimental results and predictions using Equations 7.2

7.3 Discussion of the biaxial results

7.3.1 Shear strength of unsaturated reinforced soil

As expected, in $\sigma_d - \epsilon_1$ curves (Figures 6.4 to 6.12), with an increase in suction (and associated decrease in degree of saturation) shear strength increased and the drop in post peak strength became more visible. Straw content also affected the shear strength which will be analyzed later in detail. Using total stresses, namely applied confining pressure ($\sigma_3 - u_a$) and measured deviator stress ($\sigma_d = \sigma_1 - \sigma_3$), and by means of Mohr-Coulomb's equation (Equation 7.4), cohesion (c) and friction angle (ϕ) of soil based on total stresses can be obtained. Minimum of two biaxial experiments is required to solve this equation. In order to have better accuracy three tests using different confining pressures (50, 100, and 150 kPa) were performed in this research.

$$\sigma_1 = \sigma_3 \cdot \tan^2\left(\frac{\pi}{4} + \frac{\phi}{2}\right) + 2c \cdot \tan\left(\frac{\pi}{4} + \frac{\phi}{2}\right) \tag{7.4}$$

Applied and measured minimum and maximum principal stresses, axial strain at peak stress (ϵ_p), together with total cohesion and friction angle are presented in Table 7.5. It can be inferred from this table that with an increase in suction the friction angle did not change considerably for materials (with the exception of two values: for 0% straw content at suction 55000 kPa, and for 1% straw content at suctions 3000 and 9500 kPa). But cohesion increased considerably as a result of the increase in suction stress.

Axial strain at failure generally decreased as suction increased. This occurred due to the dependency of failure type and brittleness of samples on the degree of saturation. Failure type and axial strain at peak stress were determined by bonding among soil particles as well as straw-soil interaction (for each confining pressure). In dry sand-clay mixtures connections between grains are mostly through solid bridges (see Figure 2.2) which after a certain value of strain break and the sample fails abruptly. But with an increase in water content, which fills the gap between particles, components of interparticle attractions (explained in Section 2.2.2) lose their effectiveness and solid bridges become softer. Although wet bridges can resist a smaller load, because of the existence and thickness of a water film between the clay platens, grains can more easily displace among the clays and consequently the sample fails with a larger strain. Figure 7.9 and Table 7.5 show the ϵ_p versus suction for different confining pressures and straw contents. In this figure the saturated condition is represented by 1 kPa suction. For all materials ϵ_p decreased with an increase in suction. As it can be seen in this figure, for saturated conditions diversity of ϵ_p was much more than in unsaturated conditions. The reason for this can be found in the stress-strain curves (Figures 6.4 to 6.12), in which saturated samples failed in a very soft manner and the deviator stress had an almost constant value over a wide range of axial strain; therefore, a small jump in σ_d could change the position of peak point. Mostly ϵ_p increased with an increase in σ_3 and straw content, if the other conditions were constant.

Table 7.5: Results of biaxial tests based on total stresses.

Straw content [%]	Suction [kPa]	σ_3 [kPa]	σ_1 (max) [kPa]	ϵ_p [-]	E_{50} [MPa]	E_{100} [MPa]	c [kPa]	ϕ [°]
0	0	50	174.18	0.028	61.39	4.43	13.6	28.6
		100	335.66	0.072	27.38	3.27		
		150	459.62	0.217	56.03	1.39		
	80	50	280.75	0.082	26.54	2.81	45.4	28.0
		100	433.48	0.072	30.35	4.63		
		150	559.33	0.108	25.45	3.79		
	400	50	498.47	0.020	27.05	22.42	105.8	29.0
		100	651.19	0.027	32.67	20.41		
		150	787.62	0.038	28.08	16.78		
	3000	50	1165.70	0.010	52.86	111.57	234.4	39.0
		100	1439.13	0.012	92.41	111.59		
		150	1614.76	0.013	103.67	112.67		
	9500	50	1580.69	0.011	108.183	139.15	403.2	32.0
		100	1792.23	0.012	123.88	141.02		
		150	1916.01	0.017	128.31	103.89		
	55000	50	2280.44	0.013	138.21	171.57	416.1	44.1
		100	2504.71	0.013	134.24	184.98		
		150	2850.32	0.014	164.96	192.88		
0.5	0	50	229.57	0.029	36.51	6.19	18.2	30.9
		100	370.99	0.072	51.21	3.76		
		150	542.19	0.227	16.68	1.73		
	80	50	393.61	0.084	24.11	4.09	62.9	32.4
		100	560.20	0.073	28.47	6.3		
		150	724.46	0.110	36.24	5.22		
	400	50	539.51	0.020	49.5	24.48	111.2	29.5
		100	668.28	0.028	52.35	47.36		
		150	835.07	0.039	48.02	17.57		
	3000	50	995.64	0.010	107.11	94.56	264.1	27.7
		100	1155.10	0.012	113.89	87.93		
		150	1272.36	0.013	128.58	86.34		
	9500	50	1149.65	0.013	115.14	84.59	304.0	28.9
		100	1325.00	0.012	166.91	102.08		
		150	1441.31	0.018	95.84	71.74		
	55000	50	1769.41	0.014	153.14	122.82	474.6	29.0
		100	1890.43	0.013	211.07	137.73		
		150	2061.29	0.014	212.83	136.52		
1	0	50	264.99	0.110	12.14	1.95	33.1	30.4
		100	421.99	0.082	18.06	3.93		
		150	570.02	0.108	12.99	3.89		
	0	50	457.58	0.120	17.96	3.4	83.6	30.7
		100	597.51	0.060	25.98	8.29		
		150	767.33	0.049	43.41	12.6		
	400	50	554.70	0.033	44.06	15.29	116.4	30.2
		100	708.86	0.041	41.97	14.85		
		150	857.56	0.046	43.86	15.38		
	3000	50	755.10	0.009	226.71	78.34	126.7	39.5
		100	992.25	0.013	157.2	68.63		
		150	1206.03	0.018	123.15	58.67		
	9500	50	873.63	0.011	124.19	71.52	181.3	37.1
		100	1159.31	0.012	166.39	88.28		
		150	1300.39	0.017	141.74	67.67		
	55000	50	1365.51	0.009	210.72	146.17	329.9	31.7
		100	1489.82	0.011	211.29	126.35		
		150	1695.59	0.014	190.6	110.4		

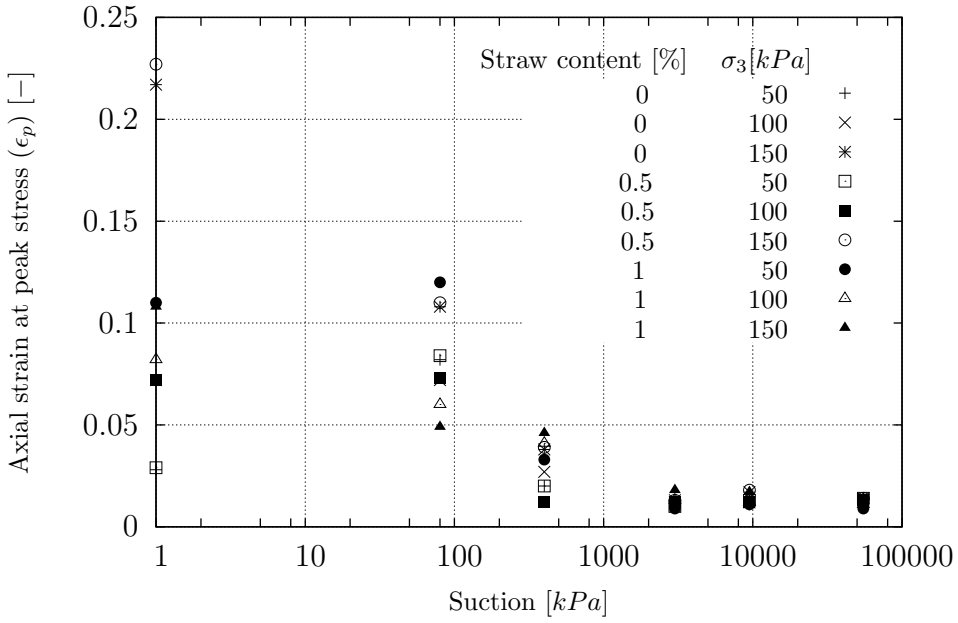

Figure 7.9: Strain at peak stress for different straw contents and confining pressures (1 kPa suction represents fully saturation).

The changes in moduli of elasticity in different conditions are presented in Table 7.5. The secant moduli of elasticity at 50% of the peak stress (E_{50}) and at peak (E_{100}) were determined as follows:

$$E_{50} = \frac{0.5 \times \sigma_d^{max}}{\epsilon_{50\%}} \tag{7.5}$$

$$E_{100} = \frac{\sigma_d^{max}}{\epsilon_p} \tag{7.6}$$

where $\sigma_d^{max} = (\sigma_1 - \sigma_3)_{max}$ is the deviator stress at peak, ϵ_p is the axial strain at peak stress, and $\epsilon_{50\%}$ is the axial strain at 50% of the maximum peak stress.

Both E_{50} and E_{100} increased rapidly with an increase in suction, which was followed by larger post peak drop in shear stress. In suctions higher than AEV with an increase in straw content E_{100} also increased. But in suctions less than AEV the opposite was observed. The reason originates from peak shear strength which with an increase in straw content increased for suctions less than AEV, and decreased for suctions higher than AEV. This phenomenon will be explained in more detail later in this section. However, dependency of moduli of elasticity on confining pressure was anticipated, but according to

the achieved results there was no meaningful relationship between moduli of elasticity and σ_3. Taibi et al. (2009) also stated that E_{50} increases with an increase in suction for soft rocks. Cho & Santamarina (2001) reported shear-wave velocity, which indicated stiffness at low strains, increased as the degree of saturation decreased for soils containing fine-grained content. But for granular material maximum velocity happens at an optimum S_r.

Figures 7.10 shows shear strength, $(\sigma_1 - \sigma_3)_{max}$, for three used materials over suctions from 0 to 55000 kPa. As we can see here, in low suctions with an increase in suction shear strength increased non-linearly and rapidly, but after a certain suction (almost residual suction) rate of increase in shear strength reduced considerably. According to Vanapalli et al. (1996), in explanation of the unsaturated shear strength behavior when drying process of soil takes place, the soils have three identifiable stages as shown in Figure 7.11:

(i) The boundary stage, in which the soil is essentially saturated. Degree of saturation in the soil does not change with increasing matric suction. In this stage the variation of shear strength is assumed to be linear.

(ii) The transition stage, (i.e. primary and secondary transition stages), in which suction $>$ AEV. In this stage S_r reduces with increasing matric suction. Specifically, the air starts to enter into the soil and the shear strength exhibits a non-linear behavior.

(iii) The residual stage. In this zone the change in the water content is very small. Beyond this stage shear strength with respect to the matric suction decreases or remains relatively constant for sandy and silty soils. However, a slight increment in the shear strength can be observed for clayey soils. The general nature of SWCC gives an indication of the shear strength behavior over a wide range of suction.

For clayey adobe bricks, Vanapalli et al. (1996) stated that the unsaturated strength is relatively high and continues to rise until it reaches the dry condition. Outcomes of this research also confirmed this statement for adobe bricks (see Figure 7.10). Escario & Juca (1989) reported an increase in shear strength for a clayey soil at suction values as high as 10 MPa. Vanapalli et al. (2000) also experimentally observed the strength of a silty soil for suction in the range of 0 to 1000 MPa. They monitored a relatively linear increment in the shear strength with an increase in suction in log-log scale. Khalili et al. (2005) measured the shear strength of a clayey silt over suctions from 0 to 400 kPa which was noticeably less than residual suction, and defined a bilinear function for shear strength versus suction, which tilted at AEV. Song et al. (2012) compared the shear strength and suction stress of silt and sand. They finally concluded that unlike sand that loses its strength as it dries, silt kept a constant strength in higher ranges of suction.

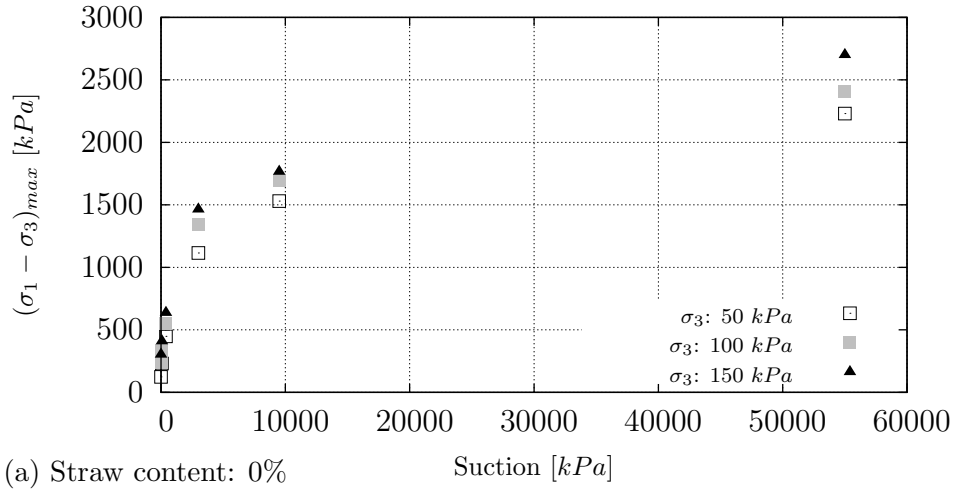

(a) Straw content: 0%

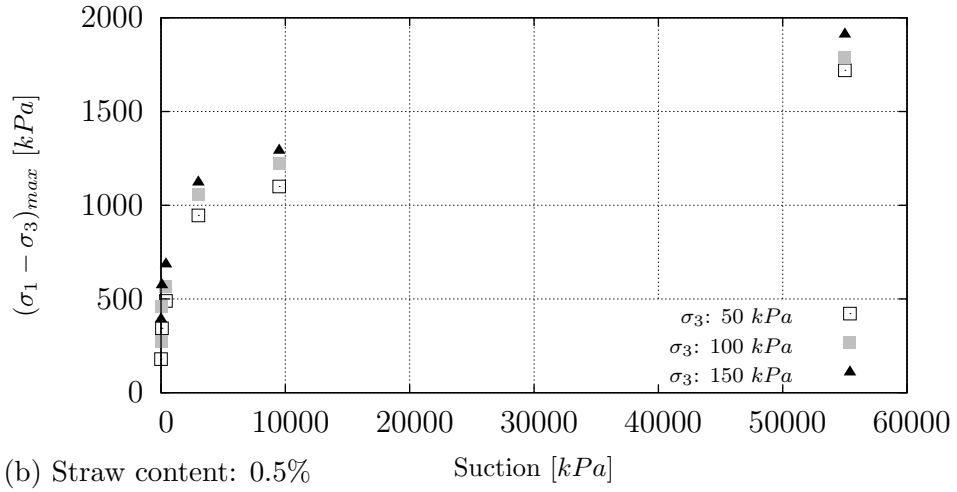

(b) Straw content: 0.5%

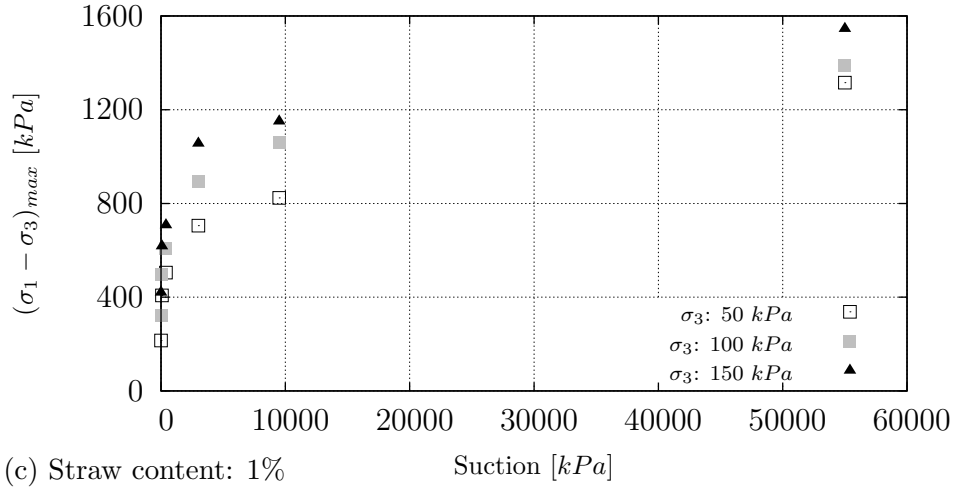

(c) Straw content: 1%

Figure 7.10: Shear strength vs. suction, experimental results for different straw contents.

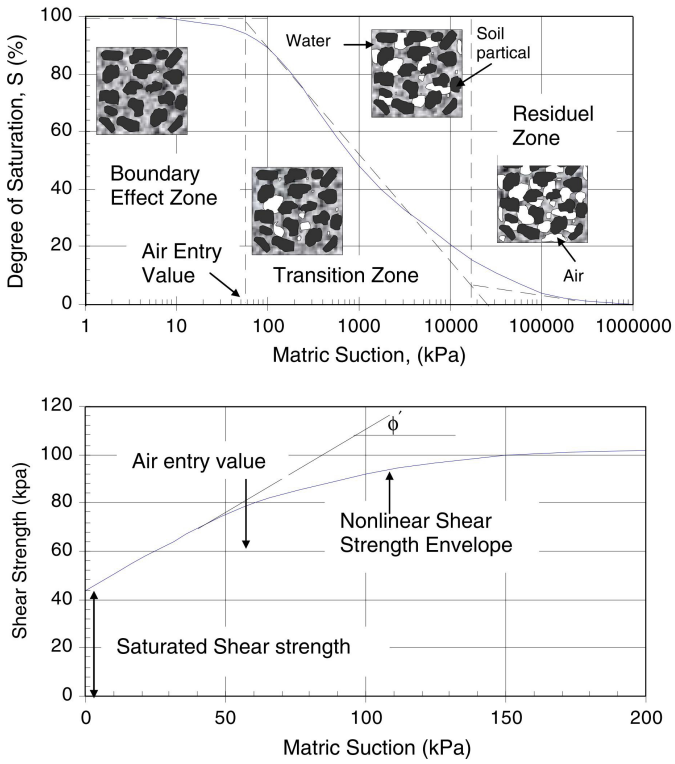

Figure 7.11: The soil-water characteristic curve and the unsaturated shear strength of a soil (Vanapalli et al. 1996).

Some other researchers (i.e. Rassam 2002, Zhan & Ng 2006, Mohamed et al. 2006, Kayadelen et al. 2007, Jotisankasa et al. 2009, and Farulla & Rosone 2012) observed shear strength of clayey soils for a range of suction from saturated conditions up to a suction higher than AEV but notably less than residual suction.

Bishop (1959) modified Terzaghi's theory to extend the effective stress idea for unsaturated soils by taking into account the two-phase nature of the pore fluid in the unsaturated soil. Bishop proposed Equation 7.7 as follows:

$$\sigma' = (\sigma - u_a) + \chi.(u_a - u_w) \tag{7.7}$$

where σ', σ, u_a, u_w, and χ are effective stress, total stress, pore air pressure, pore water pressure, and Bishop's effective stress parameter, which is 1 for saturated soils and approaches down to 0 as the soil dries. According to this equation, effective stress is always larger in a partially saturated soil compared to the same soil in fully saturated conditions.

$\chi.(u_a - u_w)$ is also called "suction stress". Suction stress characteristic curve (SSCC) has been introduced to represent the state of suction stress in unsaturated soils (Lu & Likos 2004). In this curve suction stress is drawn versus suction. Similar to SWCC, SSCC also depends on the hydraulic path and has hysteretic behavior in drying and wetting paths.

In order to predict SSCC and the shear strength of unsaturated soil, Equation 7.7 must be solved experimentally or analytically. Substituting Equation 7.7 into Coulomb's formula (Equation 7.8) the shear strength of unsaturated soils can be predicted experimentally via Equation 7.9.

$$\sigma_1' - \sigma_3' - (\sigma_1' + \sigma_3') \sin\phi' - 2c' \cos\phi' = 0 \tag{7.8}$$

$$\chi\,(u_a - u_w) = \frac{\sigma_1 - \sigma_3 - 2c' \cos\phi' - (\sigma_1 + \sigma_3 - 2u_a) \sin\phi'}{2 \sin\phi'} \tag{7.9}$$

where $(\sigma_n - u_a)$, c', and ϕ' are net total stress, and cohesion and friction angle of saturated soil respectively. Equation 7.9 determines χ using experimental data. In the literature some empirical equations have been presented to predict χ analytically:

Vanapalli et al. (1996):

$$\chi = \left(\frac{\theta}{\theta_s}\right)^{\kappa} \tag{7.10}$$

Oberg & Sallfors (1997):

$$\chi = S_r \tag{7.11}$$

Khalili & Khabbaz (1998):

$$\chi = \begin{cases} 1 & \psi < \psi_{AEV} \\ \left(\frac{\psi_{AEV}}{\psi}\right)^r & \psi \geq \psi_{AEV} \end{cases} \tag{7.12}$$

Tarantino (2007):

$$\chi = \frac{\theta - \theta_{res}}{\theta_{sat} - \theta_{res}} \tag{7.13}$$

where ψ, ψ_{AEV}, S_r, θ, θ_{sat}, and θ_{res} represent suction, air entry value (AEV), degree of saturation, volumetric water content, saturated and residual volumetric water content.

Fitting parameters κ and r in Equations 7.10 and 7.12 must be selected based on the best fit of the results. In the literature 1 for κ and 0.55 for r is suggested, however they overestimate the Bishop's effective stress parameter especially for reinforced samples. The values chosen for κ and r, which had the best fit with the experimental results, are presented in Table 7.6.

For three tested materials Figure 7.12 shows Bishop's effective stress parameter calculated from the experimental data and analytical methods introduced above. Since biaxial samples were in wetting conditions the required data for empirical equations were obtained from the wetting path of SWCC. During the wetting process, as mentioned in Section 7.2, with an increase in fiber content the amount of occluded air bubbles inside the sample and consequently the void ratio increased. This means reinforced samples under the lowest suction never reach fully saturated conditions. Equation 7.11, since it calculates χ with an absolute - not relative - parameter (S_r), showed a different trend in comparison with other curves and underestimated the range of low suctions and overestimated high suctions, especially for high straw contents, because, as mentioned before, reinforced samples in the drying path even in very low suctions still occluded air bubbles which did not let S_r return to 1. For the same reason, Equation 7.13 considerably overestimates the results in the case of fiber inclusion. In general, the methods introduced by Vanapalli et al. (1996) and Khalili & Khabbaz (1998), owing to their flexible fitting parameters (κ and r), predicted the Bishop's parameter (χ) (regarding changes in suction) better than others, especially for reinforced samples.

Table 7.6: Fitting parameters of Equations 7.10 and 7.12.

Straw content	κ	r
0 %	1.5	0.6
0.5 %	2	0.65
1 %	3	0.7

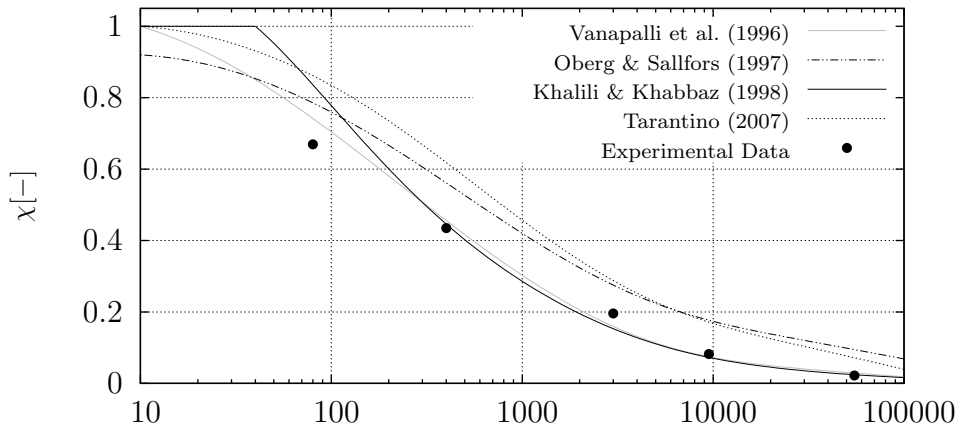

(a) Straw content: 0%

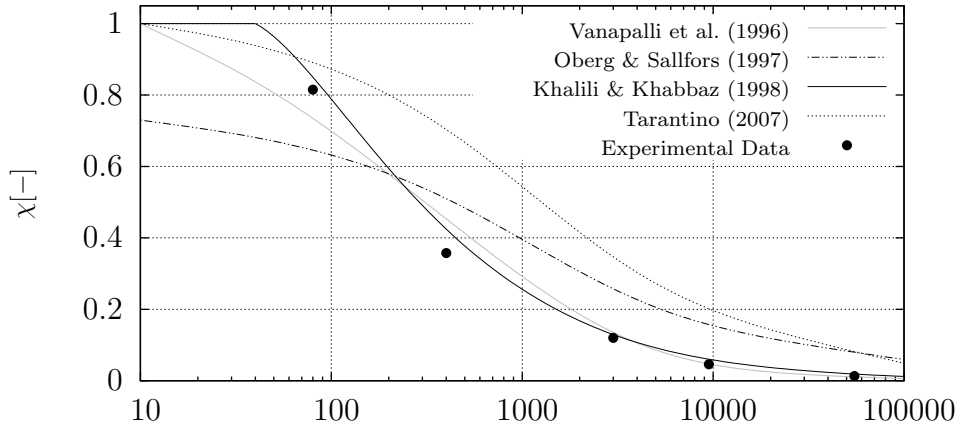

(b) Straw content: 0.5%

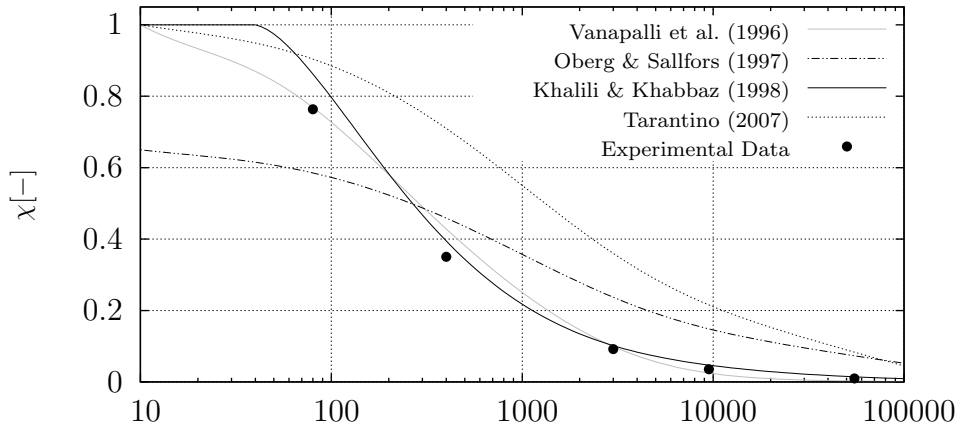

(c) Straw content: 1%

Figure 7.12: Bishop's effective stress parameter vs. suction, experimental and analytical results for different straw contents.

Effect of fiber reinforcement is more pronounced when the strain in any shear strength test increases. This means that the fibers play a role or contribute to transporting loads only if they are mobilized. As can be seen in Figure 7.13, reinforcement increased the shear strength in suctions lower than AEV (0, 80, and 400 kPa). As mentioned earlier, fibers contribute only if they are mobilized which requires a certain amount of minimum strain. In the case of low water content in which soil is stiff, fiber inclusion plays no role in the strength of the material, because the sample has a brittle behavior and fails before the fibers are activated. But in the case of higher water content soil is softer and the fiber is allowed to move among the soil matrix, therefore, fiber reinforcement can improve the shear strength of the material. The mobilized filaments contribute to carrying the load and caused an increase in shear strength. Chen & Loehr (2008) found that the resistance of fibers depends strongly on the sample's volumetric strain. Heineck et al. (2005) and Diambra et al. (2010) stated that the contribution of reinforcement is more effective after a certain level of shear strain, and at very small strains the inclusion of fiber filaments does not influence the initial stiffness and the elastic shear modulus. Similarly, Yetimoglu & Salbas (2003) also stated that at low strains fiber reinforcement does not contribute to carrying load.

But in this study, as Figure 7.13 shows, for suctions higher than AEV (3000, 9500, and 55000 kPa) shear strength decreased as the fiber content increased. This matter was due to an inverse relation between fiber content and dry density of materials (see Table 4.3 and Section 7.2.2). In addition, with regard to the fact that in high suctions failure occurred at a very small strain, and based on findings mentioned in the previous paragraph (and Figure 7.9), the reinforcement played no role in the carrying load.

As indicated also by Warren (1999), the shear strength and stiffness of adobes to a large extent depends on the water content. So, the control of humidity content of adobes may significantly contribute to their resistance in various loading conditions. Another study showing reduction in strength and increase in ductility of adobe bricks with an increase in straw content (irrespective to the straw length) has been done by Islam & Iwashita (2010). The mechanisms behind these observations can be explained as: the straw is not flexible enough to move in phases with soil particles during the drying shrinkage of adobe, either separation of straw from soil or lowering in shrinkage might occur, both of which provide less dry density and less strength for material. They also found that with an increase in water content the compressive strength of adobe decreased linearly; however, the axial strain at peak stress (ϵ_p) was independent from the water content. Similarly, the compressive strength decreased with an increase in straw content, while ϵ_p did not show

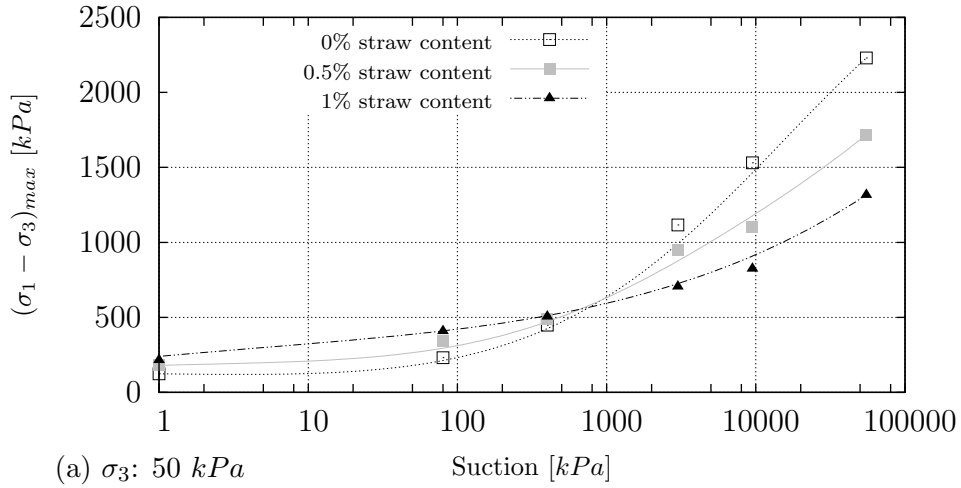

(a) σ_3: 50 kPa

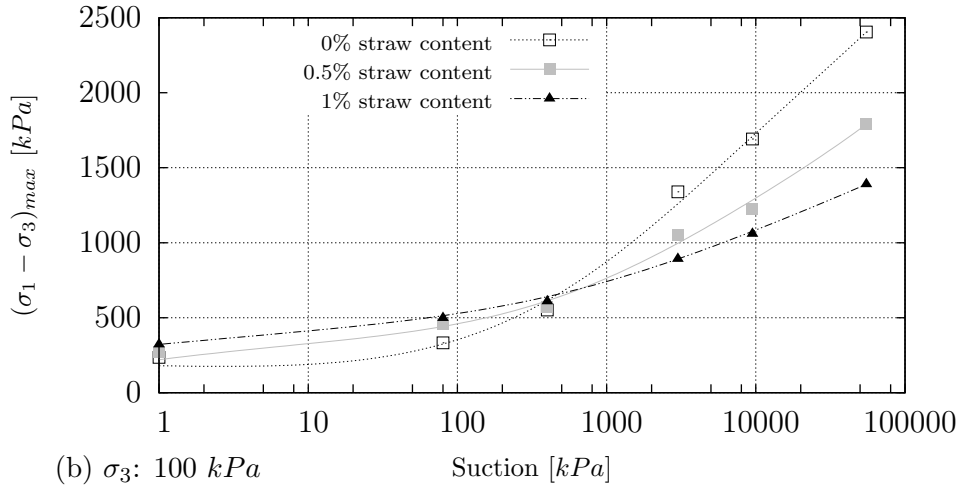

(b) σ_3: 100 kPa

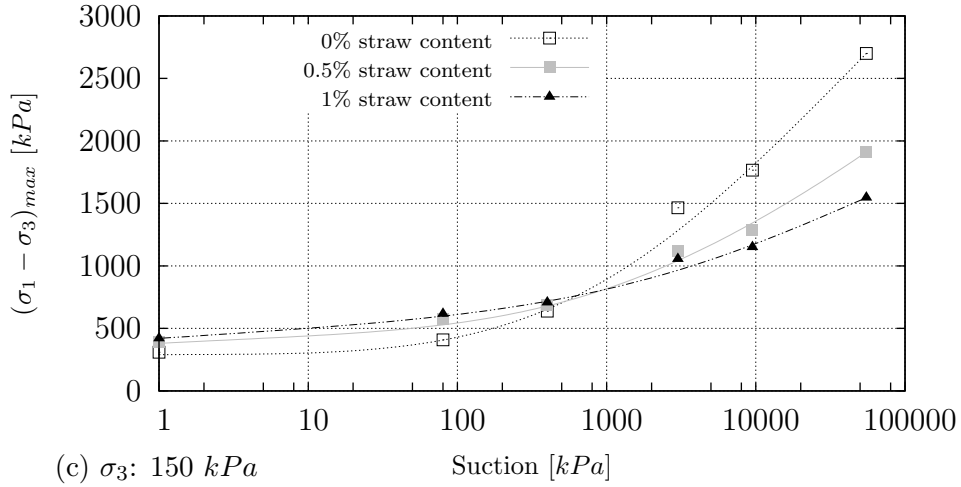

(c) σ_3: 150 kPa

Figure 7.13: Shear strength vs. suction for different cell pressures (saturated condition is represented by suction = 1 kPa).

any meaningful dependency on straw content. Most likely due to this limited strain compatibility, fiber contributions to peak strength and strain at failure were insignificant in the tests under high suctions.

7.3.2 Volumetric strain

As Figures 6.4 to 6.12 show, in volumetric behavior during shearing first contraction and then dilation were recorded. As we can see in those figures, an increase in suction maximum volumetric change (contraction) first increased but after a certain suction (close to AEV) decreased. Same trend was observed for all confining pressures and straw contents. The dependency of maximum contraction on suction can be deduced from the possibility of consolidation in saturated or low suction samples during the consolidation stage of tests. As much as the void ratio reduces, the contraction reduces as well. That is why we can expect more contraction for samples with higher suction compared to saturated samples. But this trend applies only to a certain suction. After a certain suction regarding stiffness of samples which increased rapidly with an increase in suction and due to axial strain at peak stress (ϵ_p) which reduced as suction exceeded AEV, samples failed under lesser volumetric strain and consequently contraction reduced again in this range of suction.

Maximum contraction was not only affected by degree of saturation but also by straw inclusion. Reinforcement increased the void ratio, therefore for higher straw content greater contraction was expected, which was observed in samples with suctions lower than AEV, because soft material and ductile failure allowed movement of particles over each other and contraction could freely take place and maximum contraction showed a direct relation to straw content. But for suctions higher than AEV straw content did not show a meaningful effect on maximum contraction. This could be due to two factors; (i) rigidity of samples which limited the displacement of grains independent from straw content, and (ii) almost the same axial strain at peak stress for all straw contents (presented in Figure 7.9).

Angle of dilation (ψ_d) is defined as the ratio between a volumetric strain rate and a shear strain rate. For plane strain conditions ($\epsilon_2 = 0$) it can be written in terms of the principal strain rates as below:

$$\sin(\psi_d) = \frac{-(\dot{\epsilon_1} + \dot{\epsilon_3})}{(\dot{\epsilon_1} - \dot{\epsilon_3})} \tag{7.14}$$

By straining the specimen, the angle of dilation typically increases until it reaches a maximum value. Beyond this maximum value, and by continuing to load the specimen, this angle decreases and reaches constant low value at the end of loading (i.e. in constant volume conditions).

In this study the maximum angle of dilation was affected by both suction and straw content. Figure 7.14 shows the maximum angle of dilation for all materials and confining pressures versus suction (in this figure the saturated condition is represented by suction $= 1\ kPa$). As we can see in this figure with an increase in the suction, angle of dilation generally increased. Sand grains are covered with clay platens and are connected to each other with clayey solid bridges (see Section 2.2 and Figure 4.6). In dry soils these clayey clusters are stiff and if the sample is sheared sand grains must move with their attached stiff clays which increase dilation. But bondings become softer and weaker as the water content increases, therefore the covering layer and the connections of sand grains also become softer and in shearing stage the sand grains can move over each other regardless of the position of clayey clusters and solid bridges which leads to less dilation. However, for the two highest suctions the opposite behavior was observed. The description and argumentation of this behavior require more tests and deeper analyses.

In this study straw inclusion increased the maximum angle of dilation which was more obvious for lower confining pressure (see Figure 7.14). This could be due to the higher void ratio of reinforced materials which hastens the volume change of samples. Another argument for this phenomenon can be described from the sawtooth-shape model for sliding. If we consider that sliding occurs between two rough planes represented by rigid sawtooth surfaces, the angle of dilation can be imagined more physically as the angle of teeth to the horizontal (Houlsby 1991). This means as the roughness (or the angle of teeth) increases, the angle of dilation also increases. The fiber surface was attached to the soil matrix by many clayey bridges. Fiber filaments even after failure could connect two sides of failure plane that provided a rough sliding plane as shown in Figure 7.15, which resulted in a higher angle of dilation.

Diambra et al. (2010), using triaxial tests, observed the volumetric behavior of reinforced and unreinforced soils. They reported that with an increase in fiber content under same conditions the maximum angle of dilation increased.

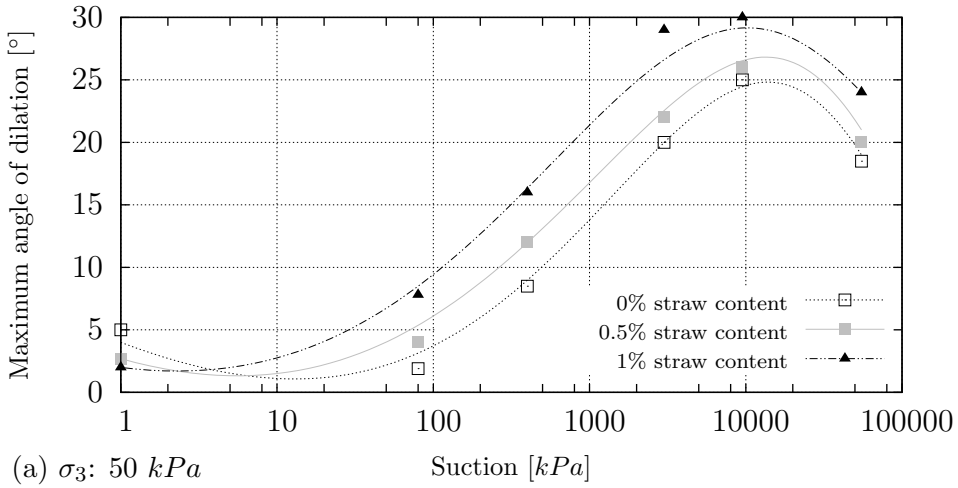

(a) σ_3: 50 kPa

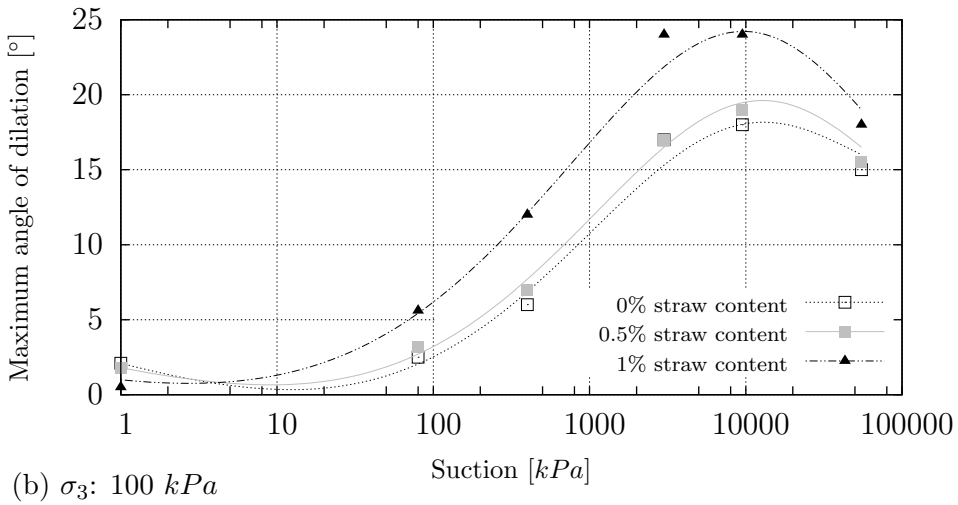

(b) σ_3: 100 kPa

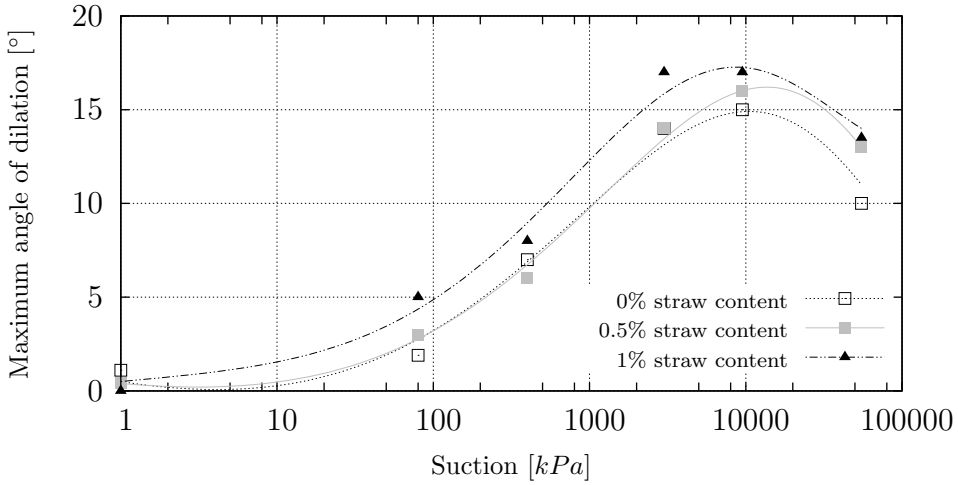

(c) σ_3: 150 kPa

Figure 7.14: Maximum angle of dilation vs. suction for different cell pressures (saturated condition is represented by suction = 1 kPa).

Figure 7.15: Roughness of failure plane caused by straw filaments.

7.3.3 Failure type and shear band inclination

Failure type was considerably affected by fiber inclusion. Unreinforced samples failed with distinct and clear shear bands (with the exception of saturated samples). Mostly upper and lower parts of the sample were separated after shearing, while in the same condition in reinforced samples failure occurred not in a single crack but in several small cracks (see Figures 3.27 and 7.16). When local cracks appeared in a specimen, some fibers across these cracks were responsible for the tension in the soil by fiber-soil connection, which effectively impeded the further development of cracks and accordingly changed the failure type of the reinforced specimens to a more ductile behavior with less distinct failure plane. The reason for this behavior is that increasing the fiber inclusion (i.e. the number of filaments per unit volume) made the soil more homogeneous and isotropic (Marandi et al. 2008 and Freilich et al. 2010). This is more pronounced in lower suctions where bondings between soil particles are weaker than the tension strength of fibers and the reinforcement effect can be more visible. The differences in the failure types explained above are obvious in Figure 7.16 in which three samples under the same suction and cell pressure but various fiber contents are shown. Cai et al. (2006) also has proven that reinforced samples show more

ductile failure compared to unreinforced samples. They clearly showed that big cracks gradually vanish and small ones appear instead while increasing the fiber content. Several other researchers also reported more ductile failure for reinforced soils (i.e. Yetimoglu & Salbas 2003, Bouhicha et al. 2005, Tang et al. 2007, Marandi et al. 2008, and Esna-ashari & Asadi 2008).

Suction as well as straw inclusion affected the mobilized shear band inclination. As the ductility of the sample increased, the shear band inclination in respect to the horizontal axis (θ_m) decreased. As Figures 6.13 and 6.14 show, with an increase in suction, greater θ_m was obtained which considerably increased (up to $\sim 20°$) over a range of suction from 0 to 55 MPa (in this figure the saturated condition is represented by suction = 1 kPa). Same trend was reported by Cruz et al. (2012). They observed a fully developed failure surface for unsaturated silty sand under plain strain conditions, with angles of 61° and 65° for suctions of 50 and 100 kPa respectively.

Fiber inclusion decreased the angle of shear band (see Figure 6.14). In Figure 7.16 three samples with the same suction and confining pressure but straw contents equal to 0, 0.5 and 1% are shown in which shear band inclinations were 69°, 68° and 63°. A factor affecting shear band inclination is the void ratio of material. With an increase in void ratio a smaller angle for shear band is probable if other conditions remain constant. This fact showed the reduction in shear band inclination by increasing fiber content (Table 4.3).

(a) (b) (c)

Figure 7.16: Specimen after shearing for suction 3000 kPa, $\sigma_3 = 50\,kPa$, and (a) 0%, (b) 0.5%, and (c) 1% fiber content.

The angles of shear band inclination measured in this study were compared to the classical prediction methods; namely Coulumb (so called static method), Roscoe (1970) (so called kinematic method), and Arthur et al. (1977) which calculate shear band inclination as: $(45° + \phi'/2)$, $(45° + \psi_d^f/2)$, and $(45° + (\phi' + \psi_d^f)/4)$ respectively, where ϕ' and ψ_d^f are the friction angle and angle of dilation at failure. Figure 7.17 evaluates the efficiency of these equations in the prediction of θ_m. As can be seen here, Coulumb's prediction gives similar values for the whole range of suction and confining pressures, but as Figure 6.13 shows, θ_m depends on suction and confining pressure. A method introduced by Roscoe (1970) gives more scattered results since ψ_d^f is also a function of suction. This method could at least follow the trend of experimental results, however, it still underestimates the θ_m. Finally, the equation of Arthur et al. (1977) probably calculates the θ_m better than previous methods, although it is not sufficiently accurate.

7.4 Discussion of the results of the wall tests

7.4.1 Volumetric changes

As discussed earlier, fiber-reinforcement is a stabilizing method implemented in order to improve the hydro-mechanical behavior of soils. One of the purposes of this method is to control the heave which appears as a result of swelling when a dry clayey soil receives water (e.g. Ayyar et al. 1989, Puppala & Musenda 2000, Cai et al. 2005, Punthutaecha et al. 2006, Cai et al. 2006, Tang et al. 2007, Al-Azzo et al. 2009, Viswanadham et al. 2009, Phanikumar & Kashliwal 2010, etc.).

This issue was also discussed in the SWCC tests of this study (see Section 7.2). Similar walls made from unreinforced and reinforced bricks had different volumetric behaviors. As a result of swelling the maximum void ratio was observed in the lowest row of bricks. Comparing Figures 6.20 and 6.21 also showed that maximum vertical displacement of the wall in a period of 1400 hours was reduced around 3.5 times with only 1% straw content. As mentioned before, initial void ratios (after wall installation and before moisture rises) for unreinforced and reinforced bricks were 0.39 and 0.57 respectively, which increased to

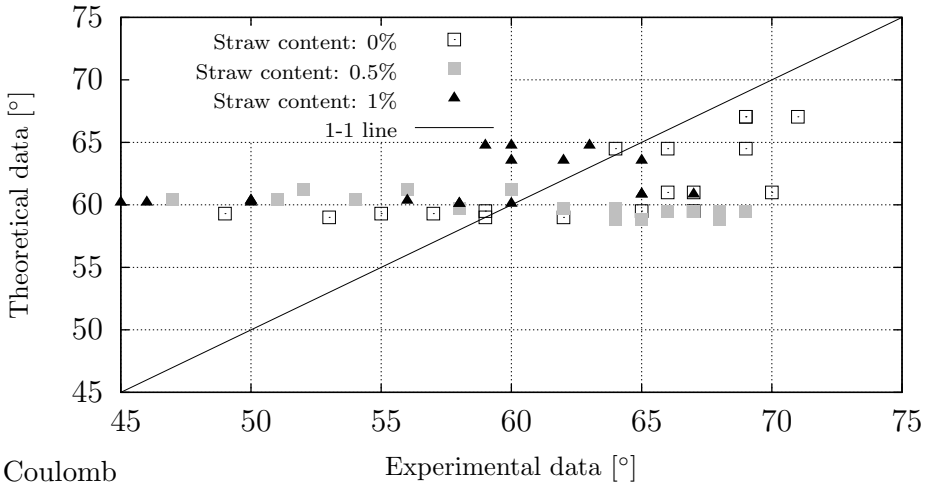

(a) Coulomb

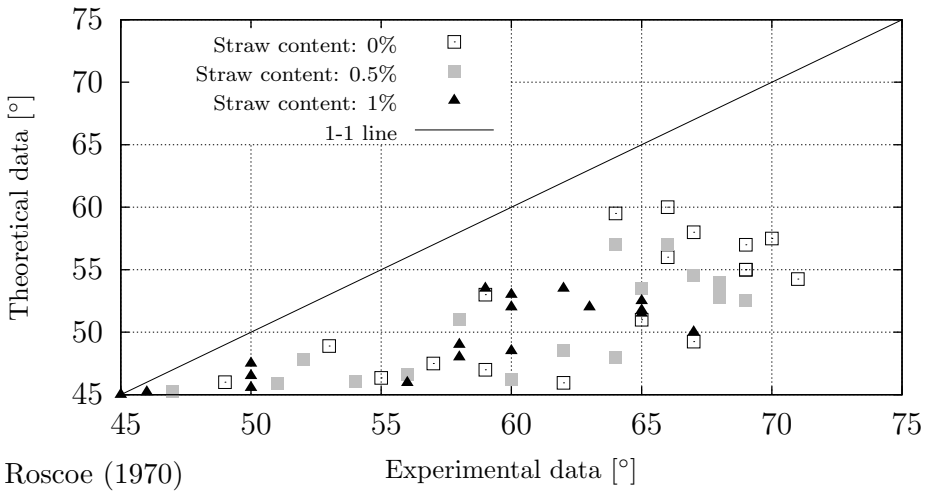

(b) Roscoe (1970)

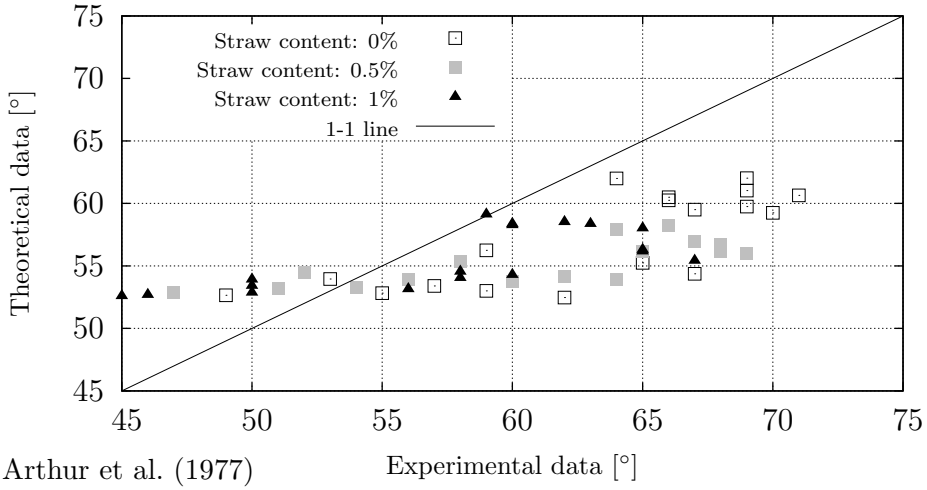

(c) Arthur et al. (1977)

Figure 7.17: Comparison between experimental and theoretical angle of shear band inclination.

0.45 and 0.59. This means reinforcement decreases the increment in void ratio ($(e_1 - e_0)/e_0$) from 15% to 3%, where e_0 and e_1 are initial and after-swelling void ratios. Figures 7.18 and 7.19 show the void ratio of different heights of the walls over time. As we can see here, although the maximum increment in void ratio were different in two walls (15 and 3%), the overall trend of volumetric behavior of reinforced and unreinforced walls were more or less similar. After around 300 to 400 hours for both walls the void ratio in the lowest row of bricks reached a maximum value, but with passing time the void ratio slightly reduced and stayed on a relatively constant value. The reason for this phenomenon was probably softening of the saturated bricks. As dry bricks received water they started swelling and the void ratio increased, but after near saturation, and in terms of the loading over the wall and the wall's self-weight, compression (or even creep) could occure and the void ratio decreased. This behavior was more pronounced in the reinfoced wall, because straw filaments limited the deformation and it took more time for the bricks to change dimensions. However, fiber-reinforcement did not have a considerable effect on the rate and level of uprising moisture, but could reduce the vertical displacement.

The so called "base ventilation countermeasure method" is used for protecting the wall against the problem of uprising moisture. This method is explained in Section 2.4.5. Evaporation of humidity from the wall to the air reduced the uprising height and rate, and consequently reduced the swelling and overall heave. By comparing Figures 6.20 and 6.22 the efficiency of the method used in controlling the heave of the protected wall can be realized. As we see in these figures, the unprotected wall had deformation up to height of around 43 cm and its maximum vertical displacement after almost 1400 hours was 2.9 mm, while for the same period of time protection reduced the height in which vertical displacement occurred to 15 cm and maximum heave to less than 1 mm. Figure 7.20 shows the void ratio of different heights of the protected wall over time. It must be mentioned here that due to the nonuniform geometry of the wall the void ratio was not the same in a horizontal plane, and what is shown in this figure is the average void ratio for each level measured from vertical and horizontal deformations. Volumetric changes in this wall were almost limited to the openings of both front and back sides (i.e. 10 cm), and increments in the void ratio reduced rapidly beyond this height.

Regarding the experimental results mentioned and discussed above and in Section 6.4, the base ventilation method can be useful for lowering the vertical displacement or heave in masonry walls. However, capability of this method depends strongly on the thickness of the wall and size of openings. In Sections 7.4.2.3 and 7.4.3 this countermeasure method is evaluated numerically for different conditions.

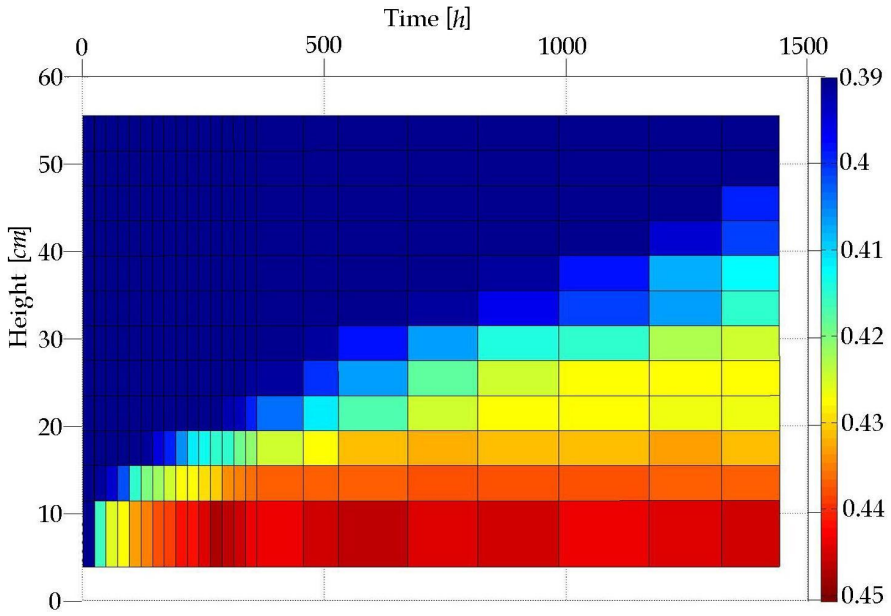

Figure 7.18: Void ratio vs. time and height of the wall (unprotected unreinforced).

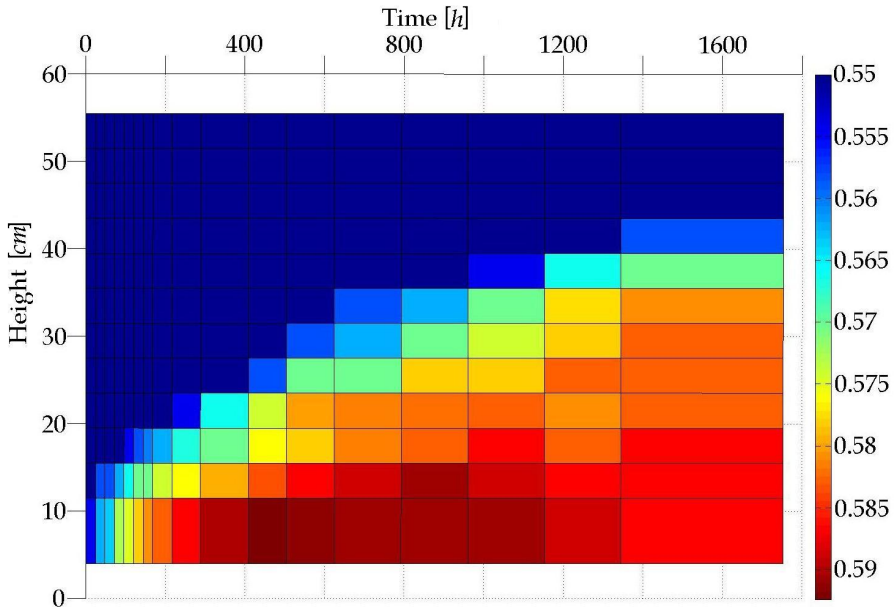

Figure 7.19: Void ratio vs. time and height of the wall (unprotected reinforced).

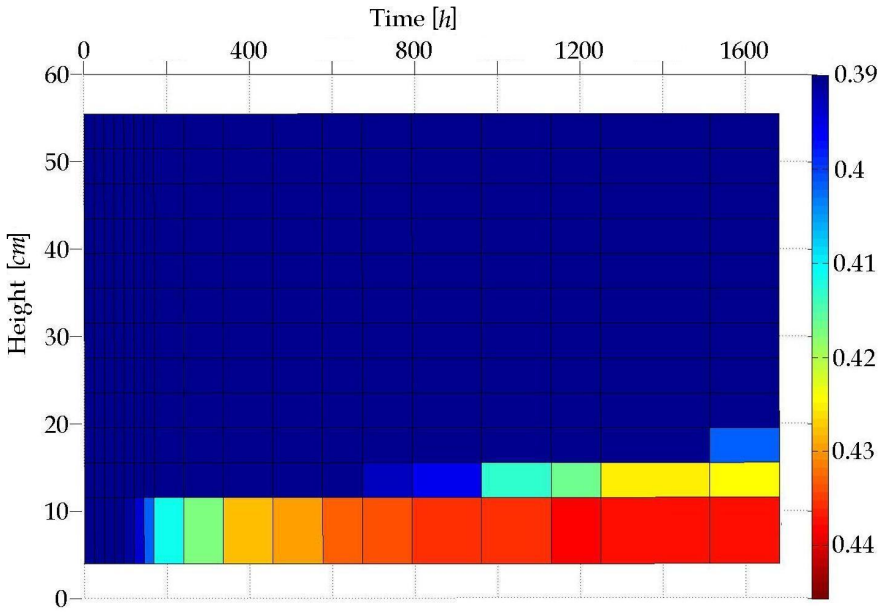

Figure 7.20: Void ratio vs. time and height of the wall (protected unreinforced).

7.4.2 Numerical simulation

Capillarity in porous media is a subject which has been much investigated, particularly in recent years. Several studies modeled water transport in unsaturated soils (i.e. Polmann 1990, Pel 1995, Mortensen 2001, and Smith 2003), and some studies analyzed and modeled uprising moisture and capillary action (i.e. Washburn 1921, Pachepsky & Scherbakov 1984, Lago & Araujo 2001, Yuan & Lu 2005, Yuan & Lu 2005, Lockington & Parlange 2004, Torres & Freitas 2007, and Mullins & Braddock 2012). In Section 3.8.5 some of these methods are explained. This study analyzes the hydraulic distribution of uprising moisture in masonry walls (introduced in Section 5.4) using the software Code-Bright 2.3. The equations used and their assumptions are as follows:

Incorporating Darcy's law (Equation 3.13) in its unsaturated form, Freeze & Cherry (1979) developed an equation for continuity of flow for transient flow through an unsaturated soil, as shown in Equation 7.15. This equation is also named the Richard's Equation.

$$\frac{\partial}{\partial z}\left[k(\psi)\left(\frac{\partial \psi}{\partial z}+1\right)\right]=\frac{\partial \theta}{\partial t} \tag{7.15}$$

One of the most fundamental parameters in uprising moisture is unsaturated hydraulic conductivity. Several empirical and statistical methods have been introduced to calculate

$k(\psi)$ as a function of some of the basic properties and variables (e.g. degree of saturation, water content, suction, saturated hydraulic conductivity, and SWCC) (see Section 3.8.4.1). In simulations of the present study SWCC was introduced using van Genuchten's equation (Tables 7.2 and 7.3). Regarding the hydraulic loading path of the bricks during the uprising process, the adapted model for the wetting curve of SWCC was used.

In the numerical simulations, relative coefficient of permeability, $k_r(\psi)$ (i.e. ratio of unsaturated to saturated coefficient of permeability) was calculated using van Genuchten's method as written in Equation 7.16.

$$k_r(\psi) = \sqrt{S_e} \cdot \left[1 - \left(1 - S_e^{1/m}\right)^m\right]^2 \tag{7.16}$$

where S_e is the effective degree of saturation defined in Equation 7.1, and m is the fitting parameter, which is assumed here to be equal to m, the fitting parameter of van Genuchten's SWCC model. Although the linearized statistical SWCC models, explained in Section 7.2, may simulate SWCC better and in a more flexible manner, because of limitations in Code-Bright in all simulations van Genuchten's model - which were existed in the software - has been used. Three walls explained in Section 5.4 were modeled numerically in the following sections.

Since uprising moisture in the unprotected wall is a 1D phenomenon (parallel to the height), it does not need to be simulated in a 3D model and a 1D or 2D model is enough. However, for the protected wall a 1D model is not enough and requires a 2D model, because the uprising of the water through the wall has a 2D distribution.

7.4.2.1 Unprotected unreinforced wall

The first numerical simulation is related to the wall with unreinforced bricks (0% straw content). In order to simulate impermeable facades, all four sides of the wall were covered with silicone glue and nylon foil. The only openings were the top and bottom surface of the wall. Water entered from the bottom surface (see Figures 5.26 and 5.32). The generated 2D model shown in Figure 7.21 has a width and height of 23×61.5 cm. Initial water pressure assigned to the material was -20 MPa,

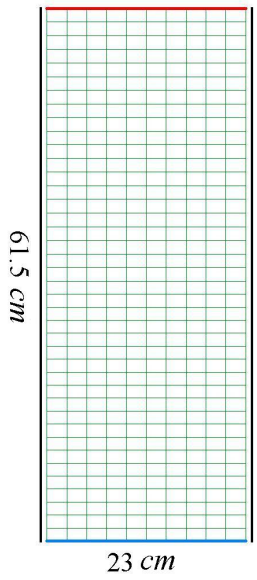

Figure 7.21: Meshes of the model simulated here, blue and red lines represent presence of water and constant initial suction, and black boundaries show the covered sides.

the initial suction of clay bricks at normally dried conditions. A constant water pressure of zero was assigned to the bottom surface of the wall that modeled the presence of free water at this face (blue line in Figure 7.21). The assigned water pressure for upper face (open to the atmosphere) was -20 MPa, the initial suction of dried bricks (red line in Figure 7.21). But no predefined constant water pressure was given to the left and right sides, which indicated that they were covered and their suction (and correspondingly their water content) were not determined by boundary conditions but by progress of the test.

Required parameters for introducing SWCC and $k_r(\psi)$ used in the simulation of this study are listed in Table 7.7. In this table parameters a, related to suction at AEV in the wetting curve, and S_{rres} and S_{rsat}, residual and saturated degrees of saturation, were determined from the wetting path of SWCC.

Figure 7.22 shows the numerically calculated gravimetric water content using the simulation mentioned above (color contour), and uprising front calculated by Washburn (1921)'s equation (the white solid curve) which was introduced in Section 3.8.5 and in Equation 3.23 and repeated here in Equation 7.17.

$$t = \frac{\theta_s(h_e + z_R)}{K_s} \ln\left(\frac{z_R + h_e}{z_R + h_e - z_f}\right) - \frac{\theta_s z_f}{K_s} \tag{7.17}$$

Table 7.7: Parameters used in simulation of unreinforced material.

Description	Parameter	Value	
	a	0.35	MPa
SWCC	m	0.5	
(van Genuchten)	S_{rres}	0.13	
	S_{rsat}	0.93	
Permeability	k_s	3.7×10^{-17}	m^2
Void ratio	e	0.39	

where z_f is the height of the wetting front, z_R is the positive pressure head imposed at z=0 (it could be zero), θ_s is the saturated water content (often taken as equivalent to the effective porosity), K_s is the saturated hydraulic conductivity, and t is time. h_e in this equation is the equilibrium height for a capillary tube but is a fitting parameter for complex porous media. Besides h_e the other required parameters are determined experimentally. In this study h_e was selected based on the best fit of the prediction results with the experimental results of four TDRs which measured water content. Washburn (1921) assumed that the uprising capillary moisture has an advancing front below which the material is saturated, however a more realistic assumption could be a uniformly distributed humidity through height of the wall. In order to adapt Washburn (1921)'s method for this study, the advancing front of uprising moisture was assumed to be the level at which water content was equal to the water content of AEV in the wetting path. The best fit occurred at $h_e = 23\,m$, gotten from experimental results (represented by white dots in Figure 7.22). The fourth point at height 45 cm did not pass the AEV during the time of the test. Comparing Washburn (1921)'s prediction and the numerical simulation of this study (Figure 7.22) explains that in spite of simplicity and age, owing to its fitting parameter, this method predicted the uprising moisture in a comparable way to the numerical modeling. This study proves that Washburn (1921)'s equation has this capability to predict the uprising moisture if experimental data over a limited time and height are available.

Figure 7.23 presents the experimental and numerical results (see Figure 5.32). Solid and dotted lines represent the experimental and numerical results respectively. The agreement between experimental and numerical results shows the reliability of the numerical model.

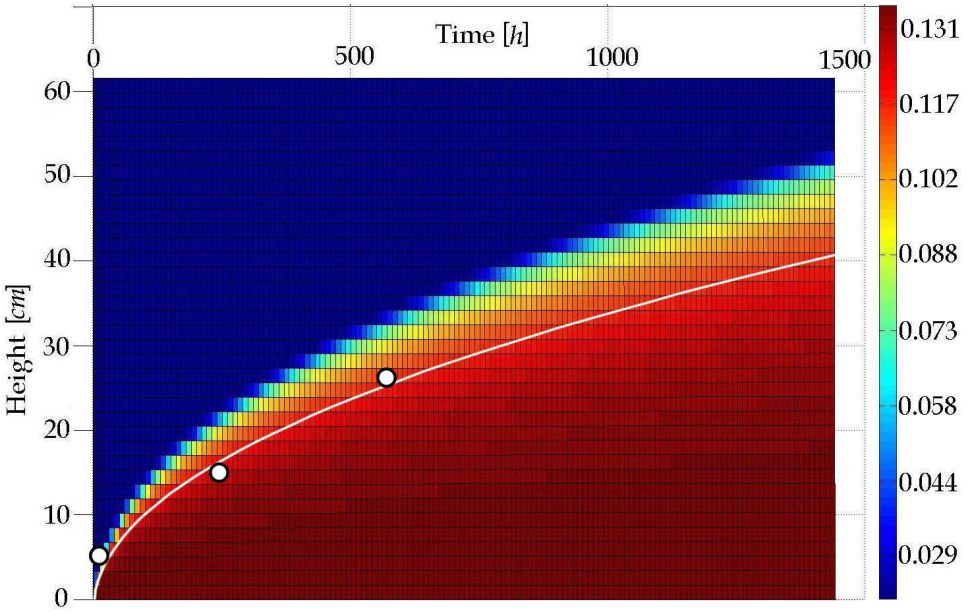

Figure 7.22: Predictions of uprising moisture in unprotected unreinforced wall. Color contour: numerically calculated gravimetric water content; solid white curve: predicted from Washburn (1921)'s equation; white dots: when TDRs showed the water content corresponding to AEV ($w_{AEV} = 11.4\%$).

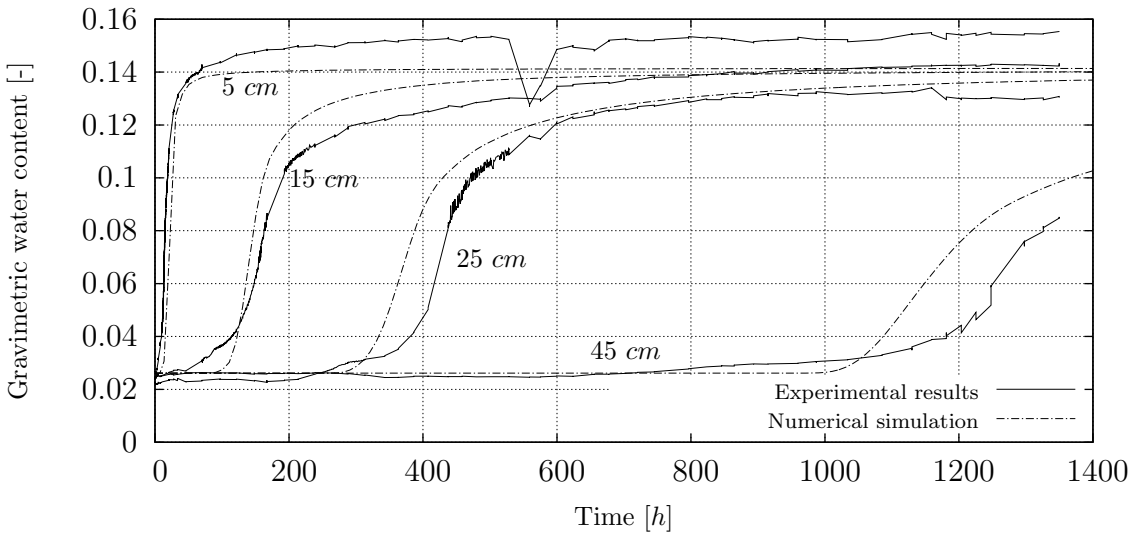

Figure 7.23: Experimental and numerical results for four positions at which TDRs were located in unprotected unreinforced wall; positions are written on the curves.

In the numerical modelings maximum or saturated S_r ($S_{r\,sat}$) was determined from the wetting path of SWCC for unreinforced material (see Figure 7.4). The water content calculated from the simulations reached the equilibrium at a value slightly higher than 0.14 (independent from swelling); however, experimental results for heights of 5 and 25 *cm* were 0.155 and 0.13 respectively. This difference was due to the swelling of the bricks. In the simulations the void ratio was assumed to be constant, but in the experimental results the void ratio varied from 0.39 to 0.45 depending on the time and height.

Figure 7.24 presents the measured and computed water content at the end of the test (after 1350 hours). The experimental results were measured from samples taken from the wall. For sampling 18 levels were considered (three levels for each row of bricks). The average of the water content of three samples from different points at each level has been taken. This figure also shows relatively good agreement between numerical and experimental results. As can be seen here, at very low heights numerical simulation underestimated the results. The reason is the same as that explained above: swelling of lower bricks that was not considered in the numerical simulation. For higher parts of the wall which remain dry until the end of the test, numerical simulation overestimates the results. This could be due to dissimilarity of laboratory conditions in which the SWCC tests and wall test were performed. Residual water content in the numerical modeling was defined from SWCC

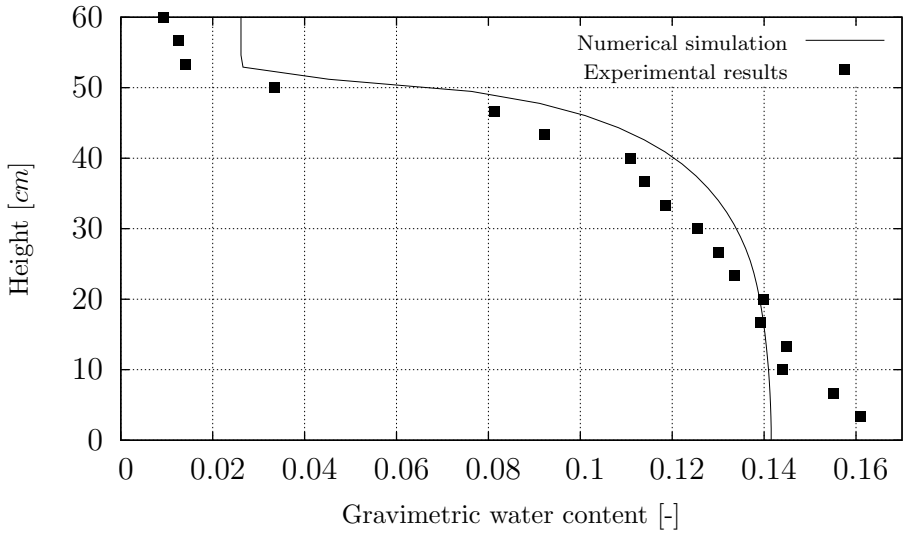

Figure 7.24: Experimental and numerical results at the end of the test in unprotected unreinforced wall.

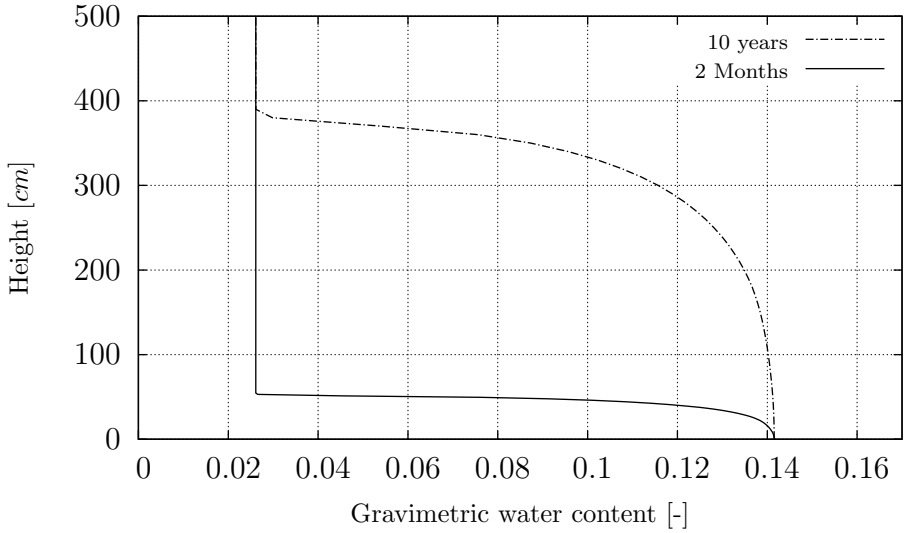

Figure 7.25: Uprising moisture in a wall after 10 years.

results. As Figure 7.1 shows, water content at the initial suction of materials (20 MPa) was slightly more than 0.02, while the measured water content of the dry bricks was less than this value.

Normally, in masonry buildings water can rise up to several meters, but in this study during the first two months of the experiment the water rose up to around 50 cm in the walls. This difference is due to the time of tests compared to the real conditions in which water may rise for more than one decade. Figure 7.25 shows uprising moisture in a 5-meter wall after 10 years. Basics of this modeling are the same as explained above.

7.4.2.2 Unprotected reinforced wall

The second numerical model simulated the wall made from straw-reinforced bricks. Besides the properties of the material used (i.e. SWCC, void ratio, and saturated permeability) other conditions (geometry, boundary and initial conditions, etc.) as well as governing theories were the same as the simulation explained in previous section. In Table 7.8 the required modeling parameters are given, which were based on SWCC results in its wetting branch (Section 7.2) and saturated permeability both of which were determined experimentally (Section 6.5). Because of occluded air bubbles inside the reinforced materials (at the lowest applied suction in the wetting path of SWCC tests), the maximum or saturated degree of saturation for reinforced material was only 0.69.

Table 7.8: Parameters used in simulation of unprotected reinforced wall.

Description	Parameter	Value	
	a	0.14	MPa
SWCC	m	0.27	
(van Genuchten)	S_{rres}	0.01	
	S_{rsat}	0.69	
Permeability	k_s	1.75×10^{-16}	m^2
Void ratio	e	0.57	

Figure 7.26 shows the predicted results for uprising moisture: the color contour is result of the numerical simulation in this study, and the solid white curve is the predicted height of advancing capillary front calculated from Washburn (1921)'s equation, Equation 7.17. Assumptions and principles of this method are described in the previous section. For this material, h_e, the Washburn (1921)'s fitting parameter, equal to 4.5 m gave the best accordance with the experimental results at four given levels in which TDRs were installed. Modelings of this study showed that Washburn (1921)'s equation has good capability in the prediction of uprising moisture (by having a fitting parameter adopted from four TDRs).

Figure 7.27 shows the numerical and experimental water content of points at which TDRs were installed. In experimental curves for conversion of TDRs' volumetric water content to gravimetric water contents (using mass-volume relationships) the void ratio varied from 0.57 to 0.59 depending on time and height. But in numerical simulations void ratio was constant. This disagreement caused the difference between numerical and experimental results in high water contents.

Figure 7.28 presents experimental and numerical water content at the end of the test (after 1750 hours). Method of sampling was like that explained in the similar observation in the previous test (unreinforced wall): 18 levels and three samples from each level for averaging. As this figure shows, the experimental and numerical results had a good agreement. For heights higher than 30 cm numerical simulation overestimated the results. This could be due to occluded air bubbles among the straw-soil matrix which reduced the water content.

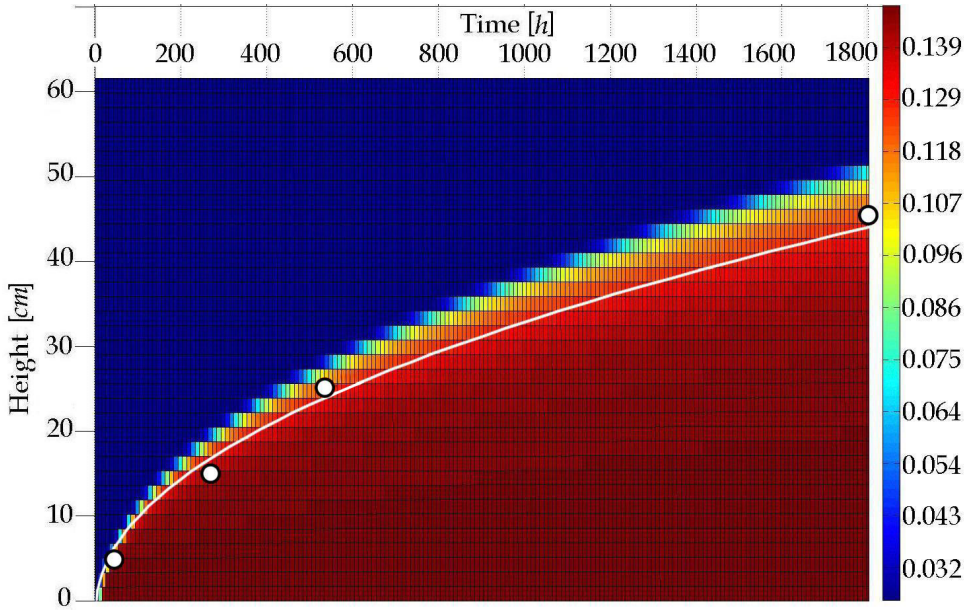

Figure 7.26: Predictions of uprising moisture in unprotected reinforced wall. Color contour: numerically calculated gravimetric water content; solid white curve: predicted from Washburn (1921)'s equation; white dots: when TDRs showed the water content corresponding to AEV ($w_{AEV} = 9.8\%$).

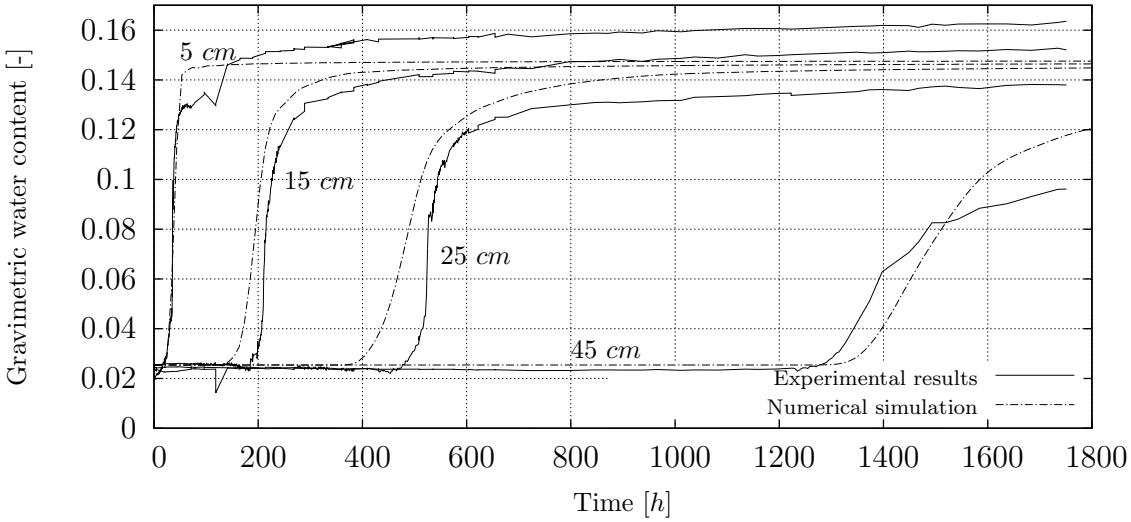

Figure 7.27: Experimental and numerical results for four positions at which TDRs were located in the unprotected reinforced wall; positions are written on the curves.

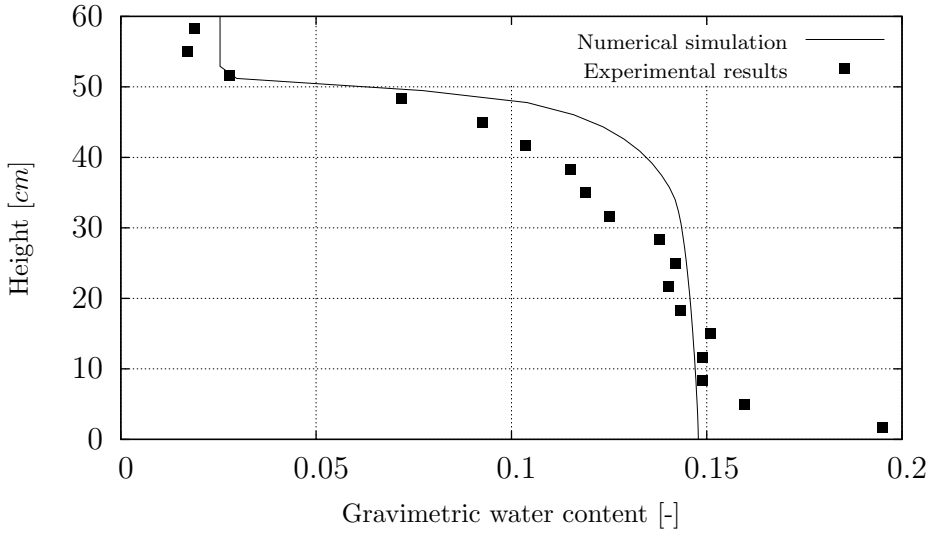

Figure 7.28: Experimental and numerical results at the end of the test in the unprotected reinforced wall.

As found in the analyses of SWCC results (Section 7.2), an increase in straw content hastened the imbibition and drainage processes in wetting and drying paths. In the wall made of reinforced material water content started to increase at heights of 15, 25 and 45 *cm* after around 200, 500 and 1300 hours, while the values were 100, 300 and 1100 hours for the unreinforced wall. This implies that reinforcement could limit the uprising rate, however not significantly. Sivakumar-Babu & Vasudevan (2008*a*) studied the effect of fiber inclusion (natural coir fibers) on seepage velocity and piping resistance of three types of soils. Their experiments were carried out for various hydraulic heads, fiber contents, and fiber lengths. It was observed that fibers reduced the seepage velocity of plain soil considerably and thus increased the piping resistance of soil. Das et al. (2009) performed one-dimensional piping tests on reinforced fly ash and concluded that reinforcement reduced seepage velocity and improved piping resistance. However, unlike what has been described here, some researchers stated that fiber inclusion increases the permeability (e.g. Maher & Ho 1994, Abdi et al. 2008, and Chegenizadeh & Nikraz 2011*b*).

In Figure 7.29 numerical color contours representing water content are located beside their concurrent photos of the wall made from reinforced bricks. In the photos the darkness of the wall's appearance shows the existence of humidity in the material. The moisture uprise can be followed visually through the wall's height in both photos and color contours. As can be seen here, similarly in both numerical modeling and visual observations, after 73 days lower parts of the wall reached its maximum water content and turned dark.

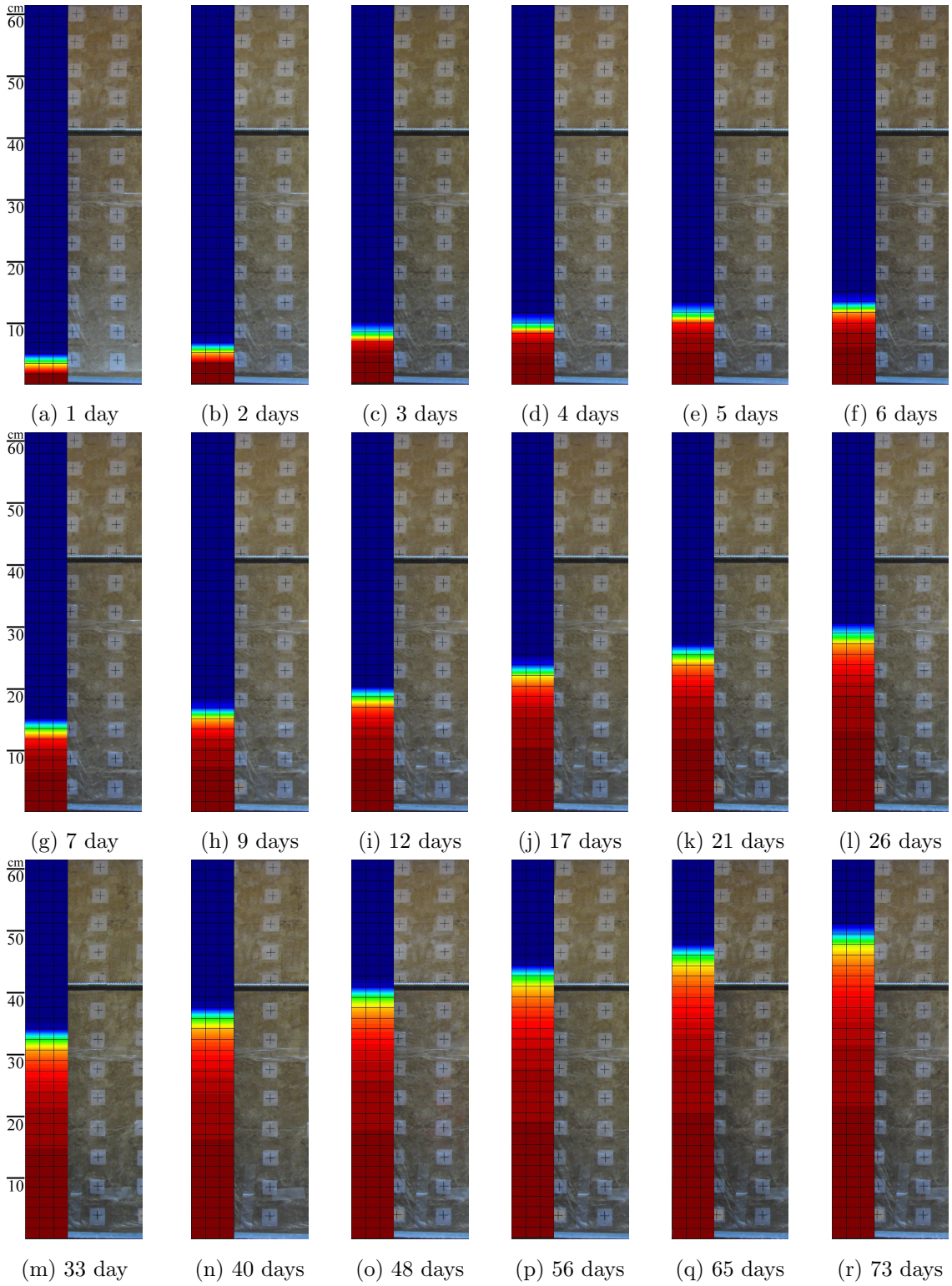

(a) 1 day (b) 2 days (c) 3 days (d) 4 days (e) 5 days (f) 6 days

(g) 7 day (h) 9 days (i) 12 days (j) 17 days (k) 21 days (l) 26 days

(m) 33 day (n) 40 days (o) 48 days (p) 56 days (q) 65 days (r) 73 days

Figure 7.29: Comparison between calculated degree of saturation (color contours) and photos of wall, after various periods, in unprotected reinforced wall.

7.4.2.3 Protected unreinforced wall

In the third model the protected wall made of unreinforced material with one of the commonly used countermeasure methods was simulated. In the so called base ventilation method two strips of openings on the front and back facades of the wall allowed evaporation from the wall's surfaces and protected the wall against problems coming from the presence of humidity in the masonry materials. Left and right sides of the wall were fully covered. In this test the height of openings was 10 *cm*. The assumptions and equations of modeling as well as material properties were the same as those described in the modeling of the unprotected wall (modeling parameters are given in Table 7.7).

Figure 7.30 shows the numerically calculated hydraulic distribution (2D) of moisture after various periods of time in the form of gravimetric water content. Figure 7.30h is the result for the end of the test (after 69 days). Its counterpart experimental result is given in Figure 6.19. As can be seen here, in the numerical simulations the assigned - constant - suction to the first 10 *cm* of the sides was the initial suction of the bricks; however, in the experiment the water content of openings also increased (see Figure 6.19). Another shortcoming of this test was the measurement of water content during the test with four TDRs, which could not cover the whole vertical cross section of the wall, but only read the water content on the four given points on the center-line (see Figure 5.33).

After more than two months moisture rose around 30 *cm*, almost half of the wall's height, while this value was much more in the unprotected wall. Figure 6.18 compares uprising in the walls at the end of tests. As the simulation of the protected wall resulted, during a period of two months, water content of facades never exceeded 0.09 while the saturated water content was around 0.14 in numerical calculations, but in the same period the lower 40 *cm* of the unprotected wall had water content of more than 0.12.

Figure 7.31 shows the numerical and experimental water content of the points at which TDRs were installed (on the center-line), and Figure 7.32 shows numerical and experimental water content at the end of the test in the center-line. Like the two previous models for lower heights of the wall, numerical simulation underestimates the results and vice versa for higher heights. As mentioned before, the reason for the underestimation in lower parts was the swelling of material which was neglected in the modeling, and the difference in higher parts was probably due to deficiency of the model to make prediction in low water contents. Probably in a high range of suction, the van Genuchten model for unsaturated hydraulic conductivity (Equation 7.16) predicts higher values for $k(\psi)$ than its real value.

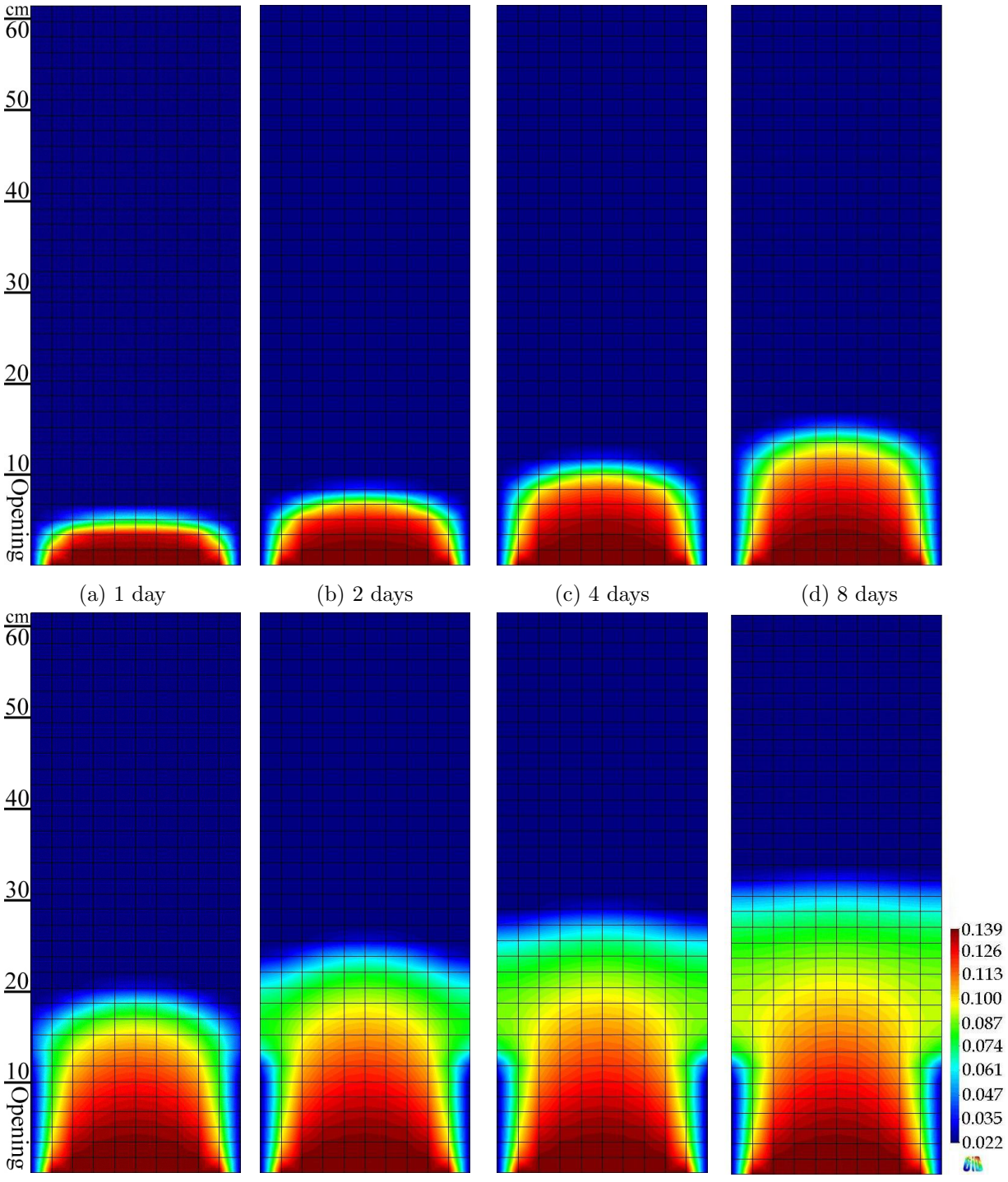

(a) 1 day (b) 2 days (c) 4 days (d) 8 days

(e) 16 days (f) 32 days (g) 48 days (h) 69 days (end of the test)

Figure 7.30: Numerically simulated degree of saturation distributed through the wall after various periods, in protected unreinforced wall.

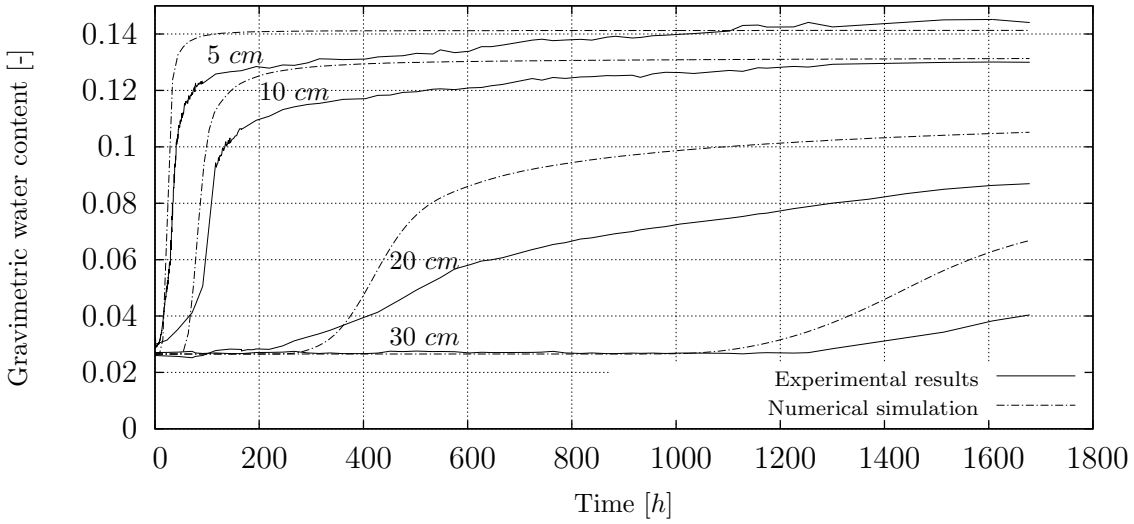

Figure 7.31: Experimental and numerical results for four positions at which TDRs were located in protected unreinforced wall; positions are written on the curves.

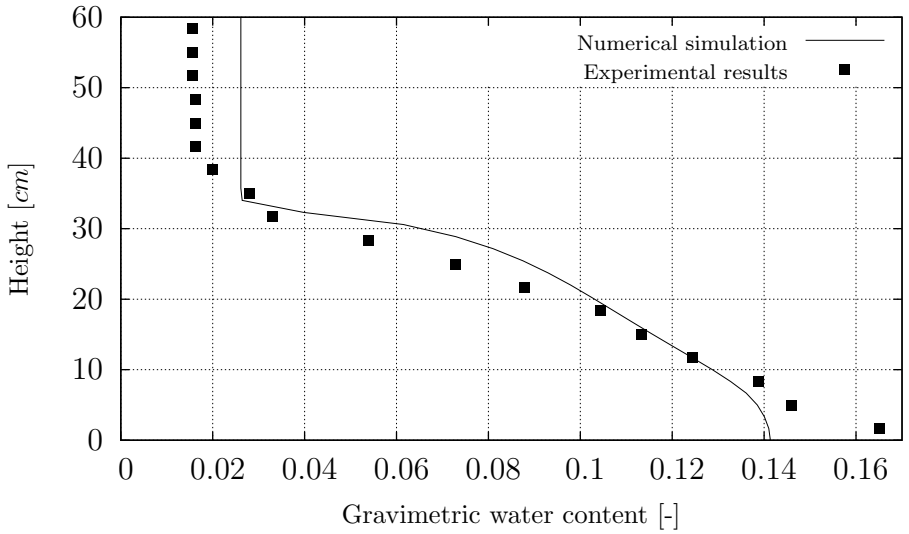

Figure 7.32: Experimental and numerical results at the end of the test in protected unreinforced wall (at the center-line).

7.4.3 Efficiency of implemented countermeasure method (base ventilation)

Not necessarily the base ventilation method can be used for all types of masonry materials, geometries, boundary conditions, bed soil, and annual fluctuations of the underground water table. Before recommending this - or any other - method its efficiency and capability must be analyzed experimentally or numerically. In order to evaluate the base ventilation method, walls with varying thicknesses and openings (b and c in Figure 7.33) were numerically simulated in this study. Boundary conditions, time, and type of material were the same in all models. In this figure black lines represent the covered areas and the blue line shows the presence of water. Modeling assumptions and parameters were like as those described in the modeling of unprotected unreinforced wall in Section 7.4.2 and Table 7.7. By changing b and c, rate and maximum rise of humidity during a given period of time was calculated. Models (M0 to M19) with a wide range of wall thickness and opening size from both sides (as listed in Table 7.9) were simulated. In this table the models are categorized based on the thickness of the walls. M0 is the unprotected wall without any ventilation (see Section 7.4.2.1), and M7 is the protected wall tested experimentally (see Section 7.4.2.3). The center-line is shown with a dashed line in this figure.

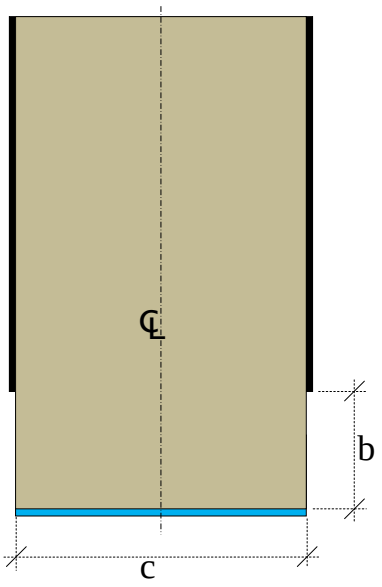

Figure 7.33: Configuration of base ventilation method used in numerical studies (cross sectional view).

Table 7.9: Configurations of simulated countermeasure methods.

Model name	c $[cm]$	b $[cm]$	b/c
M1	11.5	3.3	0.287
M2	11.5	5	0.435
M3	11.5	7.5	0.652
M4	11.5	10	0.870
M5	11.5	11.5	1
M6	23	6.6	0.287
M7	23	10	0.435
M8	23	13.2	0.574
M9	23	15	0.652
M10	23	20	0.870
M11	23	30	1.304

Model name	c $[cm]$	b $[cm]$	b/c
M12	46	13.2	0.287
M13	46	20	0.435
M14	46	30	0.652
M15	46	52.8	1.148
M16	46	80	1.739
M17	92	26.4	0.287
M18	92	40	0.435
M19	92	60	0.652
M0	0.23	0	0

Figures 7.34 to 7.37 present the water content on the center-line of the simulated walls (see Figure 7.33) with different thicknesses and opening sizes (listed in Table 7.9) after two months. From these figures the efficiency of countermeasure can be deduced. As it can be seen, the near-saturated zone after two months reduced considerably in the base-ventilated walls. It can be clearly concluded from Figure 7.34 that for thin walls this method could significantly reduce the water content in the center-line which had the maximum humidity compared to other points of the wall. As we can see in this figure, the height corresponding to 10% water content has been reduced by about 5 times (from 45 to 9 cm). Regarding the thickness of the wall (11.5 cm), this reduction in height in the weak zone can change the mechanism of failure from possibility of shearing to uniaxial compression.

As the thickness increased the inner parts of the wall receded from the openings, therefore the base ventilation method lost its efficiency for wider walls. If the thickness exceeded a certain value, the size of opening had almost no effect on the height of uprising. For walls thicker than 20 cm, openings wider than 10 cm were not helpful, and for thicknesses greater than 40 cm the base ventilation method for protecting the wall against uprising moisture probably was not a suitable countermeasure method. In historical masonry constructions different thicknesses of walls can be seen. The walls carrying gravity loads may have up to 200 cm width, but non-load carrying walls can have much smaller thicknesses of around 15 cm.

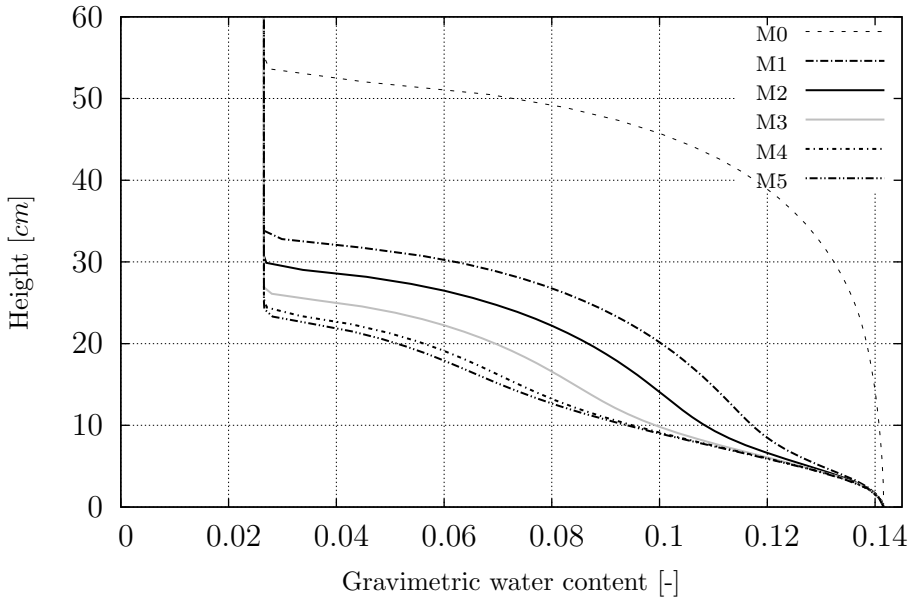

Figure 7.34: Numerically calculated gravimetric water content on the center-lines, configurations M1 to M5 (c=11.5 cm) after two months.

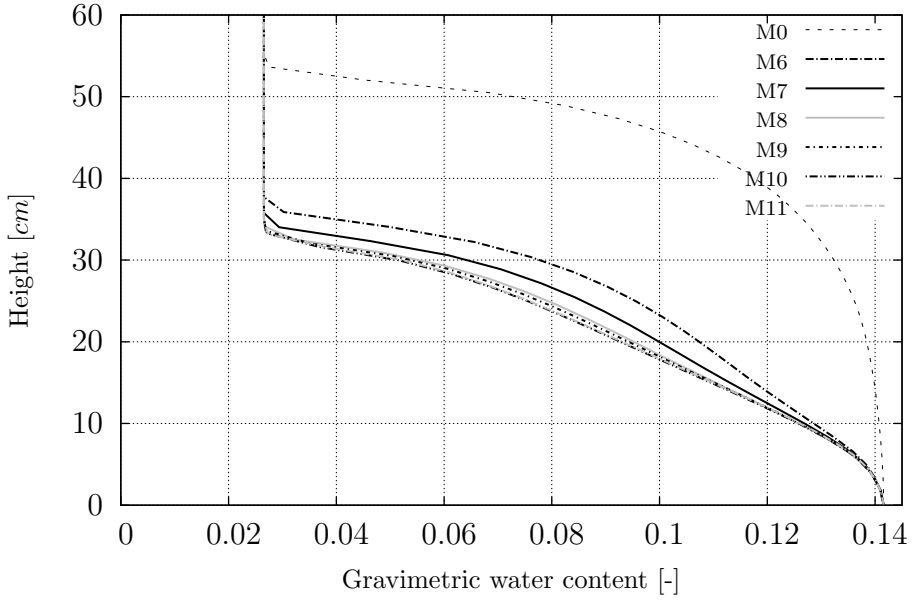

Figure 7.35: Numerically calculated gravimetric water content on the center-lines, configurations M6 to M11 (c=23 cm) after two months.

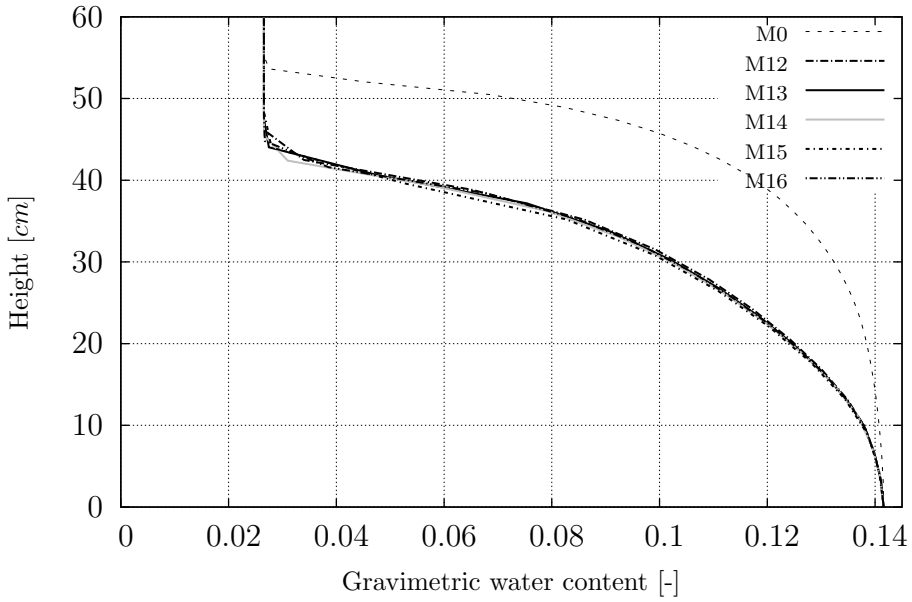

Figure 7.36: Numerically calculated gravimetric water content on the center-lines, configurations M12 to M16 (c=46 cm) after two months.

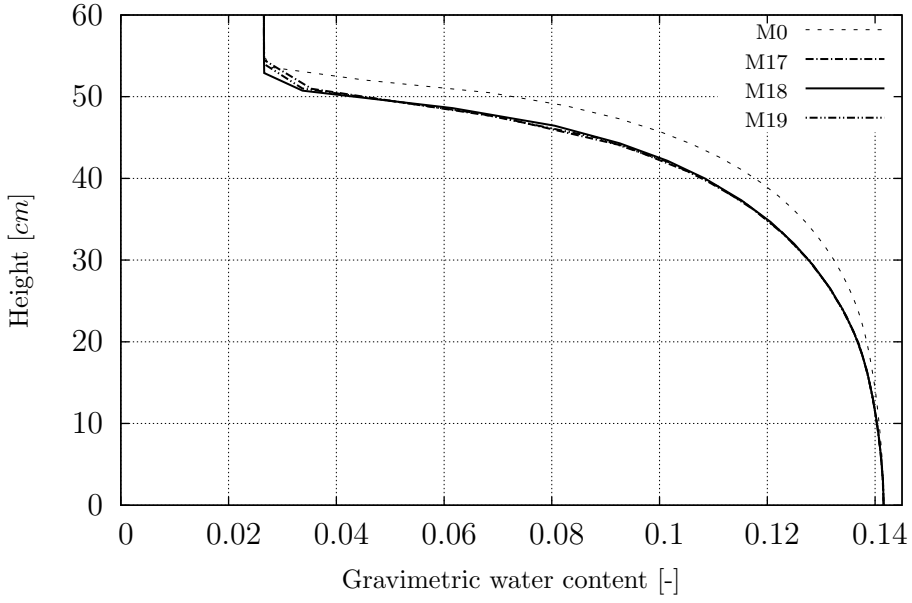

Figure 7.37: Numerically calculated gravimetric water content on the center-lines, configurations M17 to M19 (c=92 cm) after two months.

As we can see in Table 7.9, in the walls simulated numerically, the ratios of openings divided by thicknesses of the walls (b/c) has been selected same for all configurations, in order to observe if the efficiency of this method is related to this ratio or not. But as Figures 7.34 to 7.37 show, as the thickness of the wall increases, b/c loses its effectiveness. For thicker walls the inner parts are sufficient far away from boundaries to let water rise up unaffected from the openings of the faces. In actual fact, for thick walls evaporation can reduce the water content of materials near the openings.

The effectiveness of the base ventilation method is more pronounced when the duration of uprising moisture increases (even for thicker walls). Figure 7.38 shows the results of the same walls calculated in Figure 7.37 but for a period of 10 years (instead of 2 months). By comparing Figures 7.37 and 7.38 for such thick walls it can be clearly understood that the selection of a proper countermeasure method is also a function of duration of presence of water.

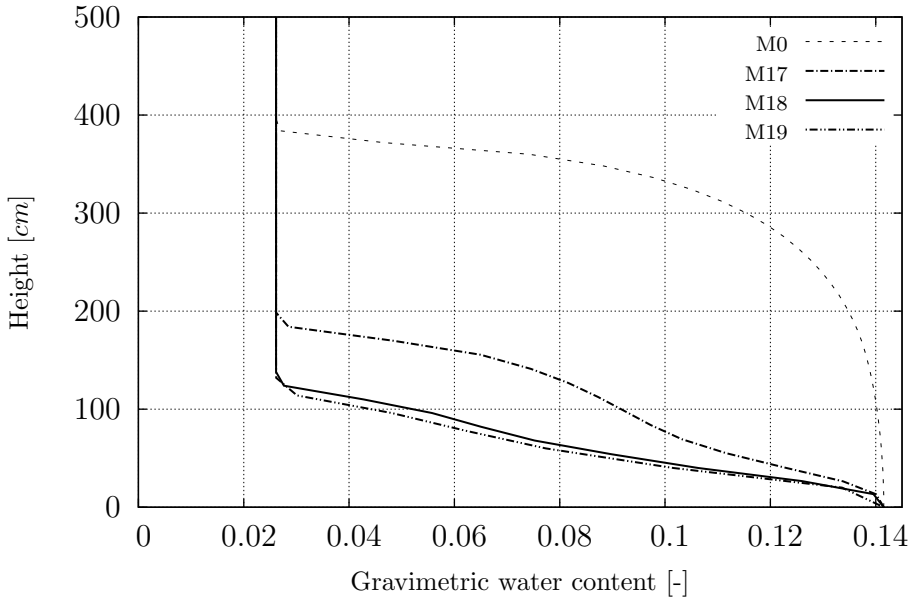

Figure 7.38: Numerically calculated gravimetric water content on the center-lines, configurations M17 to M19 (c=92 cm) after 10 years.

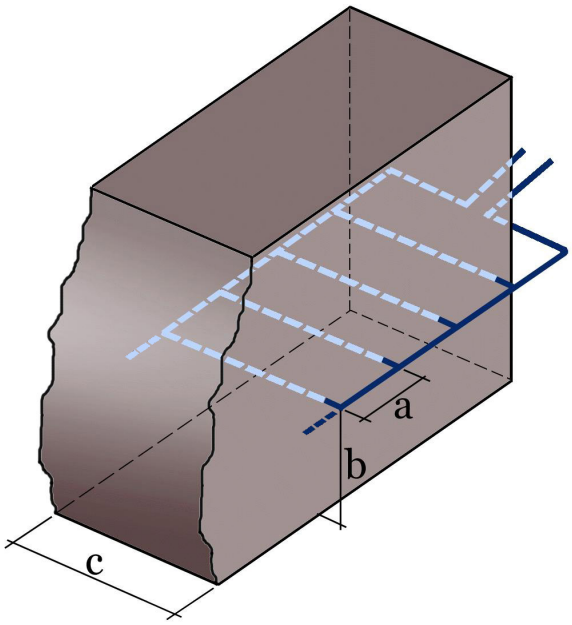

Figure 7.39: Configuration of hole ventilation method for thick walls.

7.4.4 An alternative countermeasure method (hole ventilation)

As mentioned before, for thick walls base ventilation is not an effective method. Another countermeasure method which is probably more operative for thick walls is suggested here, as shown in Figure 7.39. In this method a series of narrow holes is drilled throughout the thickness of the wall out of which humidity can evaporate. This method is called "hole ventilation". As shown in this figure, parameters a and b are the distance between the holes and the height of holes' row from the base. Since both the front and back sides of the wall are covered with impermeable facades thickness of the wall (c) does not play any role here. Circulation of this vapor accelerates the drying process. In Figure 7.39 a circulation system is drawn through which dry air is replaced with moist air via pipes and pumps.

In this study walls with 6 different distances between holes were modeled numerically, with a = 10, 20, 30, 40, 50, and 60 cm. All holes were assumed at the same elevation of $b = 0$. Total height of the model was 60 cm. Unlike the previous modelings, in which a 2D model of cross-sectional views of the wall was simulated, here 2D front views were considered. Regarding the configuration of the system, modeling of one hole in the middle of a wall with width = a is enough. Other assumptions (i.e. impermeable facades, entrance of water from bottom, governing equations, and material properties) were the

same, as explained in Section 7.4.2 and Table 7.7. In these simulations a single point represented the drilled hole, to which a constant suction equal to initial suction of bricks was assigned. In Figures 7.40 distribution of moisture in the models is shown.

Figure 7.41 compares the gravimetric water content in the vertical line in the middle of two holes (left or right borders of the model in Figures 7.40) for various hole distances. The presented results were after two months from the beginning of the test. This figure shows that as the distance between the holes increased water rose to the higher levels; however, very close holes can endanger the stability of the building, unless they are filled with any stiff and permeable material through which air can circulate, for example rods made of porous stone or steel pipes with small holes on their surfaces.

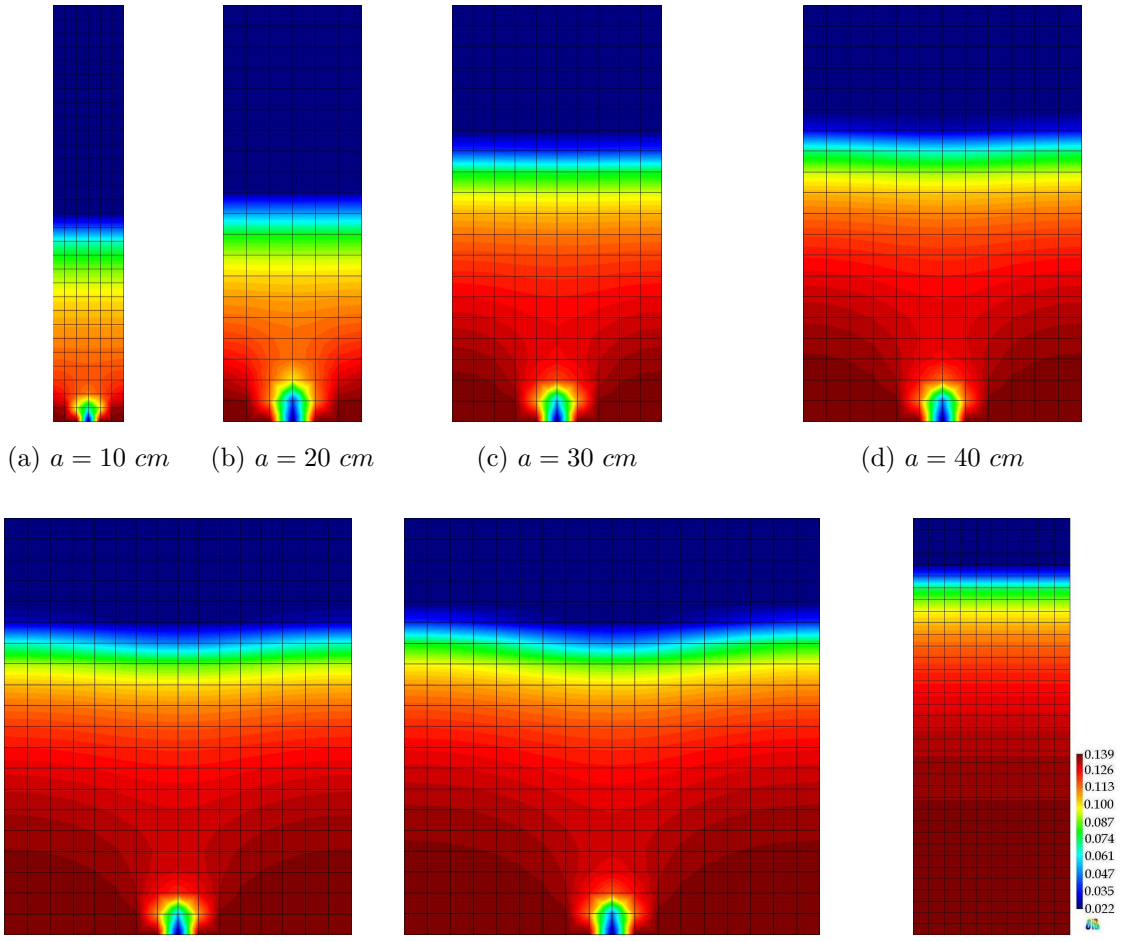

(a) $a = 10\ cm$ (b) $a = 20\ cm$ (c) $a = 30\ cm$ (d) $a = 40\ cm$

(e) $a = 50\ cm$ (f) $a = 60\ cm$ (g) unprotected wall

Figure 7.40: Numerically calculated water content in hole ventilation countermeasure method; the distance between holes are written under the photos.

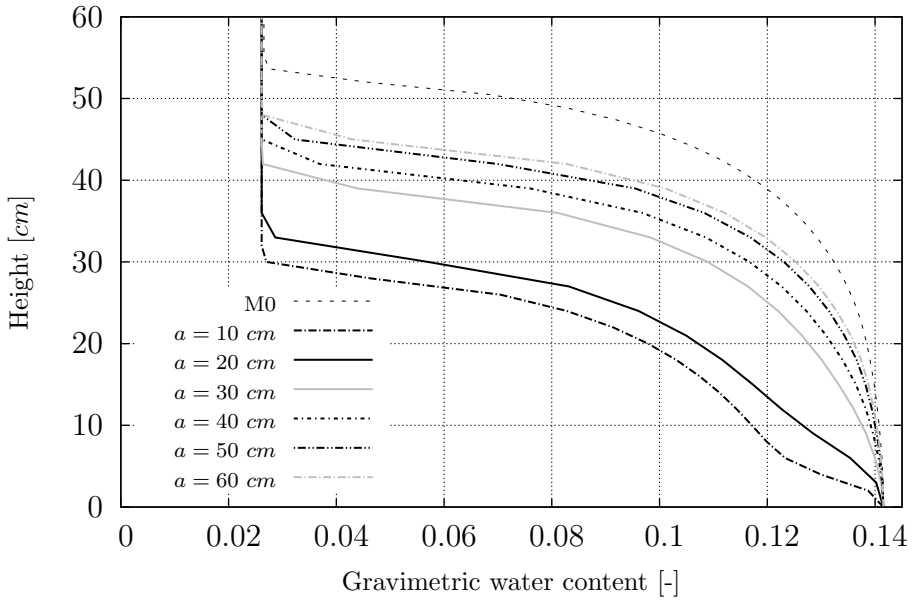

Figure 7.41: Numerically calculated gravimetric water content on the lines in the middle of two holes, $b = 0$ and a is written in the figure

The advantage of this countermeasure method is that we can select the height of the holes' row (b), which can be determined by the engineer regarding architectural possibilities, and of course the lower the holes are, the better the method works. The holes' diameter should be wide enough to let the vapor circulate through the pipes, however, one of the limitations of the analyses above on this alternative method is that the ventilation from the holes is assumed to be perfect.

7.4.5 Summary

In this chapter the influences of straw inclusion (0 to 3 gravimetric percent) on shape and parameters of SWCC were presented and discussed. Also, the influence of straw and sample size on shrinkage and swelling of reinforced soil were presented and explained. Proposed models (conventional and linearized statistical models) were adopted for simulation of the SWCC results. Results of unsaturated reinforced biaxial experiments were analyzed by calculating moduli of elasticity, effective stress parameters, effect of reinforcement on shear strength in higher and lower ranges of suction, dilatancy, and failure

type, as well as shear band inclination. Next, in the wall tests, volumetric behavior of walls subjected to uprising moisture were presented and discussed. Numerical simulations of three wall tests (unprotected unreinforced, unprotected reinforced, and protected unreinforced) were explained and discussed. Later, one common countermeasure method, namely base ventilation method, was evaluated for different configurations. Finally, an alternative countermeasure method for thick walls was suggested and its capability was numerically analyzed.

8 Conclusions and recommendations

8.1 Conclusions

This chapter presents the main conclusions and highlights drawn from the experimental and numerical studies accomplished in this thesis, recommendations and future possible researches in this field. This thesis concentrates on the manner and effects of the capillary uprising moisture phenomenon on unreinforced and straw-reinforced masonry structures. Soil-water characteristic curves of reinforced soil with straw fibers with dosages of 0 to 3 gravimetric percent were determined through Axis Translation Technique (ATT) and Vapor Equilibrium Technique (VET) depending on the suction range. Using the series of biaxial tests, shear strength, dilation and shear band inclination of reinforced soil in unsaturated conditions with a wide range of suction were investigated. Behavior of uprising moisture in large scale walls with different conditions was observed experimentally and simulated numerically. The main derived conclusions are categorized as follows.

8.1.1 Effect of straw-reinforcement on SWCC

In this study, as well as in several other studies fiber inclusion reduced the amount of shrinkage and swelling of fine-grained soils. Regarding the low percent of straw content (maximum 3%), the amount of water that could be retained by soils with various straw dosages was almost similar. But due to the influence of reinforcement on volumetric changes, the degree of saturation was a function of straw content. Void ratio of dried samples increased from 0.39 to 0.72 by the inclusion of only 3% straw. Straw filaments made a spatial structure which limited the shrinkage and swelling during drying and wetting procedures. Straw-soil interaction was also studied using SEM photos and mercury introsion porosimetry.

In the drying path of SWCCs, as the straw content of samples increased the rate of desaturation also increased (SWCCs' slopes were steeped). Amount of occluded air bubbles

had a direct relation with straw dosage. For samples with higher straw content degree of saturation at the lowest applied suction of the wetting path was considerably reduced (from $S_r = 92\%$ in unreinforced samples to $S_r = 73$, 65, 58, and 53% in samples with 0.5, 1, 2 and 3% straw content).

8.1.2 Plane strain shear strength of straw-reinforced soil

Terzaghi's effective stress idea modified by Bishop (1959) was used for the shear strength calculations of unsaturated reinforced soil. The effective stress parameter (χ) was determined using the results of biaxial tests on soils with 0, 0.5 and 1% straw inclustion under suctions from 0 (saturated) to 55 MPa. The obtained χ vs. suction showed good agreement with the methods suggested in the literature for the calculation of χ based on soil variables (e.g. SWCC parameters). Straw inclusion affected the shear strength differently in suction ranges higher and lower than AEV. In wet soils (i.e. $\psi < \psi_{AEV}$), in terms of the possibility of movement and moiblization of straw filaments in between the soil matrix, fibers took part in load bearing and their contribution increased shear strength. But in dry soils (i.e. $\psi > \psi_{AEV}$) straw-soil interactions were provided by stiff solid clayey conections which did not allow fibers to move easiliy amonge the soil grains. On the other hand, straw-reinforcement reduced the shrinkage of mixture and the void ratio of dry soil was increased in reinforced materials. Therefore straw inclusion reduced the shear strength in this range of suction. Modulus of elasticity generally decreased when suction increased, however this modulus did not present any meaningful dependency on straw content.

In general, with an increase in straw content the angle of dilatancy increased. This increment was more pronounced in higher suctions. This behavior was argued from the sawtooth-shape model for the failure plain. With an increase in straw content the roughness of sliding plane increased which was conducive to a higher amount of dilation, if other conditions were constant.

Typically, unreinforced samples failed with a clear shear band and in most cases the upper and lower parts of sample were separated after shearing (with the exception of saturated samples), while with the same condition in reinforced samples failure occurred not in a unique distinguishable crack, but in several small cracks. Fibers crossed the local cracks and carried tensile stress, which impeded the development of cracks and increased the ductility of the sample and changed the failure type from distinct failure plane to bulge

shape failure. Shear band inclination increased with an increase in suction (for around 15-20°) and decreased with an increase in straw content.

8.1.3 Observation of uprising moisture in walls

In the uprising moisture phenomenon, from the underground water table to the masonry walls, in order to observe the dependency of water content on time and height, two masonry walls were made with 0 and 1% straw reinforced bricks. Uprising rate in reinforced masonry materials was slower than that in unreinforced materials, however not significantly. Because of swelling in the bricks, both walls heaved when water rose up. But straw-reinforcement could remarkably reduce the total heave (from 3 mm to less than 1 mm). The results of these tests were compared with the numerical simulations done by software Code-Bright. The parameters used in these modelings were determined experimentally. Comparison between measured and calculated results verified the simulations, which later could be used for further modelings in practical projects in the field of conservation of masonry buildings.

In the continuation, the efficiency of a commonly used method for reducing the height and amount of risen humidity in walls was experimentally and numerically evaluated. The so called "base ventilation method" is an operative method for limiting the uprising moisture in thin walls. In this method two openings in the front and back facades of the wall allow the evaporation of humidity from the wall which reduces the uprising rate. In this study an unreinforced wall with 23 cm thickness was built and protected with this method. Height of uprising was almost half, and the maximum heave one third of that in the similar unprotected wall. In thick walls, regardless of opening size, this method could not change the uprising level adequately. Therefore, an alternative method called "hole ventilation" was suggested and simulated in this study. In this method water evaporates not from the surface but from some holes drilled through the wall's thickness, which - independently from the wall's thickness - showed the capability to keep the bricks above the holes raw dry.

Using the method introduced and evaluated in this study, engineers could predict the uprising moisture in historical masonry buildings for a period of time in which water is in contact with the foundation. In stability calculations of a masonry building, in relation to the outcomes of the shearing tests, we must assign different shear strength parameters to materials with different degrees of saturation (or suctions). This means that for lower parts of a building (which have a higher water content) weaker material must be defined.

In order to reduce the problems of this humidity, based on the configuration of the building and in relation to the architectural and structural limitations, either one of the above-mentioned countermeasure methods could be selected and analyzed numerically. Based on this numerical simulation, in stability analyses of protected buildings, shear strength parameters of moist material should also be taken into account.

8.2 Suggested future works

This thesis could be followed by several research studies in the future. Based on the findings of this study further research is suggested as follows:

- Lack of knowledge about unsaturated properties of fiber-reinforced soils is clear. Therefore, determination of the SWCC of soils reinforced with other types of fibers (natural and synthetic) and with various sample preparation methods is suggested for future research.
- Shear strength of unsaturated fiber-reinforced soils is not widely discussed in the literature. Pull-out tests of straw filaments from a soil matrix under saturated and unsaturated conditions would help us to understand the characteristics of straw-soil interaction and connection.
- In order to investigate the counter measure method (hole ventilation) introduced in this thesis, it could be experimentally evaluated in masonry walls in further research.
- With oedometer tests on the same materials used in this research, the compressibility of the material under various suctions could be determined, which is one of the required parameters in the simulation of the volumetric behavior of walls subjected to uprising moisture under different loading conditions.

Bibliography

Abdi, M., Parsapajouh, A. & Arjomand, M. (2008), 'Effects of random fiber inclusion on consolidation, hydraulic conductivity, swelling, shrinkage limit and desiccation cracking of clays', *International Journal of Civil Engineering* **6**, 284–292.

Abtahi, M., Okhovat, N., Pourhosseini, R. & Hejazi, M. (2010), Improvement of soil strength by natural fibers, *in* 'From res to des Europ prac, Bratislava, Slovak Republic'.

Adam, J., Urai, J., Wieneke, B., Oncken, O., Pfeiffer, K., Kukowski, N.abd ad Lohrmann, J., Hoth, S., van der Zee, W. & Schmatz, J. (2005), 'Shear localisation and strain distribution during tectonic faulting-new insights from granular-flow experiments and high-resolution optical image correlation techniques', *Structural Geology* **27**, 283–301.

Adrian, R. J. (1991), 'Particle imaging techniques for experimental fluid mechanics', *Annual Review of Fluid Mechanics* **23**, 261–304.

Aggarwal, P. & Sharma, B. (2010), Application of jute fiber in the improvement of subgrade characteristics, *in* 'Internatinoal conference on advances in civil engineering, Trabzon, Turkey'.

Agus, S. (2005), An experimental study on hydro-mechanical characteristics of compacted bentonite sand mixtures, PhD thesis, Faculty of Civil Eng., Bauhaus-Universität Weimar, Germany.

Agus, S., Leong, E. & Rahardjo, H. (2001), 'Soil-water characteristic curve of singapore residual soils', *Geotechnical and Geological Engineering* **19**, 285–309.

Agus, S., Leong, E. & Schanz, T. (2003), 'Assessment of statistical models for indirect determination of permeability functions from soil-water characteristic curves', *Géotechnique* **53**, 279–282.

Agus, S. S. & Schanz, T. (2003), Vapour equilibrium technique for tests on a highly compacted bentonite-sand mixture, *in* 'International Conference on Problematic Soils, Nottingham, United Kingdom, pp. 467-474'.

Agus, S. & Schanz, T. (2005), Effect of shrinking and swelling on microstructures and fabric of a compacted bentonite-sand mixture, *in* 'Proceeding of International Conference on Problematic Soils (Eds. Bilsel, H and Nalbantoglu, Z). North Cyprus Vol.2, pp. 543-550'.

Ahmad, F., Bateni, F. & Azmi, M. (2010), 'Performance evaluation of silty sand reinforced with fibers', *Geotextiles and Geomembranes* **28**, 93–99.

Aiban, S. & Znidarcic, D. (1989), 'Evaluation of the flow pump and constant head techniques for permeability measurements', *Géotechnique* **39**, 655–666.

Aitchison, G. (1965), Moisture equilibria and moisture changes in soils, *in* 'A Symposium in Print Convened by Soil Mechanics Section Commonwealth Scientific and Industrial Research Organization, Butterworths, Australia.'.

Al-Adili, A., Azzam, R., Spagnoli, G. & J., S. (2012), 'Strength of soil reinforced with fiber materials (papyrus)', *Soil Mechanics and Foundation Engineering* **48**, 241–247.

Al-Azzo, S., Salih, S. & Salim, T. (2009), 'Compressive strength and swelling properties of randomly distributed fiber reinforcement clayey soil', *Al-Taghani Journal* **22**, 160–166.

Al-Badran, Y. (2011), Volumetric Yielding Behavior of Unsaturated Fine-Grained Soils, PhD thesis, Ruhr-Universität Bochum, Germany.

Al-Mukhtar, M., Qi, Y., Alcover, J. & Bergaya, F. (1999), 'Oedometric and water-retention behavior of highly compacted unsaturated smectites', *Canadian Geotechnical Journal* **36**, 675–684.

Al-Refeai, T. (1991), 'Behavior of granular soils reinforced with discrete randomly oriented inclusions', *Geotextiles and Geomembranes* **10**, 319–333.

Al-Wahab, R. & M.A., E.-K. (1995), Using fibers to reduce tension cracks and shrink/swell in compacted clay, *in* 'Geoenvironment 2000. Geotechnical Special Publication No. 46, ASCE, New York'.

Alabdullah, J. (2010), Testing Unsaturated Soil for Plane Strain Conditions: A New Double-Wall Biaxial Device, PhD thesis, Bauhaus Universität Weimar, Germany.

Albrecht, B., Benson, C. & Beuermann, S. (2003), 'Polymer capacitance sensors for measuring gas humidity in drier soils', *Geotechnical Testing Journal* **26**, 3–11.

Alshibli, K. & Akbas, I. (2007), 'Strain localization in clay: plane strain versus triaxial loading conditions', *Geotechnical and Geological Engineering* **25**, 45–55.

Alshibli, K., Batiste, S. & Sture, S. (2003), 'Strain localization in sand: plane strain versus triaxial compression', *Geotechnical and Geoenvironmental Engineering, ASCE* **129**, 1–12.

Alshibli, K., Godbold, D. & Hoffman, K. (2004), 'The louisiana plane strain apparatus for soil testing', *ASTM, Geotechnical Testing Journal* **27**, 337–346.

Alshibli, K. & Sture, S. (2000), 'Shear band formation in plane strain experimentations of sand', *Geotechnical and Geoenvironmental Engineering, Vol. 126, No. 6, June, pp. 495-503* **126**, 495–503.

Amir-Faryar, B. & Aggour, M. (2012), 'Determination of optimum fiber content in a fiber-reinforced clay', *Testing and Evaluation* **40**.

Amirshahkarami, S. (2005), Strengthening of bam citadel, a site investigating study, Technical report, Kakh-Payeh Consultant Engineers.

Anderson, W., Goodwin, A., Pyrah, I. & Salman, T. (1997), 'Equipment for one-dimensional compression and triaxial testing of unsaturated granular soils at low stress levels', *Geotechnical Testing Journal, GTJODJ, 20 (1): 74-89* **20**, 74–89.

Arifin, Y. (2008), Thermo-Hydro-Mechanical Behavior of Compacted Bentonite-Sand Mixtures: An Experimental Study, PhD thesis, Bauhaus-University Weimar, Germany.

Arthur, J., Dunstan, T., Al-Ani, Q. & Assadi, A. (1977), 'Plastic deformation and failure in granular media', *Géotechnique* **27**, 53–74.

Ashour, T., Bahnasawey, A. & Wu, W. (2010), 'Compressive strength of fiber reinforced earth plasters for straw bale buildings', *American Journal of Agricultural Economics* **1**, 86–92.

Averjanov, S. (1950), About permeability of subsurface soils in case of incomplete saturation, *in* 'English Collection, Vol. 7, 1950, as Quoted by P. Ya Palubarinova, 1962, The theory of ground water movement (English translation by I.M. Roger Dewiest, Princeton University Press, Princeton, N.J.)'.

Ayyar, R., Krishnaswamy, R. & Viswanadham, S. (1989), Geosynthetics for foundations on a swelling clay, *in* 'International work on geotextile, Bangalore, India'.

Azadegan, O., Kaffash, E., Yaghoubi, M. & Pourebrahim, G. (2012), 'Laboratory study on the swelling, cracking and mechanical characteristics of the palm fiber reinforced clay', *Electronic Journal of Geotechnical Engineering* **17**, 47–54.

Bahar, R., Benazzoug, M. & Kenai, S. (2004), 'Performance of compacted cement-stabilized soil', *Cement and Concrete Composites* **26**, 811–820.

Bauer, G. & Oancea, A. (1996), Triaxial testing of granular soils reinforced with discrete polypropylene fibers, *in* 'First European Geosynthetics Conference on Geosynthetics: Applications, Design and Construction. A.A. Balkema, Rotterdam, The Netherlands'.

Benson, C. & Gribb, M. (1997), 'Measuring unsaturated hydraulic conductivity in the laboratory and field', *ASCE, Geotechnical Special Publication* **68**, 113–168.

Bicalho, K., Znidarcic, D. & Ko, H. (2000), 'Air entrapment effects on hydraulic properties', *ASCE, Geotechnical Special Publication* **99**, 517–528.

Bishop, A. (1959), 'The principle of effective stress', *Teknisk Ukeblad* **106**, 859–863.

Bishop, A. (1966), 'Strength of soil as engineering materials', *Géotechnique* **16**, 89–130.

Bishop, A. & Donald, I. (1961), The experimental study of partly saturated soils in the triaxial apparatus, *in* 'Fifth International Conference on Soil Mechanics and Foundation Engineering, Paris, Vol. 1, pp. 13 21.'.

Blatz, J. & Graham, J. (2003), 'Elastic-plastic modeling of unsaturated soil using results from a new triaxial test with controlled suction', *Géotechnique* **53**, 113–122.

Boominathan, S., Senathipathi, K. & Jayaprakasam, V. (1991), 'Field studies on dynamic properties of reinforced earth', *Soil Dynamics and Earthquake Engineering* **10**, 402–406.

Bouhicha, M., Aouissi, F. & Kenai, S. (2005), 'Performance of composite soil reinforced with barley straw', *Cement Concrete Compos* **27**, 617–621.

Boyd, D. (1997), *A new concept in outdoor carpeting tested*, Georgia Milepost.

Briggs, L. (1897), *The Mechanics of Soil Moisture*, US Department of Agriculture, Division of Soils, Bulletin No. 10.

Broms, B. & Casbarian, A. (1965), Effect of rotation of the principal stress axes and of the intermediate principal stress on the shear strength, *in* '6th International Conference of Soil Mechanics'.

Brooks, R. & Corey, A. (1964), *Hydraulic properties of porous media: Hydrology Papers*, Colorado State University.

Brooks, R. & Corey, A. (1966), 'Properties of porous media affecting fluid flow', *Irrigation and Drainage Division, ASCE* **2**, 61–88.

Bruce, R. & Klute, A. (1956), 'The measurement of soil moisture diffusivity', *Soil Science Society of America, Proc. 20* pp. 458–462.

Brye, K. (2003), 'Long-term effects of cultivation on particle size and water-retention characteristics determined using wetting curves', *Soil Science* **168**, 459–468.

Buckingham, E. (1907), Studies on the movement of soil moisture, Technical report, Bur. Soil Bull., 38 U.S. Dept. of Agric., Washington D.C.

Bueno, S. (1997), The mechanical response of reinforced soils using short randomly distributed plastic strips, *in* 'Almeida, editor. Recent developments in soil and Pavement mechanics. Rotterdam: Balkema'.

Bui, Q., Morel, J., Venkatarama Reddy, B. & Ghayad, W. (2009), 'Durability of rammed earth walls exposed for 20 years to natural weathering', *Building and Environment* **44**, 912–919.

Burdine, N. (1953), Relative permeability calculation size distribution data, Technical report, Transactions of the American Institute of Mining, Metallurgical, and Petroleum Engineers, 198.

Cai, Y., Shi, B., C.W.W., N. & Tang, C. (2006), 'Effect of polypropylene fiber and lime admixture on engineering properties of clayey soil', *Engineering Geology* **87**, 230–240.

Cai, Y., Shi, B., Liu, Z., Tang, C. & Wang, B. (2005), 'Experimental study on the effect of aggregate size on the strength of filled soils', *Chinese Journal of Geotechnical Engineering* **27**, 1482–1486.

Campanella, R. & Vaid, Y. (1973), Influence of stress path on the plane strain behaviour of a sensitive clay, *in* '8th International Conference on Soil Mechanics and Foundation Engineering, Moscow, USSR'.

Campanella, R. & Vaid, Y. (1974), 'Triaxial and plane strain creep rupture of an undisturbed clay', *Canadian Geotechnical Journal* **11**, 1–10.

Campbell, J. (1973), Pore pressures and volume changes in unsaturated soils, PhD thesis, University of Illinois at Urbana Champaign, USA.

Casagrande, M., Coop, M. & Consoli, N. (2006), 'Behavior of a fiber-reinforced bentonite at large shear displacements', *Geotechnical and Geoenvironmental Engineeing Engineering, ASCE* **132**, 1505–1508.

Cerato, A. & Lutenegger, A. (2002), 'Determination of surface area of fine grained soils by the ethylene glycol monoethyl ether (egme) method', *ASTM Geotechnical Testing Journal* **25**, 315–321.

Chakraborty, T. & Dasgupta, S. (1996), Randomly reinforced fly ash as foundation material, *in* 'Indian Geotechnical Conference, Madras, India'.

Cheah, J. & Morgan, T. (2009), Uku: concept to construction using flax-fibre reinforced stabilised rammed earth, *in* '11th International conference non-conventional materials and technologies, Bath, UK'.

Chegenizadeh, A. & Nikraz, H. (2011*a*), Compaction characteristics of reinforced soil, *in* '5th SASTech, Khavaran Higher-Education Institute, Mashhad, Iran'.

Chegenizadeh, A. & Nikraz, H. (2011*b*), Permeability test on reinforced clayey sand, *in* 'World Academy of Science, Engineering and Technology'.

Chen, C. & Loehr, J. (2008), 'Undrained and drained triaxial tests of fiber-reinforced sand', *Geotextiles and Geomembranes* **25**, 194–202.

Childs, E. (1969), *An introduction to the physical basis of soil water phenomena*, John Wiley and Sons Inc., New York.

Chiu, T. & Shackelford, C. (1998), 'Unsaturated hydraulic conductivity of compacted sand kaolin mixtures', *Geotechnical and Geoenvironmental Engineeing, ASCE* **124**, 160–170.

Cho, G. & Santamarina, C. (2001), 'Unsaturated particulate materials-particle-level studies', *ASCE, Journal of Geotechnical and Geoenvironmental Engineering* **127**, 84–96.

Collins, K. & McGown, A. (1974), 'The form and function of microfabric features in a variety of natural soils', *Géotechnique* **24**, 223–254.

Consoli, C., Casagrande, T., Prietto, M. & Thome, A. (2003), 'Plate load test on fiber-reinforced soil', *Geotechnical and Geoenvironmental Engineering, ASCE* **129**, 951–955.

Consoli, C., Montardo, P., Donato, M. & Prietto, M. (2004), 'Effect of material properties on the behavior of sandcementfiber composites', *Ground Improvement* **8**, 77–90.

Consoli, C., Prietto, M. & Pasa, S. (2002), 'Engineering behavior of a sand reinforced with plastic waste', *Geotechnical and Geoenvironmental Engineering, ASCE* **128**, 462–472.

Consoli, N., Heineck, K., Casagrande, M. & Coop, M. (2007), 'Shear strength behavior of fiber-reinforced sand considering triaxial tests under distinct stress paths', *Geotechnical and Geoenvironmental Engineering, ASCE, pp. 1466-1469* **133**, 1466–1469.

Consoli, N., Prietto, P. & Ulbrich, L. (1998), 'Influence of fiber and cement addition on behavior of sandy soil', *Geotechnical and Geoenvironmental Engineering* **124**, 1211–1214.

Corey, A. (1957), 'Measurement of water and air permeability in unsaturated soil', *Soil Science Society of America, Proc. 21* pp. 7–10.

Cornforth, D. (1961), Plane strain failure characteristics of a saturated sand, PhD thesis, University of London, UK.

Cornforth, D. (1964), 'Some experiments on the influence of strain conditions on the strength of sand', *Géotechnique* **14**, 143–167.

Coussy, . & Fleureau, J. (2002), *Mecanique des Sols non Satures*, Hermes Science Publications.

Coutts, P. (1995), 'Autoclaved bamboo pulp fiber reinforced cement', *Cement Concrete Compos* **17**, 99–106.

Croney, D. & Coleman, J. (1961), Pore pressure and suction in soil, *in* 'Conference on Pore Pressure and Suction in Soils, London, Butterworths'.

Cruz, A., Hoyos, L. & A., L. (2012), Unsaturated soil response under plane strain conditions using a servo/suction-controlled biaxial apparatus, *in* '2nd European Conference on Unsaturated Soils'.

Cruz, A., Hoyos, L. & Lizcano, A. (2011), A novel suction-controlled biaxial apparatus for unsaturated soils, *in* '5th Asia-Pacific Conference on Unsaturated Soils, Pattaya, Thailand, Eds: A. Jotisankasa, A. Sawangsuriya, S. Soralump, and W. Mairaing'.

Cui, Y. J. & Delage, P. (1996), 'Yielding and plastic behaviour of an unsaturated silt', *Géotechnique* **46**, 291–311.

Cuisinier, O. & Masrouri, F. (2002), Influence of a suction cycle on the hydromechanical behaviour of a swelling soil, *in* 'International Workshop on Environmental Geomechanics, Monte Verità, Switzerland (Eds L. Vulliet, L. Laloui and B. Schrefler), EPFL Press, Lausanne, pp. 175 180'.

Daniel, D. (1983), 'Permeability test for unsaturated soil', *Geotechnical Testing Journal* **6**, 81–86.

Das, A., Jayashree, C. & Viswanadham, B. (2009), 'Effect of randomly distributed geofibers on the piping behaviour of embankments constructed with fly ash as a fill material', *Geotextiles and Geomembranes* **27**, 341–349.

Davidson, J., Stone, L., Nielsen, D. & Larue, M. (1969), 'Field measurement and use of soil-water properties', *Water Resources Research* **5**, 1312–1321.

Delage, P., Audiguier, M., Cui, Y. & Howat, M. (1996), 'The microstructure of a compacted silt', *Canadian Geotechnical Journal* **33**, 150–158.

Delage, P. & Graham, J. (1996), Mechanical behaviour of unsaturated soils: Understanding the behaviour of unsaturated soils requires reliable conceptual models, *in* '1st International Conference on Unsaturated Soils (UNSAT 95), Paris, France (Eds. E.E. Alonso and P. Delage), Balkema, Rotterdam.'.

Desrues, J. (1995), Experimental strain localisation in plane strain tests on sands and weak rocks, *in* 'Dynamic Plasticity and Structural Behaviors, Plasticity'95, Osaka S. Tanimura and A.S. Khan Ed., Gordon and Breach Publ., pp. 415 418'.

Desrues, J. & Viggiani, G. (2004), 'Strain localization in sand: an overview of the experimental results obtained in grenoble using stereophotogrammetry', *International Journal for Numerical and Analytical Methods in Geomechanics* **28**, 279–321.

Desrues, L., Lanier, L. & Stutz, P. (1985), 'Localization of the deformation in tests on sand sample', *Engineering Fracture Mechanics* **21**, 909–921.

Diambra, A., Ibraim, E., Muir Wood, D. & Russell, A. (2010), 'Fibre reinforced sands: Experiments and modelling', *Geotextiles and Geomembranes* **28**, 238–250.

Dirksen, C. (1991), Unsaturated hydraulic conductivity, Technical report, In: Smith KA, Mullins CE (eds) Soil analysis. Physical methods. Marcel Dekker, New York, pp 209 270.

Drescher, A., Vardoulakis, I. & Han, C. (1990), 'A biaxial apparatus for testing soils', *Geotechnical Testing Journal* **13**, 226–234.

Dullien, F. (1992), *Porous Media: Fluid Transport and Pore Structure*, Academic Press, San Diego.

Dutta, K. & Sarda, K. (2007), 'Cbr behavior of waste plastic strip-reinforced stone dust/fly ash overlying saturated clay', *Turkish Journal of Engineering and Environmental Sciences* **31**, 171–182.

Eltantawy, I. & Arnold, P. (1973), 'Reappraisal of ethylene glycol mono-ethyl ether (egme) method for surface area estimation of clays', *Soil Science* **24**, 232–238.

Escario, V. & Juca, J. (1989), Strength and deformation of partly saturated soils, *in* '12th international conference on soil mechanics and foundation engineering, Rio De Janeiro, vol 11, pp 4346'.

Esna-ashari, M. & Asadi, M. (2008), A study on shear strength and deformation of sandy soil reinforced with tire cord wastes, *in* '4th Asian Regional Conference on Geosynthetics, Shanghai, China'.

Estabragh, A., Bordbar, A. & Javadi, A. (2013), 'A study on the mechanical behavior of a fiber-clay composite with natural fiber', *Geotechnical and Geological Engineering* **31**, 501–510.

Farulla, C. & Rosone, M. (2012), Shear strength of a compacted scaly clay from suction-controlled triaxial tests, *in* 'Unsaturated Soils: Research and Applications'.

Fauziah, M. & Nikraz, H. (2007*a*), Biaxial testing of overconsolidated clay, *in* '1st International Conference of European Asian Civil Engineering Forum, Jakarta, Indonesia'.

Fauziah, M. & Nikraz, H. (2007*b*), Stress-strain behaviour of overconsolidated clay under plane strain condition, *in* '10th Australia New Zealand conference on geomechanics, pp. 148153, Brisbane, Australia'.

Fauziah, M. & Nikraz, H. (2008), The behavior of unsaturated compacted clay under plane strain condition, *in* '3rd International Conference on Evaluation, Monitoring, Simulation, Management and Remediation of the Geological Environment and Landscape, The New Forest, Ashurst Lodge, UK'.

Fauziah, M. & Nikraz, H. (2010), 'Influence of discontinuities on the behavior of partially saturated compacted clay', *Dinamika Teknik Sipil* **10**, 9–14.

Fisher, E. (1923), 'Some factors affecting the evaporation of water from soil', *Agricultural Science* **13**, 121–143.

Fleureau, J., Bouabdallah, A., Maouchi, D. & Taibi, S. (1998), Mechanical behavior of an unsaturated loam under high stresses and high negative pressure, *in* 'Second International Conference on Unsaturated Soils, Beijing'.

Fleureau, J., Verbrugge, J., Huergo, P., Correia, A. & Kheirbek-Saoud, S. (2002), 'Aspects of the behaviour of compacted clayey soils on drying and wetting paths', *Canadian Geotechnical Journal* **39**, 1341–1357.

Fredlund, D. & Morgenstern, N. (1977), 'Stress state variables for unsaturated soils', *Geotechnical Division, ASCE* **103**, 447–466.

Fredlund, D. & Rahardjo, H. (1993), *Soil mechanics for unsaturated soils*, John Wiley and Sons Inc., New York.

Fredlund, D. & Xing, A. (1994), 'Equations for the soil-water characteristic curve', *Canadian Geotechnical Journal 31: 521-532* **31**, 521–532.

Fredlund, D., Xing, A. & Huang, S. (1994), 'Predicting the permeability function for unsaturated soils using the soil-water characteristic curve', *Canadian Geotechnical Journal 31. pp. 533-546* **31**, 533–546.

Freeze, R. & Cherry, J. (1979), *Groundwater*, Prentice Hall.

Freilich, J., Li, C. & Zornberg, G. (2010), Effective shear strength of fiber-reinforced clays, *in* '9th International Conference on Geosynthetics, Brazil'.

Freitag, D. (1986), 'Soil randomly reinforced with fibers', *Geotechnical Engineering, ASCE* **112**, 823–826.

Furumoto, K., Miki, H., Tsuneoka, N. & Obata, T. (2002), Model test on the piping resistance of short fiber reinforced soil and its application to river levee, *in* 'Geosynthetics 7th ICG-NICE, France'.

Gardner, W. (1958), 'Some steady state solutions of the unsaturated moisture flow equation with application to evaporation from a water table', *Soil Science* **85**, 228–232.

Gasparre, A. (2005), Advanced laboratory characterisation of London clay, PhD thesis, University of London, UK.

Gee, G., Campbell, M., Campbell, G. & Campbell, J. (1992), 'Rapid measurement of low soil potentials using a water activity meter.', *Soil Science Society of America Journal* **56**, 1068–1070.

Gens, A., Alonso, E., Suriol, J. & Lloret, A. (1995), Effect of the structure and volumetric behaviour of a compacted soil, *in* '1st International Conference on Unsaturated Soils (Eds. Alonso and Delage), Paris, France'.

Ghahremani, M., Ghalandarzadeh, A., Nowamooz, H. & Ghahremani, K. (2007), The undrained behavior of clayey sands, *in* '60th Canadian Geotechnical Conference, Ottawa, Canada.'.

Ghavami, K., Filho, R. & Barbosa, P. (1999), 'Behaviour of composite soil reinforced with natural fibers', *Cement Concrete Compos* **21**, 39–48.

Ghiassian, H., Poorebrahim, G. & Gray, D. (2004), 'Soil reinforcement with recycled carpet wastes', *Waste Management and Research* **22**, 108–114.

Gosavi, M., Patil, A., Mittal, S. & Saran, S. (2004), 'Improvement of properties of black cotton soil subgrade through synthetic reinforcement', *The Institution of Engineers (India)* **84**, 257–262.

Gray, D. & Ohashi, H. (1983), 'Mechanics of fiber reinforcement in sand', *Geotechnical and Geoenvironmental Engineering, ASCE* **109**, 355–353.

Gray, H. & Al-Refeai, T. (1986), 'Behavior of fabric versus fiber reinforced sand', *Geotechnical and Geoenvironmental Engineering, ASCE* **112**, 809–820.

Green, G. E. (1971), Strength and deformation of sand measured in an independent stress control cell, *in* 'Roscoe Memorial Symposium: Stress–Strain Behaviour of Soils'.

Hall, C. (1977), 'Water movement in porous building materials-i. unsaturated flow theory and its applications', *Building and Environment* **12**, 117–125.

Hambly, E. (1969), Plane strain behavior of soft clay, PhD thesis, University of Cambridge, UK.

Hambly, E. (1972), 'Plane strain behavior of remolded normally consolidated kaolin', *Géotechnique* **22**, 301–317.

Hambly, E. & Roscoe, K. (1969), Observations and predictions of stresses and strains during plane strain of wet clays, *in* '7th ICSMFE, Mexico'.

Harriette, L. (2004), The potential of flax fibers as reinforcement for composite materials, PhD thesis, Eindhoven University, the Netherlands.

Heineck, K., Coop, M. & Consoli, N. (2005), 'Effect of microreinforcement of soil from very small to large shear strains', *Geotechnical and Geoenvironmental Engineering, ASCE* **131**, 1024–1033.

Hejazi, S., Sheikhzadeh, M., Abtahi, S. & Zadhoush, A. (2012), 'A simple review of soil reinforcement by using natural and synthetic fibers', *Construction and Building Materials* **30**, 100–116.

Henkel, D. (1960), The shear strength of saturated remolded clays, *in* 'ASCE Research Conference on Shear Strength of Cohesive Soils, Boulder, Colorado'.

Henkel, D. & Wade, N. (1960), Plane strain tests on saturated remolded clay, *in* 'ASCE research conference on shear strength of cohesice soils, Boulder, Colorado'.

Hilf, J. (1965), An Investigation of Pore-Water Pressure in Compacted Cohesive Soils, PhD thesis, U.S. Dep. of the Interior, Bureau of Reclamation, Design and Construction Div., Denver.

Hoare, D. (1979), Laboratory study of granular soils reinforced with randomly oriented discrete fibers, *in* 'International Conference Soil Reinforcement, Association Amicale des Ingeniers Ansiens Eleves del LEcole Nationale de ponts et Chaussess, 1, Paris, France'.

Hoekstra, P. & Delaney, A. (1974), 'Dielectric properties of soils at uhf and microwave frequencies', *Geophysical Research* **79**, 1699–1708.

Hohn, C. (1971), Abcs of making adobe bricks, Technical report, New Mexico State University, College of Agricultural, Consumer and Environmental Sciences.

Houlsby, G. (1991), How the dilatancy of soils affects their behavior, *in* 'Tenth European Conference on Soil Mechanics and Foundation Engineering, Florance, Italy'.

Ikizler, B., Aytekin, M., Turker, E. & Yavuz, H. (2009), Effect of fibers on swelling characteristics of bentonite, *in* '2nd International Conference on New Developments in Soil Mechanics and Geotechnical Engineering, Near East University, Nicosia'.

Illuri, H. & Nataatmadja, A. (2007), Reduction of shrink-swell potential with eps inclusion, *in* '10th Australia New Zealand Conference on Geomechanics'.

Ingles, O. (1962), Bonding forces in soils, part 3: A theory of tensile strength for stabilized and naturally coherent soils, *in* '1st Conference of the Australian Road Research Board'.

Islam, M. & Iwashita, K. (2010), 'Earthquake resistance of adobe reinforced by low cost traditional materials', *Natural Disaster Science* **32**, 1–21.

Jacob, M., Joseph, S. & Pothan, L. (2005), 'A study of advances in characterization of interfaces and fiber surfaces in lingocellulosic fiber-reinforced composites', *Composite Interfaces* **12**, 95–124.

Jadhao, D. & Nagarnaik, B. (2008), Performance evaluation of fiber reinforced soilfly ash mixtures, *in* '12th Int conf of int assoc for comp meth and adv in geomech (IACMAG), Goa, India'.

Jamellodin, Z., Talib, Z., Kolop, R. & Noor, N. (2010), The effect of oil palm fibre on strength behaviour of soil, *in* '3rd SANREM conf, kota kinabalu, Malaysia'.

Jiang, H., Cai, Y. & Liu, J. (2010), 'Engineering properties of soils reinforced by short discrete polypropylene fiber', *Materials Civil Engeering, ASCE* **22**, 1315–1322.

Jotisankasa, A., Coop, M. & Ridley, A. (2009), 'The mechanical behaviour of an unsaturated compacted silty clay', *Géotechnique* **59**, 415428.

Kaniraj, R. & Havanagi, G. (2001), 'Behavior of cement stabilized fiber reinforced fly ash soil mixtures', *Geotechnical and Geoenvironmental Engineering, ASCE* **127**, 574–584.

Kayadelen, C., Tekinsoy, M. & Taskiran, T. (2007), 'Influence of matric suction on shear strength behavior of a residual clayey soil', *Environmental Geology* **53**, 981–901.

Kazragis, A. (2005), 'Minimization of atmosphere pollution by utilizing cellulose waste', *Environmental Engineering and Landscape Management* **13**, 81–90.

Key, L. (1988), 'Straw as an erosion control mulch, a technical report from us agriculture department', *Portland, Oregon,* **49**.

Khalili, N., Geiser, F. & Blight, G. (2005), 'Effective stress in unsaturated soils: Review with new evidence', *ASCE, International Journal of Geomechanics* **4**, 115–126.

Khalili, N. & Khabbaz, M. (1998), 'A unique relationship for the determination of the shear strength of unsaturated soils', *Géotechnique* **48**, 681–688.

Khedari, J., Watsanasathaporn, P. & Hirunlabh, J. (2005), 'Development of fiber-based soil-cement block with low thermal conductivity', *Cement Concrete Compos* **27**, 111–116.

Kinjal, S., Desai, A. & Solanki, C. (2012), 'Experimental study on the atterberg limits of expansive soil reinforced with polyester triangular fibers', *International Journal of Engineering Research and Applications* **2**, 636–639.

Klausner, Y. (1991), *Fundamentals of continuum mechanics of soils*, Springer-Verlag, New York.

Klute, A. (1972), 'The determination of the hydraulic conductivity and diffusivity of unsaturated soils', *Soil Science* **113**, 264–276.

Klute, A. & Dirksen, C. (1986), Hydraulic conductivity and diffusivity: laboratory methods, Technical report, In: Klute A (ed) Methods of soil analysis. 1, Physical and mineralogical methods, Madison: American Society of Agronomy; Soil Science Society of America, 2nd edn.

Koliji, A. (2008), Mechanical behaviour of unsaturated aggregated soils, PhD thesis, École Polytechnique Fédérale de Lausanne, switzerland.

Kouakou, C. & Morel, J. (2009), 'Strength and elasto-platic properties of non-industrial building materials manufactured with clay as a natural binder', *Applied Clay Science* **44**, 27–37.

Kozlowski, R. (2011), *Handbook of natural fibers: processing and applications*, Cambridge.

Kumar, A., Walia, B. & Bajaj, A. (2007), 'Influence of fly ash, lime, and polyester fibers on compaction and strength properties of expansive soil', *Materials Civil Engeering, ASCE* **19**, 242–248.

Kumar, A., Walia, B. & Mohan, J. (2006), 'Compressive strength of fiber reinforced highly compressible clay', *Construction and Building Materials* **20**, 1063–1068.

Kumruzzaman, M. & Yin, J. (2012), 'Stress-strain behavior of completely decomposed granite in both triaxial and plane strain conditions', *Jordan Journal of Civil Engineering* **6**, 83–108.

Kunze, R. & Kirkham, D. (1962), 'Simplified accounting for membrane impedance in capillary conductivity measurements', *Soil Science Society of America Proc. 26* pp. 421–426.

Lago, M. & Araujo, M. (2001), 'Capillary rise in porous media', *Journal of Colloid and Interface Science* **234**, 35–43.

Lambe, T. & Whitman, R. (1979), *Soil Mechanics*, John Wiley and Sons Inc., New York.

Le Bihan, J. & Leroueil, S. (2002), 'A model for gas and water flow through the core of earth dams', *Canadian Geotechnical Journal* **39**, 90–102.

Lee, H. & Wray, W. (1995), Techniques to evaluate soil suction - a vital unsaturated soil water variable, *in* 'First International Conference on Unsaturated Soils, Paris.'.

Lee, K. (1970), 'Comparison of plane strain and triaxial tests on sand', *Soil Mechanics and Foundation Division* **96**, 901–923.

Lee, K. & Shubeck, R. (1971), 'Plane-strain undrained strength of compacted clay', *Soil Mechanics and Foundation Division, ASCE* **97**, 219–234.

Leong, E. & Rahardjo, H. (1997), 'Review of soil-water characteristic curve equations', *Geotechnical and Geoenvironmental Engineering, ASCE* **123**, 1106–1117.

Leong, E., Tripathy, S. & Rahardjo, R. (2003), 'Total suction measurement of unsaturated soils with a device using the chilled-mirror dew-point technique', *Géotechnique* **53**, 173–182.

Li, C. (2005), Mechanical response of fiber-reinforced soil, PhD thesis, Faculty of the Graduate School of the University of Texas at Austin.

Li, C. (2009), 'Large volume, high-performance applications of fibers in civil engineering', *Applied Polymer Science* **83**, 660–686.

Likos, W., Wayllace, A. & N., L. (2005), Numerical modeling of constant flow method for measuring unsaturated hydrologic properties, *in* 'International Symposium on Advanced Experimental Unsaturated Soil Mechanics. Balkema'.

Lins, Y. (2009), Hydro-Mechanical Properties of Partially Saturated Sand, PhD thesis, Ruhr- University Bochum, Germany.

Lloret, A., Villar, M., Sánchez, M., Gens, A., Pintado, X. & Alonso, E. (2003), 'Mechanical behaviour of heavily compacted bentonite under high suction changes', *Géotechnique* **53**, 27–40.

Lockington, D. & Parlange, J. (2004), 'A new equation for macroscopic description of capillary rise in porous media', *Colloid and Interface Science* **278**, 404–409.

Loehr, J., Axtell, P. & Bowders, J. (2000), Reduction of soil swell potential with fiber reinforcement, *in* 'GeoEng2000, Melbourne, Australia, 19-24 November'.

Lu, N. & Likos, W. (2004), *Unsaturated soil mechanics*, Wiley, New Jersey.

Lu, N., Wayllace, A., Carrera, J. & Likos, W. (2006), 'Constant flow method for concurrently measuring soil-water characteristic curve and hydraulic conductivity function', *ASTM, Geotechnical Testing Journal* **29**, 111–132.

Maher, H. & Ho, C. (1993), 'Behavior of fiber-reinforced cemented sand under static and cyclic loads', *Geotechnical Testing Journal* **16**, 330–338.

Maher, H. & Ho, C. (1994), 'Mechanical properties of kaolinite/fiber soil composite', *Geochemical Engineering* **120**, 1381–1393.

Maher, M. & Gray, D. (1990), 'Static response of sand reinforced with randomly distributed fibers', *Geotechnical Engineering* **116**, 1661–1677.

Maheshwari, V. (2011), 'Performance of fiber reinforced clayey soil', *Electronic Journal of Geotechnical Engineering* **16**, 1067–1087.

Malekzadeh, M. & Bilsel, H. (2012*a*), 'Effect of polypropylene fiber on mechanical behavior of expansive soils', *Electronic Journal of Geotechnical Engineering* **17**, 55–63.

Malekzadeh, M. & Bilsel, H. (2012*b*), 'Swell and compressibility of fiber reinforced expansive soils', *International Journal of Advanced Technology in Civil Engineering* **1**.

Mansour, A., Srebric, J. & Burley, J. (2007), 'Development of straw-cement composite sustainable building material for low-cost housing in egypt', *Applied Science Researches* **3**, 1571–1580.

Marachi, N., Duncan, J., Chan, C. & Seed, H. (1981), 'Plane-strain testing of sand, laboratory shear strength of soil', *ASTM, Special Technical Publications, R. N. Yong and F.C. Townsend, Eds.* **740**, 294–302.

Marandi, M., Bagheripour, H., Rahgozar, R. & Zare, H. (2008), 'trength and ductility of randomly distributed palm fibers reinforced silty-sand soils', *American Journal of Applied Sciences* **5**, 209–220.

Masrouri, F., Bicalho, K. & Kawai, K. (2008), 'Laboratory hydraulic testing in unsaturated soils', *Geotechnical and Geological Engineering* **26**, 691–704.

Mattone, R. (2005), 'Sisal fibre reinforced soil with cement or cactus pulp in bahareque technique', *Cement Concrete Compos* **27**, 911–616.

Mendes, J., Toll, D. & Evans, F. (2012), A double cell triaxial system for unsaturated soils testing, *in* 'Unsaturated Soils: Research and Applications, Vol. 1, pp 5 10.'.

Mesbah, A., Morel, J. C., Walker, P. & Ghavami, K. (2004), 'Development of a direct tensile test for compacted earth blocks reinforced with natural fibers', *Materials in Civil Engineering* **16**, 95–98.

Michalowski, R. & Zhao, A. (1996), 'Failure of fiber-reinforced granular soils', *Geotechnical Engineering, ASCE* **122**, 226–234.

Miller, C. & Rifai, S. (2004), 'Fiber reinforcement for waste containment soil liners', *Environmental Engineering 130 (8), 981985* **130**, 981–985.

Miller, E. & Elrick, D. (1958), 'Dynamic determination of capillary conductivity extended for non negligible membrane impedance', *Soil Science Society of America Proc. 22* pp. 483–486.

Mitchell, J. (1993), *Fundamentals of Soil Behavior*, 2nd Edition. John Wiley & Sons Inc., New York.

Mochizuki, A., Min, C. & Takahashi, S. (1993), 'A method for plane strain testing of sand', *Japanese Geotechnical Society* **475**, 99–107.

Mohamed, T., Ali, F., Hashim, S. & Huat, B. (2006), 'Relationship between shear strength and soil water characteristic curve of an unsaturated granitic', *American Journal of Environmental Sciences* **2**, 142–145.

Molnár, V. (2011), Examination of pressed adobe brick, Technical report, Széchenyi István University. Department of Architecture and Building Construction, HU ISSN 1418-7108: HEJ Manuscript no.: CEA-021227-A.

Mortensen, A. (2001), Preferential Flow Phenomena in Partially-Saturated Porous Media, PhD thesis, Technical University of Denmark, Denmark.

Mualem, Y. (1976), 'A new model for predicting the hydraulic conductivity of unsaturated porous media', *Water Resources Research* **12**, 513–522.

Mullins, B. & Braddock, R. (2012), 'Capillary rise in porous, fibrous media during liquid immersion', *International Journal of Heat and Mass Transfer* **55**, 62226230.

Murray, J., Frost, D. & Wang, Y. (2000), 'The behavior of sandy soil reinforced with discontinuous fiber inclusions', *Transport Research Record* **1714**, 9–17.

Murray, T. & Farrar, M. (1988), 'Temperature distributions in reinforced soil retaining walls', *Geotextiles and Geomembranes* **7**, 33–50.

Naeini, S. & Sadjadi, S. (2009), Effect of waste polymer materials on shear strength of unsaturated clays, *in* '2nd International Conference on New Developments in Soil Mechanics and Geotechnical Engineering, Near East University, Nicosia'.

Nakai, T. (2007), Modeling of soils behavior based on tij concept, *in* '13th Asian regional Conference on Soil echnics and Geotechnical Engineering, Kolkata, (Keynote paper)'.

Nataraj, M. & McManis, K. (1997), 'Strength and deformation properties of soils reinforced with fibrillated fibers', *Geosynthetics International* **4**, 65–79.

Nübel, K. & Weitbrecht, V. (2002), 'Visualization and localization in grain skeletons with particle image velocimetry', *Testing and Evaluation* **30**, 322–329.

Neeraja, D. (2010), 'Influence of lime and plastic jute on strength and cbr characteristics of soft clayey (expansive) soil', *Global Journal of Researches in Engineering* **10**, 16–24.

Nelson, J. & Miller, D. (1992), *Expansive Soils, Problems and Practice in Foundation and Pavement Engineering*, John Wiley and Sons Inc., New York.

Ng, C. & Shi, Q. (1998), 'A numerical investigation of the stability of unsaturated soil slopes subjected to transient seepage', *Computers and Geotechnics* **22**, 1–28.

Ng, C., Zhan, L. & Cui, Y. J. (2002), 'A new simple system for measuring volume changes in unsaturated soils', *Canadian Geotechnical Journal* **39**, 757–764.

Oberg, A. & Sallfors, G. (1997), 'Determination of shear strength parameters of unsaturated silts and sands based on the water retention curve', *Geotechnical Testing Journal* **20**, 40–48.

Oda, M. & Kazama, H. (1998), 'Microstructure of shear bands and its relation to the mechanisms of dilatancy and failure of dense granular soils', *Géotechnique* **48**, 465–481.

Oda, M., Koshikawa, I. & Higuchi, T. (1978), 'Experimental study of anisotropic shear strength of sand by plane strain test', *Soils and Foundations* **18**, 25–38.

Ola, S. (1989), 'Stabilization of lateritic soils by extensible fiber reinforcement', *Engineering Geology* **26**, 125–140.

Olsen, H. (1966), 'Darcys law in saturated kaolinite', *Water Resources Research* **2**, 287–295.

Olsen, H., Nichols, R. & Rice, T. (1985), 'Low gradient per meability methods in a triaxial system', *Géotechnique* **35**, 145–157.

Orman, E. (1994), 'Interface shear strength properties of roughened hdpe', *Geotechnical and Geoenvironmental Engineering, ASCE* **120**, 758–761.

Pachepsky, Y. & Scherbakov, R. (1984), 'Determination of capillary hydraulic conductivity of soils and its dependence on suction', *Journal of Hydrology* **69**, 287–296.

Paikowsky, S. & Xi, F. (2000), 'Particle motion tracking utilizing a high-resolution digital ccd camera', *Geotechnical Testing* **23**, 123–134.

Park, S. (2001), 'Unconfined compressive strength and ductility of fiber-reinforced cemented sand', *Construction and Building Materials* **25**, 1134–1138.

Park, S. (2009), 'Effect of fiber reinforcement and distribution on unconfined compressive strength of fiber-reinforced cemented sand', *Geotextiles and Geomembranes* **27**, 162–166.

Park, S., Kim, Y., Choi, S. & Shin, E. (2008), 'Unconfined compressive strength of cemented sand reinforced with short fibers', *Korean Society of Civil Engineers* **28**, 213–220.

Pel, L. (1995), Moisture transport in porous building materials, PhD thesis, Eindhoven University of Technology, The Netherlands.

Peric, D. & Hwang, C. (2002), Experimental investigation of plane strain behaviour of georgia kaolin, *in* '8th International Symposium NUMOG VIII, Rome, Italy'.

Peters, J., Lade, P. & Bro, A. (1988), Peters j., lade p., bro a.,, *in* 'Donaghe R, Chaney R, Silver M (eds) Advanced triaxial testing of soil and rock. ASTM, STP 977. ASTM'.

Pham, Q., Fredlund, D. & Barbour, S. (2005), 'A study of hysteresis models for soil-water characteristic curves', *Canadian Geotechnical Journal* **42**, 1548–1468.

Phanikumar, B. & Kashliwal, A. (2010), Effect of fiber reinforcement on swelling behavior, *in* 'Indian Geotechnical Conference'.

Polmann, D. (1990), Application of Stochastic Method in Transient Flow and Transport in Heterogeneous Unsaturated Soils, PhD thesis, MIT, USA.

Prabakara, J. & Sridhar, R. (2002), 'Effect of random inclusion of sisal fiber on strength behavior of soil', *Construction and Building Materials* **16**, 123–131.

Pradhan, P., Kar, R. & Naik, A. (2012), 'Effect of random inclusion of polypropylene fibers on strength characteristics of cohesive soil', *Geotechnical and Geological Engineering* **30**, 12–15.

Punthutaecha, K., Puppala, J., Vanapalli, S. & Inyang, H. (2006), 'Volume change behaviors of expansive soils stabilized with recycled ashes and fibers', *Geotechnical and Geoenvironmental Engineering, ASCE* **18**, 295–306.

Puppala, A. & Musenda, C. (2000), 'Effects of fiber reinforcement on strength and volume change in expansive soils', *Transport Research Record* **1736**, 134–140.

Qu, J., Li, C., Liu, B., Chen, X., Li, M. & Yao, Z. (2013), 'Effect of random inclusion of wheat straw fibers on shear strength characteristics of shanghai cohesive soil', *Geotechnical Geological Engineering* **31**, 511–518.

Ramaswamy, S., Ahuja, M. & Krishnamoorthy, S. (1983), 'Behavior of concrete reinforced with jute, coir, and bamboo fibres', *Cement Concrete Compos* **5**, 3–13.

Ramesh, N., Krishna, V. & Mamatha, V. (2010), 'Compaction and strength behavior of lime-coir fiber treated black cotton soil', *Geomechanics and Engineering* **2**, 19–28.

Ranjan, G., Vasan, R. & Charan, H. (1996), 'Probabilistic analysis of randomly distributed fiber-reinforced soil', *Geotechnical Engineering* **122**, 419–426.

Rassam, D. (2002), 'Variation of evaporative and shear strength parameters along a tailings delta', *Canadian Geotechnical Journal* **39**, 32–45.

Ravishankar, U. & Raghavan, S. (2004), Coir stabilised lateritic soil for pavements, *in* 'Indian geotech conf, Ahmedabad, India'.

Röchter, L. (2011), Systeme paralleler Scherbänder unter Extensionim ebenen Verformungszustand, PhD thesis, Ruhr-Universität Bochum.

Röchter, L., König, D., Schanz, T. & Triantafyllidis, T. (2010), 'Shear banding and strain softening in plane strain extension: physical modelling', *Granular Materials* **12**, 287301.

Rechenmacher, A. & Finno, R. (2004), 'Digital image correlation to evaluate shear banding in dilative sands', *Geotechnical Testing* **27**, 1–10.

Rendulic, L. (1937), 'Ein grundgesetz der tonmechanik und sin experiment eller beweiss', *der Bauingenieur* **18**, 459–467.

Richards, B. (1966), The significance of moisture flow and equilibria in unsaturated soil in relation to the design of engineering structures built on shallow foundations in australia, *in* 'Symposium on Permeability and Capillarity, ASTM, Atlantic City, NJ.'.

Richards, L. (1931), 'Capillary conduction of liquids through porous medium', *Physics* **1**, 318–333.

Richards, S. & Weeks, L. (1953), 'Capillary conductivity values from moisture yield and tension measurements on soil columns', *Soil Science Society of America, Proc. 17* pp. 206–209.

Ridley, A. & Wray, W. (1995), Suction measurement: a review of current theory and practices, *in* 'Proceedings of First International conference on Unsaturated Soils.'.

Rijtema, P. (1959), 'Calculation of capillary conductivity from pressure plate outflow data with non negligible membrane impedance', *Netherlands Journal of Agricultural Science* **7**, 209–215.

Rijtema, P. (1965), An analysis of actual evapotranspiration, Technical report, Agricultural Research (Wageningen) No. 659.

Roscoe, K. (1970), 'The influence of strains in soil mechanics', *Géotechnique* **20**, 129–170.

Roscoe, K., Schofield, A. & Wroth, P. (1958), 'On the yielding of soils', *Géotechnique* **1**, 22–53.

Rowe, P. (1971), Theoretical meaning and observed values of deformation parameters for soil, *in* 'Proceedings of Roscoe Memorial Symposium, Henley-on-Thames: Foulis.'.

Rowell, M., Han, S. & Rowell, S. (2000), 'Characterization and factors effecting fiber properties', *Nat Polym Agr Compos* pp. 115–134.

Salehan, I. & Yaacob, Z. (2011), 'Properties of laterite brick reinforced with oil palm empty fruit bunch fibers', *Pertanika Journal of Science and Technology* **19**, 33–43.

Santhi, K. & Sayida, M. (2009), Behavior of black cotton soil reinforced with sisal fiber, *in* '10th National Conference on Technological Trends (NCTT09)'.

Santoni, L. & Webster, L. (2001), 'Airfields and road construction using fiber stabilization of sands', *Transport Engineering, ASCE* **127**, 96–104.

Schanz, T., Agus, S. & Tscheschlok, G. (2004), Determination of hydro-mechanical properties of trisoplast, Technical report, Research Report Bo-015/03, Laboratory of Soil Mechanics, Bauhaus-Universität Weimar, Weimar, Germany.

Schanz, T. & Alabdullah, J. (2007), Testing unsaturated soil for plane strain conditions: A new double wall biaxial device, *in* 'Experimental Unsaturated Soil Mechanics, Springer. pp. 169 178'.

Schanz, T. & Vermeer, P. (1996), 'Angles of friction and dilatancy of sand', *Géotechnique* **46**, 145–151.

Schicker, A. & Gier, S. (2009), 'Optimizing the mechanical strength of adobe bricks', *Clays and Clay Minerals* **57**, 494–501.

Segetin, M., Jayaraman, K. & Xu, X. (2007), 'Harakeke reinforcement of soil-cement building materials: manufacturability and properties', *Building and Environment* **42**, 3066–3079.

Setty, S. & Murthy, A. (1987), Behavior of fiber-reinforced black cotton soil, *in* 'IGC (87), Bangalore, India'.

Setty, S. & Rao, G. (1987), Characteristics of fiber reinforced lateritic soil, *in* 'IGC (87), Bangalore, India'.

Shibata, T. & Krube, D. (1965), Influence of the variation of the intermediate principal stress on the mechanical properties of normally consolidated clays, *in* '6th International Conference of Soil Mechanics'.

Shibata, T. & Krube, D. (1967), Contribution to discussion on plane strain tests on a saturated remoulded clay, *in* 'American Society of Civil Engineers 93, SM5'.

Sillers, W. S. (1997), The mathematical representation of the soil-water characteristic curve, PhD thesis, University of Saskatchewan, Canada.

Sivakumar-Babu, G. & Vasudevan, A. (2008*a*), 'Seepage velocity and piping resistance of coir fiber mixed soils', *Irrigation and Drainage Engineering* **134**, 485–492.

Sivakumar-Babu, G. & Vasudevan, K. (2008*b*), 'Strength and stiffness response of coir fiber-reinforced tropical soil', *Materials Civil Engeering, ASCE* **20**, 571–577.

Sivakumar, V. (1993), A critical state framework for unsaturated soil, PhD thesis, University of Sheffield, UK.

Smith, P. (2003), Numerical analysis of infiltration into partially saturated soil slopes, PhD thesis, University of London, UK.

Sobhan, K. & Mashnad, M. (2002), 'Tensile strength and toughness of soilcementfly ash composite reinforced with recycled high density polyethylene strips', *Materials Civil Engeering, ASCE* **14**, 177–184.

Song, Y., Hwang, W., Jung, S. & Kim, T. (2012), 'A comparative study of suction stress between sand and silt under unsaturated conditions', *Engineering Geology* **124**, 90–97.

Sridharan, A. & Nagaraj, H. (1999), 'Absorption water content and liquid limit of soils', *Geotechnical Testing Journal* **22**, 121–127.

Stoimenova, E., Datcheva, M. & Schanz, T. (2005), 'Statistical approach in soil-water characteristic curve modelling', *Numerical and theoretical approaches. pp. 189-200* **94**, 189–200.

Swamy, N. (1984), *New reinforced concretes*, Surry University Press.

Taibi, S., Duperret, A. & J.M., F. (2009), 'The effect of suction on the hydro-mechanical behavior of chalk rocks', *Engineering Geology* **106**, 40–50.

Tang, C., Shi, B. & Chen, W. (2006), 'Strength and mechanical behavior of short polypropylene fiber reinforced and cement stabilized clayey soil', *Geotextiles and Geomembranes* **24**, 1–9.

Tang, C., Shi, B., Gao, W., Chen, F. & Cai, Y. (2007), 'Strength and mechanical behavior of short polypropylene fiber reinforced and cement stabilized clayey soil', *Geotextiles and Geomembranes* **25**, 194–202.

Tang, C., Shi, B. & Zhao, L. (2010), 'Interfacial shear strength of fiber reinforced soil', *Geotextiles and Geomembranes* **28**, 54–62.

Tarantino, A. (2007), 'A possible critical state framework for unsaturated compacted soils', *Géotechnique* **57**, 385–389.

Tarantino, A., Mongiovi, L. & Bosco, G. (2000), 'An experimental investigation on the independent isotropic stress variables for unsaturated soils', *Géotechnique* **50**, 275–282.

Tatsuoka, F., Sakamoto, M., Kawamura, T. & Fukushima, S. (1986), 'Strength and deformation characteristics of sand in', *Soils and Foundations* **26**, 65–84.

Terzaghi, K. (1943), *Theoretical Soil Mechanics*, John Wiley and Sons, Inc., New York.

Thom, R., Sivakumar, R., Sivakumar, V., Murray, E. & Mackinnon, P. (2007), 'Pore size distribution of unsaturated compacted kaolin', *Géotechnique* **57**, 469–474.

Toker, N. (2002), Modeling the relation between suction, effective stress and shear strength in partially saturated granular media, PhD thesis, Massachusetts Institute of Technology, USA.

Topolnicki, M., Gudehus, G. & Mazurkiewicz, B. (1990), 'Observed stress-strain behavior of remoulded saturated clay under plane-strain conditions', *Géotechnique* **42**, 155–187.

Topp, G., Davis, J. & Annan, A. (1980), 'Electromagnetic determination of soil water content: Measurements in coaxial transmission lines', *Water Resources Research* **6**, 574–582.

Torres, M. & Freitas, V. (2007), 'Treatment of rising damp in historical buildings: wall base ventilation', *Building and Environmental* **42**, 424–435.

Vaid, Y. & Campanella, R. (1974), 'Comparison of triaxial and plane strain behavior of an undisturbed clay', *Geotechnical Engineering, ASCE* **100**, 207–225.

van der Waals, J. (1983), 'The thermodynamic theory of capillary under the hypothesis of a continuous variation of density', *Verhandel. Konink. Akad. Weten. Amsterdam* **1**.

van Genuchten, M. (1980), 'A closed form equation for predicting the hydraulic conductivity of unsaturated soils', *Soil Science Society of America* **44**, 892–898.

van Olphen, H. (1977), *An introduction to clay colloid chemistry*, 2nd Edition. John Wiley & Sons Inc., New York.

Vanapalli, S., Fredlund, D. & Pufahl, D. (1999), 'Influence of soil structure and stress history on the soil-water characteristics of a compacted till', *Géotechnique* **49**, 143–159.

Vanapalli, S., Fredlund, D., Pufahl, D. & Clifton, A. (1996), 'Model for the prediction of shear strength with respect to to soil suction', *Canadian Geotechnical Journal* **33**, 379–392.

Vanapalli, S., Wright, A. & Fredlund, D. (2000), Shear strength behavior of a silty soil over the suction range from 0 to 1,000,000 kpa, *in* '53rd Canadian Geotechnical Conference, Montreal, pp. 1161-1168'.

Vardoulakis, I. (1978), Equilibrium bifurcation on granular earth bodies, *in* 'Advances in the Application of Stability Analysis to Geotechnical instabilities, University of Waterloo Press, SM Study 13, Paper 3'.

Vardoulakis, I. & Goldscheider, M. (1981), Biaxial apparatis for testing shear bands in soils, *in* '10th ICSMFE, Stockholm, Vol. 4/61, Balkema, Rotterdam'.

Vardoulakis, I. & Graf, B. (1985), 'Calibration of constitutive models for granular materials using data from biaxial experiments', *Géotechnique* **35**, 299–317.

Vidal, H. (1969), 'The principle of reinforced earth', *High Res Rec* **282**, 1–16.

Viswanadham, B., Jha, B. & Sengupta, S. (2009), 'Centrifuge testing of fiber reinforced soil liners for waste containment systems', *Practice Periodical of Hazardous, Toxic and Radioactive Waste Management, ASCE, 13(1): 4558* **13**, 45–58.

Viswanadham, S. (1989), 'Bearing capacity of geosynthetic reinforced foundation on a swelling clay master of technology dissertation', *Madras (India): Indian Institute of Technology* .

Wade, N. (1963), Plane strain failure characteristics of a saturated clay, PhD thesis, University of London, UK.

Wanatowski, D. (2005), Strain Softening and Instability of Sand under plane-strain Conditions, PhD thesis, Nanyang Technology University, Singapore.

Wanatowski, D. & Chu, J. (2006), 'Stress-strain behavior of a granular fill measured by a new plane-strain apparatus', *ASTM, Geotechnical Testing Journal* **29**, 149–157.

Wanatowski, D. & Chu, J. (2007), 'Drained behaviour of changi sand in triaxial and plane-strain compression', *Geomechanics and Geoengineering* **2**, 29–39.

Wang, Y. (2006), *Recycling in textiles*, Woodhead Publishing.

Warren, J. (1999), *Conservation of Earth Structures*, Oxford.

Washburn, E. (1921), 'The dynamics of capillary flow', *Physical Review* **17**, 273–283.

Watanabe, K., Koseki, J. & Tateyama, M. (2005), 'Application of high-speed digital ccd-cameras toobserve static anddynamic deformationcharacteristics of sand', *Geotechnical Testing* **28**, 423–435.

Wheeler, S. (1986), The stress-strain behavior of soils containing gas bubbles, PhD thesis, Oxford University, UK.

White, D. J., Take, W. A. & Bolton, M. D. (2003), 'Soil deformation measurement using particle image velocimetry (piv) and photogrammetry', *Géotechnique* **53**, 619–631.

White, I., Zegelin, S., Topp, G. & Fish, A. (1994), Effect of bulk electrical conductivity on tdr measurement of water content in porous media, *in* 'Proceedings of the Symposium on Time Domain Reflectometry in Environmental, Infrastructure, and Mining Applications, Evanston, Illinois, U.S. Bureau of Mines, Special Publication'.

Wind, G. (1955), 'Field experiment concerning capillary rise of moisture in heavy clay soil', *Netherlands Journal of Agricultural Science* **3**, 60–69.

Wolf, H., König, D. & Triantafyllidis, T. (2005), 'Centrifuge model tests on sand specimen under extensional load', *International Journal for Numerical and Analytical Methods in Geomechanics* **29**, 25–47.

Wong, J., Rahardjo, H., Toll, D. & Leong, E. (2001), 'Modified triaxial apparatus for shearing-infiltration test', *Geotechnical Testing Journal* **24**, 370–380.

Wood, C. (1958), Shear strength and volume change characteristics of compacted soil under conditions of plane strain, PhD thesis, University of London, UK.

Wu, T., Loh, A. & Malvern, L. (1963), 'Study of failure envelopes of soils', *Soil Mechanics and Foundations Division, ASCE* **91**, 145–181.

Yang, H., Rahardjo, H., Leong, E. & Fredlund, D. G. (2004), 'Factors affecting drying and wetting soil-water characteristic curves of sandy soils', *Canadian Geotechnical Journal* **41**, 908–902.

Yetimoglu, T. & Salbas, O. (2003), 'A study on shear strength of sands reinforced with randomly distributed discrete fibers', *Geotextiles and Geomembranes* **21**, 103–110.

Yin, J., Kumruzzaman, M. & Zhou, W. (2007), Laboratory facilities for measuring the stress-strain-strength sehavior of soils-the state of the art, *in* 'Fourth Cross-Strait Conference on Structural and Geotechnical Engineering, Zhejiang University Press'.

Yin, Z. (1998), 'Settlement and consolidation of soil mass', *China Electric Publication House* p. (in Chinese).

Young, D. (1997), Rising damp and salt attack, Technical report, Heritage Conservation, Technical Note. South Australia, Department of Environment and Natural Resources and the City of Adelaide.

Yu, X. & Drnevich, V. (2004), 'Soil water content and dry density by time domain reflectometry', *Geotechnical and Geoenvironmental Engineering, ASCE* **130**, 922–934.

Yuan, F. & Lu, Z. (2005), 'Analytical solutions for vertical flow in unsaturated, rooted soils with variable surface fluxes', *Vadose Zone Journal* **4**, 1210–1218.

Yukselen, Y. & Kaya, A. (2006), 'Prediction of cation exchange capacity from soil index properties', *Clay Minerals* **41**, 827–837.

Yusoff, M., Salit, M., Ismail, N. & Wirawan, R. (2010), 'Mechanical properties of short random oil palm fiber reinforced epoxy composites', *Sains Malay* **39**, 87–92.

Zhan, T. & Ng, C. (2006), 'Shear strength characteristics of an unsaturated expansive clay', *Canadian Geotechnical Journal* **43**, 751–763.

Znidarcic, D., Illangasekare, T. & Manna, M. (1991), 'Laboratory testing and parameter estimation for two phase flow problems', *ASCE, Geotechnical Special Publication* **27**, 1089–1099.

Schriftenreihe des Lehrstuhls für Grundbau, Boden- und Felsmechanik der Ruhr-Universität Bochum

Herausgeber: H.L. Jessberger

1 (1979) **Hans Ludwig Jessberger**
Grundbau und Bodenmechanik an der Ruhr-Universität Bochum

2 (1978) **Joachim Klein**
Nichtlineares Kriechen von künstlich gefrorenem Emschermergel

3 (1979) **Heinz-Joachim Gödecke**
Die Dynamische Intensivverdichtung wenig wasserdurchlässiger Böden

4 (1979) **Poul V. Lade**
Three Dimensional Stress-Strain Behaviour and Modeling of Soils

5 (1979) **Roland Pusch**
Creep of soils

6 (1979) **Norbert Diekmann**
Zeitabhängiges, nichtlineares Spannungs-Verformungsverhalten von gefrorenem Schluff unter triaxialer Belastung

7 (1979) **Rudolf Dörr**
Zeitabhängiges Setzungsverhalten von Gründungen in Schnee, Firn und Eis der Antarktis am Beispiel der deutschen Georg-von-Neumayer- und Filchner-Station

8 (1984) **Ulrich Güttler**
Beurteilung des Steifigkeits- und Nachverdichtungsverhaltens von ungebundenen Mineralstoffen

9 (1986) **Peter Jordan**
Einfluss der Belastungsfrequenz und der partiellen Entwässerungs-möglichkeiten auf die Verflüssigung von Feinsand

10 (1986) **Eugen Makowski**
Modellierung der künstlichen Bodenvereisung im grundwasserdurchströmten Untergrund mit der Methode der finiten Elemente

11 (1986) **Reinhard A. Beine**
Verdichtungswirkung der Fallmasse auf Lastausbreitung in nichtbindigem Boden bei der Dynamischen Intensivverdichtung

12 (1986) **Wolfgang Ebel**
Einfluss des Spannungspfades auf das Spannungs-Verformungsverhalten von gefrorenem Schluff im Hinblick auf die Berechnung von Gefrierschächten

13 (1987) **Uwe Stoffers**
Berechnungen und Zentrifugen-Modellversuche zur Verformungsabhängigkeit der Ausbaubeanspruchung von Tunnelausbauten in Lockergestein

14 (1988) **Gerhard Thiel**
Steifigkeit und Dämpfung von wassergesättigtem Feinsand unter Erdbebenbelastung

15 (1991) **Mahmud Thaher**
Tragverhalten von Pfahl-Platten-Gründungen im bindigen Baugrund,
Berechnungsmodelle und Zentrifugen-Modellversuche

16 (1992) **Rainer Scherbeck**
Geotechnisches Verhalten mineralischer Deponieabdichtungsschichten
bei ungleichförmiger Verformungswirkung

17 (1992) **Martin M. Bizialiele**
Torsional Cyclic Loading Response of a Single Pile in Sand

18 (1993) **Michael Kotthaus**
Zum Tragverhalten von horizontal belasteten Pfahlreihen aus langen Pfählen in Sand

19 (1993) **Ulrich Mann**
Stofftransport durch mineralische Deponieabdichtungen:
Versuchsmethodik und Berechnungsverfahren

20 (1992) **Festschrift anlässlich des 60. Geburtstages von**
Prof. Dr.-Ing. H. L. Jessberger
20 Jahre Grundbau und Bodenmechanik an der Ruhr-Universität Bochum

21 (1993) **Stephan Demmert**
Analyse des Emissionsverhaltens einer Kombinationsabdichtung im Rahmen der
Risikobetrachtung von Abfalldeponien

22 (1994) **Diethard König**
Beanspruchung von Tunnel- und Schachtausbauten in kohäsionslosem Lockergestein
unter Berücksichtigung der Verformung im Boden

23 (1995) **Thomas Neteler**
Bewertungsmodell für die nutzungsbezogene Auswahl von Verfahren zur Altlastensanierung

24 (1995) **Ralph Kockel**
Scherfestigkeit von Mischabfall im Hinblick auf die Standsicherheit von Deponien

25 (1996) **Jan Laue**
Zur Setzung von Flachfundamenten auf Sand unter wiederholten Lastereignissen

26 (1996) **Gunnar Heibrock**
Zur Rissbildung durch Austrocknung in mineralischen Abdichtungsschichten
an der Basis von Deponien

27 (1996) **Thomas Siemer**
Zentrifugen-Modellversuche zur dynamischen Wechselwirkung zwischen Bauwerken
und Baugrund infolge stoßartiger Belastung

28 (1996) **Viswanadham V. S. Bhamidipati**
Geosynthetic Reinforced Mineral Sealing Layers of Landfills

29 (1997) **Frank Trappmann**
Abschätzung von technischem Risiko und Energiebedarf bei Sanierungsmaßnahmen
für Altlasten

30 (1997) **André Schürmann**
Zum Erddruck auf unverankerte flexible Verbauwände

31 (1997) **Jessberger, H. L. (Herausgeber)**
Environment Geotechnics, Report of ISSMGE Technical Committee TC 5
on Environmental Geotechnics

Herausgeber: Th. Triantafyllidis

32 (2000) **Triantafyllidis, Th. (Herausgeber)**
Boden unter fast zyklischer Belastung: Erfahrung und Forschungsergebnisse (Workshop)

33 (2002) **Christof Gehle**
Bruch- und Scherverhalten von Gesteinstrennflächen mit dazwischenliegenden Materialbrücken

34 (2003) **Andrzej Niemunis**
Extended hypoplastic models for soils

35 (2004) **Christiane Hof**
Über das Verpressankertragverhalten unter kalklösendem Kohlensäureangriff

36 (2004) **René Schäfer**
Einfluss der Herstellungsmethode auf das Verformungsverhalten von Schlitzwänden in weichen bindigen Böden

37 (2005) **Henning Wolf**
Zur Scherfugenbänderung granularer Materialien unter Extensionsbeanspruchung

38 (2005) **Torsten Wichtmann**
Explicit accumulation model for non-cohesive soils under cyclic loading

39 (2008) **Christoph M. Loreck**
Die Entwicklung des Frischbetondruckes bei der Herstellung von Schlitzwänden

40 (2008) **Igor Arsic**
Über die Bettung von Rohrleitungen in Flüssigböden

41 (2009) **Anna Arwanitaki**
Über das Kontaktverhalten zwischen einer Zweiphasenschlitzwand und nichtbindigen Böden

Herausgeber: T. Schanz

42 (2009) **Yvonne Lins**
Hydro-Mechanical Properties of Partially Saturated Sand

43 (2010) **Tom Schanz (Herausgeber)**
Geotechnische Herausforderungen beim Umbau des Emscher-Systems
Beiträge zum RuhrGeo Tag 2010

44 (2010) **Jamal Alabdullah**
Testing Unsaturated Soil for Plane Strain Conditions: A New Double-Wall Biaxial Device

45 (2011) **Lars Röchter**
Systeme paralleler Scherbänder unter Extension im ebenen Verformungszustand

46 (2011) **Yasir Al-Badran**
Volumetric Yielding Behavior of Unsaturated Fine-Grained Soils

47 (2011) **Usque ad finem**
Selected research papers

48 (2012) **Muhammad Ibrar Khan**
Hydraulic Conductivity of Moderate and Highly Dense Expansive Clays

49 (2014) **Long Nguyen-Tuan**
Coupled Thermo-Hydro-Mechanical Analysis: Experimental and Back Analysis

50 (2014) **Tom Schanz (Herausgeber)**
Ende des Steinkohlenbergbaus im Ruhrrevier: Realität und Perspektiven für die Geotechnik
Beiträge zum RuhrGeo Tag 2014

51 (2014) **Usque ad finem**
Selected research papers

52 (2014) **Houman Soleimani Fard**
Study on the hydro-mechanical behavior of fiber reinforced fine grained soils,
with application to the preservation of historical monuments